The Development of Novel Colon Targeted Drug Delivery Systems

Zuzana Hlásková

Submitted for the degree of Doctor of Philosophy

University of East Anglia

School of Pharmacy

Submitted September 2021

ABSTRACT

Oral delivery of multi-drug formulations to the colon offers many advantages to the patients suffering from diseases such as inflammatory bowel disease, including improved drug bioavailability and patients' compliance. The purpose of this project was to develop colon targeted multi-drug delivery nanosystems for oral administration using electrohydrodynamic processes. Electrospinnability of enteric polymer, hydroxypropylmethylcellulose acetate succinate (HPMCAS), was affected by the formulation and environmental factors. Beaded HPMCAS fibers were obtained, when relative humidity was controlled. Three model drugs (5-aminosalicylic acid, hydrocortisone, paracetamol) were mixed with the HPMCAS electrospinning feed solution to produce multidrug loaded nano-fibers. The drug release behaviour of electrospun multi-drug formulation did not fulfil the enteric requirements, as more than 10% of each drug was released within 2 hours in gastric pH, even though the polymeric matrices did not dissolve. The lack of enteric properties was also observed in electrospun single-drug loaded formulations. To deliver 5-aminosalicylic acid (5-ASA) into the colon without any drug loss in stomach, spherical 5-ASA loaded zein nanoparticles (NPs) were prepared by nanoprecipitation in order to incorporate them into the HPMCAS fibers. Single-step particle-in-fiber incorporation by co-axial electrospinning was not feasible. Therefore, a layered formulation (NPs in between two layers of HPMCAS fibers) was prepared instead. However, the layers of HPMCAS fibers did not protect the 5-ASA from diffusion into the acidic buffer. As the rapid drug release was anticipated to be due to the high surface areas of the electrospun fibers, significantly thicker extrudates were employed as an alternative to reduce the drug release rate. Single-drug loaded extrudates containing the same drug-polymer ratios as the single-drug loaded fibers were prepared at three different diameters. *In-vitro* dissolution data showed the surface to volume ratio of the formulation and the physico-chemical properties of the drugs are key factors influencing the enteric properties of the HPMCAS formulations.

ACKNOWLEDGEMENTS

I would like to thank my supervisors Prof Sheng Qi, Dr Andrew Mayes, and Dr Matthew Alexander for their support on this journey. Thank you for your patience, time, and insight into your experiences.

A special thanks to Prof Peter Belton, who always offered me the needed feedback and who helped me to shape this thesis.

Thanks to Dr Colin Macdonald, Bertrand Lézé, Antony Hinchliffe, Paul Disdle, and Lionel Hill for their technical support and enthusiasm to help me tackle many experimental challenges.

Thanks to my fellow researchers and mentors, Dr Muqdad Alhijjaj, Dr Janine Wilkinson, and Dr Gwenaelle Le Gall, who continuously supported me in the lab and beyond.

Thanks to my fellow PhD students, Hannah, Randa, Veronica, Enana, and Carla, who became my amazing friends. Thank you for being there for me no matter what. I could have not wished for better PhrienDs.

Thanks to my family, who have been my port in the storm in the most challenging times of my life. Thank you for cheering me on over Skype regularly and for providing me with the very much needed comfort each time I visited home. Your love gave me the strength to continue.

This project was funded by Interreg 2 Seas programme 2014-2020 co-funded by the European Regional Development Fund under subsidy contract 2S01-059_IMODE.

TABLE OF CONTENTS

LIST OF FIGURES

LIST OF TABLES

1 INTRODUCTION

The prevalence of inflammatory bowel disease (IBD) has been rising globally, with 6.8 million patients estimated to have been diagnosed in 2017.[1] IBD patients often suffer from adverse effects, since multiple drugs and/or high dosage of drug(s) are frequently required and systemic absorption can occur.[2] With patient's compliance in mind, there is a need to investigate colon targeted multi-drug delivery systems that could be delivered orally and in a controlled manner, which would consequently improve the drugs' potency and bioavailability and decrease their adverse effects. Orally delivered drugs to colon need to be protected from premature release in the stomach and its acidic pH, which can easily degrade the drug.[2] Once the drugs reach the colon intact, they need to either penetrate the mucus barrier, which covers and protects the epithelium from pathogens and foreign particles, or release immediately before the mucus is renewed (every 4 - 6 hours), to avoid their entrapment and flush.[3] In this project, a pH-responsive polymer HPMCAS (grade H) is investigated as a potential carrier for three model drugs: 5-aminosalicylic acid (5-ASA), hydrocortisone (HYD), and paracetamol (PAR), using electrospinning as a primary preparation technique.

1.1 Colon Anatomy and Physiology

Colon (also called large intestine or large bowel) is approximately 1.5 m long tube following small intestine and terminating in the anus.[4,5] The small intestine and colon are separated by the ileocecal valve which works on the same principle as a sphincter. The ileocecal valve is created from intestinal mucosa and prevents faecal material from getting back into the small intestine. The undigested food (mostly cellulose and water) passes through the ileocecal valve to the cecum, then it continues to the ascending colon, transverse colon, descending colon, sigmoid colon, and rectum, respectively. At the beginning of the colon, an appendix is attached to the cecum. This small dead-end tube is formed predominantly by lymphatic tissue and is believed to be a vestigial organ, meaning it used to be a bigger organ with a specific function. Nowadays, the purpose of the appendix is not known, although some theories about its immune function have appeared.[5] The transverse and sigmoid colon are attached to the abdominal wall with the mesentery. The mesentery is not common for ascending and descending colon, although it is present in 12% and 22% of people, respectively.[4] The structural layers of the colon are from outside to the lumen: serosa, longitudinal muscle, circular muscle, submucosa, mucosal muscle, mucosa and epithelium.[5] The longitudinal muscle is condensed into three bands, which is called taenia coli.[4] This

makes the rest of the colon to "squeeze" into and therefore, creating the typical pockets called haustra. Haustra serve to enhancing the absorption surface. The epithelial layer contains many Goblet cells and submucosal glands producing mucus, which is the only secretion occurring in the colon.[5] This viscoelastic mucus layer protects the epithelial barrier of the colon from the external environment. Mucus is a gel containing crosslinked and entangled mucin fibers.[6,7,8] Mucin fibers are formed by linkage of mucin monomers coated by proteoglycans and are approximately 3-10 nm in diameter and roughly 15 nm long. Mucus layer contains approximately 90-98% water.[6] However, mucus is not formed only by mucin. It consists of salts, lipids, proteins, different macromolecules, cells, bacteria and cellular debris.[6,8] The ion, lipid, and protein content together with water percentage influence the viscoelasticity of mucus. The mucus viscosity is usually 1,000 – 10,000 times higher than water viscosity.[6,9] Colonic mucus layer thickness is 100 μm on average, but experiences great variations.[6] Mucus is continuously renewed and discarded. Its lifetime in human colon is predicted to be approximately 4-6 hours.[6] This clearance mechanism serves as protection of epithelial cells from the pathogens and foreign particles present, to which it was found to be highly adhesive.[8]

The function of the colon is removing water from the ileal effluent. Together with water (approx. 80% water[5] from 1 litre of effluent per day[4]), the salts, minerals and vitamins are absorbed.[4,5,10] The vitamins, such as vitamin K, riboflavin, thiamin, biotin, and folic acid, are produced by colonic microflora (trillions of bacteria).[5] The colonic activity is greatly reduced by sleep and increased by mental stress.[4]

1.2 Inflammatory Bowel Disease and its Treatment

Inflammatory bowel disease (IBD) can be divided into two groups based on distribution, clinical behaviour and histological characteristics.[11,12] The first group is ulcerative colitis, which is distributed only in colonic mucosa. On the other hand, the second group, Crohn's disease, is spread over all layers of gastrointestinal tract (GIT).[11,13,14] Ulcerative colitis characteristics vary dependently on the disease activity level. In mild ulcerative colitis, often only the rectum is affected. But in severe stage, there is high ulceration, most of the mucosa is lost and the colon dilatation is rapidly increased. Patients in all stages suffer from diarrhoea and rectal bleeding.[12] Crohn's disease patients are usually young women (15 – 35 years) suffering from abdominal pain, weight loss and diarrhoea.[11] Crohn's disease diagnosis is based on thickened areas of GIT wall with inflammation, ulceration and fissuring of the mucosa.[12] NHS statistics predicted that in 2017, one person

in every 250 was affected by IBD in UK, while ulcerative colitis was slightly more frequent.[13] IBD increases the risk of colorectal cancer.[12]

The treatment is symptomatic and similar for both groups.[11,12] The anti-inflammatory derivatives of 5-aminosalicylic acid (5-ASA) are used mainly for active ulcerative colitis. For severe ulcerative colitis but also for active Crohn's disease, corticosteroids (hydrocortisone, methylprednisolone, beclomethasone, budesonide, tixocortol) are often prescribed. Patients suffering from chronic disease are often prescribed immunosuppressants such as azathioprine or mercaptopurine. Nowadays, the severe forms of IBD are treated also with biological therapies (infliximab, adalimumab, certolizumab pegol). Crohn's disease patients can be prescribed metronidazole or ciprofloxacin to avoid fistulising of perineum. Beside many other drugs (immunoglobulins, interleukins, interferons, heparin, short-chain fatty acids etc.), which can be tried as IBD treatment, nutritional and dietary therapy may be beneficial. In ulcerative colitis patients, surgery (colectomy) is often performed to avoid long-term corticosteroid therapy and also to lower the risk of colorectal cancer.[12]

A common symptom of all IBD patients, which brings them to their physician's office, is a pain. Although, the pain should be thoroughly evaluated, the determination of the source (inflammation, secondary complications, functional pain, chronic pain) is often very complicated. M. J. Docherty et al.[15] suggest starting the management of the pain of patients with active IBD by paracetamol if escalating of the existing therapy is not sufficient on its own. Despite their higher effectivity, non-steroidal anti-inflammatory drugs (NSAIDs) and opiates should be used with caution due to the higher risk of side effects.[15] The well-known gastrointestinal side effects of NSAIDs[16,17] are linked with a potential of NSAIDs to increase the inflammation in the IBD.[18,19,20,21] Selective COX-2 inhibitors are believed to be safer due to the reduced risk of their gastrointestinal toxicity.[22,23] Nevertheless, they are associated with potential cardiovascular side effects.[24,25] The opiates are frequently prescribed for severe pain. However, their risks (side effects, abuse, and diversion to other patients) lead to major concerns and patients need to be therefore closely monitored while using the opiates. Regular exercise, physical therapy, and psychotherapy (including antidepressants) are often prescribed alongside the medication.[15]

1.3 Multi-drug formulations

Thanks to a rapid development of medical sciences, the length of human life has been prolonging globally. In 2019, it was predicted the average length of life would be 69.9 and

74.2 years for men and women, respectively. Although, there is a significant difference between life expectancy at birth in low income countries (62.7 years) and high income countries (80.8 years).[26] The World Health Organization (WHO) estimated that 63% (36 million) of all deaths that occurred globally in 2008 were caused by noncommunicable (chronic) diseases. According to WHO's projections, the number of deaths from chronic conditions will increase to 55 million by 2030.[27] The World Economic Forum predictions from 2011 suggest the noncommunicable diseases will cause a loss of US$ 47 trillion by 2030, which is equal to 75% of global gross domestic product (GDP) calculated in 2010.[28]

Complex combination therapies, consisting of multiple drugs (often over five different medicines) taken more than once daily, are commonly prescribed to treat chronic diseases. This leads to low medication adherence, which can decrease to 30% only, depending on factors such as patients' age or the level of clinical intervention.[29,30] This often results in further health complications, as the patient does not receive sufficient therapy, as well as negative side effects. This vicious cycle is exacerbated with physicians who tend to intensify the already complex treatment plan when they notice the patients' condition has worsened.[31] To simplify the administration of the medicines, compliance aids such as weekly or monthly trays are frequently introduced. However, these aids come with several disadvantages. The preparation of the trays is time consuming, it is prone to errors,[32] and once removed from the original packaging, the manufacturer cannot guarantee the medicine's condition. For example, the change of packaging can increase the rate of the medicine's degradation.[33,34] Additionally, this can bring a professional risk to the pharmacists and clinicians since the medicine is referred to as 'unlicensed' when not in original packaging. Most importantly, the actual contribution of these aids to the patient's compliance has not been supported by sufficient evidence.[35,36] Therefore, there is a pressing need for development of formulations delivering multiple drugs at once, preferably in a controlled manner, so the medicine could be administered only once a day.

Even though combined therapy has been used since the era of great civilisations (e.g., herbal teas and ointments) and frequently used in the form of a pill since the 1940s, when the first multivitamins reached the market, the development of multidrug formulations have experienced a boom only over the last two decades. It was thanks to Wald and Law, who introduced the term PolyPill in 2003 and estimated that this type of formulation could prolong the lives of one third of British people by up to 12 years.[37] In between 2013 and 2018, a total of 93 multidrug formulations was approved by the Food and Drug

Administration (FDA) and European Medicines Agency (EMA). The improvement in patients' compliance was observed in clinical trials of e.g., cardiovascular diseases, hypertension[38] or HIV[39] treatments. However, multidrug formulations are not beneficial only to the patients. The pharmaceutical companies are motivated by the potential extension of their patents as well as the reduction of costs related to the manufacturing (e.g., single product pipeline, reduced packaging). Last but not least, the cost reduction also projects into the prescribing and dispensing of the medicines.[40]

1.3.1 Approaches to Multi-drug Formulations

Although, the PolyPill concept was introduced as one pill treating all patient's diseases, pharmaceutical industry and most research studies tend to focus on either combination of drugs targeting one disease or combining drugs in order to decrease adverse effect of one of the drugs (e.g., combination of aspirin and omeprazole, when omeprazole protects the stomach from the adverse effects of aspirin by reducing the gastric acidity).[31] The different multi-drug formulations and their development are summarised in the two following tables. Table 1.1 lists and describes the molecular and supramolecular structures used for multi-drug delivery, including examples of either clinical or studied formulations. Preparation methods used to develop the multi-drug formulations are described in the Table 1.2, also including examples of relevant formulations.

Table 1.1. Summary of the molecular and supramolecular structures used for multidrug delivery, their principles, and examples of the clinical or studied formulations.[31,41]

Structure	Principle	Example
Codrugs and Molecular Conjugates (Molecular)	A covalent linkage between two or more synergistic pharmacophores, which is broken once a target tissue is reached. Either linked directly using e.g., ester, amide, and azo bonds (a fixed molar ratio of the drugs, potential dosage issues due to the differences in drugs potency) or via a linker such as peptide (drugs activated through enzymatic degradation of the peptide).	• Salazopyrin®, combination of sulfapyridine and mesalazine (Crohn's disease, first approved in 1950)[42] • Benorilate (paracetamol-aspirin)[43]
Macromolecules (Molecuar)	Combination of natural macromolecules such as DNA, RNA, and proteins or synthetic molecules with limitless monomer choice.	• Mongersen: a synthetic 21-mer antisense oligonucleotide hybridizing with complementary mRNA, resulting in decrease of Smad7 protein expression, which is overexpressed in IBD mucosal tissues.[44]
Ionic Conversion (Supramolecular)	Ionic liquid drugs consisting of drugs counteracting one another as anions and cations in a solution.	• Examples of cations[45]: morpholinium, phopshonium, pyridinium, imidazolium • Examples of anions[45]: inorganic halides and sulfates, organic acetates and phosphates

Structure	Principle	Example
Cocrystals (Supramolecular)	Cocrystals are formed by hydrogen bonding between the functional groups (e.g., carboxylic, amide, and hydroxyl) of the drugs. Solubility, permeability, stability, and potency of the drugs can be improved this way.[46,47]	• Entresto®, a cocrystal of sacubitril and valsartan for heart failure treatment.[48]
Cyclodextrins (Supramolecular)	Cyclodextrins are cyclic oligosaccharides consisting of a ring created by glucose subunits linked together by glycosidic bonds - creating a potential to encapsulate hydrophobic drugs in their hydrophobic core (depending on steric effects) and link hydrophilic drugs onto their hydrophilic exterior.	• Hydroxypropyl-β-cyclodextrin in formulation with hydrocortisone (increase of the hydrocortisone bioavailability in the aqueous humor and cornea)[49]
Liposomes (Supramolecular)	Liposomes are vesicles created by phospholipid bilayer around aqueous compartment, which can encapsulate lipophilic drugs within the bilayer and hydrophilic drugs inside the compartment.	• Vyxeos® (daunorubicin and cytarabine) for acute myeloid leukemia.[50]

Structure	Principle	Example
Nano- and Microparticulates (Supramolecular)	Using nano- and microparticles as a carrier which can co-encapsulate two or more drugs, usually composed of biodegradable materials. Recently, mesoporous silica nanoparticles became of interest due to their ability of loading drugs into their pores using a solvent free system. These pores can be controlled by so called ‘gatekeepers’ that open the pores in response of a specific stimulus, allowing for a targeted/controlled drug release.	• Abraxane®, a nanoparticle formulation of paclitaxel and albumin, increasing paclitaxel delivery levels through endogenous albumin pathways.[51]
Metal-Organic Frameworks (Supramolecular)	Metal-Organic Frameworks are porous crystalline scaffolds formed by the inorganic ions or clusters coordinated to organic ligands. The pores can entrap drug molecules, allowing for controlled release.[52]	• studies of delivery of nitrous oxide (prevention of coagulation)[53,54]
Polymeric Structures (Supramolecular)	Polymeric structures can be constructed to possess a number of domains that entrap different drug molecules, enabling separation and controlled release of multiple APIs at a rate that is suitable for the drugs' pharmacokinetic characteristics.[55]	• PLGA as most commonly used polymeric carrier[56,57] • contraceptive polymeric implants[58]

Table 1.2. Summary of preparation methods used for multidrug delivery, their principles, and examples of the formulations prepared by these methods.[31,41]

Method	Principle	Examples
Extemporaneous preparation	Mixing products together.	• Prepared in clinical practice by pharmacists
Traditional formulation approaches	Direct compression, dry granulation, spray drying, and wet granulation.[59,60]	• Over the counter remedies to treat coughs and colds
Extrusion-spheronisation	Extrudates (filaments) are created by extrusion of a blend of the drug(s) and excipient(s) (which can be bound together with binders or water).[61] Spheronisation is a process to create small spheres or pellets from the extrudates. Each drug can be extruded and spheronised separately to be combined into the formulation in a desired ratio.[62]	• Contraceptive formulations Implanon® (3-ketodesogestrel in a core covered with an ethylene vinyl acetate membrane)[63] and NuvaRing (etonogestrel and ethinyl estradiol in a coaxial fiber consisting of two types of polyethylene vinylacetate copolymers)[64]
3D printing	3D printing enables personalised medicine, combining all of the patients' medicines into one tablet, allowing each drug to follow a specific release profile.	• Currently, only approved (FDA) formulation is single-drug ZipDose® technology branded SPRITAM (antiepileptic levetiracetam).[65]
Solid dispersion	Solid dispersion is a molecular dispersion of a drug in amorphous excipient, improving the drugs' bioavailability.[66]	• Ezetimibe-lovastatin: sucrose beads layered with a glass solution of the drugs and Soluplus (enterically coated with Eudragit L100 and Eudragit L100-55)[67]
Multilayer formulations	Multilayer formulations takes advantage of layer by layer construction of tablets, meshes, oromucosal films, and thin layer films adhered onto silica based nanoparticles.	• Multilayer coatings created by biomimetic calcium phosphate and polyelectrolytes, releasing biological growth factors[68]

1.3.2 Clinical Considerations for Use of Multi-drug Formulations

Although potential interaction of the drugs through synergy is one of the advantage of multidrug formulations, it is important to study how the drugs in the particular combination affects each other to avoid their potential interaction through dangerous synergy (or antagonism). While a combination of e.g., bisoprolol (hypertension and heart failure treatment) and acyclovir (antiviral) improves bioavailability of both medicines, there is no clinical use for such a combination even though the drugs are not antagonists and do not contraindicate each other. The sought after synergy is the one that has a clinical use. For example, a combination of co-amoxicillin (a broad-spectrum antibiotic) and amoxicillin (a β-lactam antibiotic) where clavulanic acid in co-amoxicillin protects the amoxicillin from degradation by β-lactamases produced by the bacteria.[31]

The synergistic effect can often be confused with a so-called additive effect. Although, there is evidence that combination therapies have better outcomes than use of individual drugs in cancer treatment, recent studies suggest this is not due to the synergy but rather due to the increased probability that one of the drugs will have the targeted therapeutic effect.[69]

It is also important to keep on mind that each drug comes with potential adverse side-effects. Combining several medications into one tablet then leads to difficulties when a cause of adverse effects need to be identified. There is also a risk that a combination of drugs will cause new unencountered side-effects. This is especially dangerous as many of the newly developed formulations have prolonged release, which makes reversing of the side effects even more difficult.

Lack of flexibility in dosage adjustments is an enduring problem coming with multidrug formulations. This is caused mainly by fixed molar ratios of the drugs in most of the formulations. Additionally, there are combinations, in which a synergistic effect of the drugs occurs only at specific molar ratios (e.g., Vyxeos® - a liposomal cancer medicine[50]). For this reason, FDA and other organs recommend to prescribe multidrug formulations only to patients who are already stabilised on multiple drugs (and specific dosages compatible with the multidrug formulations).[31]

1.4 Colon targeted oral drug delivery

Keeping in mind patients' compliance, the most convenient and also most common administration is the oral route. Oral administration of the drug to the colon can experience many drawbacks, such as dissolving in the stomach or intestinal fluid resulting in low doses reaching the colon and in often observed side effects arising mainly from systemic toxicity.[2,14,70,71] Therefore, protecting the drug from absorption in the upper gastrointestinal tract is required to keep the drug in its intact form until it reaches the colon, including the part in between the cecum and transverse colon.[2,7,14]

From the upper to the lower GIT, the enzymatic activity, motility, and fluid content continually decrease, while pH level and viscosity increase. These properties bring different challenges to the colon delivery systems due to the effects they have on the dosage forms as well as the pharmacokinetic and pharmacodynamic behaviour of the drugs. The average colonic fluid volume is approximately 13 ml, while the range was calculated to be 1 – 44 ml.[72] The low fluid volume may affect the dissolution of the drugs and subsequently the drugs' bioavailability. The solubility of the drugs is also affected by the colonic pH, which can be altered by a diet. For example, a diet rich in carbohydrates reduces colonic pH due to the high concentration of short chain fatty acids produced by fermentation of the polysaccharides.[73] A similar effect can be observed when polysaccharide based drugs are delivered to the colon (e.g., laxative lactulose fermented into lactic acid).[74] The diet also affects the enzymatic activity since the undigested food components (carbohydrates, proteins, fats) serve as substrate for these colonic enzymes.[75] The presence/absence of the food affects the intestinal-colonic transit time of the dosage form as well as the time of administration and the type of the dosage form itself. The healthy individuals showed approximately 52 hours long transit time, while only ~24 hours transit times were observed for patients suffering from ulcerative colitis.[76] The transit is generally delayed during sleep and by use of smaller delivery systems such as particles (compared to capsules which are transited faster).[77]

The influence of upper GIT could be also overcome by rectal administration, but this route brings challenges with respect to reaching the proximal colon, spreading capacity of the formulation and its retention time. [70,71]

1.4.1 Conventional drug delivery approaches

Nowadays, either the immediate release or controlled release (extended release, delayed release and timed release) drug delivery systems such as tablets, gelatine capsules, oral suspensions or oral powders are on the market.[71] Several strategies of colon targeting are used and studied nowadays. These methods, their principles, and examples of corresponding studied or marketed systems and materials are summarized in the Table 1.3.

Table 1.3. Colon targeting strategies for drug delivery. [2,71, 78, 79]

Method	Principle	Studied/Marketed systems and materials
Prodrug formation	Prodrug is an inactive derivative of an active drug (parental drug) formed by covalent linkage of the drug and a carrier. The release of parental drug is obtained either spontaneously or by enzymatic activity of colon microflora.	• Azo bond conjugates • Cyclodextrin conjugates • Glycoside conjugates • Glucuronate conjugates • Dextran conjugates • Polypeptide conjugates • Polymer conjugates
Coating with pH-sensitive polymers	The drug formulation is coated with polymer, which dissolves, disintegrates, or swells in alkaline pH.	• Eudragit® (L 100; S 100; L- 30D; FS 30D; L 100-55) • Polyvinyl acetate phthalate • Hydroxypropyl methylcellulose phthalate (50; 55) • Cellulose acetate phthalate • HPMCAS
Coating with biodegradable polymers	The coating of formulation is degraded by colonic microflora (enzymes).	• Azo-polymers
Embedding in polysaccharide matrices	The drug is released from the matrices via matrix swelling or degradation due to the action of colonic microflora (polysaccharidases).	• Amylose • Chitosan • Chondroitin sulfate • Cyclodextrin • Dextran • Guar gum • Pectin • Xylan

Method	Principle	Studied/Marketed systems and materials
Embedding in pH-sensitive matrices	Drug is released from the matrices via matrix swelling or degradation due to the change of pH towards alkaline values.	• Eudragit® S
Bioadhesive systems	Drug formulation is coated with a polymer, which adheres to colonic mucosa.	• N- (2-hydroxy propyl) methacrylamide (HPMA) copolymers
Time released systems	Multicoated drug formulation passes the stomach and after that, the drug is released after a lag time equivalent to the small intestine transit time.	• Eudragit® (RL; RS; FS; E; L) • Hydroxypropylcellulose • Hydroxypropylmethylcellulose acetate succinate • Ethyl cellulose • Time Clock®
Pressure controlled systems	The release of drug is triggered by pressure arising from peristaltic movements.	• Ethyl cellulose • Eudragit® S
Osmotic controlled systems	The drug formulation is encapsulated into the semipermeable membrane system, from which it is released due to the osmotic pressure generated by the solvent entry.	• OROS-CT system (Alza corporation)
Redox-sensitive polymeric systems	The drug release is triggered due to the system response to the colonic redox potential.	• Azo compounds • Disulphide compounds
Coating with microparticles	The drug formulation is coated with or encapsulated into the microparticles.	• Silica microparticles
Combination of above	Complex systems utilising more than one method of targeting in one.	• Pulsincap™ (pH-sensitive properties and timed release) • CODES™ (pH-sensitive properties and polysaccharides)

The principle of **pH dependent targeting** is based on gradually increasing pH in gastrointestinal tract (from stomach to colon). Polymers or other materials, which disintegrate, swell or dissolve in an alkaline environment, protect the drug from release in the acidic environment of the stomach and preferably in the neutral environment of the small intestine as well.[2,78] Many of the pH based systems currently available on the market are taking advantage of enteric coating, which protects the drug from acidic environment and is often made of methacrylic acid based polymers which are known as Eudragit®.[70,71,80,81] The shelfed products are usually gelatine capsules coated with this Eudragit® enteric layer (e.g., 5-ASA in Asacol®, Salofac®, Claversal®, etc.), since enterically coated gelatine capsules are manufactured easier than complex systems.[80] In one of these complex systems, the enteric coating is accompanied with a timed-release layer usually made of hydroxypropyl cellulose (Figure 1.1).[70,71] After the enteric coating dissolution, the time-release layer of swellable hydrophobic polymer slowly erodes. Once the erosion reaches the core tablet, the drug is rapidly released.[70,81]

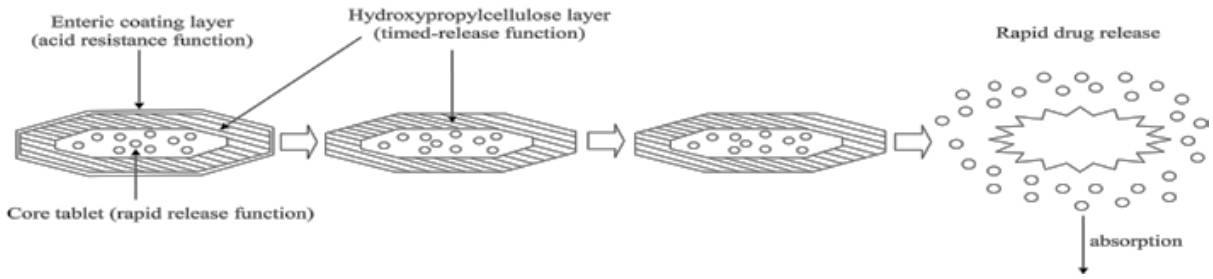

Figure 1.1. Enterically coated timed-release tablet with rapid release function.[70]

Second complex system combining pH sensitivity and time release is called Pulsincap™.[71,79] This system holds the drug in a water insoluble body which is plugged with a hydrogel sealing the opened end. The plugged end is then covered with a water soluble cap and the capsule is then enterically coated. This means, the enteric coating protects the capsule in the stomach and then quickly dissolves following the gastric emptying which enables the water soluble cap to dissolve in the intestinal fluid. Then the hydrogel plug starts to swell until it is ejected which results in the drug release.[71] The Pulsincap™ system and its principle can be seen in Figure 1.2.

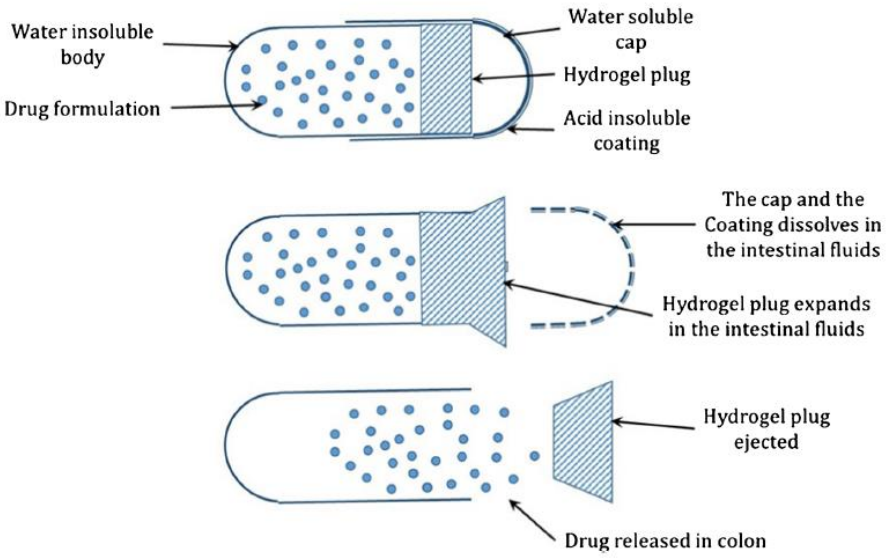

Figure 1.2. Pulsincap™ system and its principle of the drug release.[71]

CODES™ system combines enteric coating together with polysaccharide lactulose, which is enzymatically degraded by colonic microflora. The tablet containing drug and lactulose is coated with acid soluble material (Eudragit E) and then overcoated with enteric layer (Eudragit L). When the enteric coating is dissolved, the acid-soluble layer protects the tablet from dissolution in the alkaline environment of the small intestine. Once the tablet reaches the colon, the colonic microflora starts to degrade the lactulose into short-chain fatty acids, which acidifies the environment around the tablet and dissolves the acid soluble material enabling the drug release.[70,80,81] The lactulose could be potentially replaced with isomalt, which performed similarly *in vitro* and *in vivo*.[82] The CODES™ system and its mechanism of drug release can be seen in Figure 1.3.

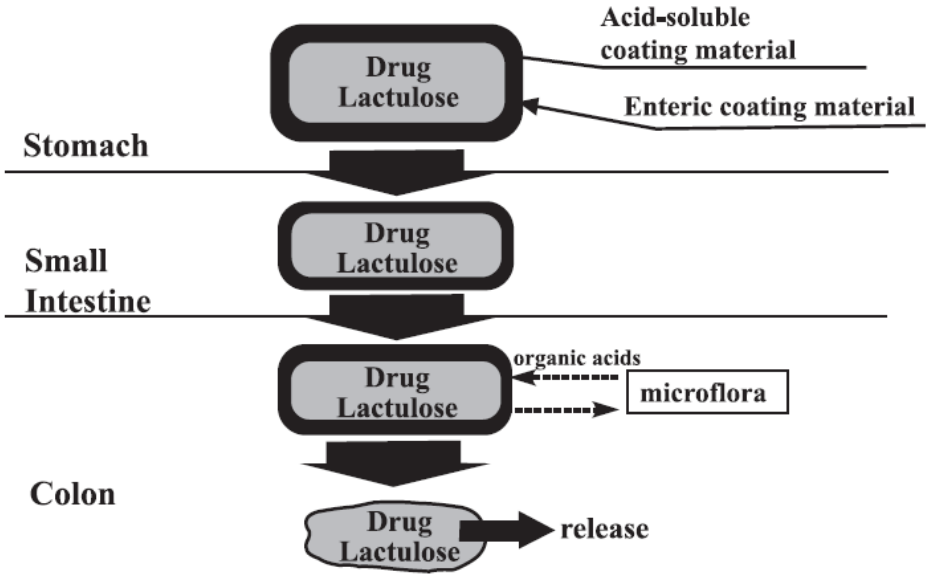

Figure 1.3. CODES^{TM} system and its mechanism of drug release.[80]

However, pH sensitive drug delivery systems can suffer from colonic pH variations among healthy individuals and also between healthy and diseased people. The pH values in different parts of GIT are listed in Table 1.4, comparing the healthy individuals[2] and IBD patients, where in UC patients, the pH values depend on disease activity and on the other hand, in CD patients, the pH reaches approximately the same values irrespective of the disease activity[14].

Table 1.4. Comparison of pH values through GIT in healthy individuals and IBD patients.[2,14]

GIT part	pH (healthy individuals)	pH (IBD patients)
Stomach	1-2 (4 during digestion)	without major changes
Small intestine	6-7	without major changes
Colon	7-8	2.3-5.5 (UC); 5.3 (CD)

Time Clock® is a **time-dependent** drug delivery system. A tablet or a capsule is coated with a hydrophobic-surfactant layer. This layer is applied as an aqueous dispersion. Therefore, the water soluble polymer is added, which helps the coating to adhere to the core tablet or capsule. The coating then rehydrates and redisperses in an aqueous environment of the GIT for the time which is proportional to the layer thickness. Once the coating is dispersed, the drug is released.[83] The Time Clock® systems can be also enterically coated.[84] However, the transit times can vary among individuals as well as pH levels. In some subjects, the drug can release already in the small intestine, while in other individuals the onset of drug release never occurs, since the drug stays intact for the whole transit time.[79] Also

variations among healthy and diseased individuals can be observed. For example, more rapid transit times are observed in IBD (UC) patients[85], IBS patients[86] or in patients suffering from diarrhoea and carcinoid syndrome[87].

Alza corporation trademarked the OROS® system working on the **osmotic pressure** principle.[88] The push-pull unit measures 4 mm in diameter and can be used as a single unit or up to 6 units can be encapsulated into a gelatine shell. The push-pull unit consists of drug layer and push layer, both covered with a semipermeable membrane and overcoated with an enteric layer. On the drug layer end, the orifice is drilled which enables controlled release of the drug once the enteric coating is dissolved and water is able to enter the unit causing the push layer to force the drug layer out. [2,70,88,89] The OROS® system is described in Figure 1.4.

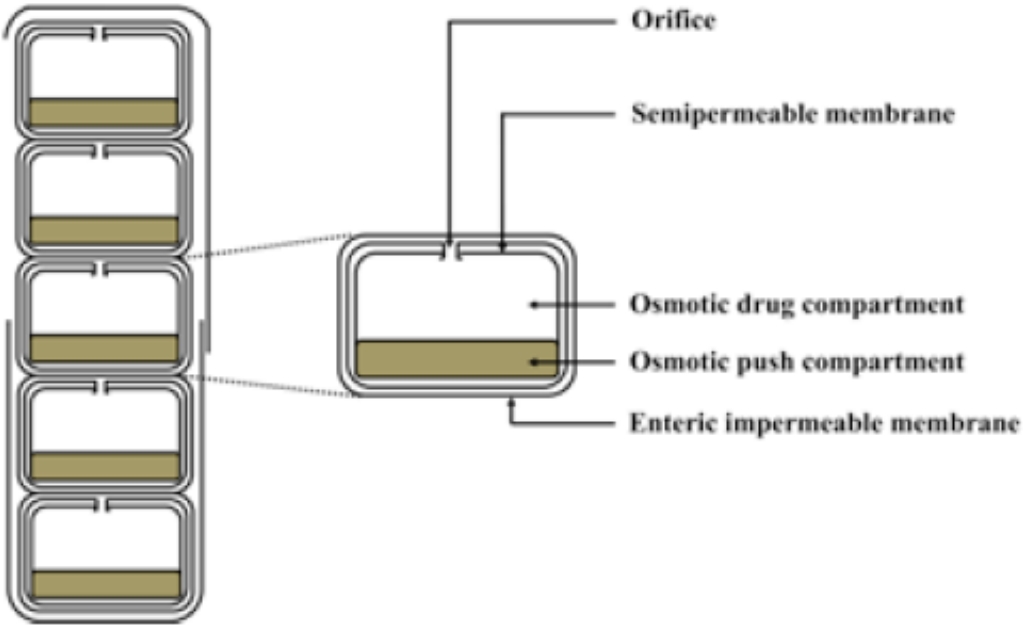

Figure 1.4. OROS (Alza corporation) osmotic drug delivery system.[70]

1.4.2 Micro- and nano-systems under investigation

The colon targeted drug delivery efficacy can be enhanced by use of micro- and nano-systems. The smaller carrier size improves drug bioavailability at diseased tissues, reduces systemic adverse effect and also lower drug concentrations can be used to achieve the same result as with the conventional systems. In inflamed tissue, the nano-systems were observed to overcome the physiological changes, such as different transit time, pH level, intestinal volume and mucosal integrity, better than conventional systems.[90,91] Table 1.5 summarises

current strategies in colon targeted micro- and nano- drug delivery, explains their principles and shows some examples of materials and preparation methods used in particular studies.

Table 1.5. Approaches to colon targeted micro- and nano- drug delivery systems.[14,91]

Approach	**Principle**	**Material; Size Range; Preparation**
Size dependent systems	Reduced size improves the colonic residence time and enhances the efficacy of drug delivery to the colon. An epithelial enhanced permeability and retention effect (eEPR)[90,91] can be observed. Reduced size can also help to avoid the rapid elimination in case of diarrhoea because of the effective uptake of carrier by inflamed tissue and cells.[92,93]	• Polystyrene; μm and nm; purchased from Polysciences Ltd. (Eppenheim, Germany)[94] • Ethyl cellulose; nm; emulsification solvent evaporation technique using different surfactants[95] • PLGA; nm; oil/water emulsification-solvent evaporation method[96]

Approach	Principle	Material; Size Range; Preparation
Surface charge dependent systems	Carriers with positive or negative charge electrostatically interact with inflamed tissue. Since this type of interaction can occur with different components of GIT (bile acids, mucins, etc.), additional targeting mechanism is usually required.	Positively charged carriers (adhere via interaction between carrier and negatively charged mucosa): • Eudragit RL; nm; modified solvent displacement method[97] • Chitosan-functionalised PLGA; nm; solvent evaporation technique[98] • Trimethylchitosan; nm; ionic complexation/gelation method[99] • Chitosan coated liposomes; nm; dry film rehydration method[100] Negatively charged carriers (adhere via interaction between carrier and positively charged proteins in inflamed tissue): • DSPG liposomes; nm; lyophilisation and rehydration[101] • Nanostructured lipid carriers; nm; high-pressure homogenization[93] • PLGA; nm; solvent evaporation technique[98] • PLGA; nm; oil/water emulsification method[102,103]
PEGylation dependent systems	Using of PEG hydrophilic surface and neutral charge to hinder interactions with mucus and other intestinal/colon components.[104,105,3]	• PLGA; nm; nanoprecipitation[106] • Nitroxide radical-containing nanoparticle; nm; assembly of an amphiphilic block copolymer that contains stable nitroxide radicals in an ether-linked hydrophobic side chain[107]
pH dependent systems	Works on the principle of continuous increasing of pH level in the GIT (enteric coating).	• Eudragit® S100; nm; “water-in-oil-in-water” method[99]

Approach	Principle	Material; Size Range; Preparation
Biodegradable systems	Using of materials which are enzymatically degraded in colon.	• PLGA; nm; oil/water emulsification method[103] • Silica nanoparticles (SiNPs); nm; covalent binding of 5-ASA to the SiNPs surface[108] • gelatine nanoparticles in PCL microparticles oral delivery system (NiMOS); nm and µm; ethanol precipitation method under controlled conditions of temperature and pH followed by optimized protocol to form NiMOS[109,110] • PLA Nanosystems embedded in hydrogels; nm and µm; double emulsion/solvent evaporation[111]
Redox systems	Using of materials which degrade in presence of reactive oxygen species (ROS). The high ROS level is caused by inflammation.	• Thioketal nanoparticles; nm; oil-in-water single-emulsion procedure[112]
Active targeting dependent systems	Using of ligands coupled to the surface of drug delivery carriers. Specific ligands react to disease induced changes, such as receptor expression. [92,113]	• Polystyrene nanoparticles coated with antibodies; nm; antibodies were absorbed onto the surface of nanoparticles by incubation in a buffer[114]

1.5 Fabrication of micro- and nano-systems via electrohydrodynamic and nanoprecipitation methods

In this project, electrospray, electrospinning, and nanoprecipitation are used as the main preparation techniques. Electrospraying and electrospinning are both also called ElectroHydroDynamic Processes (EHDP), which are techniques of liquid atomisation and spinning by means of electrical forces.[115,116] Nanoprecipitation is a technique, in which phase

separation occurs after a material dissolved in appropriate solvent is mixed with a so-called antisolvent.[117]

1.5.1 EHDP: Electrospray and Electrospinning

The predominantly used mode of EHDP (both electrospray and electrospinning) is a cone-jet mode. The conductive liquid flows out from a capillary nozzle, to which high potential is applied. If the applied potential is sufficient, the electrical stress caused by free charges at the surface of the exiting liquid leads to formation of a conical shaped meniscus called Taylor cone. The Taylor cone is further elongated into a highly charged jet, which either disrupts into primary droplets at some point (**electrospray**) or elongates and whips towards the collector resulting in fibers (**electrospinning**).[115,116]

In the **electrospray** droplet formation, the electrostatic repulsion, the kinetic energy of the liquid and the surface tension on the liquid-gas interface play the main roles. The primary droplets shrink due to solvent evaporation. Since the shrinkage causes increased charge concentration, the droplets often experience Rayleigh disintegration or Coulomb fission after the solvent evaporation. This means the already shrunk droplets are broken up into even smaller droplets to balance the charge concentration. These disruptions lead to polydisperse particles, which is the reason why they should be avoided. This can be achieved by discharging of the produced droplets using e.g. a corona neutralizer consisting of discharging stainless steel ring or needle, which is connected to a separated high potential source and is placed opposite to or around the nozzle.[115] Finally, the droplets are solidified and particles are deposited on a collector.[118] The scheme of particle formation can be seen in Figure 1.5.

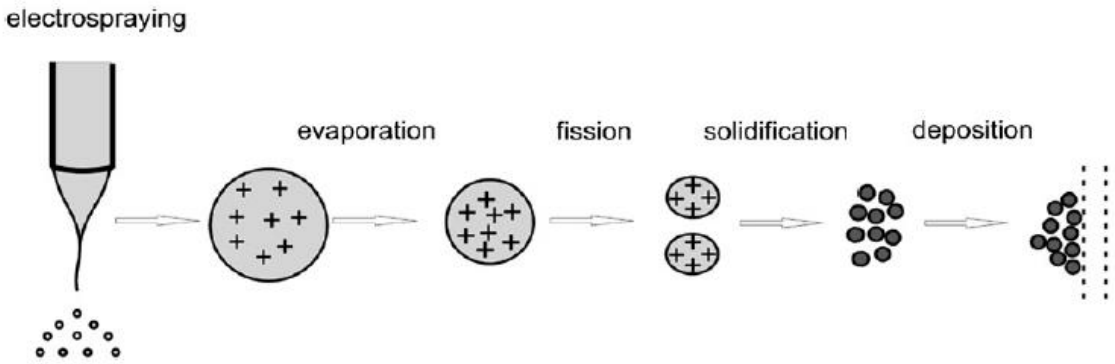

Figure 1.5. Steps of electrospray particle formation.[118]

In the **electrospinning** process, polymers of higher molecular weights are used to achieve sufficiently high axial tension in the jet.[115,116] The electrospun fibers can range from nano- to micrometres in diameter, can be up to three metres long, and are collected as a non-woven fibrous mat.

Both electrospray and electrospinning apparatus are almost the same, as both require a high voltage electric supply, one electrode connected to a conductive nozzle and another one connected to a conductive collector. In the case of processing material solution, which is the type of EHDP used in this project, a solution reservoir such as a syringe and a pump for a liquid feed (e.g., syringe pump, pressure pump) are also required. A representative scheme of an electrospray setup is shown in Figure 1.6. This setup would be equally functional for electrospinning if sufficient axial tension in the jet was reached. In that case, the liquid jet would not disrupt into droplets as shown in the diagram but would elongate and whip towards the collector. Different types of EHDP setups are discussed in more detail in Chapter 2.

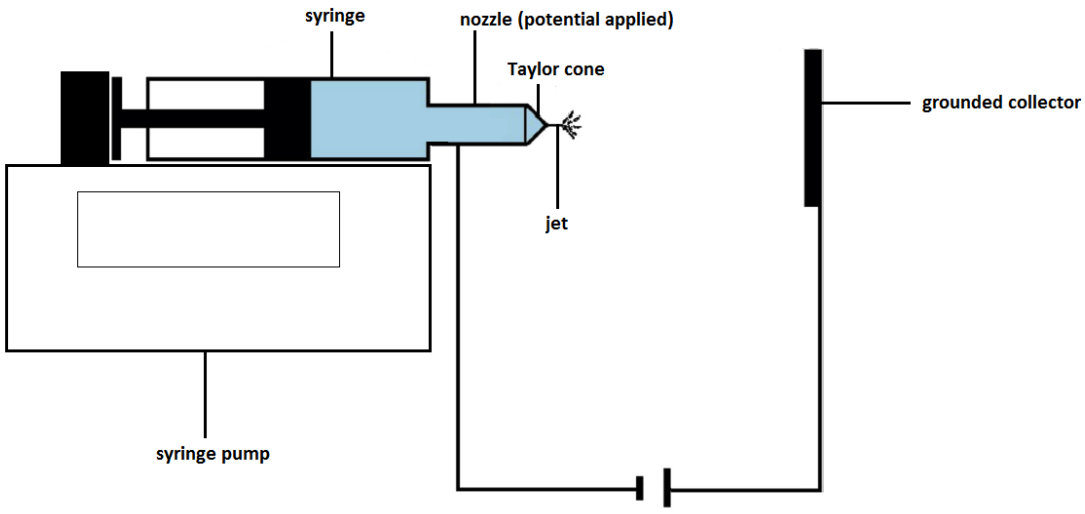

Figure 1.6. A representative scheme of electrospray setup.[115]

1.5.2 EHDP: Formulation and Process related parameters

There are a number of liquid properties influencing the electrospray and elecrospinning outcome. These are mainly conductivity, viscosity, and surface tension at the liquid-gas interface. When using electrohydrodynamic processes in pharmaceutics, mainly polymers, but also different carriers, are used to enable controlled drug release or targeted local drug delivery. The carrier type, molecular weight, and their concentration influence the process critically as well as the solvent physicochemical properties. Because EHDP occurs

only if the electric stress overcomes surface tension, organic solvents with low surface tension are commonly used alongside water, which is frequently used in electrospinning. The solvent properties influence the surface morphology of the particles and fibers significantly. Finally, adding the API into the solution may change the liquid properties substantially.[115,119]

In electrospinning, increased conductivity of the solution (by the use of solvent with higher conductivity or by adding salts) shows improved quality of the fibers and lower beading of the fibers, since the increased conductivity stretches and accelerates the jet. On the other hand, lower dielectric constant leads to longer stable process due to the reduction of bending instability (because of lower charge density). The viscosity is another important parameter in electrospinning. The fiber diameter increases with increasing concentration of the solution. No fibers are formed when the viscosity is too low due to insufficient polymer chain entanglement but also when the viscosity is too high since the electrical charges are insufficient to stretch the solution.

The electrospray cone-jet mode is feasible when conductivity of solution is in the range of 10^{-11} to 10^{-1} S m^{-1},[120] but commonly the range of 10^{-8} to 10^{-4} S m^{-1} is used. The cone-jet mode forms in a certain range of flow rate and potential. The most important factor influencing the diameter of the jet and consequently the size of particles is the flow rate. Both potential and geometry of the nozzle affect the jet diameter and the current, which is transported by the jet, negligibly. To achieve near monodisperse droplet sizes in a stable cone-jet mode, operation near the minimum flow rate is required. For low viscosity solutions, the minimum flow rate depends directly on permittivity and surface tension of the solution and indirectly on the density and conductivity of the solution.[121] If the solution is highly viscous, the equation may look different. It is suggested that in such a case, the minimum flow rate directly depends on solution permittivity and squared diameter of the nozzle, and indirectly depends on the viscosity of the solution.[122] However, the liquid viscosity influences only the jet breakup. But it does not affect the current within the jet or the jet diameter. High liquid viscosity delays the jet breakup resulting in the elongated jet of electrospinning. Since the jet carries the net charge, the jet can experience nonsymmetric perturbations resulting in moving the small portion of the jet slightly off axis. This leads to whipping, because the charge along the rest of the jet pushes that small portion even farther away from the axis. Due to the whipping, high tensile stresses arise and this results in jet thinning.[121]

Using polymer solutions, the solidification process and the particle/fiber morphology depend on the correct balance of solvent evaporation rate, polymer diffusion and polymer chain entanglement.[115,119] If the solvent, for example DCM, possesses high vapour pressure, its boiling point is low and therefore the solvent evaporation is fast. Using this type of solvent may lead to formation of highly porous or even hollow structures, since the time for polymer chain entanglement is short. On the other hand, by choosing a solvent with low evaporation rate (low vapour pressure, high boiling point) smooth particles of smaller size can be achieved. However, there is a risk of a weaker chain entanglement causing two different maxima in size distribution. Using water as a solvent may lead to coronal discharge in the air, therefore aqueous solutions are electrosprayed either in vacuum or inert gas environment.[119]

1.5.3 EHDP: Advantages and Disadvantages

EHDP methods are nowadays used across different fields because of their numerous advantages. The main advantages of the EHDP products (fibers and particles) are seen in high surface to volume ratio, high porosity, and in the case of pharmaceutical use, high drug loading efficiency and its molecular dispersion due to the fast evaporation of the solvent. The experimental setup is relatively cheap and can be very flexible. Different cone-jet setups then enable preparation of customised micro- or nano-systems with tailored properties. The setup can be modified in different steps, e.g. by using of different types of nozzle (single, co-axial, or tri-axial), different collectors (dry collector or solution) or working in different environments (atmospheric pressure vs vacuum).[116,115]

Electrospinning is often considered as a green technology as there is a potential to avoid harmful organic solvents. Electrospray can produce particles smaller than 1 μm of various materials. The size distribution of the particles is usually narrow if a stable cone-jet mode is obtained. Since the droplets are highly charged, their self-dispersing properties lead to almost no agglomeration and coagulation. Using of electric field allows easy control of the droplets' motion.

Among the disadvantages of electrospray cone-jet method is the rather narrow operating window, meaning the number of factors influencing the stability of cone-jet mode is high and the factors are very complex and interdependent.[115] Another disadvantage of EHDP is possible degradation of the drug encapsulated into the particles or loaded into the fibers due to different factors such as high electrical potential, temperature or shear stress in

the nozzle.[115,123] Finally, the upscaling of the methods for industrial usage is still challenging due to the low production rate of both techniques.

1.5.4 Nanoprecipitation Method

Nanoprecipitation is a bottom-up technique, in which the particles are formed via nucleation, growth, and precipitation. This is achieved by mixing the drug and/or the carrier material dissolved in appropriate solvent (dissolved parent phase) with a so-called antisolvent. Amongst others, change of the solubility, pH, or temperature are the most common factors inducing the phase separation.[124]

The **nucleation** is activated through the change in the system's equilibrium, caused by either supersaturation (exceeded solubility equilibrium) or supercooling (system temperature dropping below the phase transformation point). In order to reduce high Gibbs free energy caused by either supersaturation or supercooling, atomic or molecular clusters are formed.[125] Depending on the size of the clusters, subcritical and supercritical nuclei are formed. The supercritical nuclei are larger than the critical size that allows further growth, while the subcritical nuclei are smaller than the critical size and dissociated back into the dissolved parent phase. In pharmaceutical nanoparticle preparation, homogenous nucleation, happening spontaneously and forming nuclei uniformly throughout the system, prevails over heterogeneous nucleation, occurring in the presence of foreign entities serving as a nucleating surface (e.g., impurities, dust, and rough surface of the container).[126,127] One of the most important factors influencing the properties of the nanoparticles is the rate of nucleation (number of nuclei formed in a unit volume of a solution per unit time). Small, monodisperse nanoparticles are achieved by rapid and uniform nucleation, when formation of a high number of nuclei causes a rapid drop in the supersaturation level, followed by termination of the nucleation and beginning of the growth process. Bigger and polydisperse nanoparticles are formed via slower nucleation rates since the supersaturation level decreases over a longer period of time, allowing formation of nuclei of various and larger sizes. The mixing technique highly affects the uniformity and rate of nucleation in the antisolvent nanoprecipitation.[128,129]

The nucleation occurs simultaneously with the **growth** process. The growth is described as growth in size caused by adsorption of so-called growth species (formed and diffused reactants) on the surface of the nuclei. Alongside the kinetics of the nucleation and growth, both diffusion and surface mechanisms are significant factors affecting the

continuous growth and the final size distribution of the nanoparticles.[130] The time required to complete homogenous mixing of the solutions divided by the time required for the critical nucleation concentration to be reached gives the dimensionless Damköhler number (Da) which determines whether the growth is controlled by diffusion (Da<<1) or the surface (Da>>1) or both (Da ~ 1).[128] Monodisperse particles can be obtained by controlling the growth with the diffusion of the monomers from the bulk solution to the surface of the nuclei. Such diffusion controlled growth can be achieved by increasing the viscosity of the bulk solution or by creating a layer which protects the nanoparticles from the monomers' diffusion.[128,130] Surface controlled growth occurs when the diffusion of the monomers from the bulk solution to the surface of nuclei is very rapid and can have two mechanisms – mononuclear and polynuclear.[130] The mononuclear growth occurs layer by layer and leads to polydisperse particles since the growth rate is dependent on the surface area of the nuclei. On the other hand, the polynuclear growth is relatively uniform, affected by temperature only and leads to monodisperse particles, as the concentration of the growth species is sufficiently high to start growing a second layer before the first is fully finished.[128,130]

1.6 Aims and Objectives of the Project

The general aim of this project was development of a colon targeted multidrug nanoformulation for oral administration, prepared predominantly by electrospinning and electrospray techniques. For this purpose, the enteric HPMCAS polymer and zein protein were selected as excipients to carry three model drugs used in IBD treatment: 5-aminosalicylic acid (5-ASA), hydrocortisone (HYD), and paracetamol (PAR). The three main objectives of the project are summarised below, including a brief description of tasks which were performed to achieve these aims.

- **Preparation of blank HPMCAS electrospun fibers**

Electrospinning of blank HPMCAS fibers has not been described in the literature prior this project. Therefore, formulation, process, and environment related factors affecting electrospinnability of the enteric HPMCAS polymer were studied to obtain blank HPMCAS electrospun fibers. Physico-chemical properties of the blank HPMCAS fibers were characterised and compared with the raw material. (Chapter 3)

- **Preparation of colon targeted multi-drug loaded HPMCAS electrospun formulation**

HPMCAS fibers containing three model drugs (5-ASA, HYD, PAR) were electrospun based on the process knowledge obtained through preparation of the blank HPMCAS fibers. Physico-chemical properties of the drug loaded formulations were characterised as well. (Chapter 3)

Drug release profiles from the multi-drug loaded HPMCAS electrospun formulation did not fulfil the enteric requirements of the colon-targeted formulation as the drugs were released prematurely (Chapter 3) and therefore encapsulation of the drugs into zein nanoparticles incorporated into the HPMCAS fibers was explored.

  - Electrospray and nanoprecipitation were compared as preparation techniques of zein nanoparticles (blank and loaded with 5-ASA) followed by physico-chemical and drug release profile characterisation of the particles. (Chapter 4)
  - Feasibility of incorporation of 5-ASA loaded zein nanoparticles into HPMCAS electrospun fibers in a single step was studied, followed by physico-chemical characterisation. (Chapter 5)

- **Study of drug release profiles from the multi-drug loaded HPMCAS electrospun formulation**

Since incorporation of the drug loaded nanoparticles into the HPMCAS fibers proved to be unsuccessful, drug release profiles of individual model drugs from the electrospun HPMCAS fibers were studied more closely. For this purpose, single-drug loaded HPMCAS fibers were electrospun and characterised. (Chapter 5)

  - As none of the single-drug loaded electrospun formulations fulfilled the enteric requirements, the potential effect of fiber diameter on the drug release was further studied. To obtain different diameters of the fibers, filaments containing the same drug-polymer ratios as the electrospun fibers were prepared by hot melt extrusion. (Chapter 5)

2 MATERIALS & METHODS

In this chapter, physico-chemical properties of the used materials and experimental considerations of the formulation processes are described. Details of equipment, materials, and procedures performed in this project are given in the relevant chapters discussing the experimental results.

2.1 Model Drugs

Three model drugs (5-aminosalicylic acid, hydrocortisone, and paracetamol) commonly used in the treatment of inflammatory bowel disease (IBD) were selected to be delivered simultaneously in the nanofibrous formulation. The model drugs are further described below. Their structures and physico-chemical properties are then summarised in the Table 2.1.

2.1.1 5-Aminosalicylic Acid (5-ASA)

5-Aminosalicylic acid (5-ASA), also called mesalamine or mesalazine, is an anti-inflammatory drug. Even though, 5-ASA mode of action is uncertain, it is considered to act locally on intestinal tissue, as its systemic absorption is low.[131,132,133] It is believed, the drug supresses the metabolism of arachidonic acid there, leading to inhibition of mucosal inflammation mediated by cyclooxygenases and lipoxygenases.[133] Mesalamine is an active moiety of various prodrugs such as sulfasalazine (sulfapyridine linked to 5-ASA by an azo bond).[132,134] The dose of 5-ASA range between 2.4 and 4.8 g per day.[131]

5-ASA, a small hydrophilic organic molecule,[131] is obtained in a form of tan to pink crystalline powder (needle like crystals) which can darken when exposed to air.[134] The powder is non-hygroscopic and slightly soluble in water (0.84 mg/ml at 20 ˚C). It is readily soluble in dilute hydrochloric acid and in dilute alkali hydroxides. Very low solubility was observed in dehydrated alcohol, acetone, and methyl alcohol. 5-ASA is practically insoluble in chloroform, ether, butyl alcohol, ethyl acetate, n-hexane, methylene chloride, and propyl alcohol.[135] Computed partition coefficient $\log P = 0.46 \pm 0.34$ (ACD/logP program; Advanced Chemistry development, Toronto, Canada) suggests an equivalent preference for hydrophilic and hydrophobic environment.[134] Dissociation constant (pKa) was determined for each of three 5-ASA functional groups: 2.09 (carboxylate group), 5.26 (amino group), and 13.64 (hydroxyl group).[134,135]

2.1.2 Hydrocortisone (HYD)

Hydrocortisone (HYD), also known as cortisol, is a corticosteroid used as fast-acting anti-inflammatory medicine due to its glucocorticoid and mineralocorticoid activity (lesser extent).[136] In the IBD treatment, HYD is prescribed for a short period of time (3 - 6 weeks) to induce remission, followed by a gradual decrease of dosage before being replaced by another medication serving as maintenance therapy.[137] Hydrocortisone is obtained as a white, odorless powder, which is poorly soluble in water (0.28 mg/ml at 25 °C). Three polymorphic forms of hydrocortisone are known: orthorhombic forms I (most stable) and III (metastable), and monoclinic form II (metastable).[138]

2.1.3 Paracetamol (PAR)

Paracetamol (PAR), also known as acetaminophen, is a commonly used over-the-counter analgesic and antipyretic with weak anti-inflammatory properties. It is also an analgesic of first choice when it comes to the management of pain caused by the IBD.[15] Paracetamol is also a widely used component of various multidrug formulations used for cold and flu treatment. The usual oral dose of paracetamol is 0.5 – 1 g every 4 to 6 hours, with maximum of 4 g per day.[139] Compared to opioids, there are no problems with dependence and tolerance with paracetamol. However, PAR shows a so-called ceiling of efficacy, when increasing the dose above this threshold does not improve the therapeutic effect.[139] Paracetamol is obtained as crystalline white powder. Three polymorphs of paracetamol are known: monoclinic form I (stable), orthorhombic form II (metastable), and form III (unstable).[140]

Table 2.1. Structures and physico-chemical properties of the model drugs: molecular weight (M), dissociation constant (pKa), partition coefficient (logP), solubility in water, Biopharmaceutical Classification System class, melting point (T_m), glass transition (T_g), and polymorphic forms.[135,141,142]

Model Drug	Structure	M (g/mol)	pKa	logP	Solubility in water	BCS class*	T_m (°C)	T_g (°C)	Polymorphic forms
5-Aminosalicylic acid	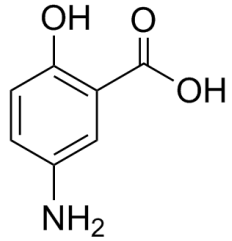	153.14	2.09; 5.26; 13.64	0.46 ± 0.34	0.84 g/L at 20 °C	IV	Degrades before melting	-	-
Paracetamol	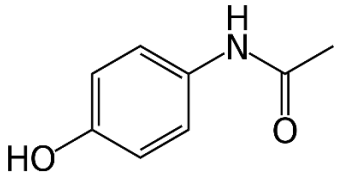	151.16	9.5	0.46	14 g/L at 20 °C	III	169	26	I, II, III
Hydrocortisone	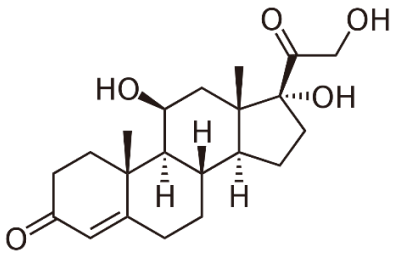	362.5	12.6	1.6	0.28 g/L at 25 °C	II	224	86	I, II, III

* Class I - high permeability, high solubility; Class II - high permeability, low solubility; Class III - low permeability, high solubility; Class IV - low permeability, low solubility.

2.2 Excipients

Three different excipients were used in this project. Enteric hydroxypropylmethylcellulose acetate succinate (HPMCAS) was used to electrospin the multidrug loaded fibrous formulations. Zein nanoparticles were prepared by electrospray and nanoprecipitation, where the feasibility of loading 5-ASA into these particles was studied. Finally, polyvinylopyrrolidone (PVP) was used as an auxiliary excipient to produce a formulation combining the 5-ASA loaded zein nanoparticles and the HPMCAS fibres.

2.2.1 Hydroxypropylmethylcellulose acetate succinate (HPMCAS)

Hydroxypropylmethylcellulose acetate succinate (HPMCAS) is a synthetic polymer also known as hypromellose acetate succinate in pharmaceutical industry. This white to off-white powder is a mixture of acetic acid and monosuccinic acid esters of hydroxypropylmethyl cellulose. HPMCAS is an approved pharmaceutical excipient for oral formulations. It is commonly used as an enteric coating agent for tablets, capsules, and granules as well as a solid-dispersion carrier to improve drug bioavailability. The polymer is physiologically inert and its solubility is controlled by pH of the solvent. It is practically insoluble in water, ethanol, and hexane. HPMCAS is tasteless and may have a faint odour of acetic acid. The polymer is produced in three different grades: L, M, and H. Different content of acetyl and succinoyl groups in these three grades leads to a solubility of each grade in different pH (see Table 2.2).[143]

Table 2.2. HPMCAS grades and their solubility in different pH, depending on the various acetyl, succinoyl, methoxyl, and xydroxypropoxy content in each grade.[143]

Grade	Acetyl Content	Succinoyl Content	Methoxyl Content	Hydroxypropoxy Content	Soluble in pH
L	5 – 9%	14 – 18%	20 – 24%	5 – 9%	> 5.5
M	7 – 11%	10 – 14%	21 – 25%	5 – 9%	> 6
H	10 – 14%	4 – 8%	22 – 26%	6 – 10%	> 6.8

HPMCAS is hygroscopic and hydrolyses to acetic acid and succinic acid at sustained levels of elevated humidity. Therefore, the polymer must be stored in a well-closed container in a cool, dry place. Due to its high molecular weight (10 – 500 kDa) and insolubility in water causing low oral bioavailability, the daily intake limit is set to 560 mg (Inactive Ingredient Database).[143] In this project, granulated AquaSolve^{TM} HPMCAS of grade H was used as an enteric carrier for colon targeted oral formulation.

2.2.2 Zein

Zein is a protein with molecular weight about 22 - 27 kDa and is found in the endosperm of corn kernels.[144] This protein with amphiphilic properties contains high concentration of glutamic acid (21 – 26%), leucine (20%), proline (10%), and alanine (10%), but shows a low nutritional value due to the deficiency of basic and acidic amino acids (tryptophan, lysine).[145] The high content of nonpolar amino acid residues in the core of the protein covered with hydrophilic glutamine turns defines the solubility behaviour of the protein (see the structure in Table 2.3). Zein is insoluble in water but can be dissolved in aqueous ethanol (e.g., 70% v/v), where it can form small globules with diameters between 150 and 550 nm.[146] It can also be dissolved in the presence of high concentrations of urea, high concentrations of alkali (pH ≥ 11), or anionic detergents.[145] Zein's "bricklike" structure also allows carrying other molecules inside and sustained drug release.[146] Commercial zein is a mixture of several peptides (α-, β-, γ- and δ-zein), which possess different molecular weight, solubility and amino acid sequence.[147] α-Zein creates approximately 80% of the total prolamin present in corn and is soluble in 95% ethanol. Its peptide composition is very similar to the whole zein. Starch gel electrophoresis showed two major bands at 22 and 24 kDa belonging to α-zein. β-Zein is richer in histidine, arginine, proline, and methionine, when compared to α-zein. This relatively unstable zein is soluble in 60% ethanol and insoluble in 95% ethanol. Three bands were found for β-zein in the gel electrophoresis: 14, 22, and 24 kDa.[145] Zein is biodegradable and FDA approved as a food-grade ingredient.

2.2.3 Polyvinylopyrrolidone (PVP)

Polyvinylopyrrolidone (PVP) is an amorphous polymer obtained as a hygroscopic white powder. PVP is a linear non-ionic polymer, which is pH stable. The polymer is hydrophilic and highly polar, and therefore soluble in water and organic solvents. PVP can be plasticised by addition of water or the organic plasticisers. It is known for its adhesive and cohesive properties.[148] In pharmaceutical industry, PVP is widely used for solid dispersions and has been reported to form complexes with BCS class II drugs, improving their aqueous dissolution properties.[149] PVP is physiologically inert and it is manufactured in several molecular weights. In this project, PVP k90 was used, which has molecular weight in the range of 1,000,000 – 1,700,000 Da.[148]

Table 2.3. Structures and physico-chemical properties of the excipients: molecular weight (M), glass transition (T_g), and solubility in water.[143,145,148]

Excipient	Structure	M (g/mol)	T_g (°C)	Solubility in water
HPMCAS	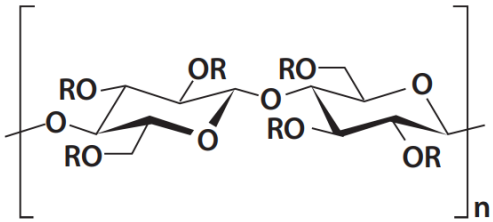 **R**= -H, -CH_3, -C(O)CH_3, -C(O)$CH_2CH_2CO_2H$, -[$CH_2CH(CH_3)O$]$_m$**R**^{1} **R**^{1}= -H, -CH_3, -C(O)CH_3, -C(O)$CH_2CH_2CO_2H$	10,000 – 500,000	123	Insoluble (pH dependent)
Zein	glutamine turns α-helix 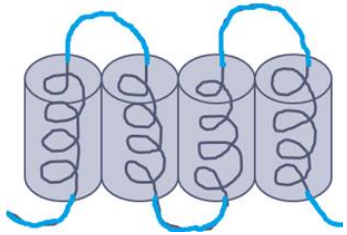 glutamine turns	22,000 – 27,000	161	Insoluble
PVP k90	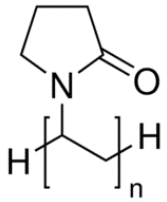	1,000,000 – 1,700,000	177	Highly soluble

2.3 Formulation Processes

2.3.1 Electrospinning

The electrospinning setup can be either vertical or horizontal, resulting in no difference in the fiber morphology.[150] While traditional setup uses one high voltage source, R. Jaeger et al.[151] introduced an additional high voltage source in a form of a ring electrode into the system to reduce the electrostatic field at the tip of the nozzle (see Figure 2.1).

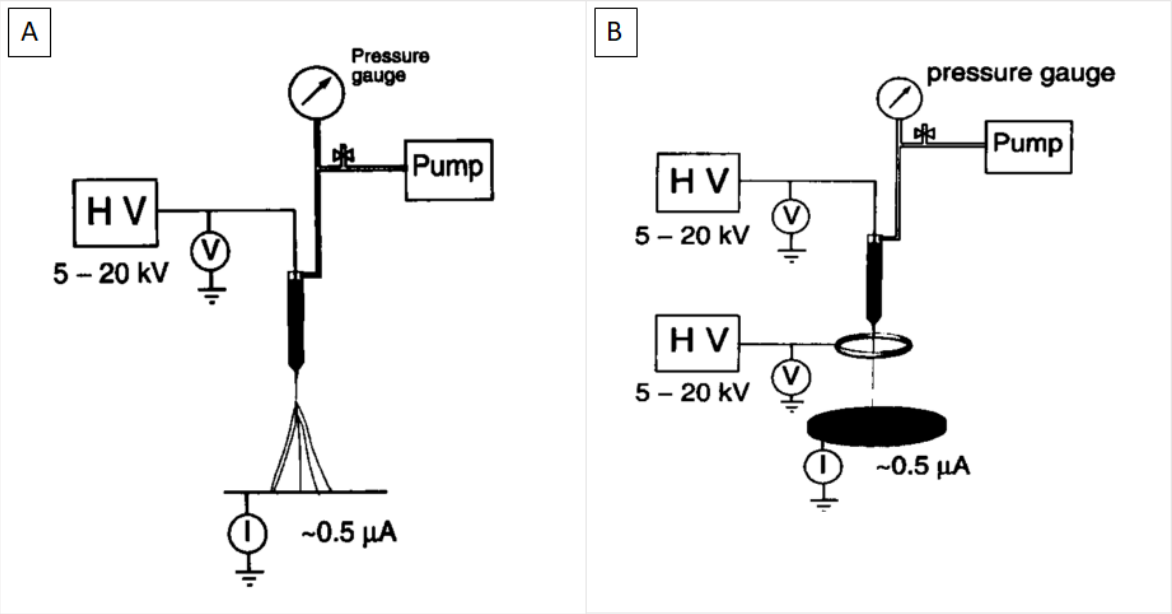

Figure 2.1. Experimental layout of the (A) one-electrode and (B) two-electrodes setups. Adapted from R. Jaeger et al. (1998).[151]

The fibers can be collected on various collectors. Over 10 different types of collectors are described in detail by W. E. Teo et al.[152] in their review on electrospinning design and nanofiber assemblies. Fibers consisting of several layers, typically called core-shell, can be produced by introduction of co-axial (two layers) or tri-axial nozzle (three layers) and corresponding number of extra feed solution pumps. In the co-axial electrospinning, the core feed solution is pumped through the inner nozzle and the shell feed solution is pumped through the outer nozzle. In the case of the tri-axial electrospinning, a middle layer separating the core and shell is introduced. In principle, the core feed solution does not need to be electrospinnable as the process is mostly affected by the outer shell solution.[153,154] In pharmaceutical application, the core-shell fibers has a great potential in multidrug delivery, when each fiber layer consists of different drug(s) in a corresponding polymeric carrier. This way, drugs with different physico-chemical properties such as logP and subsequently different release profile can be delivered in a single formulation. Equally, a multiphasic drug release can be obtained from the core-shell fibers, when an immediate drug release from the

shell is followed by a controlled release from the core.[155] A biphasic drug release is commonly used in delivery of non-steroidal anti-inflammatory drugs (NSAIDs), antihypertensive, antihistaminic, and anti-allergic agents.

2.3.2 Electrospray

The electrospray setup is the same as the electrospinning setup. However, a closed chamber with air/nitrogen flow is often introduced to reduce the evaporation of solvents and to form smaller particles with smoother surface.[156] Although the stable cone-jet is the most commonly used spraying mode, different modes such as dripping, microdripping, simple-jet, and multiple cone spraying have been studied. The spraying mode is determined by the competing electric stress and surface tension on the liquid-gas interface, together with the kinetic energy of the feed solution leaving the nozzle.[119] It is not uncommon that the particles are not deposited on the collector only but also different parts of the setup such as inside walls of the chamber or the ground needle. This is due to incomplete discharge of the particles during the process. To reduce the charge of the particles and to increase the particle deposition efficiency, the ring electrode is often introduced together with the gas flow, as the trajectory of the particles can be easily controlled when the particles are completely discharged.[157] A. Rezvanpour et al.[158] reported that the particle collection efficiency was determined by solution flow rate, nitrogen flow rate, ring voltage, and nozzle voltage. They also observed the difference between the electric potential on the nozzle and the ring played a key role in the particle collection efficiency. Other contributing factors included durations of the process, polymeric materials, and electrical conductivities of solutions. Study of A. Rezvanpour and C. Wang[159] shows the maximum collection efficiency at 80% on the grounded aluminium flat plate, which was increased to 90% after introduction of an auxiliary electric field created by an additional flat plate connected to a high voltage supply and placed a few centimetres above the original flat collector.

2.3.3 Nanoprecipitation

Nanoprecipitation process is controlled by several interdependent parameters. Most common driving force of the nanoprecipitation is supersaturation.[160] The supersaturation degree is a ratio of the solute concentration in the binary solvent-antisolvent mixture after mixing and the equilibrium solubility of the solute in the solvent-antisolvent mixture. Increasing the degree of the supersaturation leads to increased nucleation rate and decrease of the particle size.[160] However, high degree of supersaturation shortens the time required to start the precipitation process. Unless a highly efficient mixing is involved in the process,

precipitation will occur before homogenous mixing of solvent and antisolvent is reached, resulting in large polydisperse particles.[161] Mixing process is therefore considered to be the most crucial step in production of monodisperse nanoparticles. Uniform mixing leads to uniform supersaturation throughout the binary mixture, reducing the Ostwald ripening effect.[162] The mixing process is also affected by the solvent and antisolvent miscibility, as this affects the homogeneity of the nucleation step and consequently the particle size distribution. Cheng et al.[163] studied the effect of the solvent on the PLGA particle size, observing that use of the solvents with high miscibility with the antisolvent leads to smaller particle size.

Beside the solute concentration in the solvent phase and the solute solubility in the bulk solvent, which can be also regulated by environmental factors such as temperature, the volume ratio between the solvent and the antisolvent is another key parameter regulating the supersaturation.[164] In principle, decreasing the solvent-antisolvent ratio leads to decrease of the solute equilibrium solubility in the binary mixture and reduction of the Ostwald ripening.[164,165] Selection of the solvent with a good solute dissolving capacity is therefore important to minimize its volume and also to simplify its removal after the precipitation step. However, experimental results in the literature suggest that changing the solvent-antisolvent ratio by either reducing the solvent volume or by increasing the antisolvent volume can have opposite effects on the size of the particles as well as their drug loading efficiency. For example, Budhian et al.[166] observed that particle size decreased and drug loading efficiency increased when the solvent volume was decreased. However, Limayem Blouza et al.[167] studied the effect of increasing the antisolvent volume. In this case, the size of the nanoparticles increased, while the drug encapsulation efficiency decreased.

To increase the nanosuspensions stability and decrease the aggregation of the particles, wide range of stabilisers have been used in nanoprecipitation. The stabilisers can be e.g., polymers or surfactants and stabilise the particles either sterically or statically.[168] The stabilisers should be selected based on their ability to adsorb onto the surface of the particles. The higher the adsorption affinity of the surfactant towards the solute is, the faster the adsorption process will be, resulting in smaller particle size.[169] The concentration of the stabiliser is a key parameter in the stabilisation but also nanoprecipitation process. Aggregation is promoted when the critical concentration of the stabiliser is exceeded. In case of the polymeric stabilisers, the polymeric chains will get entangled due to their flocculation. The surfactants on the other hand, will create micelles, increasing the Ostwald ripening effect.[162]

3 ELECTROSPUN FIBERS

3.1 Introduction

The overall objective of this chapter was to develop and study colon targeted multidrug delivery systems produced by electrospinning technique. For this purpose, HPMCAS polymer was selected as the excipient to provide the enteric properties. Three drugs commonly used in IBD treatment, 5-aminosalicylic acid (5-ASA), paracetamol (PAR), and hydrocortisone (HYD), were selected as model drugs. This chapter describes a method of electrospinning of HPMCAS (grade H) without any additives to obtain beaded fibers, even though only unsuccessful attempts to electrospin the pure HPMCAS polymers (grade LF) were described in the literature[170] prior to this project. It was observed that relative humidity played a significant role in the electrospinning of the polymer. Therefore, the effect of relative humidity on the electrospinning of blank and drug loaded fibers was studied more closely in this chapter. The SEM scans of the beaded fibers were further analysed to observe fiber diameter and its distribution as well as the size and distribution of the beads. To understand the morphology of the fibers better, the effect of solution properties (viscosity, conductivity, surface tension) on the fiber structure was examined. The fibers were further assayed by TGA to determine whether all solvent was successfully evaporated during the electrospinning process. To assess the crystallinity of the formulations, the drug distribution within the electrospun fibers, and the potential inter-molecular interactions in between the polymer and the drugs, all samples were characterised by (M)DSC, ATR-FTIR, and PXRD. Finally, the drug release was evaluated by LC-MS in case of the multidrug and by UV-VIS spectrophotometry in case of the single-drug loaded formulations.

3.2 Materials and Methods

3.2.1 Materials

5-aminosalicylic acid (5-ASA) and Hydrocortisone (HYD) were purchased from Acros Organics, US. Paracetamol (PAR) was purchased from Sigma Aldrich, US. HPMCAS was kindly gifted by Ashland, US. Acetone and ethanol were purchased from VWR, France. DMSO was purchased from Fisher Scientific, UK. Hydrochloric acid and PBS tablets (pH = 7.4) were purchased from Sigma Aldrich, US. MilliQ (MQ) water was produced using a Purelab ultra (ELGA LabWater, UK).

3.2.2 Enteric fibrous film fabrication

Clear solutions of different concentrations of HPMCAS in pure acetone, ethanol, and a binary solvent system of acetone and DMSO in various ratios were prepared and tested for its electrospinning abilities, using nanofiber electrospinning unit (Tong Li Tech, China), a syringe pump (Cole-Parmer, US), 22G emitter (Avectas:Spraybase, Ireland) and flat or rotating drum collectors. Humidity in the system was controlled with N_2 flow.

3.2.3 Imaging of the electrospun samples

SEM analysis was performed to visualise the surface of the fibrous formulations. The electrospun samples (either peeled or including the aluminium foil substrate) were directly attached onto SEM specimen stubs by double-sided tape and coated with gold using a Polaran SC7640 sputter gold coater (Quorum Technologies) prior to imaging. The blank and the multidrug loaded fibers were imaged by Zeiss EVO HD15 scanning electron microscope and the single-drug loaded formulations were scanned by Gemini 300 series scanning electron microscope (Zeiss, Germany). The Image J software was used to measure the fiber diameter and the size of the beads, when 100 values were averaged for each.

3.2.4 Physico-chemical characterisation of the fibrous films

Viscosity of the electrospinning solutions was measured by the Discovery Hybrid Rheometer (TA Instruments, Delaware, United States) equipped with a 2°, 40 mm cone-and-plate geometry and a solvent trap. The method was set to be a flow ramp procedure from 0.1 to 400s^{-1} at 21 ˚C for 120 seconds. The measurement was done in triplicate to calculate the average viscosity ± SD. The rheological profiles were analysed in TRIOS (TA Instruments, Newcastle, USA) software. The viscosity values were read at the value of shear rate which simulated the flow of the electrospun solution through 22G nozzle, considering the flow rate used in electrospinning process. The calculation of the shear rate ($\dot{\gamma}$) was based on the Hagen-Poiseuille equation:[171]

$$\dot{\gamma} = \frac{(4 \cdot V)}{\pi \cdot R^3 \cdot t}$$

Where V is the volume of the solution, t is the time of the flow, and R is the radius of the nozzle.

Conductivity was measured with conductivity probe (Mettler Toledo, US) in triplicates, when temperature was monitored at the same time.

Surface tension was measured by a pendant drop technique using 22G nozzle. The data were analysed by the FAMAS software, and the temperature was monitored during the measurements.

Thermal analyses of raw materials, physical mixes, and all formulations were performed with TGA and (M)DSC. TGA analysis was performed using TGA 5500 discovery series (TA Instruments, UK), when samples in an open aluminium pan were analysed in different temperature ranges with a heating rate 10 °C/min. The (M)DSC analysis was performed with a TA Universal Q2500 Discovery series differential scanning calorimetry (TA Instruments, Newcastle, USA). Samples of 0.5 – 3 mg were analysed in standard crimped aluminium pans (TA Instruments, Newcastle, USA), which were pierced to reduce the moisture effect on the analysis. The dry nitrogen gas purged through the DSC cell at a flow rate of 50 ml/min. The mass of each empty standard pan was matched with a mass of an empty reference pan. Different temperature ranges were used for individual materials and formulations depending on their decomposition temperatures obtained from the TGA analysis. In the DSC analysis, the heating and cooling rate was 10 °C/min. The heating rate in the MDSC method was 2 ˚C/min and the amplitude was 0.31 ˚C for 60 seconds. The glass transitions were found in the normalised reversing heat flow, while the melting points were searched in the non-reversing (normalised) heat flow. To treat both the TGA and (M)DSC data TRIOS (TA Instruments, Newcastle, USA) software was used. All the thermal analyses were performed in triplicates.

ATR-FTIR experiments were performed using a Vertex 70 spectrometer (Bruker Optics Ltd., Coventry, U.K.) fitted with an internal reflection diamond Attenuated Total Reflectance (ATR) accessory (Specac Ltd., Orpington, U.K.) equipped with diamond internal reflection element. All ATR-FTIR spectra were measured from 650 to 4000 cm^{-1}, in absorbance mode using a scanning resolution of 4 cm^{-1} with 32 repeated scans. To treat the data, OPUS software (Bruker Optics Ltd., Coventry, U.K.) was used. The samples were measured in three repeats.

PXRD analyses were performed at ambient conditions using a Thermo ARL Xtra X-ray diffractometer (Thermo Scientific, Switzerland). The X-ray Cu Kα1 source (λ = 1.540562 Å) with a voltage of 45 kV and a current of 40 mA were used. The samples were scanned over an angular scan range $5° < 2\theta < 60°$ with a 0.02° step width and scan speed of 1 s/step.

3.2.5 *In vitro* drug release from multidrug loaded fibers

Drug release profiles from multidrug loaded samples were obtained from experiments using dissolution bath and dissolution baskets. The sink volume was 500 ml and 5 ml samples were withdrawn at each time point. The bath was kept at 37 ˚C and the rotation of the baskets was 70 rpm. The fibers were fitted into HPMC capsule for easier manipulation. The filled capsules were placed into the baskets and the baskets were immersed into hydrochloric solution (pH = 1.2) for two hours. After that, the baskets were removed and transferred into PBS buffer (pH = 7.4), where the temperature and the rotation speed were kept the same. In both buffers, the sink volume was kept constant by adding 5 ml of fresh corresponding buffer after each dissolution sample was withdrawn. The weight of each fibrous sample was calculated, so the sink conditions were followed, and the drug was detectable by the **LC-MS** assay developed by Lionel Hill, a platform manager at John Innes Centre (Norwich, UK). The drugs were separated on the 50×2.1mm 2.6µ Kinetex XB C18 column (Phenomenex, USA), using an Acquity UHPLC system (Waters). The following gradient of acetonitrile versus 0.1% formic acid in water, run at 600µl.min^{-1} and 35°C:

time (minutes)	% acetonitrile
0	0
1.3	30
1.8	100
2.3	100
2.4	0
3.8	0

The samples were kept at 20 °C prior to injection. The strong needle wash was acetonitrile with 0.01% formic acid and the weak needle wash was water. 5-ASA, PAR, and HYD retention times were 0.33 min, 0.82 min, and 1.70 min, respectively. Waters Xevo TQS tandem mass spectrometry system was used to quantify the drug content. Spray chamber was kept at 500 °C desolvation temperature, the flow rate of the desolvation gas was 900 L.hr^{-1}, and the flow rate of the cone gas was 150 L.hr^{-1}.

The nebuliser pressure was 7 bar. The MS detector collected the following mass transitions:

	fragment mass	collision energy
5-ASA	53.1546	28
Cone voltage 36V	80.1754	22
Precursor *m/z* 154.1319	92.1581	16
Paracetamol	65	24
Cone voltage 24V	93	20
Precursor *m/z* 152.2	110.1	14
Hydrocortisone	105.1	40
Cone voltage 26V	121.1	24
Precursor *m/z* 363.2	309.2	16
	327.2	16

3.2.6 *In vitro* drug release from single-drug loaded fibers

Drug release from single-drug loaded formulations was performed in shaking water bath (100 rpm) at 37 ˚C, using beakers and closed dissolution baskets, assuring simple manipulation of the fibers during the transfer from hydrochloric solution (pH = 1.2) into PBS buffer (pH = 7.4) after two hours. The dissolution was performed under sink conditions, when the sink volume was 50 ml and the samples taken at each time point were 0.5 ml. The sink volume was kept constant with the corresponding buffer. The concentrations were measured by **UV-VIS spectrophotometry**, using a CLARIOstar® Plus microplate reader (BMG Labtech, Germany) and quartz 96 well plate and a MARS Data Analysis Software (BMG Labtech, Germany). The standard curves were produced for each drug in both hydrochloric solution (pH = 1.2) and PBS buffer (pH = 7.4). The absorbance maxima were found at 302 nm and 332 nm for 5-ASA in hydrochloric solution (pH = 1.2) and PBS buffer (pH = 7.4), respectively. Absorbance maximum did not shift for PAR and HYD, showing absorbance maximum at 244 nm and 248 nm in both buffers, respectively. Concentrations of the drugs were calculated at each time point following Beer-Lambert law and further corrected, considering the addition of the fresh buffer after withdrawing each sample.

3.3 Results and Discussion

3.3.1 Feasibility of electrospinning of HPMCAS

The processability and fiber forming ability of the carrier polymer, HPMCAS, was tested in the first instance. First, blank formulation was optimised in terms of spinnability. The preliminary screening was performed on a flat collector and fibers were assessed with optical microscope. After unsuccessful trials to electrospin HPMCAS in pure ethanol or acetone due to rapid solvent evaporation, acetone:DMSO binary mixture was selected as a common

solvent for HPMCAS and all three model drugs in sufficient concentrations. Concentration of the polymer as well as the ratio of the solvents in the binary mixture were screened (see Table 3.1).

Table 3.1. Electrospinnability screening of the HPMCAS solution to find optimal polymer concentration, ratio of acetone and DMSO in the binary solvent mixture, needle size (G), flow rate, and distance in between the nozzle and collector to achieve fibers with minimal beading and no moisture uptake after electrospinning (wet).

HPMCAS %(w/v)	Acetone:DMSO (v:v)	G	Flow Rate (nl/s)	Distance (cm)	Product	Wet
12	7:3	18	278	14	Particles/Droplets with few fibers	Y
12	7:3	18	100	14	Particles/Droplets with few fibers	Y
16	7:3	18	200	14	Heavily beaded fibers	Y
18	3:2	18	100	14	Heavily beaded fibers (large beads)	Y
18	3:2	18	300	14	Heavily beaded fibers	Y
18	1:1	18	300	24	Heavily beaded fibers (large beads)	Y
18	3:2	22	100	14	Heavily beaded fibers (small beads)	Y
18	3:2	22	200	14	Heavily beaded fibers (small beads)	Y
20	3:2	18	200	14	Beaded fibers (small beads)	Y
20	3:2	22	200	20	Beaded fibers (small elongated beads)	N

Based on the findings in Table 3.1, 20% (w/v) HPMCAS in acetone:DMSO (3:2; v:v) was selected as an optimal candidate. The flow rate was set to 0.72 ml/h (200 nl/s), the distance in between collector and emitter was 20 cm, and 22G emitter was used in all following experiments. It was observed that humidity level significantly affects the electrospinning process and final structure of the fibers. Centres of the fibrous mats collected on a flat collector dissolved due to the moisture absorption from air within one hour of electrospinning even at RH as low as 40 ± 2%. This suggests that hygroscopic properties of HPMCAS are increased with increased surface to volume ratio of the fibers, since the powder form is reported to absorb less than 3% of water content at RH < 50% (at 25 °C).[143] Therefore, a combination of a rotating drum as a collector (60 rpm) and a scanning nozzle (50 mm/s) was introduced to achieve even thickness of the fibrous mat within the samples. The effect of relative humidity on the structure of the HPMCAS fibers was further tested by producing electrospun samples at room temperature at four different RH values: RH = 50 ± 2%, RH = 40 ± 2%, RH = 30 ± 2%, and RH = 23 ± 2%. In all four cases, beaded polydisperse fibers were observed in SEM scans with mean fiber diameter of

511.3 ± 221.1 nm, 400.7 ± 179.0 nm, 495.5 ± 217.2 nm, and 177.5 ± 100.7 nm, respectively (see Figure 3.1). However, the fibers produced at RH = 23 ± 2% are not continuous and the beads are more spherical than in the samples electrospun at higher RH, suggesting the decrease of relative humidity could lead to the switch between electrospinning and electrospray, even though the concentration of the polymer remains unchanged.

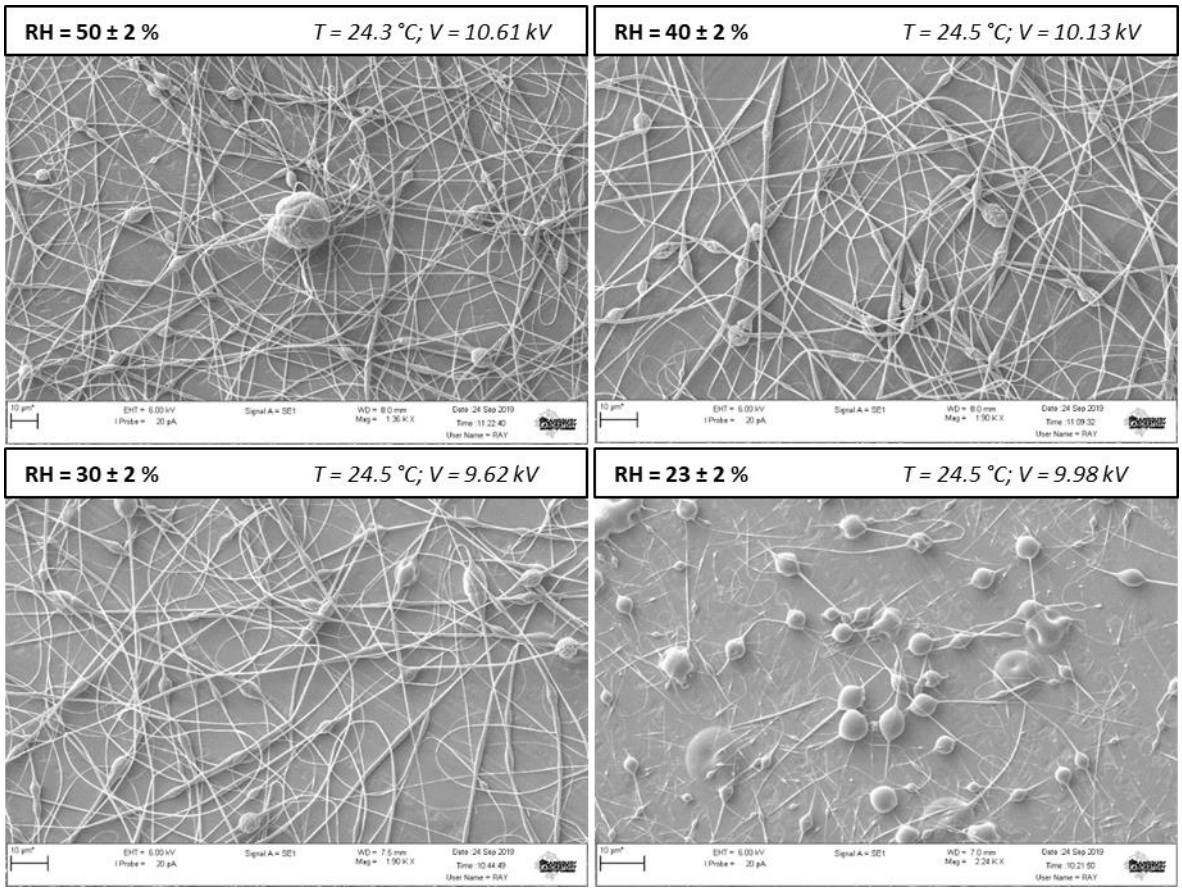

Figure 3.1. Representative SEM scans of electrospun blank HPMCAS formulation showing different structure of fibers at various relative humidity.

The distribution of the fiber diameter and the bead length/width ratio is compared for the four blank HPMCAS samples in Figure 3.2. The histograms were produced from 100 manual ImageJ measurements of each fiber diameter, bead length (along the fiber axis), and bead width (perpendicular to the fiber axis). The broadest peak of fiber diameter distribution can be found in the sample electrospun at RH = 50 ± 2%, where the most abundant fiber diameter is in 300 – 600 nm range (histogram A1). In this sample, two peaks of the bead length/width ratio can be seen in histogram B1, one for the ratio in the range of 2 – 3 and another for the ratio >5. This suggests the beads are mostly elongated and irregular. Fibers

with diameter of 200 – 300 nm and 400 – 500 nm were found to be the most abundant in the sample electrospun at RH = 40 ± 2% (histogram A2). The bead length/width ratio of this sample shows a broad peak over all ranges, beside the range 0 – 1 (histogram B2). The blank HPMCAS sample electrospun at RH = 30 ± 2% shows a distinct peak for fiber diameter in the range of 400 – 600 nm (histogram A3) and for the bead length/width ratio of 2 – 3 (histogram B3). The last set of histograms, belonging to the sample electrospun at RH = 23 ± 2%, shows significantly thinner fibers with the most abundant diameter in the range of 0 – 200 nm (histogram A4) and more spherical beads with most abundant bead length/width ratio of 0 – 2 (histogram B4), compared to the samples produced at higher RH.

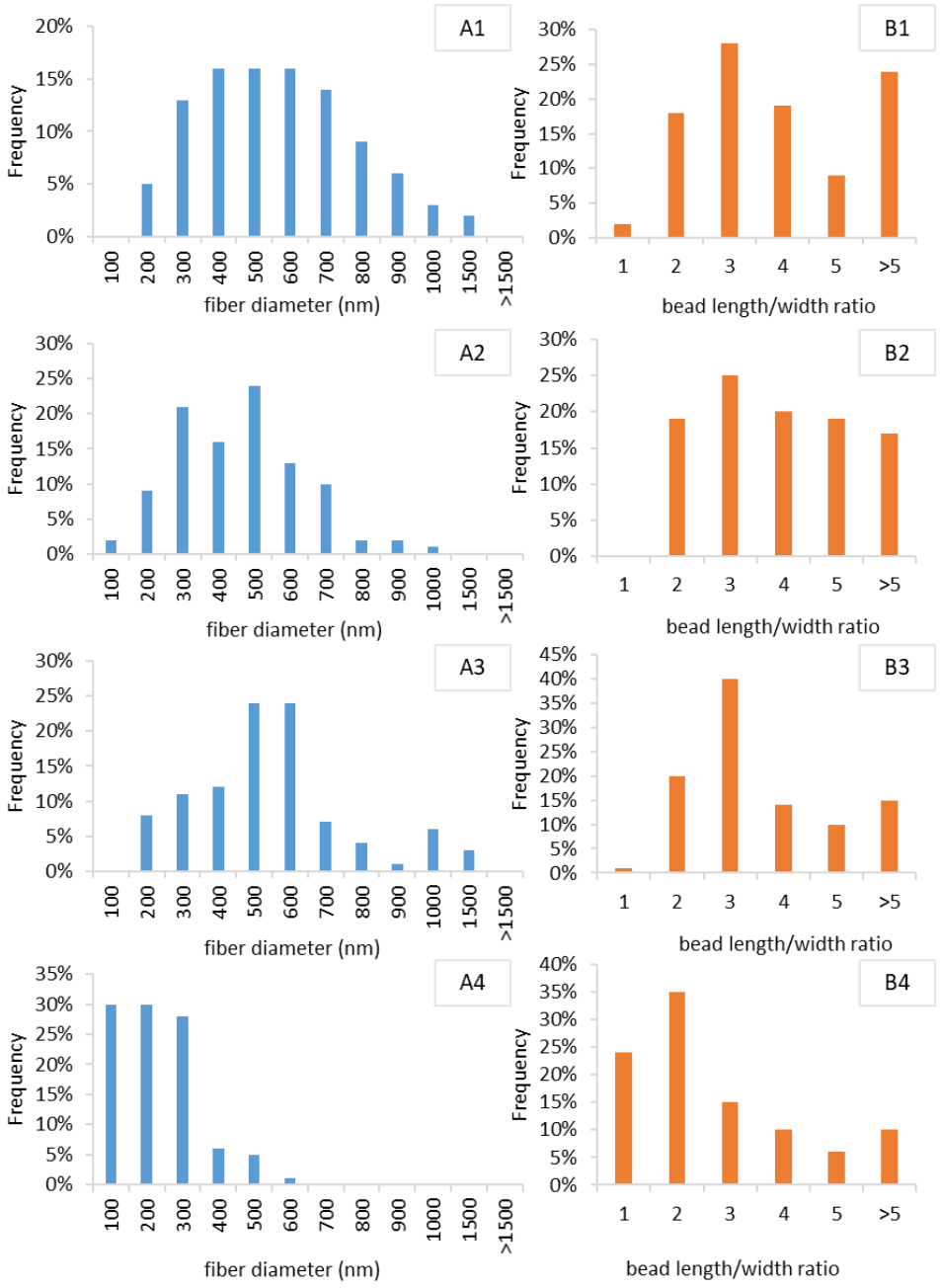

Figure 3.2. Histograms describing different (A) distribution of fiber diameter and (B) length/width ratio of beads formed in electrospun blank HPMCAS samples at various relative humidity: (1) RH = 50 ± 2%; (2) RH = 40 ± 2%; (3) RH = 30 ± 2%; (4) RH = 23 ± 2%.

From the evidence in the literature, the humidity effect on the fiber diameter and the beads formation seems to be material specific, since the fiber diameter as well as the bead formation can both increase and decrease with decreasing humidity, depending on the physico-chemical properties of the polymer.

Polymers rapidly precipitating at the presence of water such as polystyrene or polyetherimide showed increase in fiber diameter when relative humidity is increased.[172,173] This might be due to the precipitation occurring on the surface of the electrospinning jet further preventing its elongation. On the other hand, water soluble polymers such as polyvinyl alcohol or cellulose acetate manifested decreased fiber diameter when the humidity was increased, due to the thinning of the solution (concentration and viscosity) by the water from the air.[174,175] The fiber diameter can be increased in the lower humidity as well due to the faster solvent evaporation. This was demonstrated by Golin (2014) on core-shell fibers, where the poly(ethylene glycol) core was covered with poly(caprolactone) shell.[176] These findings in the literature suggest the water sensitive polymers are significantly affected by the relative humidity and need to be electrospun at the optimal relative humidity. The HPMCAS is hygroscopic and swells before disintegration in pH above 7.[143] All obtained blank HPMCAS fibers were polydisperse, while a significantly higher frequency of the lower fiber diameter was observed in the lowest RH (23 ± 2%). This suggests the swelling property could be one of the factors influencing fiber diameter of electrospun HPMCAS in various relative humidity.

The humidity affects the beading of the fibers as well. Even in this case, the properties of the polymer affect the way how humidity influences the beading formation. For example, the water soluble polyethylene oxide showed higher degree of beading and fusing when the relative humidity was increased.[177,178] This might be explained by water droplet formation on the jet accelerating through the environment with high relative humidity. These droplets can also thin the solution as mentioned earlier, which can lead to the breakage of the fibers. This was reported in poly(ethylene glycol) fibers by Nezarati et al. (2013).[179] On the other hand, the water insoluble polymers such as polystyrene showed increased beading in the fibers electrospun at lower humidity, suggesting the water in air increases viscoelasticity of the polymeric solution.[172] Based on these findings, the decrease of the bead formation would be expected with decreasing humidity due to the polarity of the HPMCAS. However, more spherical beads together with the breakage of the fibers in the low relative humidity suggest the HPMCAS behaves as a non-polar polymer during the electrospinning process due to its hygroscopicity. Overall, the humidity plays a significant role in the electrospinning of HPMCAS and the balance needs to be established to avoid excessive beading leading to the breakage of the fibers (low RH) as well as the excessive water uptake at higher humidity.

Although highly affected by environmental conditions (e.g., temperature and humidity), the physico-chemical properties of the polymer feed solution are commonly measured and adjusted prior electrospinning (at their initial states) to achieve desired morphology of the electrospun fibers. Literature states three main reasons for bead formation: low viscosity of the polymer solution (potentially caused by low concentration and/or low molecular weight of the polymer), high surface tension, and low charge density.[180] To find potential explanation of the beading occurring in the blank HPMCAS fibers (see Figure 3.3), the viscosity, surface tension, and conductivity of the electrospun solutions were measured. The viscosity value was read at a shear rate of 28.4 s^{-1}, which was the closest to the calculated value of 29.6 s^{-1}, using the Hagen-Poiseuille equation to simulate the flow (0.72 ml/h) of the electrospun solution through 22G nozzle (0.205 mm radius). The temperature was fixed at 21 ˚C. Even though the solvent trap was used during measurements of the rheological profiles of the solutions, the standard deviation for the replicates appeared to be high due to the acetone fast evaporation during each measurement. Acetone:DMSO (3:2; v:v) viscosity (η) was 13 ± 3 mPa.s, compared to 856 ± 34 mPa.s measured for the blank 20% (w/v) HPMCAS solution. The conductivity of the solutions was measured at 20 – 22 ˚C. The binary solvent's conductivity (κ) was 0.377 ± 0.006 µS, which was increased to 3.373 ± 0.065 µS after adding the HPMCAS polymer. The surface tension was measured by the pendant drop technique. The surface tension of the acetone:DMSO (3:2; v:v) mixture $\gamma = 31.5 \pm 1.1$ mN/m (at 21 ˚C) is close to the calculated value using values of the pure solvents. Surface tension of pure acetone is stated to be 25.2 mN/m, while the value for DMSO is 43.54 mN/m, both at 20 ˚C. Adding the HPMCAS polymer to reach 20% w/v concentration increases the solution's surface tension to 41.7 ± 4.8 mN/m. As well as the humidity effect on electrospinning, the workable ranges of viscosity, conductivity, and surface tension are material specific. To avoid the formation of the beads, the change of the DMSO in the solvent might be considered to decrease the surface tension. However, 5-ASA, one of the model drugs is highly soluble in DMSO, while almost insoluble in other solvents without acidifying (which would lead to the polymer precipitation). Beading formation could be also reduced by adding salts into the electrospinning solutions, causing reduced surface tension and increased conductivity leading to increased stretching of the fibers.[181] The addition of the salts was not studied due to the potential crystallisation of the salts, which would disrupt the structure of the fibers and affect the drug release from the drug loaded formulations.

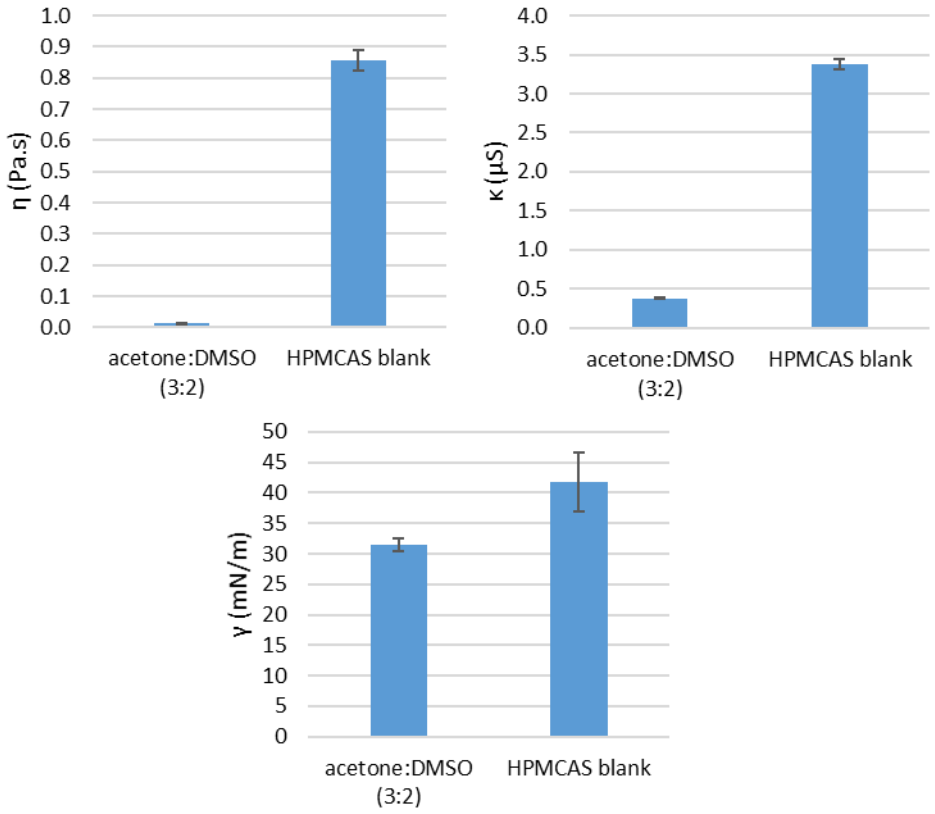

Figure 3.3. Solution properties of acetone:DMSO (3:2, v:v) binary mixture and 20% (w/v) HPMCAS in acetone:DMSO (3:2, v:v): viscosity (η) measured at shear rate of 28.4 s^{-1} at 21 ˚C (top left), conductivity (κ) measured at 20 - 22 °C (top right), and surface tension (γ) measured at 21 ˚C (bottom middle).

To confirm the electrospun fibers contained no residual solvent from the electrospinning process, TGA analysis was performed on samples immediately after the production. The focus was put mainly on DMSO residue due to its high boiling point (189 °C)[181] and therefore slow evaporation rate. For this reason, the TGA method was modified to include 15 minutes long isothermal step at 189 °C. In Figure 3.4, TGA thermograms of blank HPMCAS fibers electrospun at various relative humidity are compared with a TGA thermogram of the raw HPMCAS powder. No significant weight loss was observed at 189 °C in any of the electrospun samples, confirming the DMSO was fully evaporated during electrospinning. Only electrospun sample of blank HPMCAS at RH = 23 ± 2% showed weight loss of 2.8% at 100 ˚C. The increased water absorption from air in this sample could be explained by the thinner fiber diameter increasing the surface to volume ratio significantly.

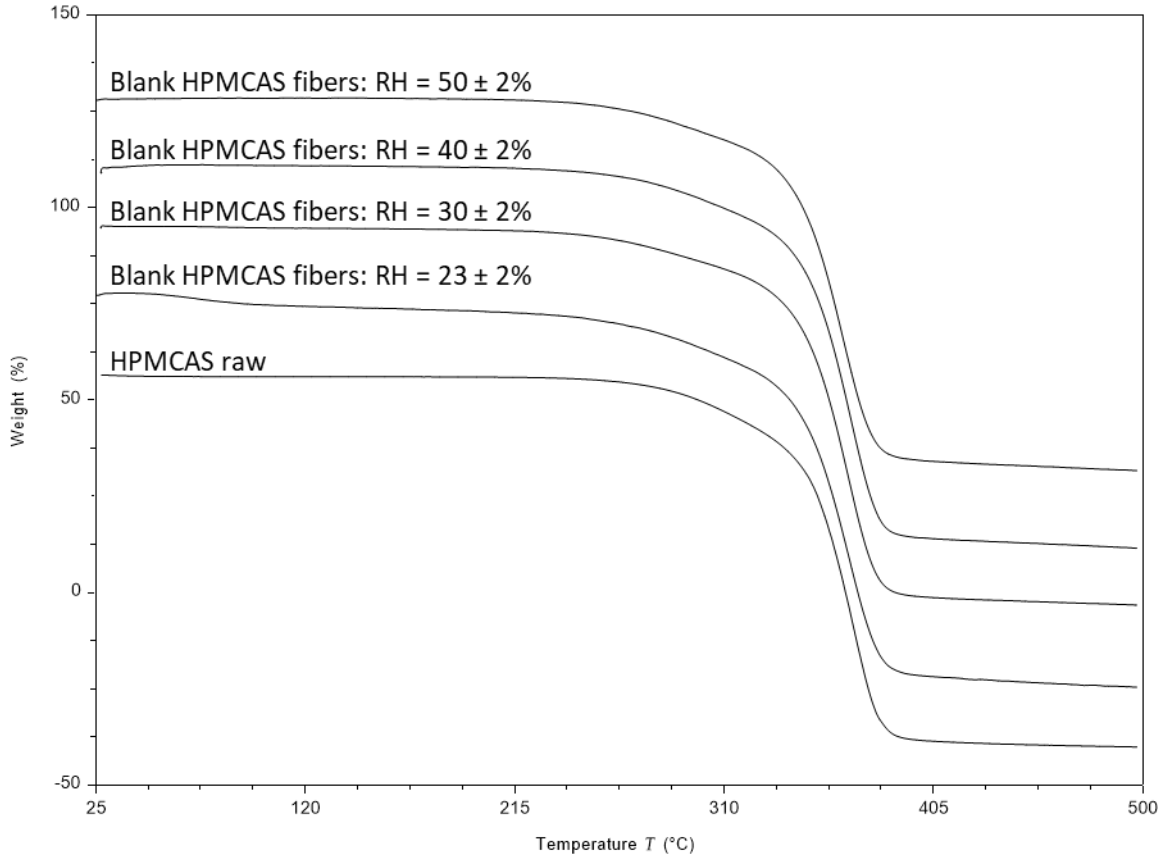

Figure 3.4. TGA thermograms of electrospun blank HPMCAS samples at various relative humidity compared to unprocessed HPMCAS powder, confirming no residual DMSO left in the electrospun samples.

DSC thermogram of the raw HPMCAS powder and MDSC thermogram of the blank HPMCAS fibers electrospun at RH = 30 ± 2% were obtained to compare glass transitions of the raw material and processed formulation (see Figure 3.5). The raw HPMCAS powder showed glass transition at 123 ˚C (mid-point), which corresponds with the manufacturer's report. The electrospun blank HPMCAS fibers showed glass transition at 126 ˚C (mid-point). No significant shift of the glass transition after electrospinning suggests the polymer structure is not affected by the acetone:DMSO (3:2; v:v) solvent mixture and further electrospinning process. This was confirmed with ATR-FTIR analysis, which showed identical spectra of the raw HPMCAS powder and the blank HPMCAS fibers electrospun at RH = 30 ± 2% (see Figure 3.6).

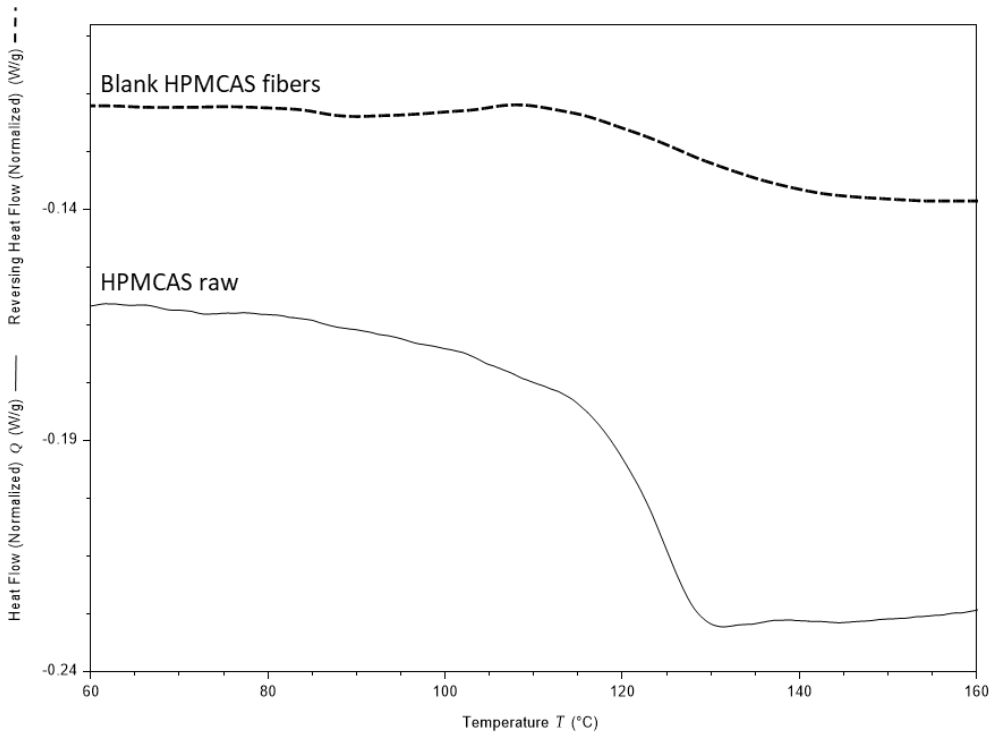

Figure 3.5. DSC thermogram of HPMCAS powder (solid line, y-axis = heat flow [W/g]) and MDSC thermogram of blank HPMCAS fibers electrospun at RH = 30 ± 2% (dashed line, y-axis = reversing heat flow [W/g]), showing no significant shift in the glass transition after electrospinning of the polymer.

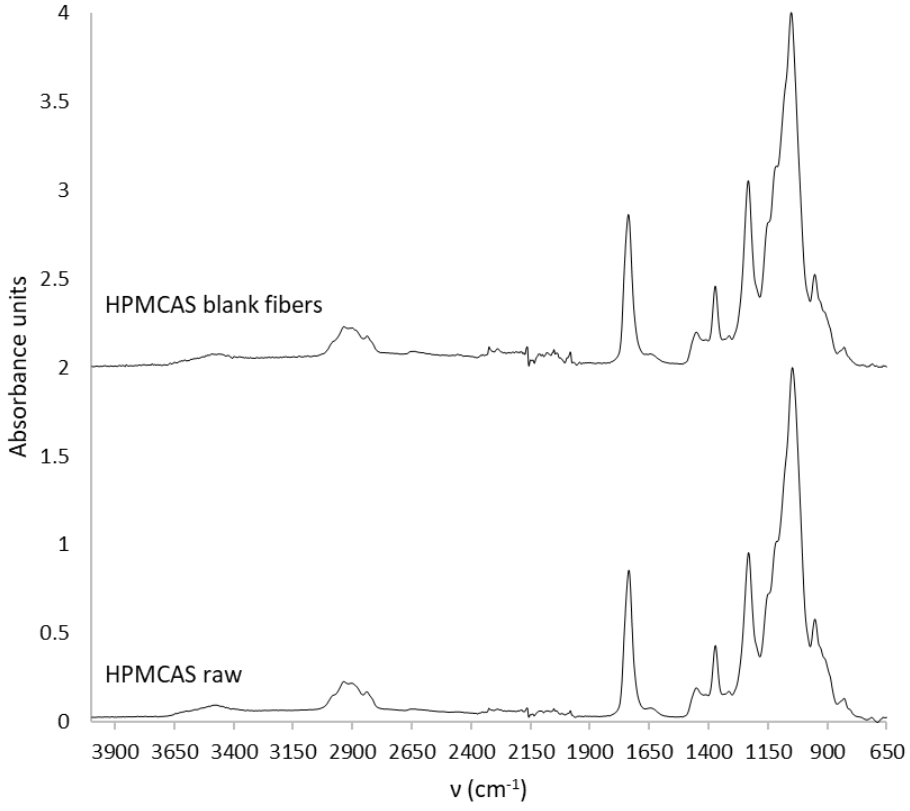

Figure 3.6. ATR-FTIR spectra of HPMCAS powder and blank HPMCAS fibers electrospun at RH = 30 ± 2%, confirming the polymer structure is unaffected by the electrospinning process.

The fibers were first collected on an aluminium foil covered collector, where the foil served as a substrate. However, the structure of the foil did not allow the fibrous mat to be peeled in one piece. Therefore, numerous materials such as PET, Teflon, parafilm, or mesh thin plastic sheets were tested as a sample substrate, including direct electrospinning on the stainless steel drum. Electrospinning substrate is required to be conductive or thin enough to avoid creating a barrier in between the nozzle and collector, which would interrupt the grounding of the collector. The only material which did not interfere with the electrospinning process and allowed a sufficient peelability was a commercially available grease proof baking paper with silicon coating. The structure of aluminium foil and the grease proof paper was compared under optical microscope (see Figure 3.7), showing regular tight pattern of aluminium foil caused by the rolling step in the aluminium foil manufacturing process while the grease proof paper shows irregular pattern coming from the initial paper structure which was treated with the silicon coat. Beside structural pattern, the potential drop in electrostatic force when using grease proof paper instead of aluminium foil could be another explanation of the increased peelability from the latter substrate. All further drug loaded samples were therefore collected on the grease proof paper only.

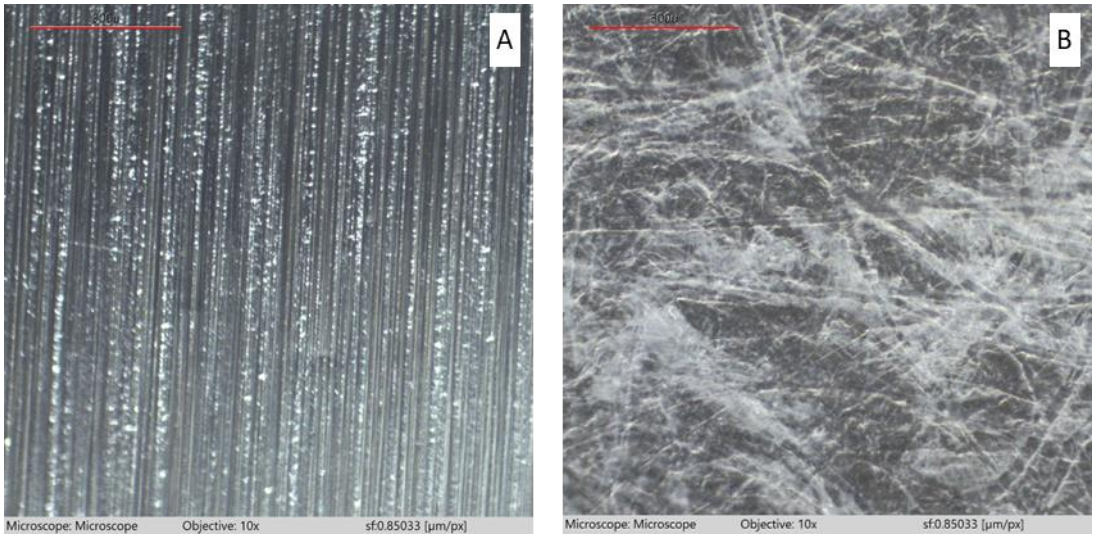

Figure 3.7. Microscopic structure of (A) aluminium foil and (B) grease proof paper used as a substrate for electrospinning of HPMCAS fibers; scale bar of 300 µm (red line).

3.3.2 Multidrug loaded HPMCAS fibers

The direct electrospinning of three drug substances in HPMCAS fiber has its advantage of being a single-step process, which would reduce the manufacturing cost and the HPMCAS should still maintain the colonic site-specific drug release. 5-ASA, PAR and HYD were added to 20% (w/v) solution of HPMCAS in acetone:DMSO (3:2; v:v) to obtain 7%, 8%, and 2% loading, respectively. This formulation is further referred to as MIX-HPMCAS fibers. The effect of the relative humidity on the electrospinning process and electrospun formulations was again studied at room temperature and at RH = 50 ± 2%, RH = 40 ± 2%, RH = 30 ± 2%, and RH = 23 ± 2%. Based on SEM scans (see Figure 3.8), fibers obtained at 30 ± 2% relative humidity were selected as best candidate for multidrug film based formulation, even though beading occurred. The mean fiber diameter of this formulation was 285.4 ± 147.5 nm. Besides beading, MIX-HPMCAS fibrous mats electrospun at relative humidity above 30 ± 2% showed significant fusing of the fibers. Their mean fiber diameter was 541.0 ± 342.0 nm and 521.9 ± 248.8 nm at RH = 40 ± 2% and RH = 50 ± 2%, respectively. Thin heavily beaded MIX-HPMCAS fibers were produced at RH = 23 ± 2% showing mean fiber diameter of 148.8 ± 73.7 nm.

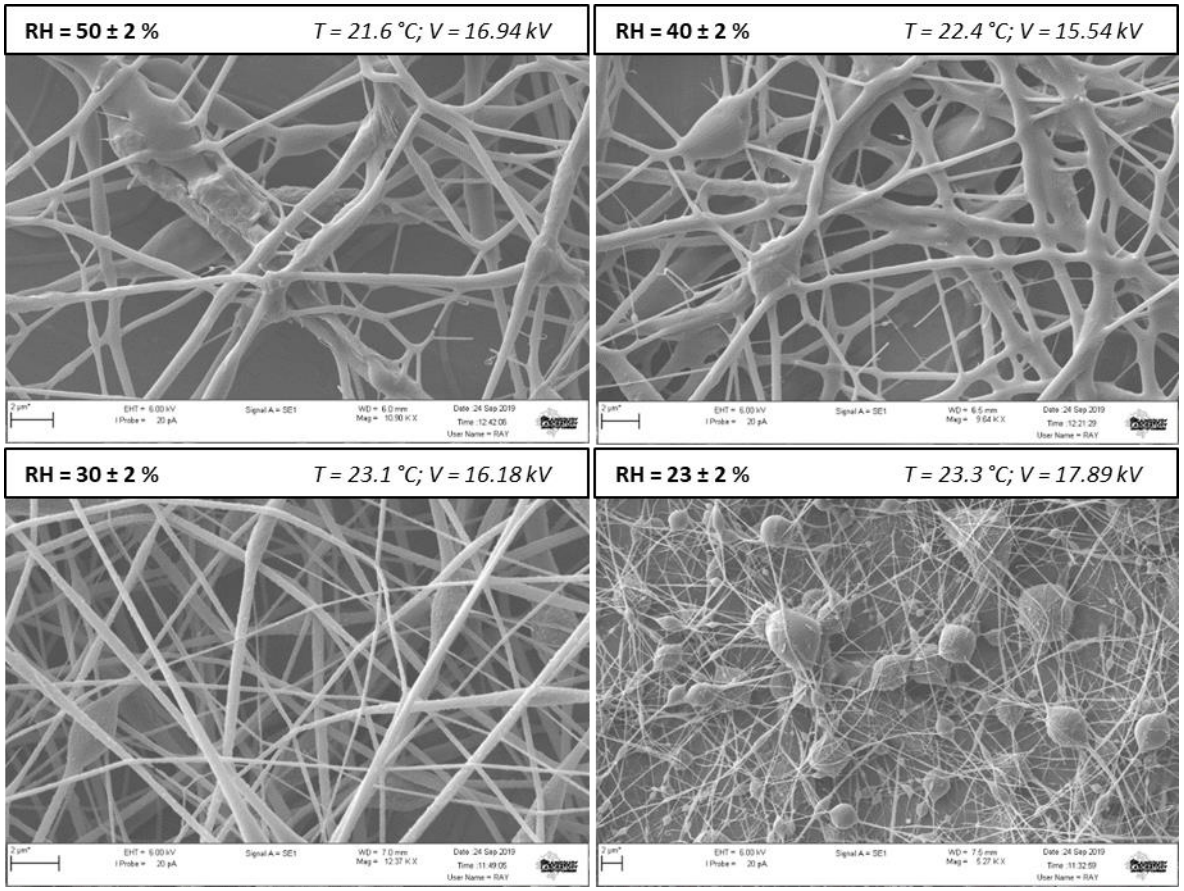

Figure 3.8. Representative SEM images of electrospun 3-drug loaded formulation MIX-HPMCAS fibers showing the effect of relative humidity on the fiber structure.

The standard deviation of the fiber diameter was very high in all four samples, therefore histograms showing frequency of individual fiber diameter ranges and histograms comparing the shape and distribution of the beads in each sample were produced (see Figure 3.9). MIX-HPMCAS fibers electrospun at RH = 50 ± 2% show the most abundant fiber diameter in the 400 – 500 nm range (histogram A1) and bead length/width ratio in the range of 2 – 3 (histogram B1). Fibers with diameter of 300 – 400 nm and 500 – 600 nm were found to be the most abundant in the sample electrospun at RH = 40 ± 2% (histogram A2). This sample was the most polydisperse out of the four MIX-HPMCAS electrospun samples. The bead length/width ratio of this sample shows to be most abundant in the 1 – 3 range (histogram B2). The MIX-HPMCAS sample electrospun at RH = 30 ± 2% shows a tailing peak for fiber diameter with the maximum at 100 – 200 nm (histogram A3). The bead length/width ratio of 1 – 2 is the most abundant in this sample (histogram B3). Significantly thinner fibers with the most abundant diameter in the range of 100 – 200 nm (histogram A4) were observed in the MIX-HPMCAS sample electrospun at RH = 23 ± 2%. More spherical

beads with most abundant bead length/width ratio of 1 – 2 and >10% increase of beads in the 0 – 1 bead length/width ratio (histogram B4), compared to the samples produced at higher relative humidity.

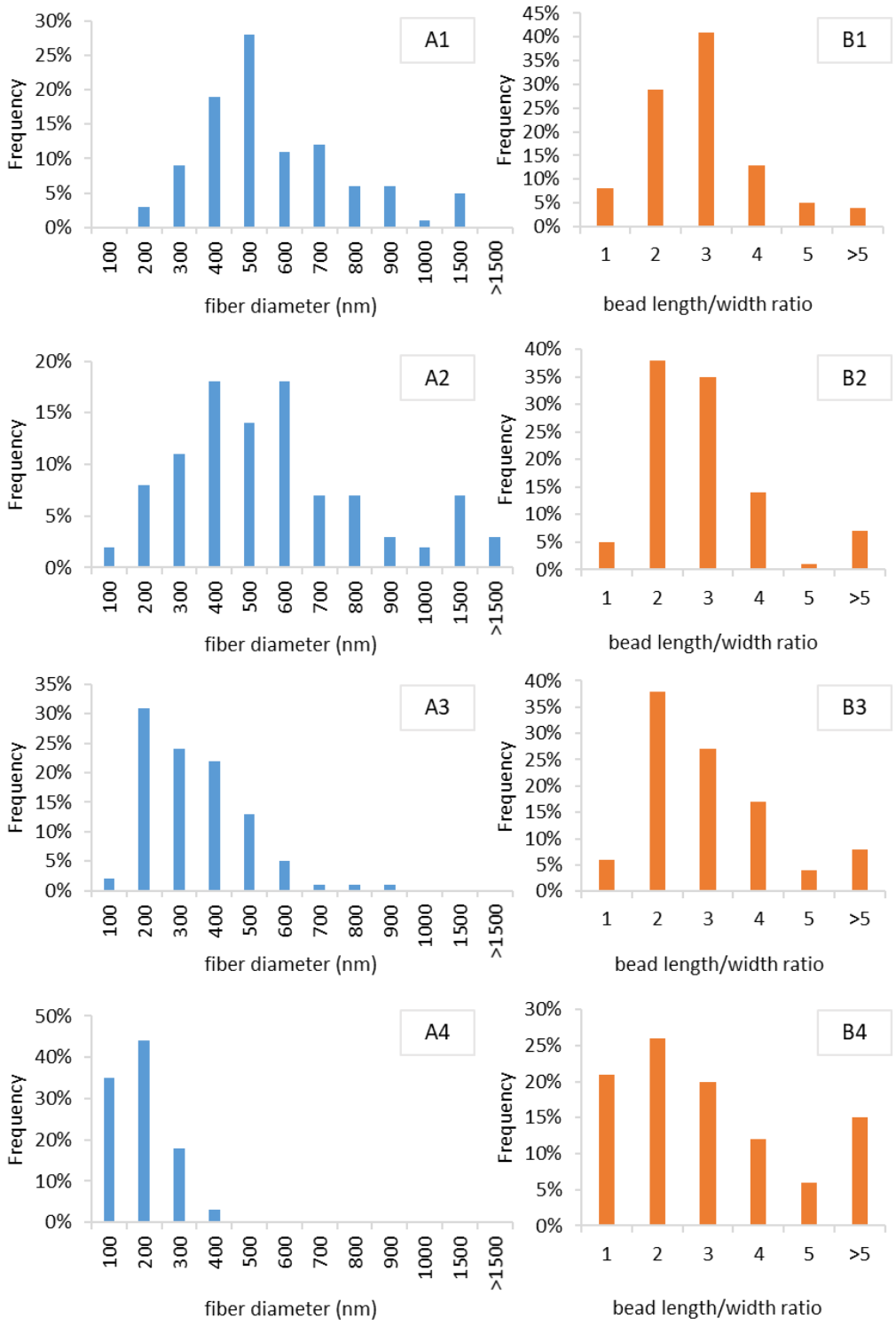

Figure 3.9. Histograms describing different (A) distribution of fiber diameter and (B) length/width ratio of beads formed in electrospun MIX-HPMCAS samples at various relative humidity: (1) RH = 50 ± 2%; (2) RH = 40 ± 2%; (3) RH = 30 ± 2%; (4) RH = 23 ± 2%.

The viscosity, surface tension, and conductivity of the MIX-HPMCAS solution were measured and compared with the values for blank HPMCAS solution and the binary solvent mixture (see Figure 3.10). Even though the concentration of the HPMCAS did not change, the solution properties were significantly affected by the addition of the three model drugs. Viscosity (η) of the solution significantly decreased from 856 ± 34 to 638 ± 66 mPa.s. The surface tension (γ) significantly decreased from 41.7 ± 4.8 to 33.2 ± 1.4 mN/m. The drop in both, the viscosity and surface tension, suggests the mixture of the drugs behave as a plasticiser. The conductivity (κ) of the solutions rapidly increased from 3.373 ± 0.065 to 32.57 ± 0.45 μS due to the acidic properties of 5-ASA. Even though the conductivity significantly increased, the voltage necessary to create the Taylor cone had to be increased by >5 kV at each relative humidity compared to electrospinning of the blank HPMCAS samples. Solutions with higher conductivity and lower surface tension are known to be less prone to the beading formation. However, the beading seems to be driven mostly by the viscosity of MIX-HPMCAS solution.

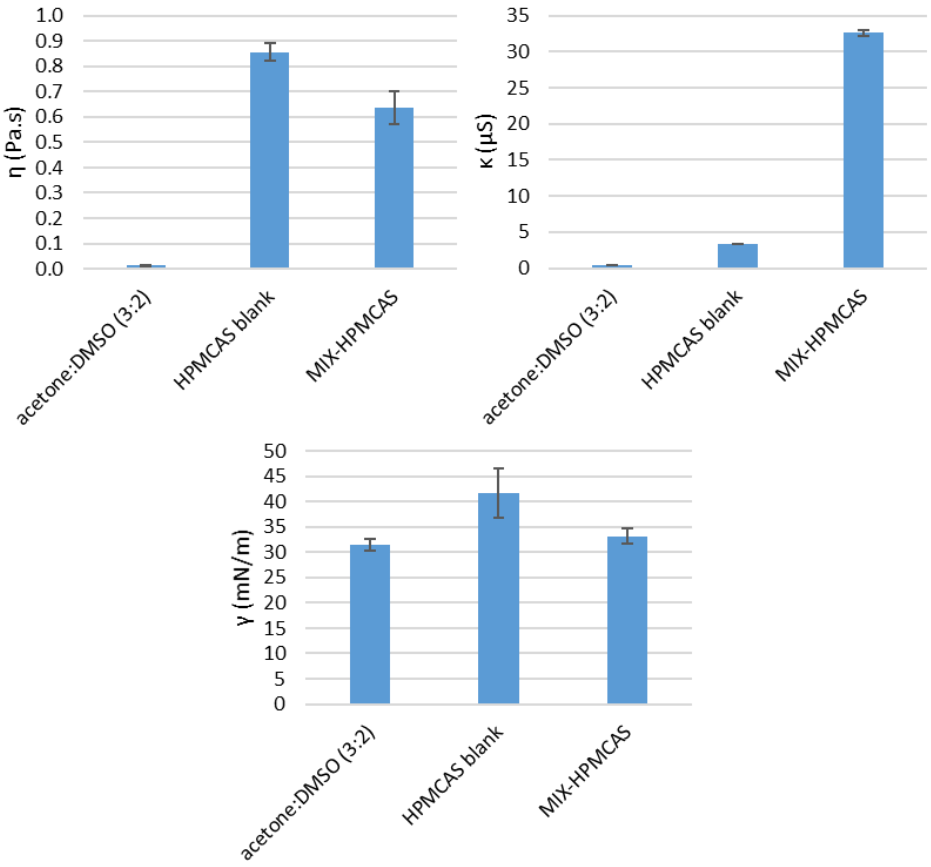

Figure 3.10. Solution properties of MIX-HPMCAS compared to blank HPMCAS solution and the solvent binary mixture in terms of viscosity (η) measured at shear rate of 28.4 s^{-1} (top left), conductivity (κ) measured at 20 - 22 °C (top right), and surface tension (γ) measured at 21 ˚C (bottom middle).

Further characterisation of drug loaded formulations was performed. Moisture uptake by the MIX-HPMCAS fibers was studied by TGA (see Figure 3.11). MIX-HPMCAS fibers electrospun at RH = 50 ± 2% showed 12.3% weight loss at 100 ˚C, suggesting the fused MIX-HPMCAS fibers absorbed significantly more air moisture than the blank HPMCAS fibers electrospun at the same relative humidity. However, no significant weight change (<3%) at 100 ˚C was observed in MIX-HPMCAS fibers electrospun at RH = 40 ± 2% and lower, even though the MIX-HPMCAS fibers electrospun at RH = 40 ± 2% showed significant fusing as well.

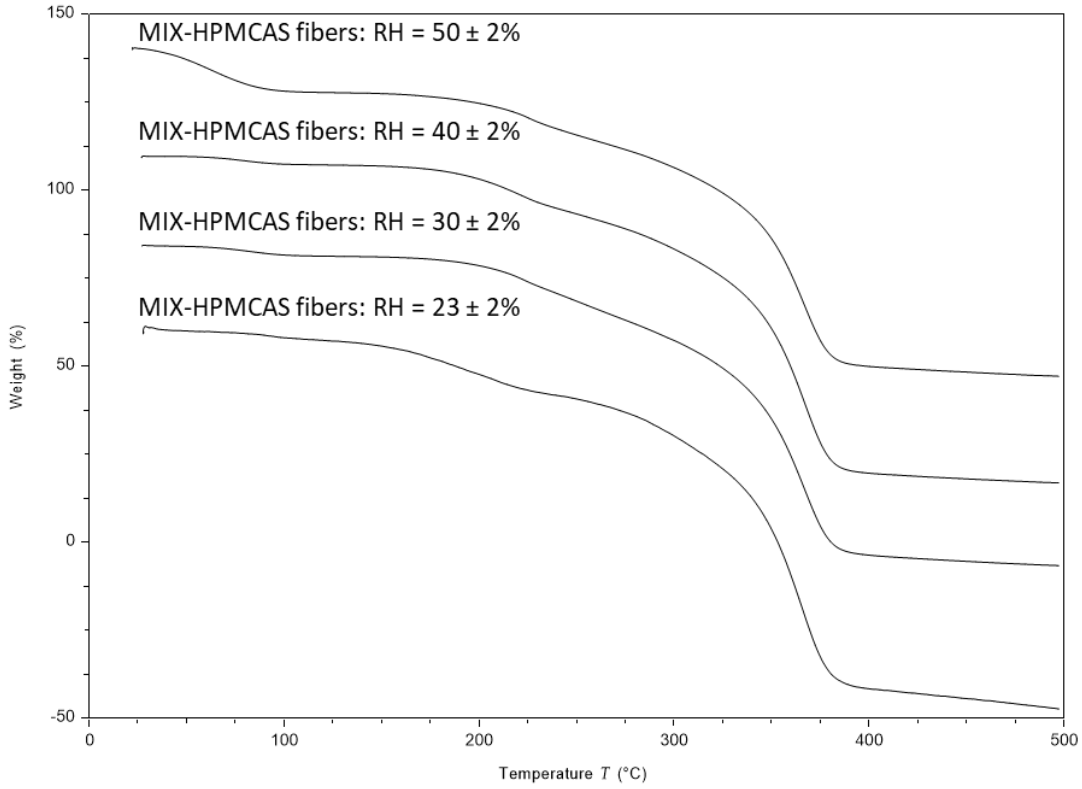

Figure 3.11. TGA thermograms of MIX-HPMCAS fibers electrospun at RH = 50 ± 2%, RH = 40 ± 2%, RH = 30 ± 2%, and RH = 23 ± 2%, showing significant moisture uptake by fibers electrospun at RH = 50 ± 2%.

TGA proved there was no residual solvent left in the fibers after electrospinning by introducing the 15 minutes long isothermal step at 189 °C. In Figure 3.12, blank HPMCAS fibers electrospun at 30% relative humidity are compared with MIX-HPMCAS fibers electrospun at RH = 30 ± 2%, MIX-HPMCAS physical mix and individual drugs. Both MIX-HPMCAS fibers and physical mix showed 6.5 - 7.5 % weight loss at 189 °C. This weight loss is associated with PAR, which decomposes at the same temperature, as it is the boiling point of DMSO. The reproducibility of weight loss at 189 °C between

MIX-HPMCAS fibers and physical mix suggests this weight loss belongs to PAR decomposition only and no DMSO residues are trapped in the MIX-HPMCAS fibers.

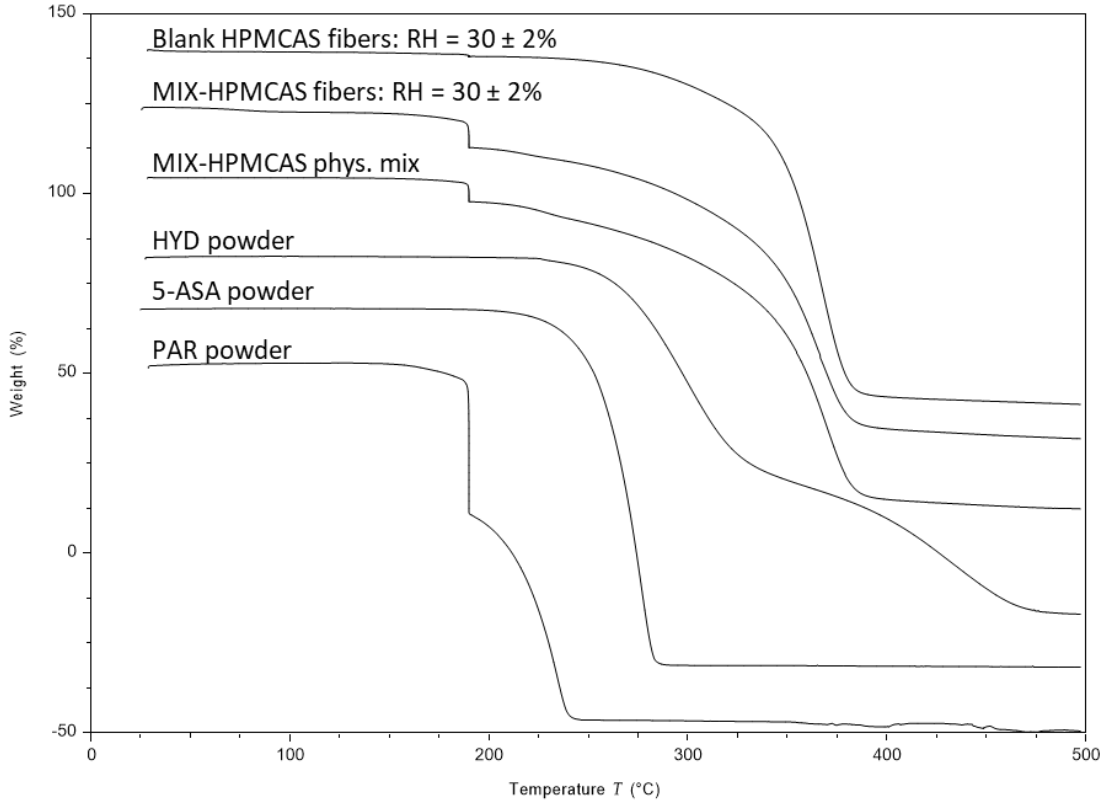

Figure 3.12. TGA thermograms of blank HPMCAS fibers and MIX-HPMCAS fibers compared to MIX-HPMCAS physical mix and individual drug powders, showing no residual solvent left in fibers after electrospinning.

MDSC thermograms showed significant depression of the single glass transition of the MIX-HPMCAS fibers electrospun at RH = 30 ± 2% when compared with physical mix (see Figure 3.13). This suggests all three drugs are amorphous and molecularly dispersed in HPMCAS when electrospun together with the polymer. No melting point for PAR was detected in MDSC thermogram of the physical mix before 180 °C. This together with significant depression of glass transition compared to HPMCAS powder suggests ball-milling (as the preparation method for the physical mixture) of the mixture could partially amorphise the drugs. Melting points for 5-ASA and HYD cannot be seen in the MDSC thermograms because the mixture decomposes before the melting points could be observed. 5-ASA decomposes before its melting occurs and HYD melting point onsets at 223 °C.

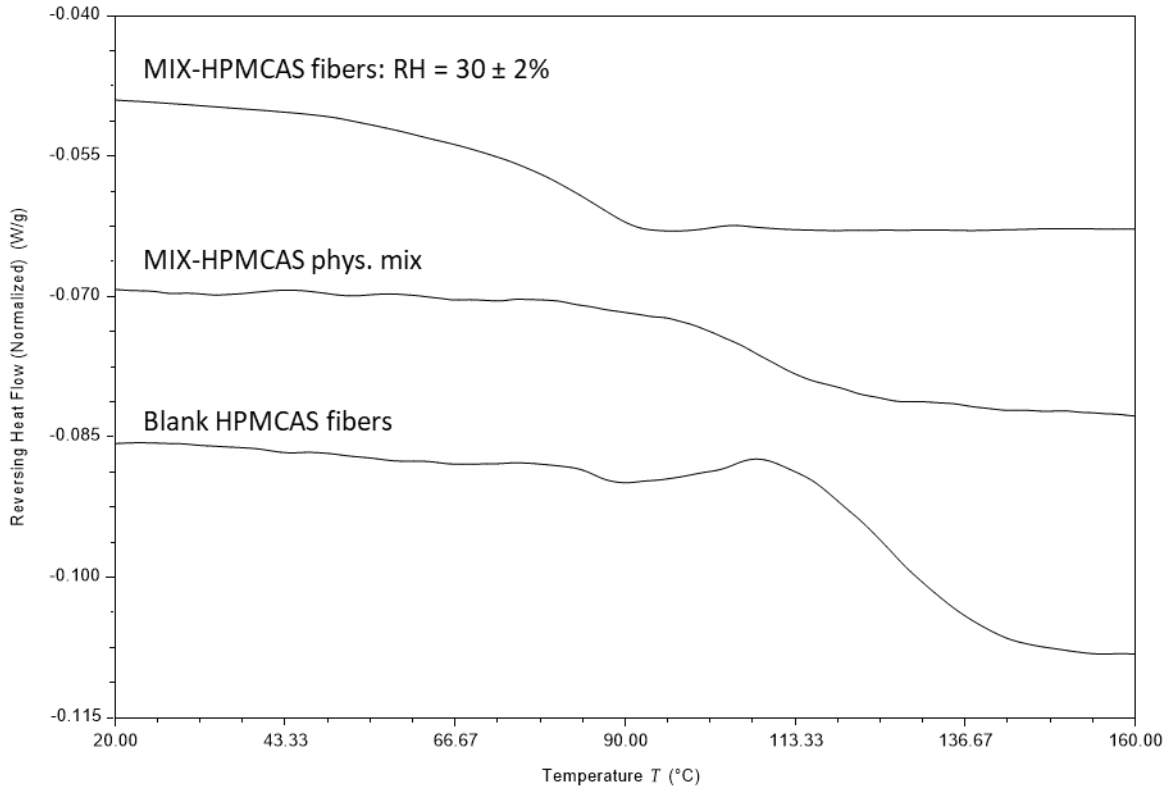

Figure 3.13. MDSC thermograms of blank HPMCAS fibers, MIX-HPMCAS physical mix, and electrospun MIX-HPMCAS formulation showing significant glass transition depression in physical mix and further glass transition depression in MIX-HPMCAS fibers.

ATR-FTIR spectra in Figure 3.14 showed no significant shifts of polymer or drugs peaks suggesting no strong specific interaction in between all four compounds in the MIX-HPMCAS fibers and physical mix. The peaks belonging to the drugs are less intense and broader in the MIX-HPMCAS fibers, suggesting the drugs are molecularly dispersed in the fibers.

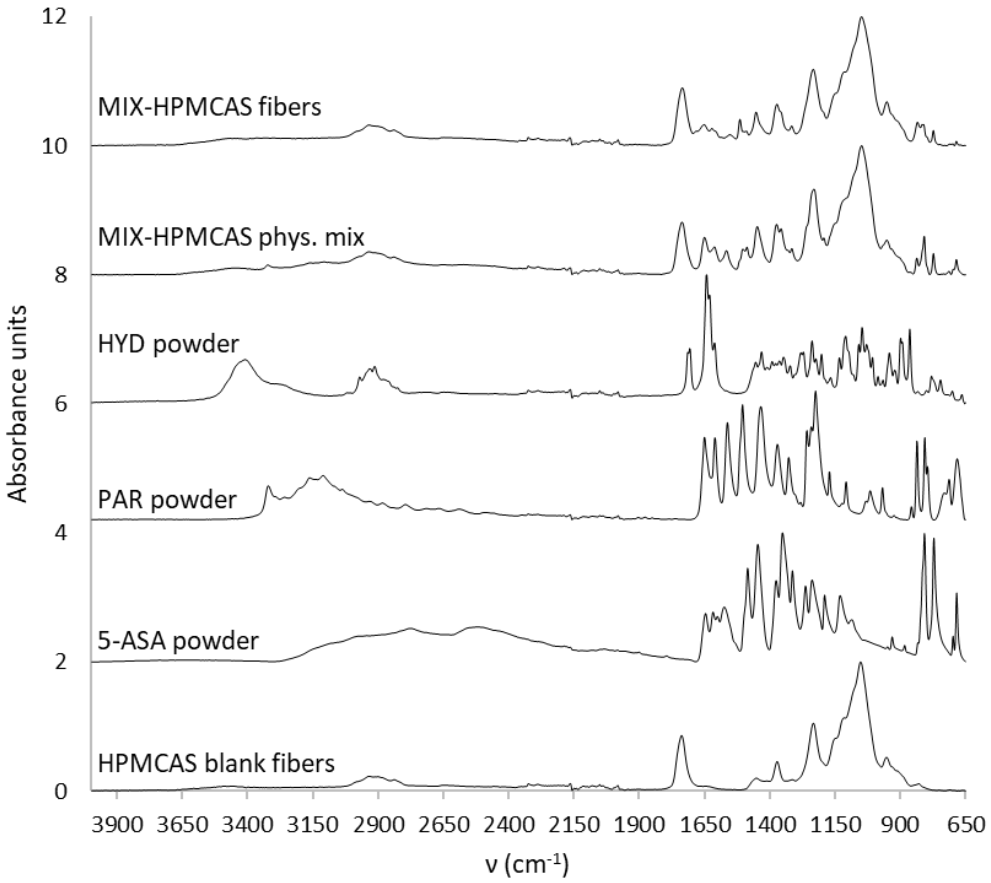

Figure 3.14. ATR-FTIR spectra of MIX-HPMCAS fibers, MIX-HPMCAS physical mix, individual drugs (5-ASA, PAR, HYD) and blank HPMCAS fibers, suggesting no inter-molecular interaction in between all four compounds in the MIX-HPMCAS fibers and physical mix.

Amorphous state of the MIX-HPMCAS fibers was confirmed with PXRD diffractograms showing amorphous halo for the fibers, while crystalline peaks belonging to the three drugs can be observed in MIX-HPMCAS physical mix (see Figure 3.15).

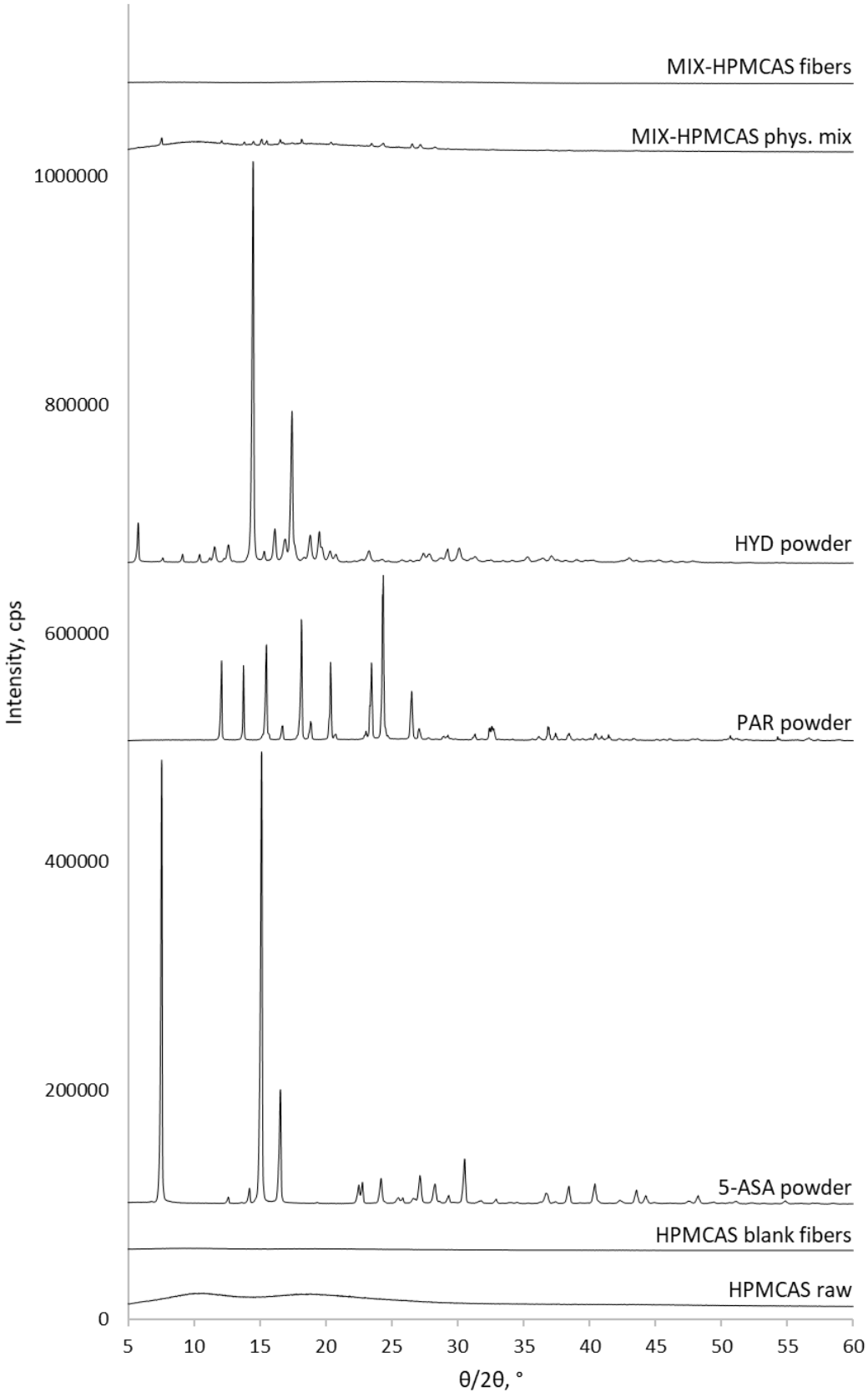

Figure 3.15. PXRD diffractograms of MIX-HPMCAS fibers, MIX-HPMCAS physical mix, individual drugs (5-ASA, PAR, HYD), blank HPMCAS fibers and HPMCAS powder, showing the MIX-HPMCAS fibers are fully amorphous.

All three analyses (MDSC, ATR-FTIT, PXRD) together confirmed the molecular dispersion of the three drugs in the MIX-HPMCAS fibers, which should allow rapid release of the drugs from the HPMCAS fibers once the colonic pH > 7 is reached. The dissolution experiment was performed in sink conditions at 37 ˚C, using baskets in dissolution vessels. Each MIX-HPMCAS fibers replicate was fitted into an HPMC capsule since there is a high probability the industrial preparation of such formulation would involve this final step to allow easier manipulation. The filled capsules in the dissolution baskets were immersed into hydrochloric solution (pH = 1.2) of pH = 1.2 for the first two hours, mimicking the stomach environment and transition time. After two hours, the baskets with the undissolved fibers (containing the rest of the unreleased drugs) were transferred from the hydrochloric solution (pH = 1.2) into vessels with PBS buffer of pH = 7.4, to study the drug release in the colonic pH. The samples were assayed with LC-MS to obtain drug release profiles of each drug (see Figure 3.16). The HPMC capsule dissolved within first 20 minutes of the dissolution, keeping the drug release at zero levels at the first time point (10 min). After two hours, 65 ± 8% of 5-ASA, 66 ± 6% of PAR, and 19 ± 4% of HYD was released in pH = 1.2, even though the HPMCAS fibers were not dissolved. This shows the HPMCAS fibers did not fulfil the enteric requirements (<10% of drug released at pH = 1.2) for any of the three drugs. The slower release of HYD can be explained by its higher degree of hydrophobicity. 5-ASA and PAR did not show any additional release in pH = 7.4, when the drug concentration plateaued at 65 ± 10%, suggesting almost all drug was released in gastric pH. Release of HYD reached 59 ± 4% after 6 hours in pH = 7.4. These values suggest the drug loss occurred. This could happen before and during the fiber transfer from pH = 1.2 to pH = 7.4 where possible disintegration of the (undissolved) fibrous mat would result into a leak of the small mat fragments into the hydrochloric solution (pH = 1.2) through the basket mesh.

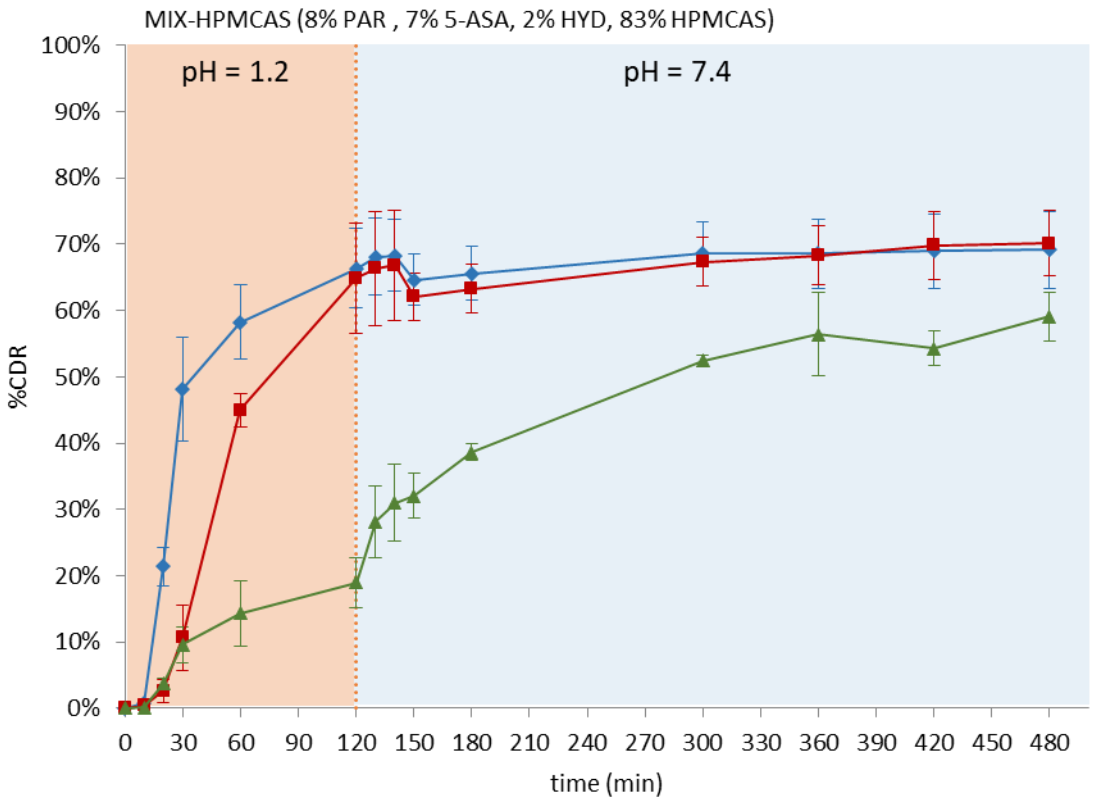

Figure 3.16. Drug release from electrospun MIX-HPMCAS formulation, simulating the pH transition from stomach acidic pH = 1.2 to colonic pH = 7.4 at 2 hour time point. Blue diamonds show release of PAR, red squares release of 5-ASA, and green triangles release of HYD.

3.3.3 Single-drug loaded HPMCAS fibers

To study the lack of enteric properties of MIX-HPMCAS fibers, three additional control samples containing one of each individual drug were prepared. The drug loading percentage was kept the same as in MIX-HPMCAS for each drug. The HPMCAS concentration was kept fixed 20% (w/v) and the drugs were added accordingly, 7% of 5-ASA in 5-ASA-HPMCAS, 8% of PAR in PAR-HPMCAS, and 2% of HYD in the HYD-HPMCAS. Samples were electrospun at RH = 30 ± 2% under the same process conditions as MIX-HPMCAS. However, -5 kV was applied on the rotating drum to increase the grounding and stability of the Taylor cone. Representative SEM images of 5-ASA-HPMCAS, PAR-HPMCAS, and HYD-HPMCAS electrospun samples are shown in Figure 3.17. All three samples manifested polydisperse beaded fibers. The mean fiber diameter of 5-ASA-HPMCAS, PAR-HPMCAS, and HYD-HPMCAS was 355.9 ± 185.7 nm, 556.1 ± 308.9 nm, and 426.6 ± 275.3 nm, respectively.

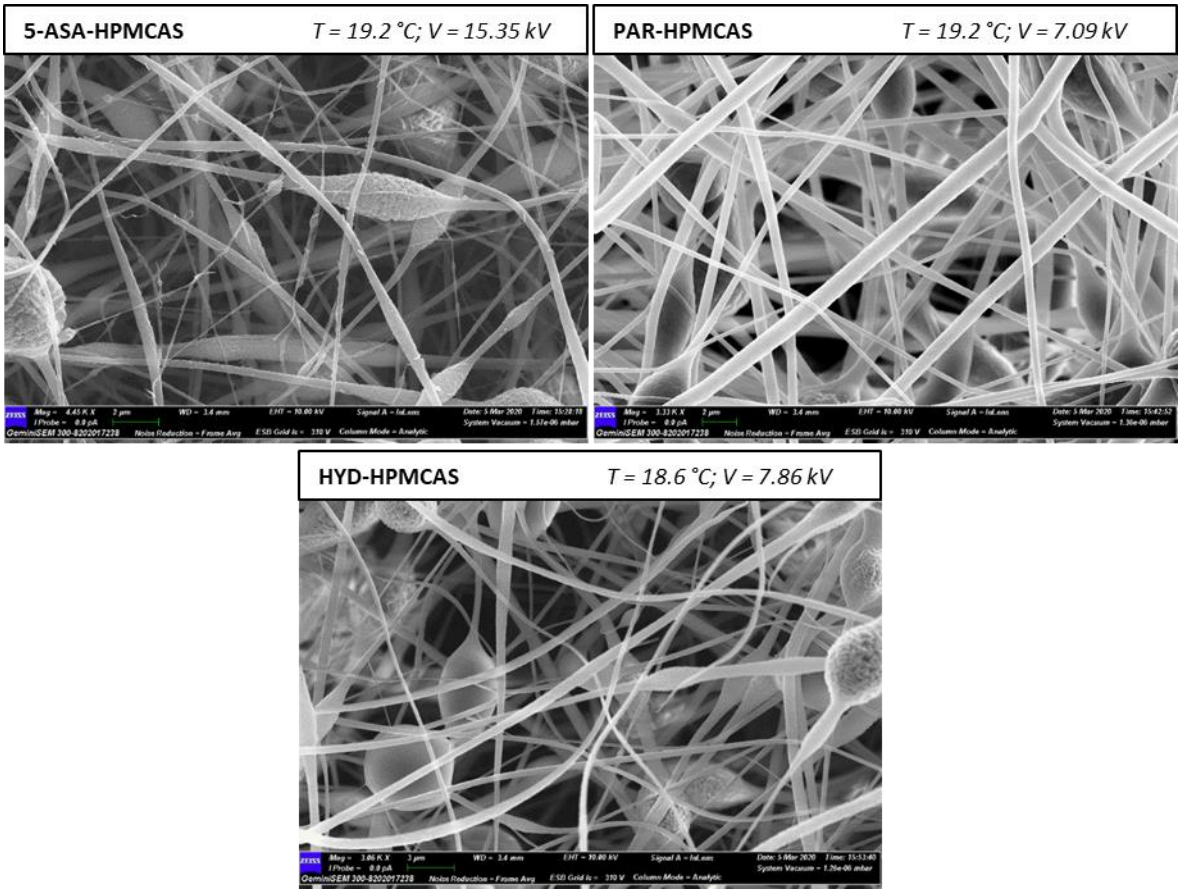

Figure 3.17. Representative SEM images of single-drug loaded HPMCAS fibers electrospun at RH = 30 ± 2%, showing beaded fiber structure in each sample.

Due to the high standard deviation, the distribution of the fiber diameter is shown in histograms describing the frequency of each fiber diameter range. The histograms were produced for bead length/width ratio as well (see Figure 3.18). 5-ASA-HPMCAS fibers' diameter was most abundant at 200 – 400 nm (histogram A1), while the bead length/width ratio was most abundant in the range of 1- 2 (histogram B1). PAR-HPMCAS fibers showed two maxima in fiber diameter (histogram A2). The most abundant fiber diameter of these fibers was in the range of 300 – 400 nm and the second peak was found at the 1000 – 1500 nm range. Beads of the PAR-HPMCAS fibers were more elongated compared to 5ASA-HPMCAS fibers, showing peak maximum at the 2 – 3 bead length/width ratio range as well as 14% of the beads in the bead length/width ratio >5 (histogram B2). HYD-HPMCAS fibers also showed two peaks in the fiber diameter histogram, the most abundant fiber diameter was found at the 200 – 300 nm ratio and the second peak was found at the 1000 – 1500 nm range (histogram A3). The maximum of the bead length/width ratio

was found in the range of 1 – 2 (histogram B3). However, 21% and 15% of the HYD-HPMCAS beads were in the bead length/width ratio of 3 – 4 and >5, respectively.

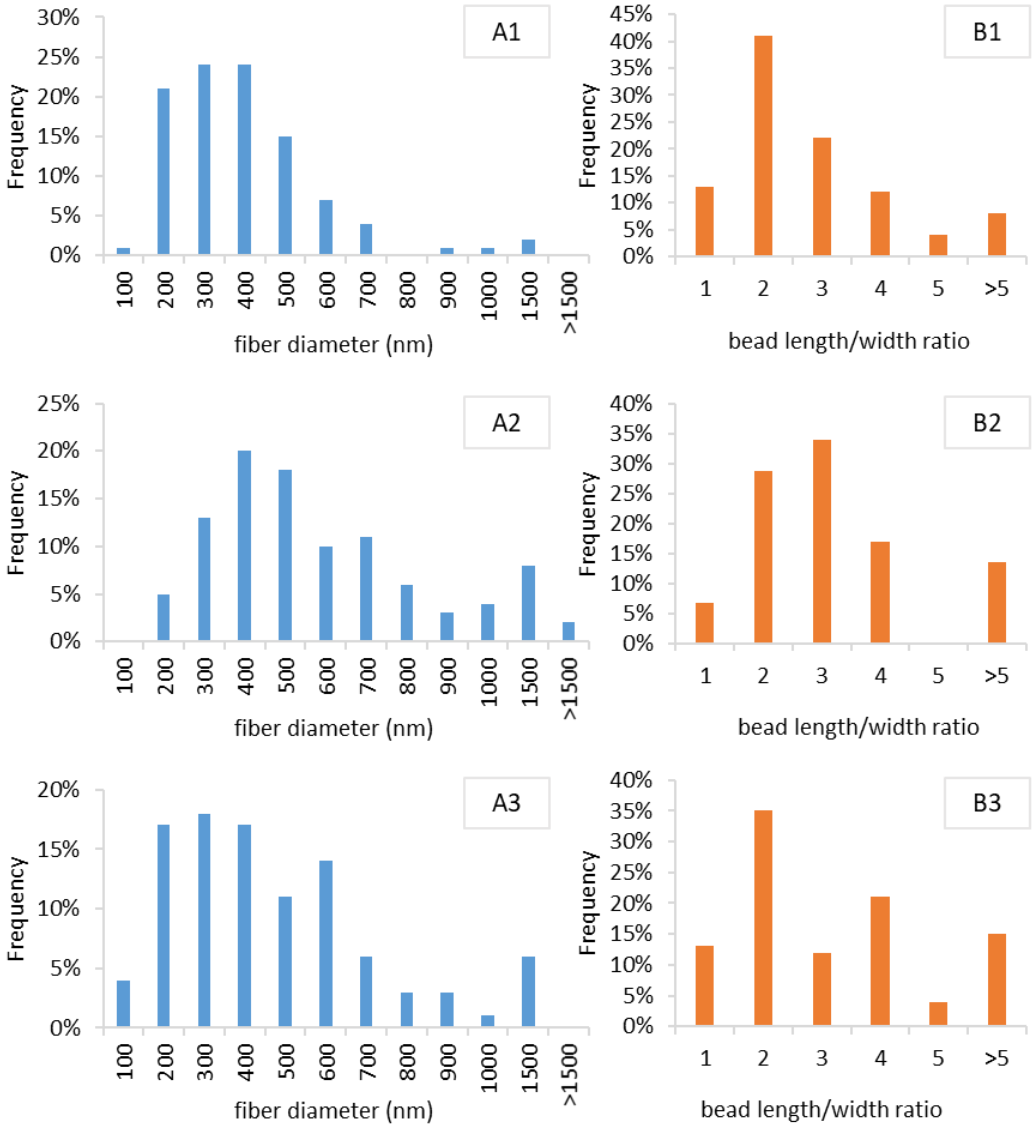

Figure 3.18. Histograms describing different (A) distribution of fiber diameter and (B) length/width ratio of beads formed in electrospun single-drug loaded HPMCAS fibers at RH = 30 ± 2%: (1) 5-ASA-HPMCAS fibers; (2) PAR-HPMCAS fibers; (3) HYD-HPMCAS fibers.

The viscosity, surface tension, and conductivity were measured for all three single-drug loaded solutions and compared with the values of MIX-HPMCAS solution, blank HPMCAS solution and the binary solvent mixture (see Figure 3.19). Even though the concentration of the HPMCAS stays fixed, the solution properties were significantly affected by the addition of each of the three model drugs. Viscosity (η) of the solution significantly decreased for

5-ASA-HPMCAS and HYD-HPMCAS solution compared to the blank HPMCAS solution. Even though the mean viscosity decreased for the PAR-HPMCAS solution as well, the standard deviation was too high to determine significant change. None of the single-drug loaded solutions' viscosity significantly differed from each other or from the viscosity of the MIX-HPMCAS solution. The mean surface tension (γ) decreased significantly for 5-ASA and HYD loaded solutions compared to blank HPMCAS solution, but no significant decrease was observed for PAR-HPMCAS solution. None of the single-drug loaded solutions' surface tension showed significant difference from surface tension of multi-drug MIX-HPMCAS solution. When single-drug loaded solutions were compared in between each other, 5-ASA-HPMCAS showed significantly lower surface tension than PAR-HPMCAS solution (and no other significant difference were found). Compared to the blank HPMCAS solution, the conductivity rapidly increased for 5-ASA-HPMCAS, while it significantly decreased in both PAR-HPMCAS and HYD-HPMCAS solutions. This confirms the 5-ASA was the main reason for the high MIX-HPMCAS conductivity. However, the conductivity of the MIX-HPMCAS solution was significantly higher than in 5-ASA-HPMCAS solution, suggesting the mixing of the three drugs plays certain role on the conductivity too.

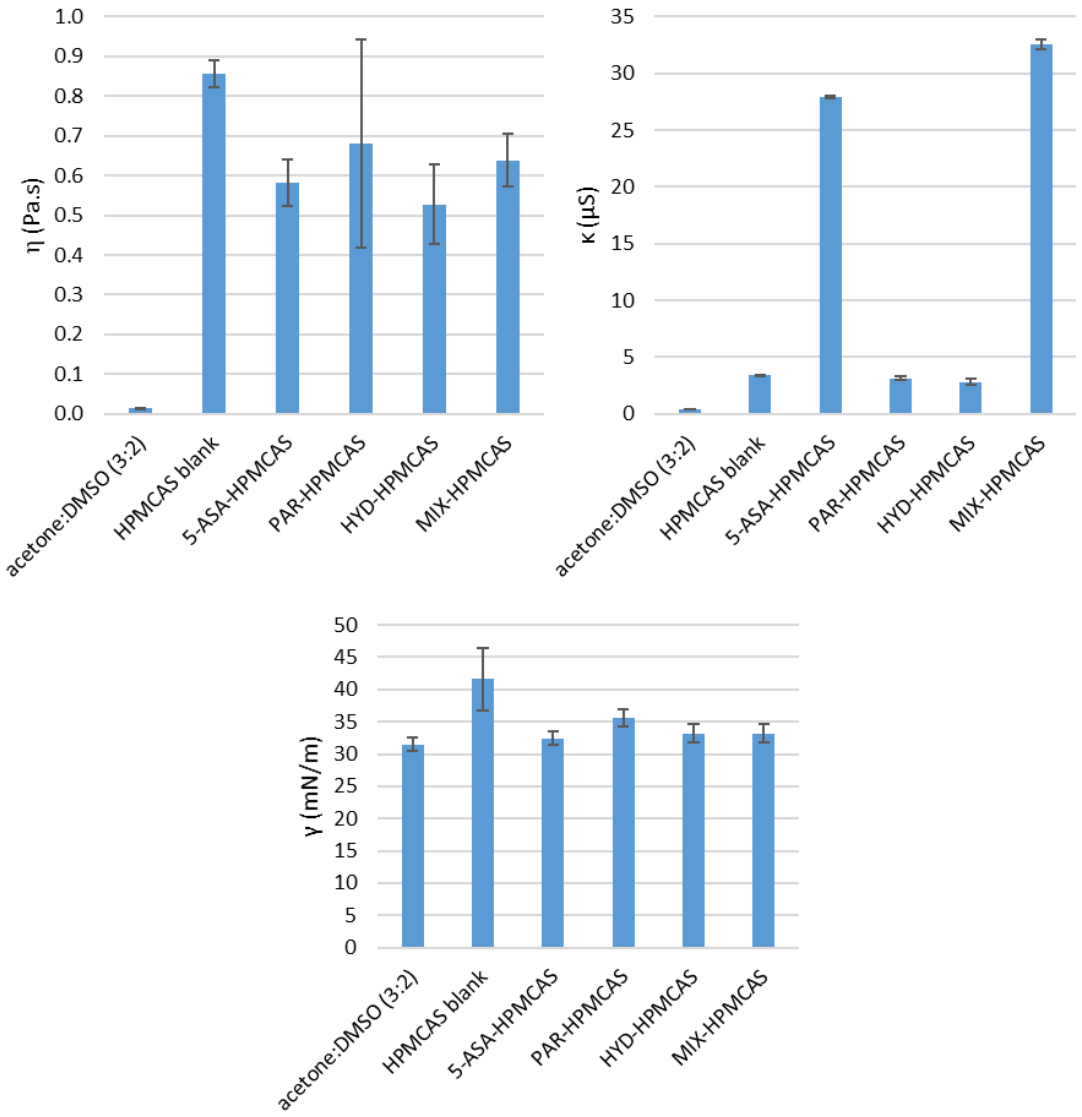

Figure 3.19. Properties of single-drug loaded HPMCAS electrospinning solutions: viscosity (η) measured at shear rate of 28.4 s^{-1} at 21 ˚C (top left), conductivity (κ) measured at 20 - 22 °C (top right), and surface tension (γ) measured at 21 ˚C (bottom middle).

TGA analysis showed no significant moisture absorption (<3%) by the electrospun single-drug loaded fibers. The thermograms of the individual single-drug loaded fibers compared to their physical mixes are shown in Figure 3.20.

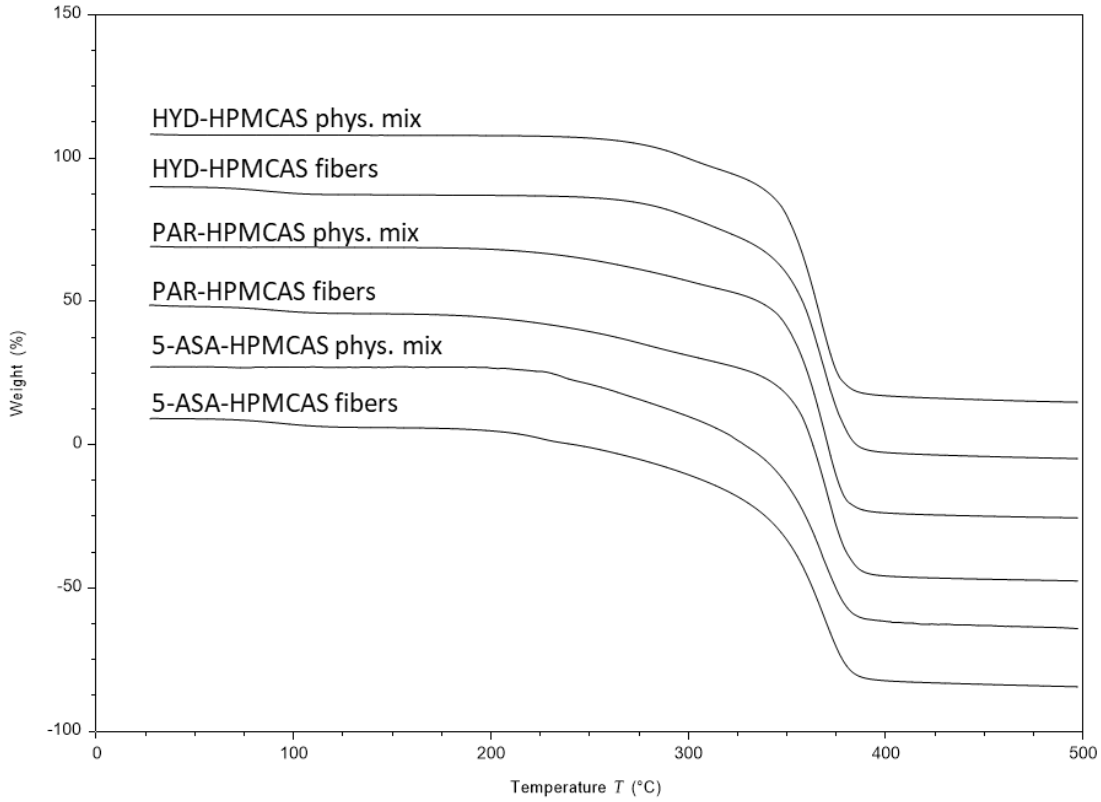

Figure 3.20. TGA thermograms of single-drug loaded HPMCAS fibers and their physical mixes, showing the consistent moisture uptake by electrospun fibers.

MDSC analysis shown significant depression of the single glass transition in all three single-drug loaded fibers compared to their physical mixes, suggesting full molecular dispersion of the drug in the HPMCAS polymer (see Figure 3.21). As it could have been seen previously in the case of MIX-HPMCAS, no melting point of the PAR was detected before 180 ˚C. Melting points of 5-ASA and HYD were not possible to detect due to the nature of the drugs. However, glass transitions of 5-ASA-HPMCAS and HYD-HPMCAS physical mixes (124 ˚C and 125 ˚C, respectively) were not significantly depressed compared to the glass transition of HPMCAS powder, suggesting the preparation of the physical mix by ball milling did not affect the crystalline state of the drugs. On the other hand, glass transition of the PAR-HPMCAS physical mix was depressed to 108 ˚C. This indicates the PAR is prone to amorphisation by ball milling process possibly due to its lower melting point (169 ˚C) compared to the other two drugs.

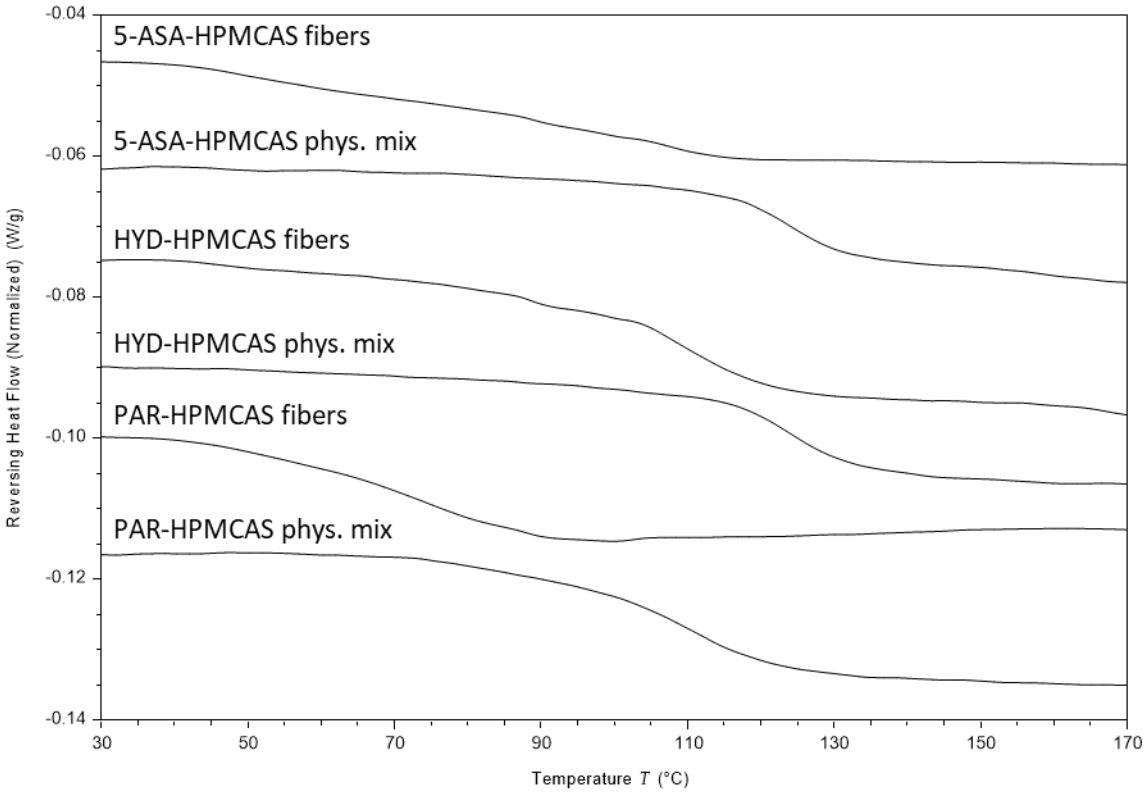

Figure 3.21. MDSC thermograms of single-drug loaded HPMCAS fibers, showing depression of single glass transition in each electrospun sample compared to their physical mixes.

No significant shifts of the peaks were found in the ATR-FTIR spectra of the single-drug loaded fibers compared to their physical mixes and the spectra of the individual drugs and blank HPMCAS fibers (see Figure 3.22). This indicates no specific interactions in between the drugs and the polymer in both physical mixes and electrospun formulations. However, broader peaks were found in the electrospun single-drug loaded samples, suggesting the lower state of crystallinity in these samples.

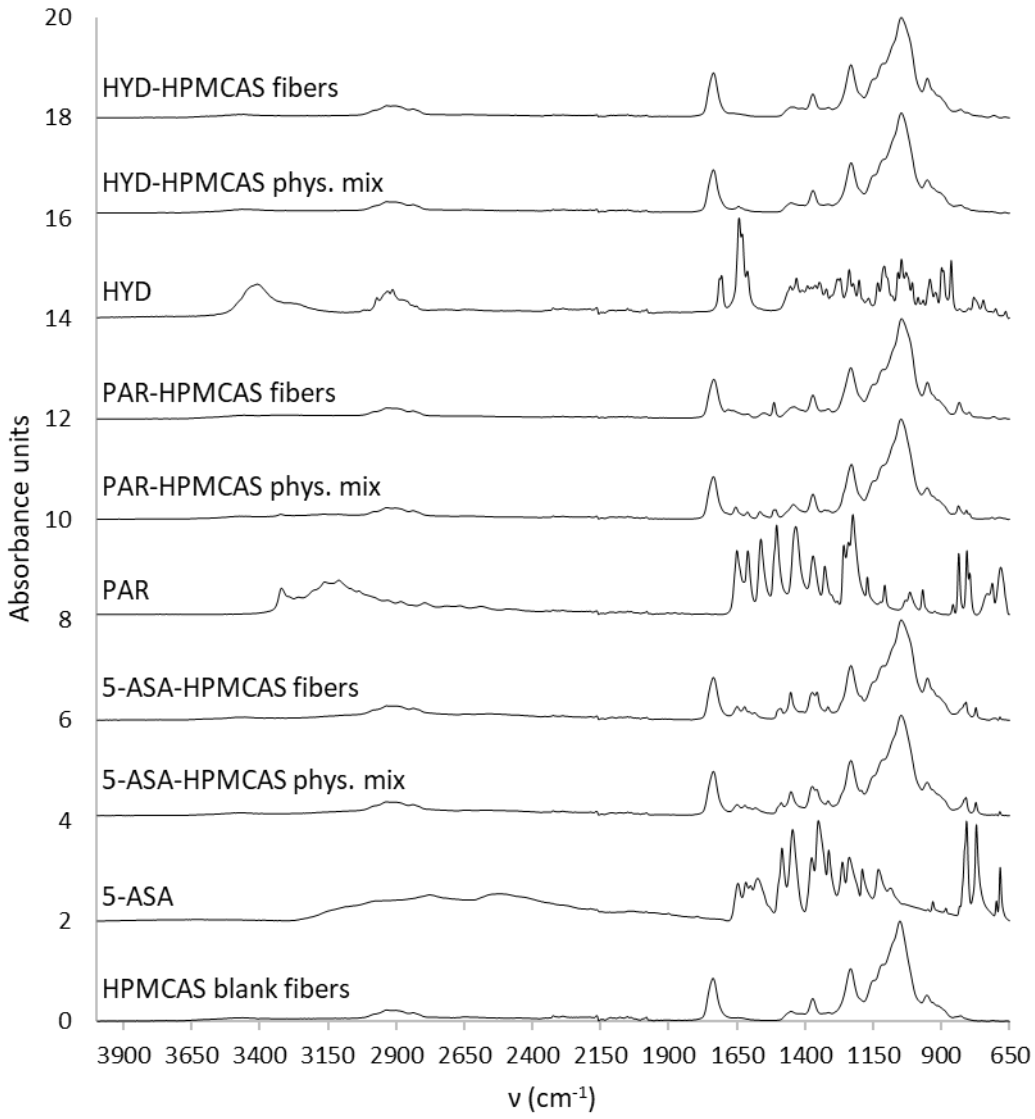

Figure 3.22. ATR-FTIR spectra of single-drug loaded HPMCAS fibers, their physical mixes and individual drugs compared to blank HPMCAS fibers, suggesting no inter-molecular interaction in between individual drugs and the polymer.

PXRD diffractograms confirmed the amorphous state of the electrospun single-drug loaded fibers compared to their physical mixes, which presented with crystalline peaks belonging to each of the three dugs (see Figure 3.23). PXRD confirmed crystallinity of PAR-HPMCAS physical mix even though no melting point was observed in MDSC. This suggests the paracetamol dissolves in the polymer with the increasing temperature, amorphising the mixture. PXRD together with MDSC, and ATR-FTIR analyses confirmed the molecular dispersion of the drugs in the electrospun fibers.

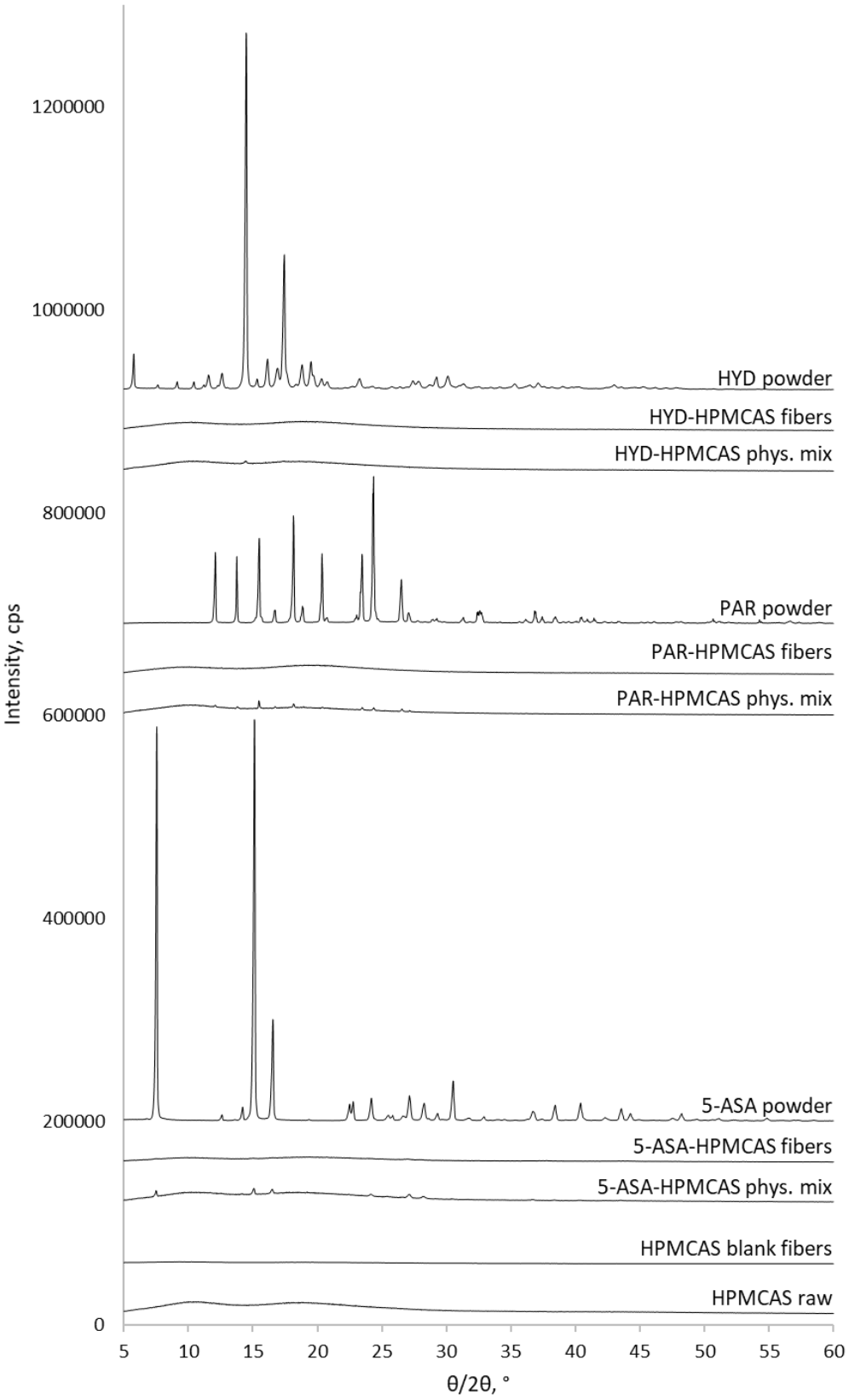

Figure 3.23. PXRD diffractograms of single-drug loaded HPMCAS fibers, their physical mixes and individual drugs compared to blank HPMCAS fibers and HPMCAS powder, showing fully amorphous electrospun formulations.

Drug release from the single-drug loaded fibers was performed in sink conditions at 37 ˚C and assayed by UV-VIS spectrophotometry (see Figure 3.24). Fibers were not fitted into an HPMC capsule in this case due to the absorption signal interference (as no chromatographic separation preceded the assay). The fibers in the dissolution baskets were immersed into hydrochloric solution (pH = 1.2) for the first two hours, followed by the transition into the PBS buffer of pH = 7.4. The single-drug loaded fibers did not fulfil the enteric requirements (<10% of drug released at pH = 1.2). Even though the HPMCAS fibers were not dissolved in pH = 1.2, 76 ± 7% of 5-ASA, 57 ± 15% of PAR, and 15 ± 4% of HYD was released after two hours, indicating no significant difference compared to the drug release from MIX-HPMCAS fibers. The following release in PBS showed a significant difference only in case of the HYD and its release from HYD-HPMCAS fibers, when compared with MIX-HPMCAS fibers. Only 33 ± 10% of HYD was released after 6 hours in PBS (compared to 59 ± 4% from MIX-HPMCAS fibers). Since the hydrocortisone loading and therefore intensity of its absorption signal in UV-VIS spectrophotometry were low, the signal could have interfered with the absorption of HPMCAS polymer, which tends to elevate the sample baseline in high concentrations. As the HYD-HPMCAS samples in PBS buffer (pH = 7.4) contained the highest concentration of HPMCAS, this could also lead to slower dissolution of the fibers due to possible saturation in the sink media. These experiments confirmed the polymer fibers did not lose its enteric properties due to the high drug loading quantity or mixing of the drugs together in MIX-HPMCAS fibers. The effect of the fiber diameter on the enteric properties was therefore studied and the findings are presented in Chapter 5.

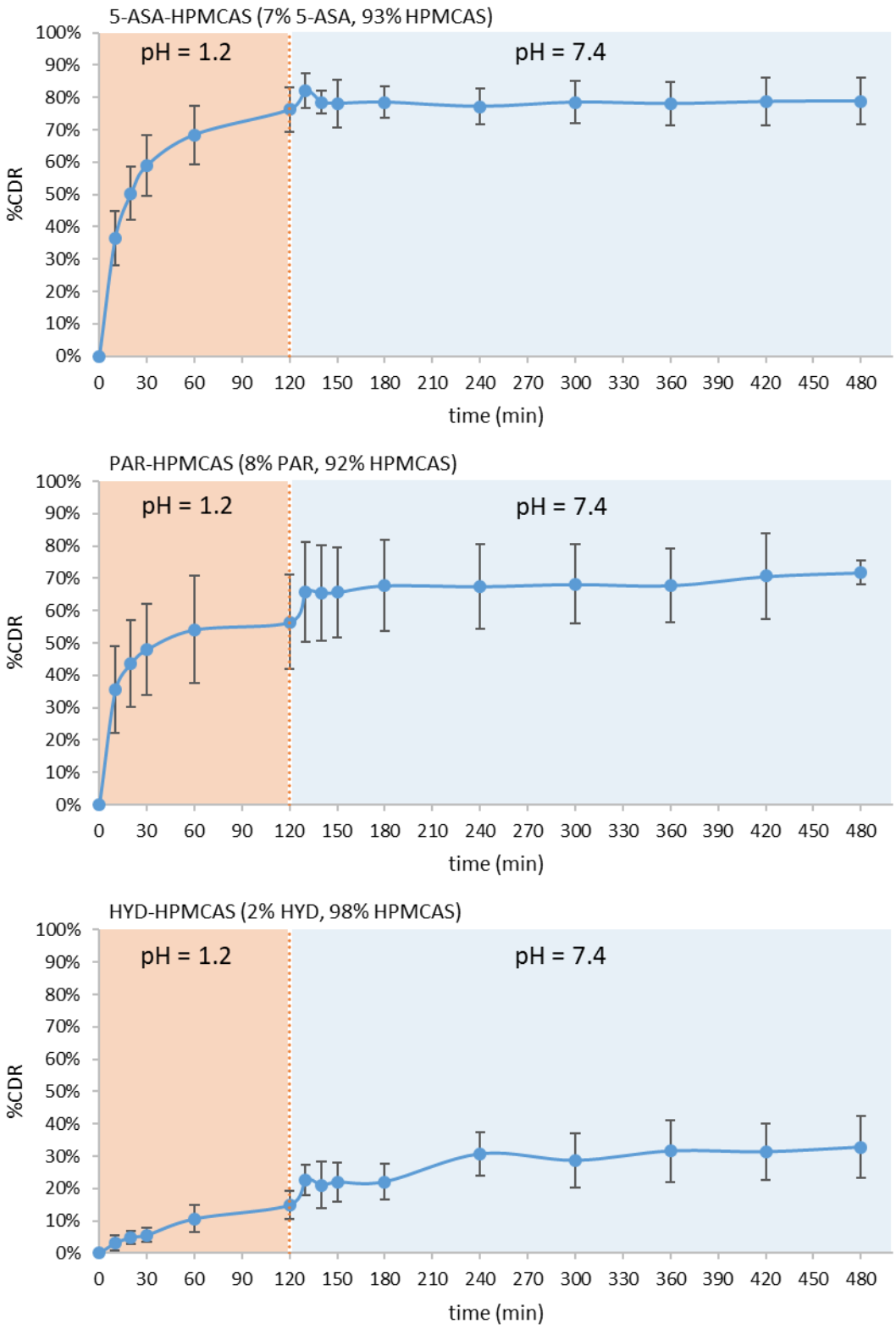

Figure 3.24. Drug release from single-drug loaded electrospun HPMCAS formulations (top: 5-ASA-HPMCAS, middle: PAR-HPMCAS fibers, bottom: HYD-HPMCAS fibers), simulating the pH transition from stomach acidic pH = 1.2 to colonic pH = 7.4 at 2 hour time point.

It is interesting to compare findings in this chapter with a study published by Liu et al. in 2020, describing theophylline loaded HPMCAS (AS-MG) electrospun fibers.[182] Smooth fibers were obtained from 12wt% solutions in methanol:DCM (4:6, v:v), however beading occurred at the highest reported drug loading of 4%. The relative humidity was not monitored in this case. Even though the authors stated that the drug release was not affected by the acidic pH, the drug release profiles clearly show that more than 60% of the theophylline was released in each case within two hours in gastric pH. This would support the theory that the enteric properties of the HPMCAS are lost due to the high surface to volume ratio of the electrospun fibers. However, it seems the polymer was not supplied from a commercial manufacturer and the physico-chemical characterisation of the pure polymer does not correspond with the reported data. The glass transition was not identified from the thermograms due to high water content and the TGA analyses showed two-step degradation with the first step starting already at 121 ˚C, while only one-step degradation is shown in the commercially supplied polymers and is not observed before 200 ˚C for any of the available grades. The FT-IR fingerprint of the HPMCAS (AS-MG) is also different, missing a distinct peak at 1372 cm^{-1} and one of the shoulders (1150 cm^{-1}) of the broad 1047 cm^{-1} peak. This suggests the polymer used in these experiments was not pure HPMCAS polymer.

Various studies of electrospinning other enteric polymers such as Eudragit L100 and S100 can be found in the literature, as the electrospinning process of these polymers is not as complex as in the case of HPMCAS. However, the evaluation of the performance of Eudragit fibers for targeted drug delivery is not uniform among these studies, as some of the drugs are protected from release in acidic pH (e.g., diclofenac sodium loaded Eudragit L100-55 fibers prepared by Shen et al.[183]), while others leach out (e.g., 5-fluorouracil loaded Eudragit S100 fibers studied by Illangakoon et al.[184]). Burgess et al.[185] decided to study this phenomenon further by comparison of electrospun Eudragit S100 fibers (both monolithic and core-shell) loaded with one of the four model active ingredients (benzoic acid, 1-naphthoic acid, 1-naphthylamine, and 9-anthracene carboxylic acid). They found out the acidity/basicity and molecular weight were the most important factor affecting the ingredient release profile when acidic species and ingredients of higher molecular weight were released slower in acidic media. Burgess et al. observed these trends in both monolithic and core-shell fibers, while the ingredient release from core-shell fibers was reduced when compared to its monolithic equivalent.

Even though, PAR is less acidic and of lower molecular weight (151 g/mol) compared to 5-ASA (153 g/mol), no significant difference in the release of these two drugs from the HPMCAS electrospun fibers was observed after two hours in acidic media (in both multi-drug and single-drug loaded fibers). However, the HYD (363 g/mol) was released significantly slower compared to PAR and 5-ASA, suggesting a larger difference in molecular weight might be necessary to affect the release profile if the trends observed in Eudragit fibers were applicable to the HPMCAS fibers.

3.4 Conclusion

The HPMCAS was confirmed to be electrospinnable without adding any additives. Beaded fibers were obtained from 20% (w/v) HPMCAS solution in acetone:DMSO (3:2, v:v). The quality and the structure of the fibers was significantly affected by relative humidity, showing thinner and broken fibers with more spherical beads in decreased humidity (RH = 23 ± 2%). The multidrug loaded MIX-HPMCAS followed the same pattern, however significant fusing was observed at RH>30 ± 2%. Therefore, RH = 30 ± 2% was selected as optimal humidity for the electrospinning of the drug loaded formulations, as well as use of rotating drum as a collector to assure even thickness of the fibrous mat. The acetone:DMSO (3:2, v:v) was fully evaporated from the collected fibers in all cases, as proved by TGA analysis. All the drugs in drug loaded formulations were confirmed to be molecularly dispersed. This was concluded from results of (M)DSC, ATR-FTIR, and PXRD analyses. None of the drug loaded fibrous formulations complied with the enteric requirements (more than 10% of each drug was released within two hours in gastric pH). Despite significantly higher total drug load (17%), the MIX-HPMCAS and single-drug loaded fibers did not show significantly different release profiles of each drug in gastric pH, suggesting the loss of enteric properties is caused by the increased volume to surface ratio of the fibers and not by overloading of the formulations.

4 ZEIN NANOPARTICLES

4.1 Introduction

A different delivery system has to be proposed due to the HPMCAS fibers leaking the drugs in gastric environment. However, the electrospun fibers are still pH respondent and do not dissolve in pH = 1.2 and therefore, they were considered as a potential carrier for incorporated drug loaded nanoparticles. For this purpose, zein nanoparticles loaded with 5-ASA were developed. Zein was selected for its mucoadhesive properties,[186] which would increase the potency of the drug due to the time of the particles spent on the colonic wall. 5-ASA was selected as it is the most widely used drug in management of the IBD out of the three model drugs and due to its precipitation ability in excess of water. Two preparation methods of the blank zein nanoparticles are compared in this chapter: the electrospray, and the anti-solvent (precipitation) techniques. Drug loaded zein nanoparticles were further developed by anti-solvent method only due to low yield and redispersion ability of the electrosprayed nanoparticles. All prepared nanoparticles were imaged either by SEM and/or TEM to estimate their size. Precipitated nanosuspensions were also characterised by DLS and the zeta potential of the blank zein nanoparticles was measured. Further physico-chemical properties of all formulations were characterised by TGA, DSC, ATR-FTIR, and PXRD. The drug release from the precipitated nanoparticles was performed in PBS (pH = 7.4) and assayed by LC-MS.

4.2 Materials and Methods

4.2.1 Materials

Zein was purchased from ACROS Organics, US. 5-aminosalicylic acid (5-ASA) was purchased from Acros Organics, US. Ethanol (EtOH) was purchased from VWR, France. MilliQ (MQ) water was produced using a Purelab ultra (ELGA LabWater, UK). Hydrochloric acid and PBS tablets were purchased from Sigma-Aldrich, US.

4.2.2 Electrosprayed nanoparticles preparation

The zein was precisely weighted and then dissolved in a corresponding volume/weight of solvent to obtain aimed concentration. The solutions were stirred overnight and double filtered using PES syringe filters of 0.45 and 0.2 μm pore size, respectively. Clear solutions were then vertically electrosprayed, using a custom made system consisting of a syringe pump (Cole-Parmer, USA), 1 ml plastic syringe (Terumo, Japan), metal 30G needle (Spraybase, Ireland) and a plate collector covered with aluminium foil. The parameters were

optimised based on the solution, using a CCD camera to observe the Taylor cone and a multimeter to monitor the electrical current.

4.2.3 Precipitated nanoparticles preparation

Blank precipitated NPs were prepared by anti-solvent method mixing filtered zein solution in 70% EtOH aq. (v/v) and Milli-Q water in different concentrations of zein and different solvent/anti-solvent proportions. To obtain drug loaded NPs, mixtures of zein and 5-ASA dissolved in 70% EtOH aq. (v/v) together with correspondent volume of HCl were precipitated with Milli-Q water. The nanosuspensions were freeze dried for the purpose of further characterisation.

4.2.4 Size distribution and zeta potential of the nanoparticles

Zetasizer Nano (Malvern Instruments Ltd, Malvern, UK) was used to study size distribution (DLS) in backscattering mode (173°) as well as the zeta potential of precipitated blank zein nanosuspensions. In all DLS methods, 'protein' was set as a material, using Malvern standard selection. The other parameters were set based on the ethanol concentration in the aqueous nanosuspension solvent, based on the approximation that viscosity of the sample equals to viscosity of dispersant. For each dispersant concentration, number of ethanol moles was calculated based on tabulated density (0.7893 g/cm^3) and molar mass (46 g/mol) of ethanol. Then tabulated viscosity values were matched with the calculated number of moles. Finally, dielectric constant of the dispersant was estimated based on the volume ratio of the two solvents, using tabulated values for water (80) and ethanol (24). Since all tabulated values were read at 20 ˚C, each DLS method was also set to 20 ˚C.

The suspensions of precipitated nanoparticles were also characterised by JEOL JEM2010 200 kV transmission electron microscope (TEM) (JEOL, Japan). TEM samples of electrosprayed zein nanoparticles were prepared by electrospraying of the nanoparticles directly on the grids.

Electrosprayed and freeze dried precipitated particles were imaged by SEM. The particle samples were directly attached onto SEM specimen stubs (the electrosprayed nanoparticles on the aluminium substrate) by double-sided tape and coated with gold using a Polaran SC7640 sputter gold coater (Quorum Technologies) prior to imaging. The electrosprayed nanoparticles were imaged by a JSM 5900LV field emission scanning electron microscope (Jeol Ltd., Japan) equipped with a tungsten hairpin electron gun. The precipitated nanoparticles were scanned by Zeiss Supra 55 VP FEG SEM (Zeiss, Germany). The Image J

software was used to analyse the particle diameter distribution, when 100 values were averaged for each.

4.2.5 Physico-chemical characterisation of the nanoparticles

Thermal analyses of raw materials, physical mixes, and all formulations were performed with TGA and DSC. For instruments details see Chapter 3. The mass of each empty standard pan was matched with a mass of an empty reference pan. At first, the samples were heated to 75 °C and after a 5 min isothermal step, they were cooled back to 20 °C, both at 20 °C/min rate, to reduce the moisture of the samples and to avoid an interference of the relaxation broad peak with the glass transition of zein. These three initial steps were followed by a ramp heat-cool-reheat method at 10 °C/min rate. Two 1-minute isothermal steps were introduced in between each heating and cooling pair. Different temperature ranges were used for individual materials and formulations depending on their decomposition temperatures obtained from the TGA analysis. All the thermal analyses were performed in triplicates.

ATR-FTIR and **PXRD** experiments were performed using the same equipment and methods as in Chapter 3.

4.2.6 *In vitro* drug release and drug loading efficiency

The zein NPs were tested for the drug release in shaking incubator at 37 °C. The NPs suspension was transferred into dialysis bag and these were inserted into 50 ml of PBS buffer, pH = 7.4. LC-MS TOF method was developed to assay the 5-ASA. Drug was separated on RP C18 column (Thermo Scientific™ Acclaim™ 120, 2.1 x 250 mm, 5 µm) and detected with Agilent MS-TOF detector at 40 °C. To assess the drug loading efficiency of the precipitated zein NPs, the suspensions were filtered with centrifuge filter units (Amicon, Merck) and the supernatant was analysed by LC-MS.

4.3 Results and Discussion

4.3.1 Electrosprayed zein nanoparticles

Electrospray (EHDA) was selected as a first nanoparticle preparation method due to its advantages such as monodispersity, high drug loading efficiency, and vast process modification possibilities with potential to prepare final formulation, drug loaded nanoparticles incorporated into the enteric fibers, in a single step production.[115] Gomez-Estaca et al.[187] and Bhushani et al.[188] reports on zein electrosprayed nanoparticles were used as a starting point to find the optimal conditions of the process. For this purpose,

the formation and stability of Taylor cone were monitored by a CCD camera and electrical current measurements. It was observed the diameter of the nozzle played an important role in a Taylor cone stability, which directly affects the size distribution of the particles. This corresponds with the findings that the surface tension and viscosity of the electrosprayed solutions are among the key factors influencing the particle formation and size.[115] The nozzle gauge and/or the shear rate within the nozzle are often omitted parameters in the EHDA literature, leading to decreased reproducibility of the experiments. In this study, the 30G stainless steel needle was selected as the best candidate since the Taylor cone was more stable in comparison with bigger diameter needles. Therefore, the 30G nozzle was used for all processes which are further discussed. In the Figure 4.1, representative images of the Taylor cone are showed. When a flow rate and a distance between nozzle tip and collector were fixed, a shape of the Taylor cone improved with increasing concentration of zein (see figures A and C, showing 1.75% (w/v) and 2.5% (w/v) zein in 80% (v/v) EtOH (aq.), respectively). Although the feed solutions were double filtered (PES 0.45 μm and 0.2 μm syringe filters, in this order) before electrospraying, zein tendency to precipitate in excess of water reduced the stability of the process over the time. In the Figure 4.1 A, white precipitated protein on the surface of the nozzle is showed. These precipitates could block the needle and therefore, the process was often restarted after the nozzle was wiped with the solvent. The buildup of the precipitates on the surface of the nozzle and potentially inside of the needle tip also increased the occurrence of the precipitates on the edge of a nozzle, which grew in a form of short (often branched) fibers (see Figure 4.1 B). The formation of these fiber-like precipitates increased with frequency of the instabilities in the Taylor cone, despite the filtration of the zein solution and no visible zein precipitates on the surface of the nozzle. In further shown data, only processes, which were stable for the time required for further particle characterization, are discussed. For future works, hydrophobic coating of the nozzle surface was considered to avoid the precipitation issues.

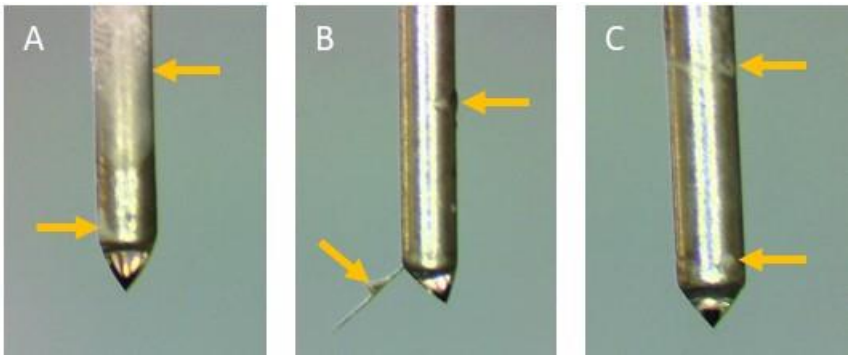

Figure 4.1. Representative images of a Taylor cone shape improving with increasing concentration/potential (from A to C, 1.75% (w/v), 2% (w/v), and 2.5% (w/v) zein in 80% (v/v) EtOH (aq.)) at a fixed flow rate and electrospray process issues such as zein precipitation on all three nozzles (pointed at with orange arrows).

In this study, a 0.5 µl/min flow rate was fixed for all experiments. The process parameters as well as the protein and ethanol concentrations used in each experiment are summarized in the Table 4.1. Each feed solution was electrosprayed at 13, 17.5, and 22.5cm needle tip - collector distance (further referred to as "distance"). Only the 5% (w/v) zein solution was not possible to electrospray at distance longer than 13 cm due to the increased precipitate formation corresponding to the increased potential required for the process. High voltage was also required at the 22.5 cm distance for an acidified 2.5% (w/v) zein solution due to its high conductivity. This experiment was not conducted due to the safety reasons. The voltage required to reach the stable Taylor cone increased with the zein concentration and the distance. Only outlier was observed, when 1.75% (w/v) zein solution was electrosprayed, requiring highest potential at the middle distance. No regular pattern in the electric current values measured in this study was found, which correlates with the findings in the literature.[189] The electrical field density decreases with the increasing distance, which causes decrease of the electrical current when voltage is fixed. However, increased voltage increases the electrical current following a current-voltage profile specific to the feed solution. Y. Si et al.[189] also reported the current-voltage profiles can change when polarity of the voltage is switched from positive to negative, showing a turning point in the profile followed by a steeper growth, which was suggested to be caused by a corona discharge. The current is also known to be increased with the feed solution's conductivity.[190] This was observed in the acidified 2.5% (w/v) zein solution at 13 cm, where the highest current was measured. However, the current significantly dropped at 17.5 cm for this solution, showing even lower value than 3% (w/v) zein solution in 80% (v/v) EtOH (aq.). The particle size was estimated from SEM and TEM images (using manual measurements in ImageJ software), where spherical and non-spherical particles forming clusters could be seen for all studied

concentrations of zein and electrospray parameters used (see Figure 4.2). The change in the distance but also the change in the concentrations of zein and/or ethanol and the change of conductivity did not cause any significant change in the particle diameter due to high standard deviation (13 – 37% and 34 – 52% of corresponding mean size calculated from SEM and TEM measurements, respectively). This as well as the irregularity of the particles' shape might be caused by the instability of the cone-jet mode not visible by the CCD camera and not detected by the current measurements. Low resolution of the SEM instrument, staining of the zein NPs with PTA for imaging with TEM (both causing a possible error in manual measurements), as well as placing the copper TEM grids directly on the collector (causing potential changes in the electric field) could have also affected the value of the standard deviation. Therefore, the size distribution was further studied in the particles electrosprayed from the 2.5% (w/v) zein solution in 80% (w/w) EtOH (aq.).

Table 4.1. Summary of electrosprayed zein solutions, process conditions, and estimated diameter of prepared particles. All solutions were double filtered (0.45 μm followed by 0.2 μm PES syringe filter) and electrosprayed vertically at room temperature and humidity, using 0.5 μl/min flow rate, and 30G nozzle.

Zein conc. (w/v)	Solvent	Distance (cm)	Voltage on nozzle (kV)	Voltage on collector (kV)	Current (nA)	Mean Diameter (nm)
1.75%	80% (v/v) EtOH (aq.)	13	5	-5.301	123.0	100 ± 30
		17.5	5	-8.491	144.0	101 ± 17
		22.5	5	-7.773	130.0	100 ± 15
2%		13	5	-6.628	114.2	108 ± 26
		17.5	5	-7.939	116.2	108 ± 19
		22.5	5	-12.373	210.4	101 ± 21
2.25%		13	5	-7.207	124.6	101 ± 19
		17.5	5	-6.857	141.6	93 ± 25
		22.5	5	-9.990	160.4	117 ± 26
2.5%	80% (v/v) EtOH (aq.)	13	5	-5.109	131.8	100 ± 15
		17.5	5	-6.899	150.2	126 ± 20
		22.5	5	-8.418	143.0	107 ± 25
	80% (w/w) EtOH (aq.)	13	4.500	-5	236.0	164 ± 73
		17.5	8.429	-5	220.6	139 ± 51
		22.5	10.622	-5	371.8	134 ± 64
	80% (w/w) EtOH (aq.) + HCl (0.009M)	13	8.148	-5	517.6	101 ± 34
		17.5	12.140	-5	424.8	97 ± 50
		22.5	too high conductivity → too high potential needed			
3%	80% (v/v) EtOH (aq.)	13	5	-5.688	138.6	137 ± 51
		17.5	5	-8.896	181.0	129 ± 17
		22.5	5	-8.639	451.8	140 ± 26
	80% (w/w) EtOH (aq.)	13	6.811	-5	164.6	156 ± 55
		17.5	8.450	-5	245.2	176 ± 65
		22.5	10.651	-5	259.8	150 ± 56
4%	80% (v/v) EtOH (aq.)	13	5	-6.088	156.8	131 ± 25
		17.5	5	-6.151	160.4	127 ± 35
		22.5	5	-7.975	177.8	140 ± 36
5%		13	5	-9.862	167.4	143 ± 31
		17.5	too high zein concentration → too many precipitate formation			
		22.5				

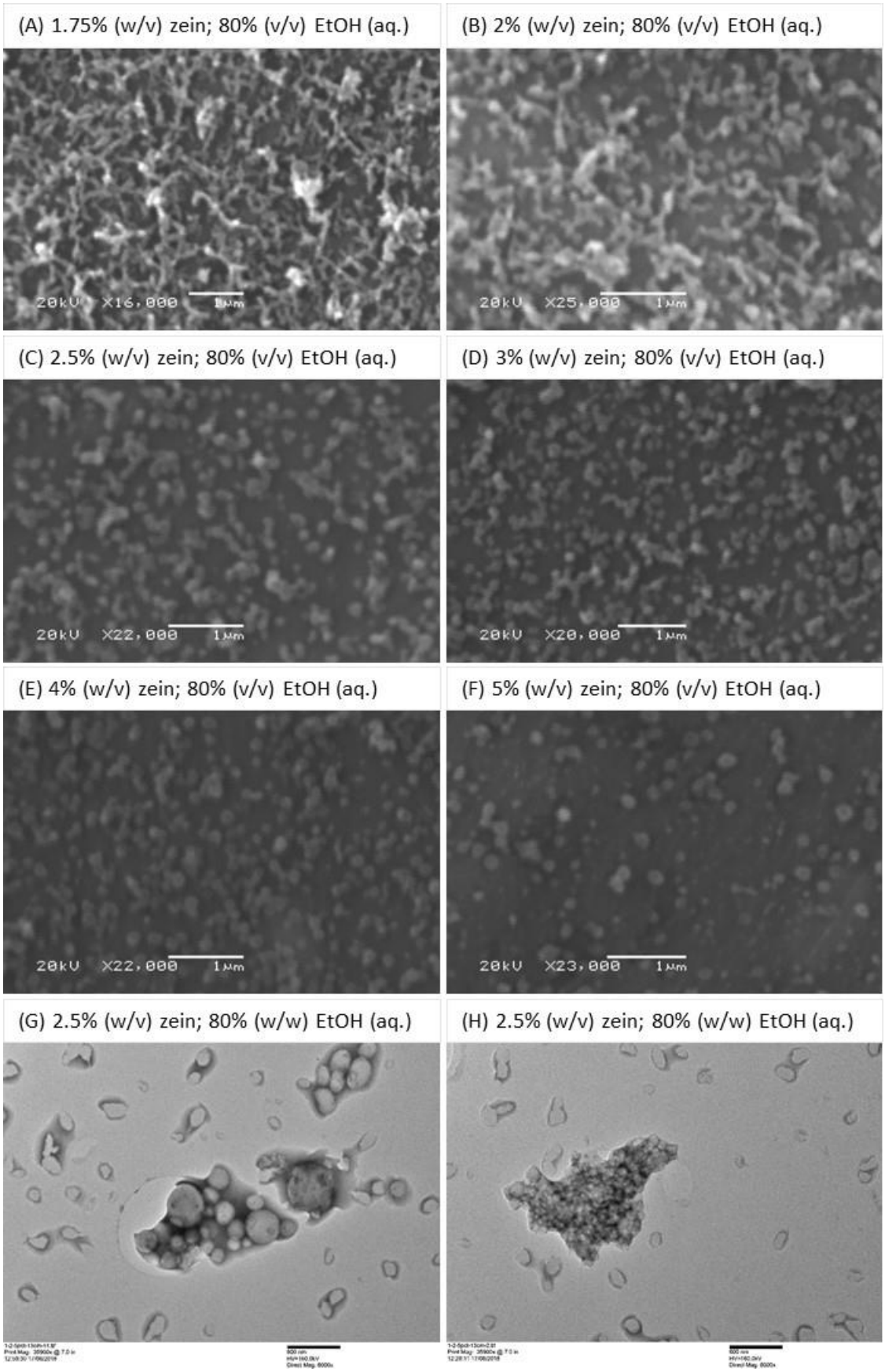

Figure 4.2. Representative SEM and TEM images of zein nanoparticles electrosprayed at 13 cm distance, showing both spherical and non-spherical particles with tendency to cluster and no significant difference in particle diameter when (A – F) zein and (G, H) ethanol concentration increased.

The Figure 4.3 A shows different diameter distribution profiles of the spherical particles electrosprayed from the 2.5% (w/v) zein in 80% (w/w) EtOH (aq.) depending on the nozzle-collector distance. However, in all three distances, the maximum at 100 – 200 nm and tailing of the distribution profile were observed. The distribution of the length/width ratio of the non-spherical particles showed little difference when nozzle-collector distance was changed (see Figure 4.3 B). Most of the non-spherical particles' length was less than 1.5 times longer than their width and a decreasing distribution profile with increased length/width ratio can be seen for all three distances.

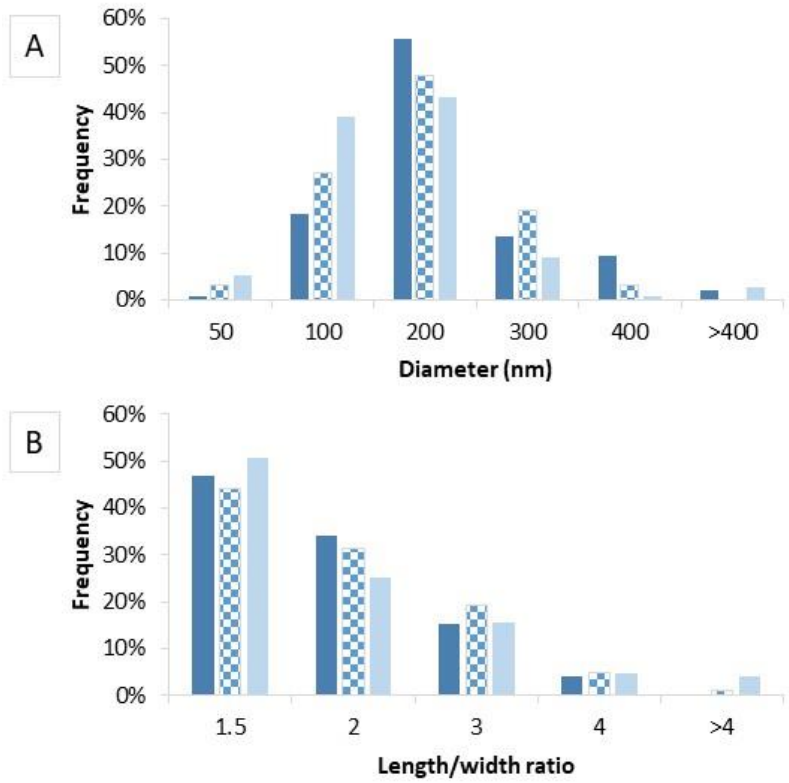

Figure 4.3. Distribution of (A) spherical particle diameter and (B) length/width ratio of non-spherical particles electrosprayed from double filtered 2.5% (w/v) zein in 80% (w/w) EtOH (aq.) solution at 13cm (solid dark blue), 17.5 cm (checked), and 22.5 cm (solid light blue) nozzle-collector distance.

This formulation electrosprayed at 13 cm was selected as a representative sample for physico-chemical characterization of the zein EHDA particles. The thermal analysis showed the EHDA particles decomposed faster than pure zein powder, when 10 ± 1% weight loss was found at 267 °C and at 280 °C, respectively (see Figure 4.4). This could be associated with the higher surface energy as well as faster water uptake (~3% weight loss at 100 °C in the EHDA particle sample compared to pure zein with weight loss of ~1%) found in the nanoparticle sample due to the increased surface to volume ratio. In Figure 4.5, no significant

depression of the particles' glass transition (mid-point at 160 ± 1 °C) was observed when compared to pure zein powder (mid-point at 162 ± 1 °C).

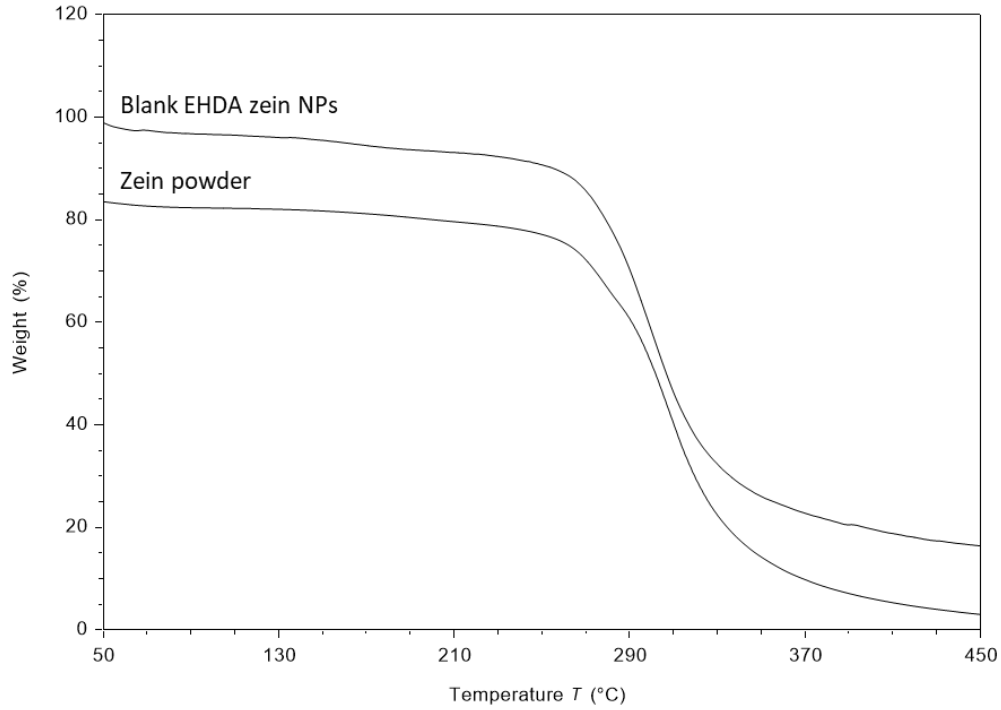

Figure 4.4. A TGA thermogram of blank electrosprayed (EHDA) zein NPs (2.5% (w/v) zein in 80% (w/w) EtOH (aq.)) showing a faster rate of decomposition (10 ± 1% weight loss at 267 °C) compared to pure zein powder (10 ± 1% weight loss at 280 °C).

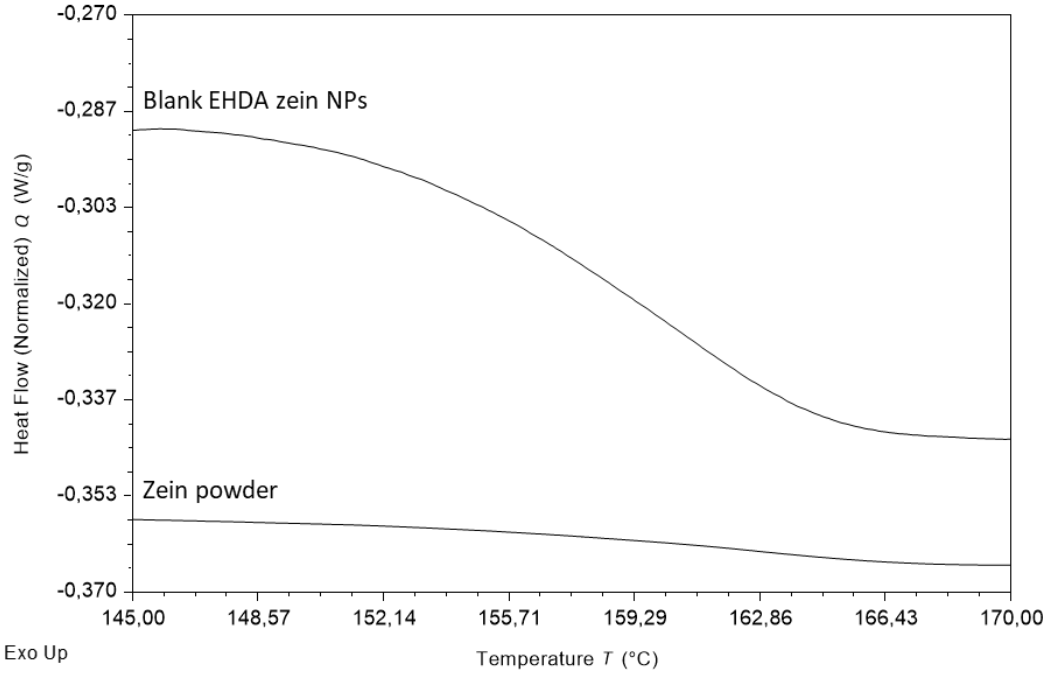

Figure 4.5. A DSC thermogram of blank electrosprayed (EHDA) zein NPs (2.5% (w/v) zein in 80% (w/w) EtOH (aq.)) showing no significant glass transition depression (mid-point at 160 ± 1 °C) compared to pure zein powder (mid-point at 162 ± 1 °C).

The Figure 4.6 shows an ATR-FTIR analysis of the EHDA particles compared to pure zein powder and lists the important protein bands and their relative intensities in both samples. Significant shifts of the amide I and amide II (~1530 cm^{-1}) peaks to higher wave numbers were observed in the EHDA particles. Amide I peak is associated with the C=O stretching, while the amide II peaks result predominantly from in-plane N-H bending vibrations accompanied with C-N and C-C stretches.[191] The most intense band in both spectra was the amide I. The intensities of the rest of the bands decreased in the EHDA particles' spectrum compared to the pure zein spectrum. The amide III is predominantly assigned to in-phase combination of N-H in-plane-bending and C-N stretching. This band is very sensitive to protein secondary structure changes. Although S. Cai and B. R. Singh[191] claims amide III peaks in the range of 1245 – 1220 cm^{-1} correspond to β-sheets, these peaks cannot be used as a single determiner of the protein secondary structure, as many different vibrations could contribute to these peaks. However, together with the shift of the amide I peak, this suggests the decrease of β-sheets and increase of α-helices in the zein secondary structure after electrospraying from 80% (w/w) EtOH (aq.).[192]

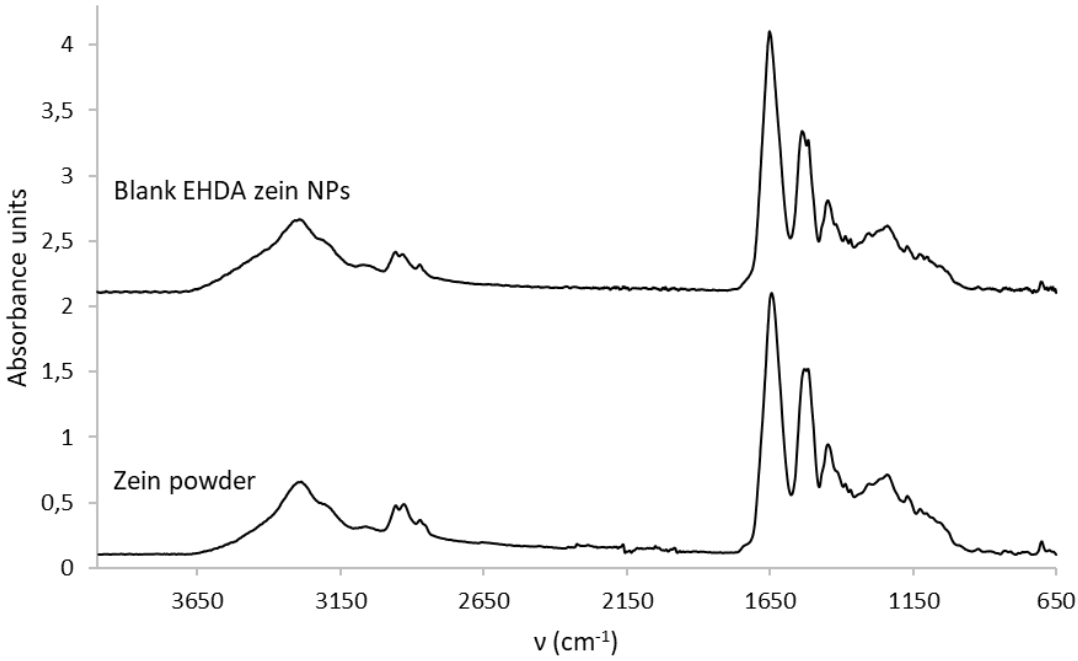

Protein Band	Pure zein		EHDA zein NPs	
	v (cm^{-1})	RI (%)	v (cm^{-1})	RI (%)
Amide I, ~1650 cm^{-1}	1645	100	1652	100
Amide II, ~1530 cm^{-1}	1529	72	1538	62
Amide II, ~1515 cm^{-1}	1518	72	1516	58
C-N Stretch, ~1445 cm^{-1}	1448	45	1447	35
Amide III, ~1240 cm^{-1}	1240	34	1241	26

Figure 4.6. ATR-FTIR spectra and a table of important protein bands (significant shifts highlighted in grey) observed in blank electrosprayed (EHDA) zein NPs (2.5% (w/v) zein in 80% (w/w) EtOH (aq.)) and pure zein powder, suggesting a secondary structure of zein changed after electrospraying.

Drug loaded zein particles were not further prepared by EHDA due to its extremely low yield caused by low flow rate and concentration of protein required to obtain a stable cone-jet mode. The drug loading efficiency and the drug release studies would not be possible to perform due to the limits of detection of quantitative methods.

4.3.2 Precipitated zein and 5-ASA loaded zein nanoparticles

Because of a low throughput of electrospray, precipitation method with higher yield was further used to prepare NPs. Following the ternary phase diagram for zein solubility in ethanol and water (see Figure 4.7)[145], 5% (w/v) zein solution in 70% EtOH (aq., v/v) was tested to develop the most suitable anti-solvent method.

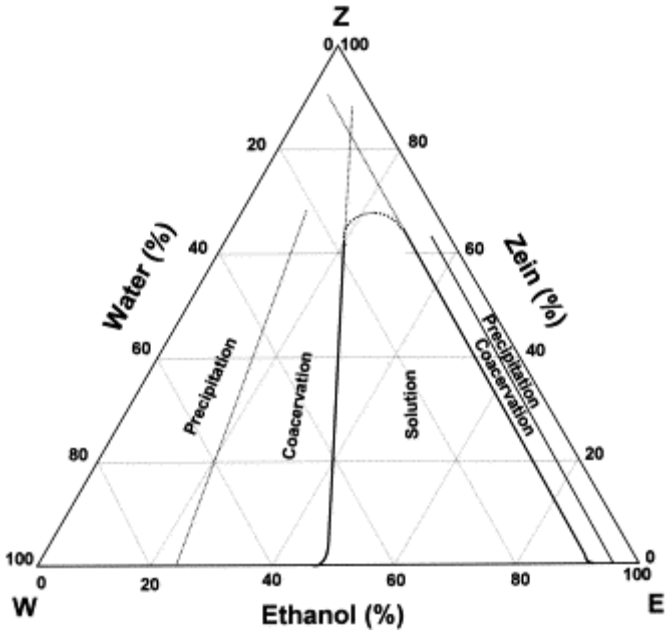

Figure 4.7. Ternary phase diagram for the solubility of zein in ethanol and water.[145]

DLS was selected as a quick screening assay. First, the 5% (w/v) zein solution in 70% EtOH (aq., v/v) was analysed before precipitation occurred (see Figure 4.8). The DLS method was set using tabled values for viscosity, refractive index, and dielectric constant of both ethanol and water at 20 ˚C.[193] The analysis showed two broad overlapping peaks in the range of 122 – 3091 nm (dark blue line) in the cloudy solution. Therefore, the solution was filtered through a PES (0.45 μm) syringe filter. However, the solution still was not clear of any particles within this range after the filtration (light blue line). The second filtration step was introduced, using the PES (0.2 μm) syringe filter. This step reproducibly filtered the zein solution, so the particles present were only in the 5 – 44 nm range (black line). Double filtered 5% (w/v) zein solution in 70% EtOH (aq., v/v) was used for all following experiments to ensure the particles found in the precipitated nanosuspensions were not present in the zein solution before mixing with anti-solvent.

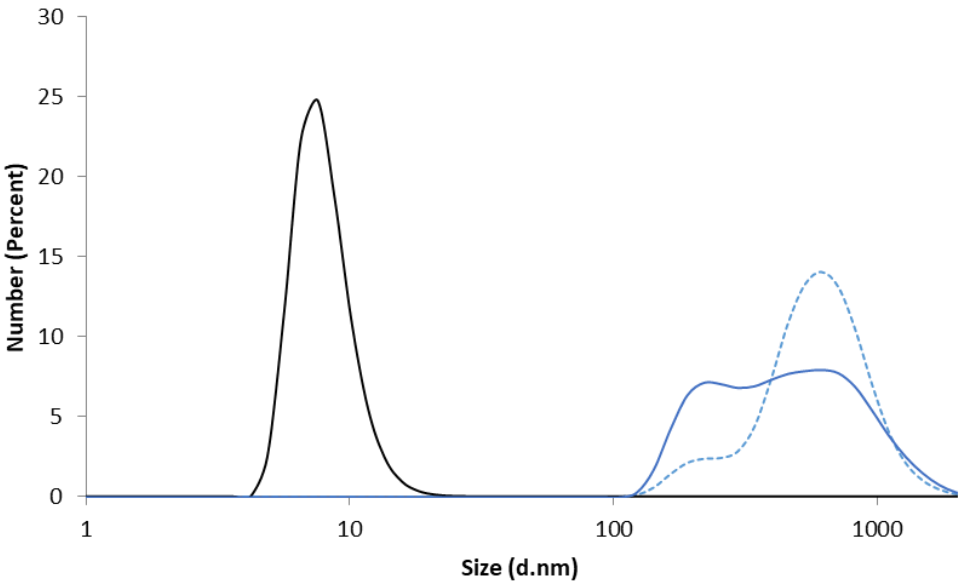

Figure 4.8. The effect of filtration of the 5% (w/v) zein solution in 70% EtOH (aq., v/v) (dark blue line), using a PES (0.45 µm) syringe filter (light blue dashed line) first and a PES (0.2 µm) syringe filter (black line) as a second step.

A precipitation ratio of solvent and anti-solvent was then screened to ensure the highest concentration of the NPs was obtained. One mL of the double filtered clear yellow zein solution was transferred and vigorously mixed using the micro pipette with corresponding volume of MQ water to reach 7%, 7.78%, 8.75%, 14%, and 23.34% EtOH (v/v) in the milky nanosuspensions. The DLS method was amended for each of the EtOH concentration. The increasing concentration of EtOH in the nanosuspensions did not show a significant effect on the particle size (see Figure 4.9). The polydispersity index (PdI)[194] was lower than 0.15 in all cases. Higher concentration of the EtOH was not studied to not overstep the border between precipitation and coacervation. Therefore, mixing the zein solution with the MQ water in the 1:2 volumetric ratio to reach 23.34% of EtOH in the final nanosuspension was selected as the preparation method to reach the highest possible concentration of the NPs.

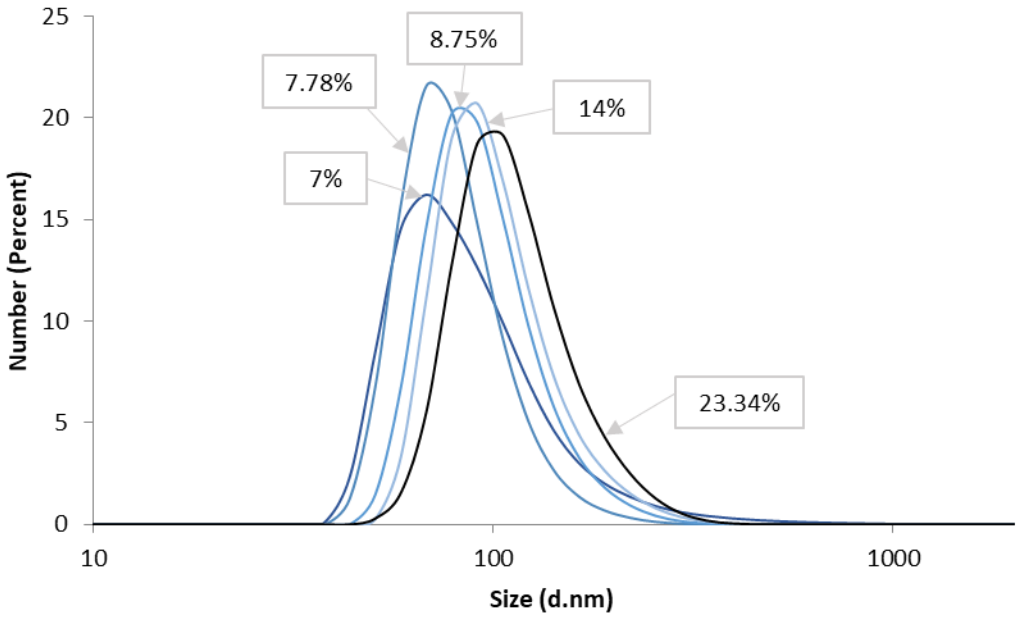

Figure 4.9. Size of the precipitated zein NPs depending on the concentration of EtOH in the nanosuspension, suggesting EtOH concentration does not affect the particle size significantly (black line for 23.34% EtOH).

The 5-ASA was selected as a model drug due to its low solubility in water and therefore, its possibility to co-precipitate with zein. 5-ASA is readily soluble in acidified solvents, therefore, 0.3M HCl solution in 70% EtOH (aq., v/v) was used as an initial solvent for the model drug. A solution of 25 mg/ml concentration was analysed by DLS which showed a single peak at 220 nm, potentially belonging to the impurities coming from the raw 5-ASA powder with 99% purity as this peak was observed in 10 times lower concentration of the drug as well and therefore, could not be assigned to supersaturation. The 5-ASA solution was filtered through a syringe filter with pore diameter of 100 nm. The solution was clear and beige, which is caused by the colour of the 5-ASA powder (beige-brown to grey). The oxidation process was studied by a visual comparison of the colours of the solutions in an open flask and in a flask, which was filled with argon gas and sealed, both at room temperature. A change of colour was observed in the solution in the open flask after 8 days (light brown), while the colour of the solution in the argon filled flask stayed unchanged. This corresponds with the findings of J. Jensen et al. (1992) who described autooxidation of 5-ASA in aqueous solutions as a formation of self-coupled polymeric species.[195] The precipitation properties of the drug solution were tested following the same anti-solvent method as in the preparation of the blank zein NPs and analysed by DLS. The filtered 5-ASA solution before precipitation showed a peak at 0.7 ± 0.1 nm, which was shifted to 369 ± 121 nm after addition of the MQ water (see Figure 4.10). The peak after precipitation

is irregularly shaped, suggesting high degree of polydispersity. However, the size is significantly different to the blank zein NPs, suggesting the DLS method could be potentially used as a quick indicator of successful loading of the drug into the NPs. The drug loaded zein NPs (further referred to as 5-ASA-zein NPs) were prepared by mixing corresponding volumes of double filtered zein solution and filtered 5-ASA solution to obtain 5%, 10%, and 20% drug loading ratios, resulting in different zein and HCl concentration in each drug loading percentage. The size of the particles in the mixture of 5-ASA and zein solutions (referred to as 5-ASA-zein solution) was checked by the DLS and showed a peak at 7.5 nm, corresponding to the peak of double filtered zein solution. 5-ASA-zein solution was precipitated using the same anti-solvent method as in the blank zein NPs and 5-ASA particles preparation, showing a peak at 85 ± 29 nm for 5% drug loading, which can be seen in Figure 4.10.

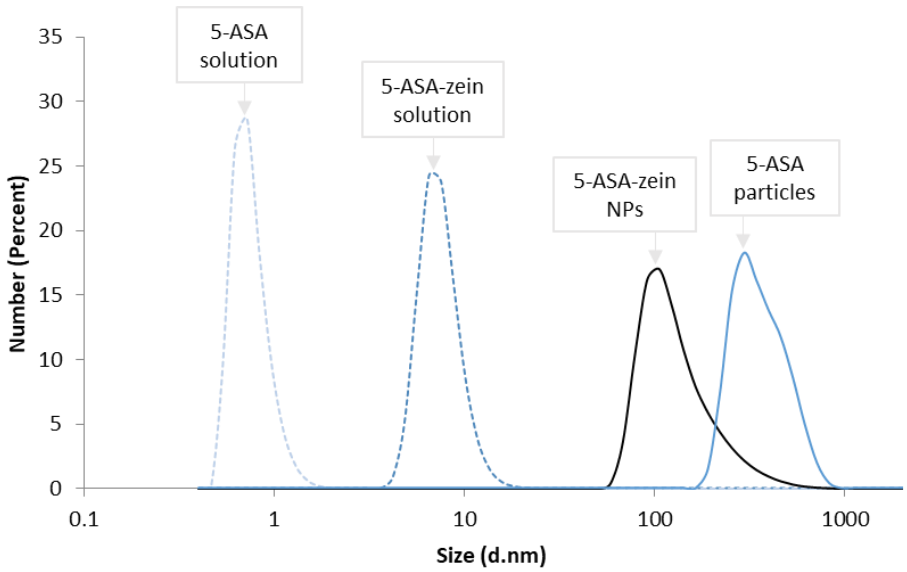

Figure 4.10. Size distribution of particles found in filtered 5-ASA solution, 5-ASA-zein solution, and precipitated suspensions of 5-ASA-zein NPs and 5-ASA precipitates measured by DLS shows four significantly different peaks, suggesting the 5-ASA was loaded into the zein particles.

The effect of both protein and HCl concentration on the size of the blank zein NPs was further studied by DLS. Following the mixing pattern used in the preparation of drug loaded NPs, 5 samples with decreasing concentrations of protein and increasing concentrations of HCl were prepared and compared to samples of the same protein concentration without acidification. Figure 4.11 shows the protein concentration on its own does not affect the size of the particles significantly (see the solid bars). However, the increased concentration of HCl combined with decreasing concentration of protein shows a potential for size control of the zein particles (see the chequered bars). There was no significant difference in size of the

particles between the non-acidified and acidified particles in the range of 15 – 12 mg/ml of zein, corresponding to the 0.009 – 0.0027M HCl concentration in the nanosuspensions and mimicking the conditions for preparation of 5 – 15% drug loaded NPs. A significant difference in between the sizes of the acidified and non-acidified particles could have been seen at the 11 and 6 mg/ml of zein, mimicking 20 and 50% drug loading conditions, respectively. There was also a significant difference in between the sizes of the acidified particles themselves in this range as well as compared to the 15 mg/ml zein concentration (mimicking 5% drug loading conditions), suggesting decreased pH leads to the increased size of the particles as well as their polydispersity level. This corresponds with findings of J. Bouman et al.,[196] who observed higher hydration rates and swelling capacity values for zein in pH = 1, compared to the pH = 6.8. From this point, drug loaded 5-ASA-zein NPs were compared to the corresponding acidified blank zein NPs due to the potential pH effect on the nanoparticle structure.

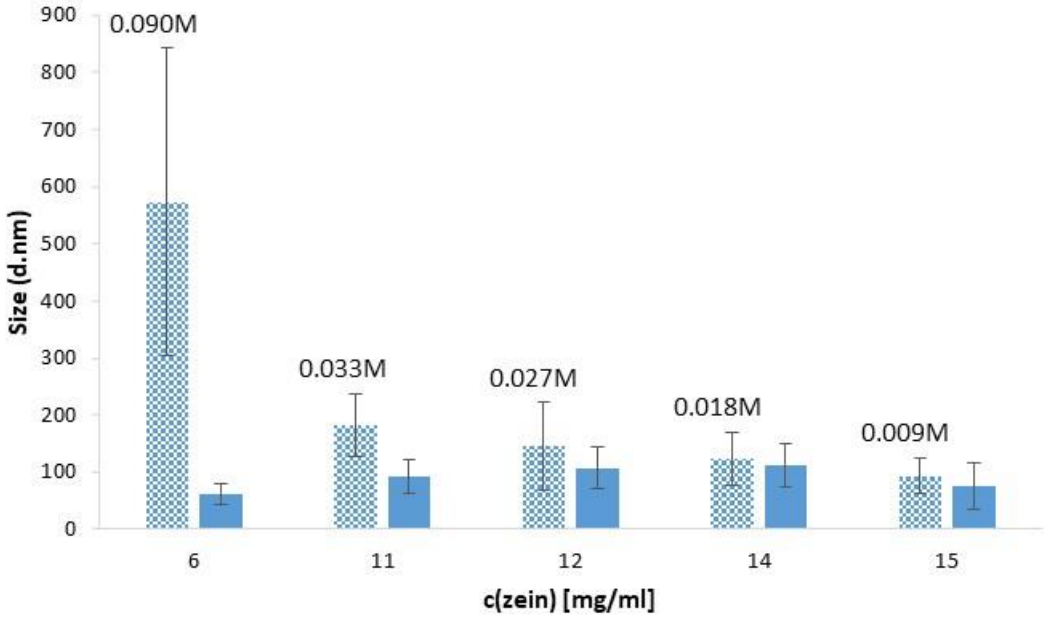

Figure 4.11. Influence of zein and HCl concentrations on blank zein NPs size, showing a significant particle size increase with pH drop from 0.033M to 0.090M HCl. No significant effect of protein concentration was observed in this zein concentration range.

In the Table 4.2, sizes of the blank acidified and drug loaded 5-ASA-zein nanoparticles measured by DLS are compared, with no significant difference in between the sizes of the drug loaded NPs and their corresponding blank. However, gradual increase in the mean size as well as the standard deviation can be observed with the increased HCl concentration in both drug loaded and blank NPs with a significant difference found in between 5 and 20%

loading (corresponding blanks). This observation suggests the addition of the 5-ASA does not affect the size of the NPs and the pH is the sole controlling factor.

Table 4.2. DLS size comparison of blank (acidified) and drug loaded 5-ASA-zein NPs.

Drug Loading	Blank NPs (d.nm)	5-ASA-zein NPs (d.nm)
5%	93 ± 31	85 ± 29
10%	123 ± 47	125 ± 45
20%	183 ± 55	190 ± 61

With the further step – an incorporation of the 5-ASA-zein NPs into the HPMCAS fibers (see Chapter 5) - in mind, the stability of the double filtered zein solutions, prepared drug loaded nanosuspensions and their corresponding blanks was tested by DLS at room conditions. No particles bigger than 50 nm were found in the double filtered zein solution after 7 days (see Figure 4.12). Immediately after filtration, the PdI was 1, even though only single sharp peak at 7.5 nm was found in the analysis. This high PdI could be assigned to some particle sizes found outside the instrument's cut-off range, most likely few large particles which are given higher weight in the z-average and consequently PdI calculations. The PdI was gradually decreasing over the course of the 7 days, suggesting the large particles were settling down.

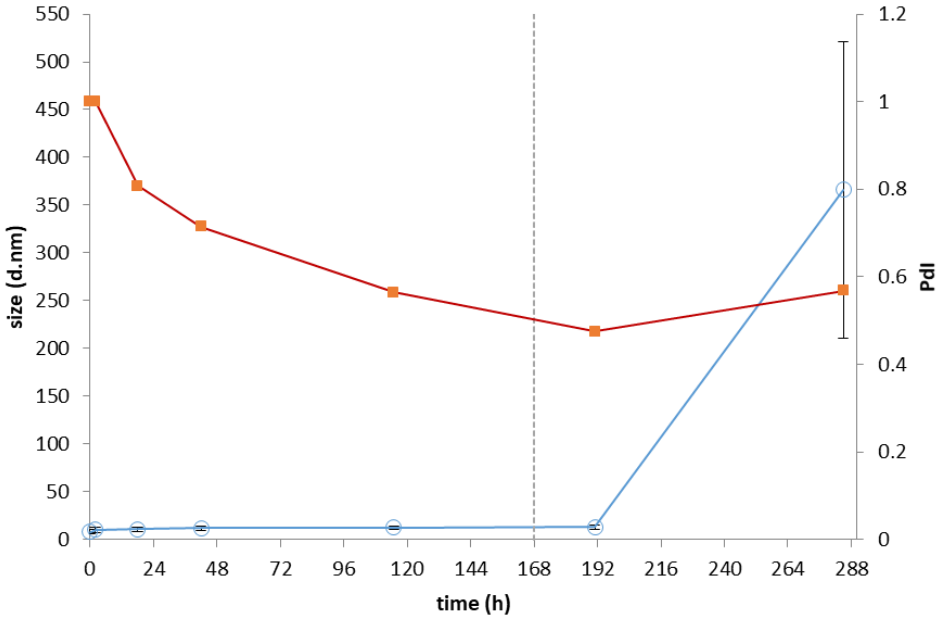

Figure 4.12. Stability of double filtered 5% (w/v) zein solution in 70% EtOH (aq.) measured by DLS, showing stable size of the particles (blue circles) and decreasing PdI (red squares) for at least 7 days (168 hours).

Stability of the blank non-acidified zein NPs is described in Figure 4.13, showing both the size (blue crosses and line) and the PdI (orange squares and line) of the nanosuspension are stable over the course of two weeks, after which the PdI increases above the value of 0.2.

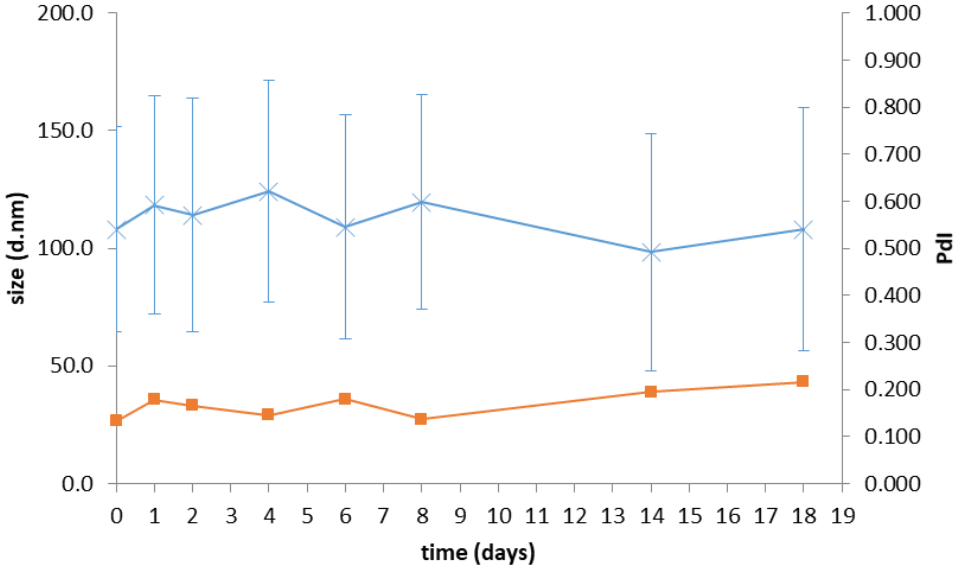

Figure 4.13. DLS stability study of blank non-acidified zein NPs, showing the particle size (blue crosses) and the PdI (orange squares) were stable for 14 days (PdI ≤ 0.2).

On the other hand, the 5-ASA solution polymerises by the oxidation process as mentioned earlier, and therefore the 5-ASA-zein solution was always prepared from freshly dissolved and filtered 5-ASA solution, followed by immediate preparation of the drug loaded NPs. The stability of their mean size (black line and filled markers) is described in Figure 4.14, compared to the corresponding acidified blank zein NPs (grey line and unfilled markers). There was no significant difference in the mean size found over the period of 8 days in any of the observes sample. Also, no significant difference in the size of the particles was found when corresponding pairs of blank and drug loaded nanosuspensions were compared (see Table 4.3). Although, this data could suggest the stability of the nanosuspensions over the 8 days period, the nanosuspensions were always prepared fresh when intended for further processing. This is because of the 5-ASA oxidation as well as the value of the standard deviation/polydispersity of the samples, which is too large to significantly prove whether any changes such as drug leak could have happened over the time.

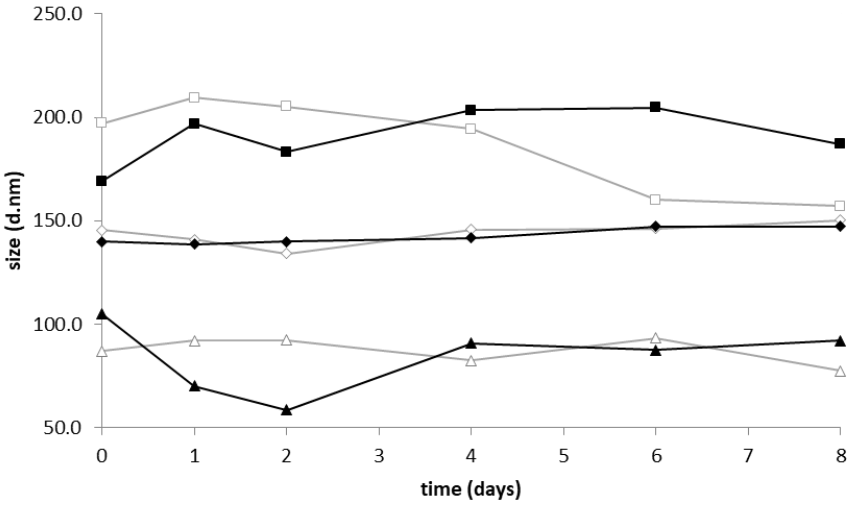

Figure 4.14. DLS stability study of 5-ASA-zein NPs (black line) mean size compared to the corresponding acidified blank zein NPs (grey line); the particle size of the 5%, 10%, 20% drug loading/corresponding HCl concentrations in blank NPs is represented by solid/hollow triangles, diamonds, and squares, respectively.

Table 4.3. Summary of mean particle size and standard deviation (nm) of drug loaded zein NPs and their corresponding acidified blanks measured by DLS.

Day	Blank zein NPs (5%)	5-ASA-zein NPs (5%)	Blank zein NPs (10%)	5-ASA-zein NPs (10%)	Blank zein NPs (20%)	5-ASA-zein NPs (20%)
0	87 ± 33	105 ± 36	145 ± 42	140 ± 53	197 ± 59	169 ± 64
1	92 ± 36	70 ± 38	141 ± 52	139 ± 54	210 ± 95	197 ± 70
2	92 ± 42	58 ± 35	134 ± 59	140 ± 54	205 ± 73	183 ± 120
4	82 ± 39	91 ± 36	146 ± 52	142 ± 47	194 ± 61	203 ± 84
6	93 ± 47	88 ± 53	146 ± 37	147 ± 47	160 ± 36	205 ± 59
8	77 ± 43	92 ± 49	150 ± 57	147 ± 55	157 ± 42	187 ± 62

Zeta potential of the zein solution before precipitation was measured to compare with the zeta potential of the nanosuspensions. Zein solution in aqueous 70% (v/v) ethanol showed a single broader peak of zeta potential at 1.99 mV compared to a sharp peak at 25.3 mV measured for non-acidified blank zein NPs. However, zeta potential of acidified solutions and nanosuspensions was not possible to measure due to their high conductivity.

All nanosuspensions were imaged by TEM to study the shape of the particles (see Figure 4.15). Phosphotungstic acid (PTA) solution at pH = 7 was used to stain the protein NPs. Spherical, polydisperse particles were observed in all samples, showing majority of the particles having smooth surface. A porosity could have been observed in some, especially

larger particles. When the same PTA staining technique was used for the 5-ASA precipitates sample (drug on its own), no particles were found on the grid. Therefore, a vapour staining method, using RuO_4, was used to stain the 5-ASA particles. Round structures with the 70 ± 36 nm diameter were observed after the vapour staining. No bigger crystals were found on the grid, while highly irregular peak at 369 ± 121 nm was observed for the same nanosuspension in DLS.

The nanosuspensions were further freeze dried to obtain a powder form for further physico-chemical characterisation of each sample. These were imaged by SEM to observe whether the freeze drying affects the size and the shape of the particles. The particles stayed spherical after freeze drying, while the 5-ASA crystallised into the large plates shaped crystals. Beside spherical particles, large 5-ASA crystals were found in 5-ASA-zein NPs (10%) and 5-ASA-zein NPs (20%), suggesting the drug was either not fully loaded into these protein particles or the drug leaked from the particles during the freeze drying (see Figure 4.17). The porosity of the protein particles, both blank and drug loaded, was more visible in the freeze dried samples, even in the particles with smaller size. This suggests the form of drying could have impacted the physical structure of the protein nanoparticles, even though the size of the particles did not change significantly.

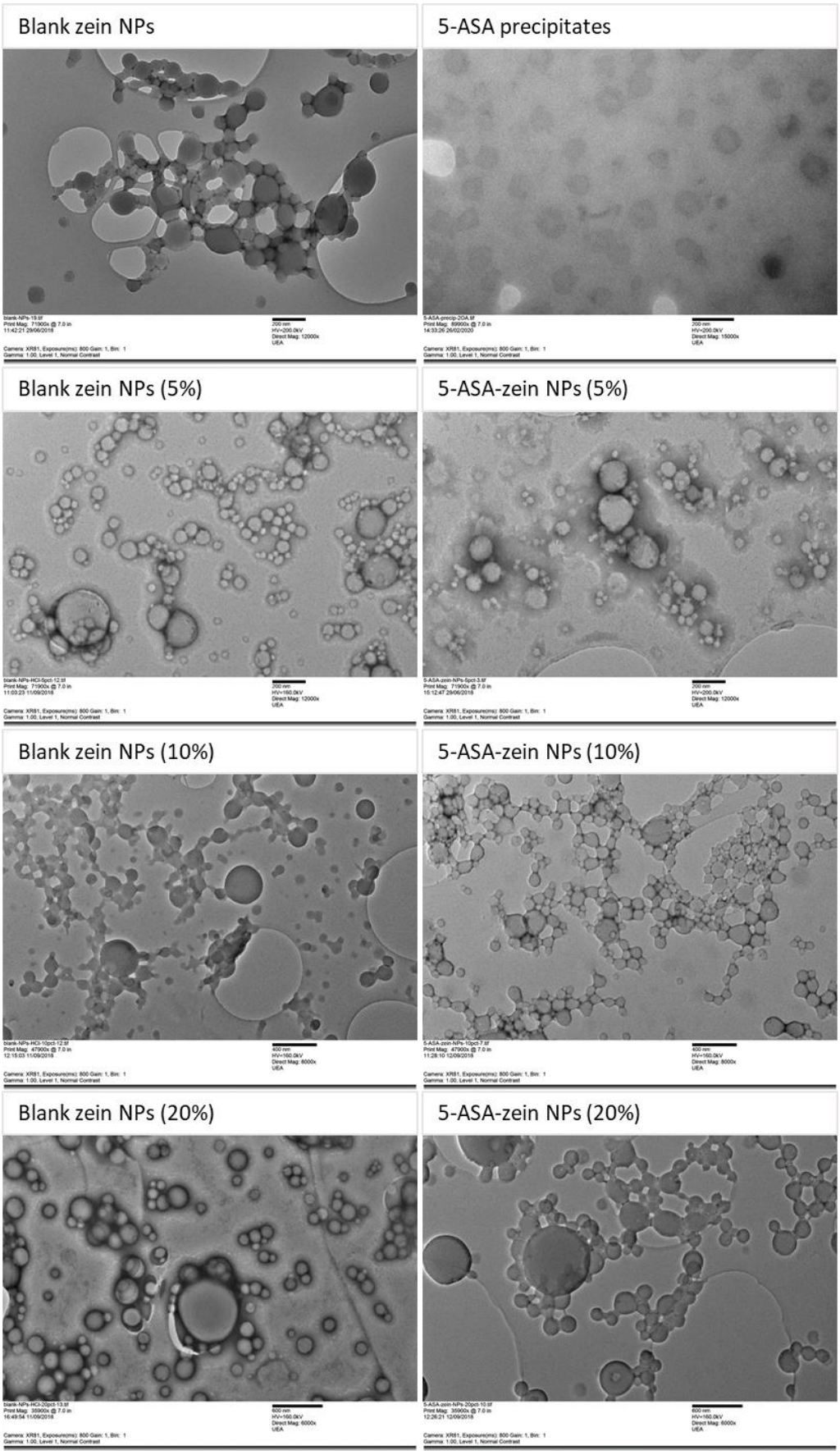

Figure 4.15. Representative TEM images of suspensions of blank zein NPs, 5-ASA precipitates, 5-ASA-zein NPs (5%, 10%, 20%) and their corresponding blanks.

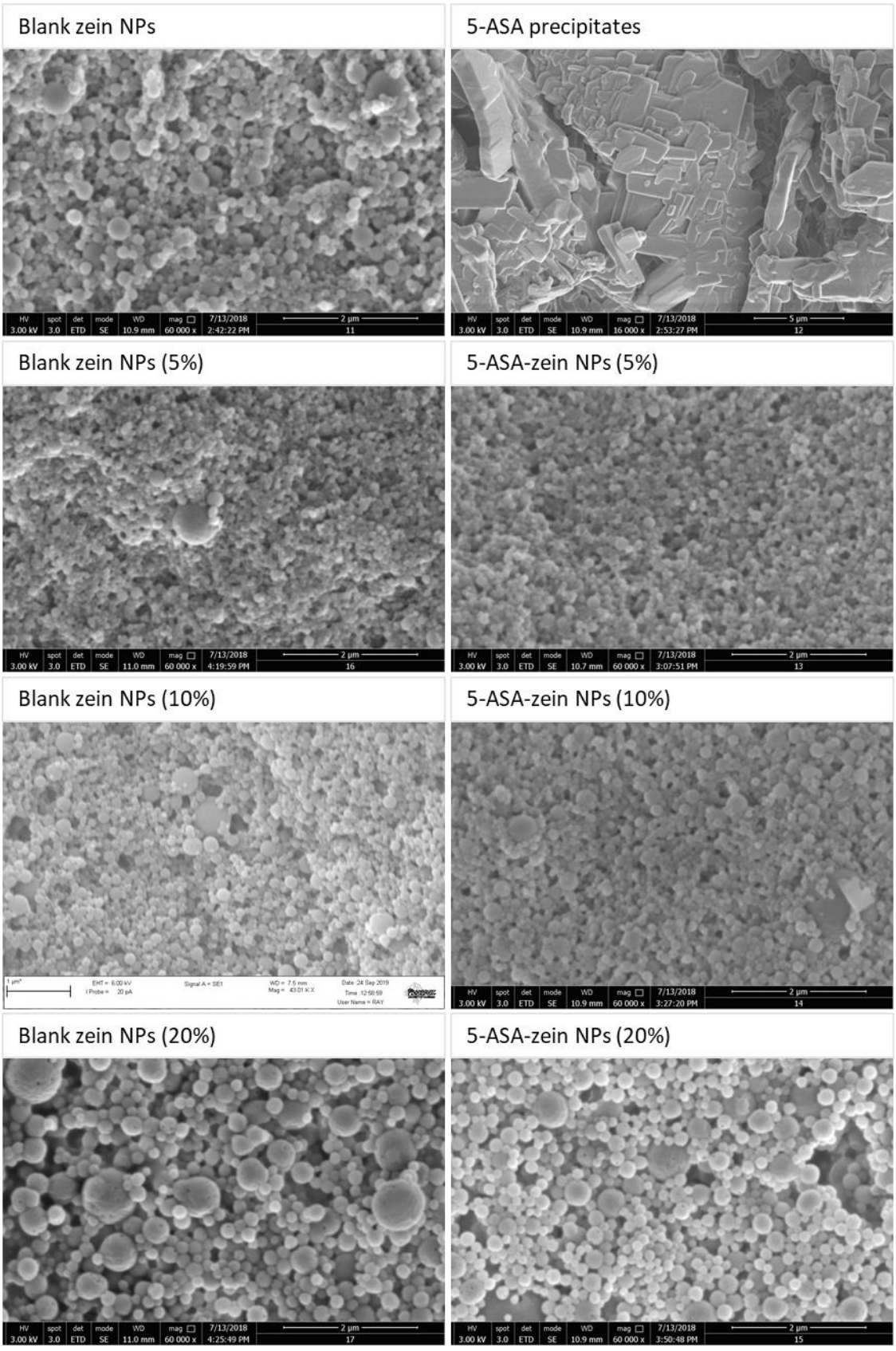

Figure 4.16. Representative SEM scans of freeze dried blank zein NPs, 5-ASA precipitates, 5-ASA-zein NPs (5%, 10%, 20%) and their corresponding blanks.

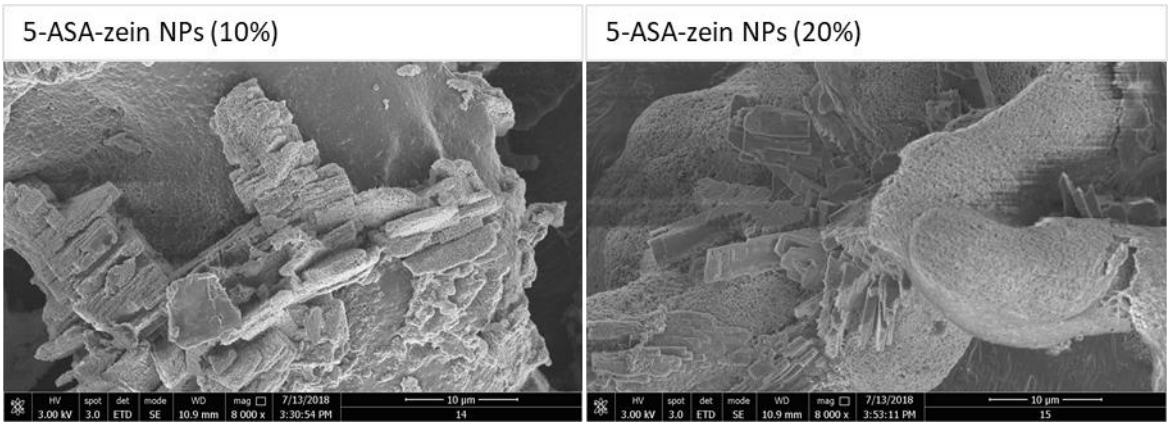

Figure 4.17. Representative SEM scans of freeze dried 5-ASA-zein NPs (10% & 20%), showing presence of 5-ASA crystals.

The mean size of all the protein particles (blank and drug loaded) was measured from both TEM and SEM images manually, using ImageJ software. The data obtained from all three different techniques measuring size, including DLS, showed no significant difference in the mean size of the particles, suggesting the size of the particles is not significantly affected by the staining or freeze drying (see Figure 4.18). This also proved the DLS being an effective quick method for the particle size determination.

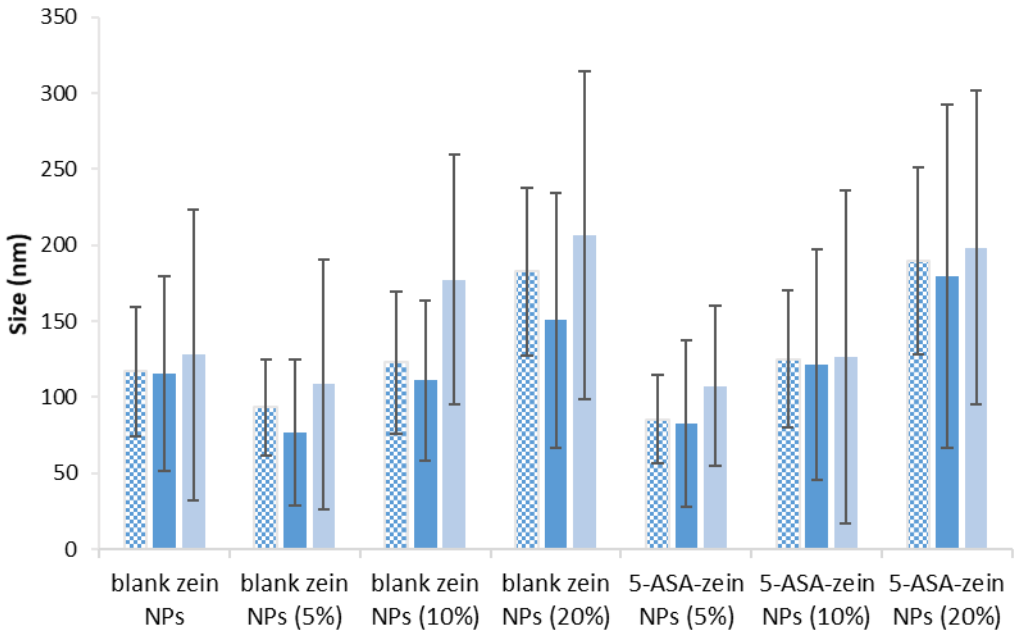

Figure 4.18. Size measurement by DLS (chequered), TEM (solid dark blue), and SEM (solid light blue), showing no significant difference in between DLS and TEM measurements of the nanosuspensions as well as in between the nanosuspensions and freeze dried NPs measured by SEM.

Due to the acidification of the 5-ASA solution, the form of the created salt had to be identified. For this purpose, the acidified 5-ASA solution in 70% EtOH (aq., v/v) as well as

the precipitated suspension of the drug in 23.34% EtOH (aq., v/v) were freeze dried to obtain their powder form, further referred to as 5-ASA solution and 5-ASA precipitates, respectively. First, the thermal analysis was performed. 5-ASA is known for its high thermal stability and decomposition before its melting occurs.[134] Therefore, the DSC technique was not used in the 5-ASA form determination. However, TGA showed a two-step degradation for both 5-ASA solution and 5-ASA precipitates, compared to a single step degradation of 5-ASA powder (see Figure 4.19). The first step of the degradation shows 19 – 20% of the weight loss in both cases, which corresponds with the molecular mass ratio of the HCl in the 5-ASA chloride salt (19.44%). This could be potentially used as a drug encapsulation efficiency quantification method. The 7 °C difference in between the first step decomposition onsets of 5-ASA solution (162 °C) and 5-ASA precipitates (155 °C), suggests two different forms of the salt being present in the two samples. There was no significant loss of free water (<0.5% weight loss at 100 °C) observed in either of the three samples.

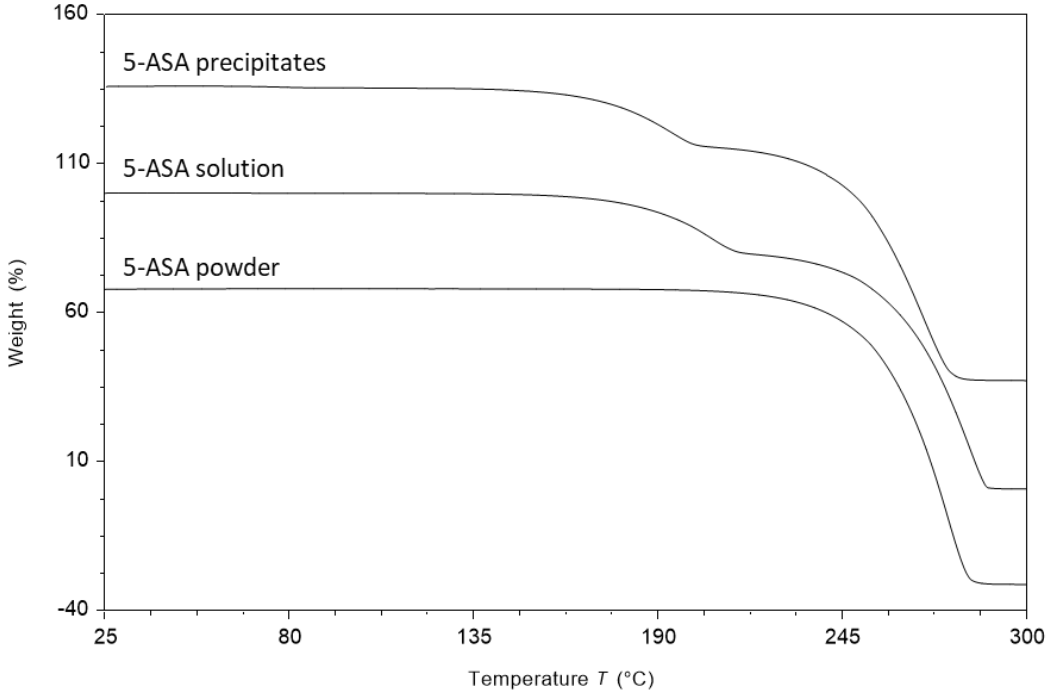

Figure 4.19. TGA thermograms of freeze dried 5-ASA solution and 5-ASA precipitates compared to pure 5-ASA powder, suggesting the first decomposition steps of 5-ASA chloride salts correspond to the weight loss of HCl.

All three powders were further characterised by ATR-FTIR (see Figure 4.20 and Table 4.4). The absorption bands of 5-ASA powder corresponded with findings in literature.[134] The assignments of the 5-ASA powder bands are as follows: O-H stretching associated with the hydroxyl groups at 2776 cm^{-1} (hydrogen bond in COO-H), C=O stretching at 1645 cm^{-1} (carboxylic group), NH_2 bending at 1616 cm^{-1}, C-C stretching mode at 1485 and 1447 cm^{-1}, O-H deformation of the hydroxyl groups at 1375 and 1352 cm^{-1}, in plane bending mode at 1263 – 1190 cm^{-1}, C-O stretching at 1130 cm^{-1}, and C-H bond out of plane bending mode as well as ring deformation of the aromatic group at 808 – 685 cm^{-1}. Most of these bands were significantly shifted in 5-ASA solution and 5-ASA precipitates samples and showed different relative intensities, suggesting a primary amine chloride salt was formed by the acidification process. These two samples showed absorption bands at the same wavenumbers, however the relative intensities of the bands decreased in all the 5-ASA precipitates' bands but the one at 1207 cm^{-1} (100% intensity). This change of relative intensities could suggest a different crystal lattice structure since no significant moisture difference was found in the TGA analysis.

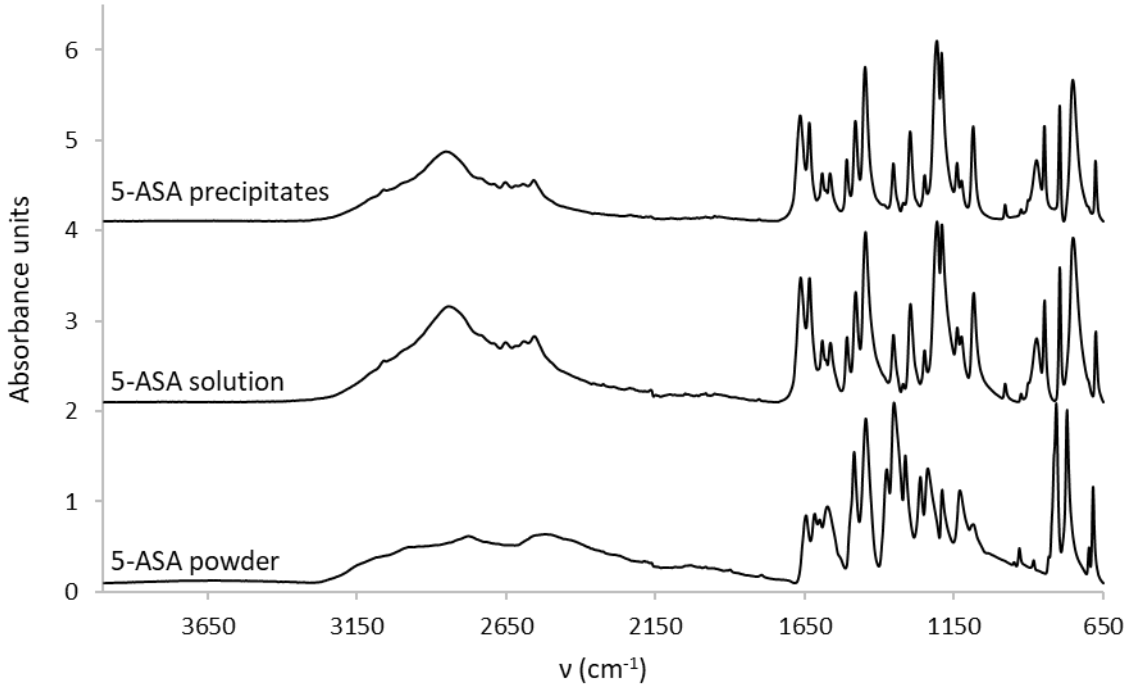

Figure 4.20. ATR-FTIR spectra of freeze dried 5-ASA solution and 5-ASA precipitates showing significant band shifts compared to pure 5-ASA powder, suggesting a primary amine chloride salt was formed by the acidification process.

Table 4.4. Summary of the ATR-FTIR absorption bands' wave numbers (ν) and their relative intensities (RI); showing assigned peaks highlighted in grey.

5-ASA		**5-ASA solution**		**5-ASA precipitates**	
***v* (cm^{-1})**	***RI***	***v* (cm^{-1})**	***RI***	***v* (cm^{-1})**	***RI***
Broad overlapping peaks at ~ 3300 – 1680 cm^{-1}		Broad overlapping peaks at ~ 3300 – 2250 cm^{-1}			
-		3059	23%	3059	18%
2776	26%	2845	53%	2845	39%
-		2652	33%	2652	22%
		2618	31%	2618	20%
		2592	34%	2592	21%
		2556	37%	2556	23%
1645	37%	1666	69%	1666	59%
1616	38%	1634	69%	1634	55%
1601	35%	1591	34%	1591	27%
1574	42%	1565	33%	1565	27%
-		1509	36%	1509	34%
1485	73%	1480	61%	1480	56%
1447	91%	1448	93%	1448	86%
1375	63%	-			
1352	100%	1354	37%	1354	32%
1313	71%	1297	54%	1297	50%
1263	59%	1248	29%	1248	26%
1238	64%	1207	100%	1207	100%
1190	52%	1191	98%	1191	93%
1130	51%	1140	41%	1140	32%
-		1124	36%	1124	23%
1086	33%	1086	60%	1086	53%
949	12%	980	10%	980	9%
932	19%	-			
883	13%	874	35%	874	34%
833	15%	847	56%	847	53%
808	100%	797	74%	797	64%
771	96%	752	91%	752	78%
698	20%	-			
685	53%	676	39%	676	33%

Therefore, PXRD analysis was performed. In Figure 4.21, PXRD diffractograms of the three samples were compared to the XRD patterns of 5-ASA, 5-ASA Cl^-, and 5-ASA Cl^- . H_2O, obtained from Cambridge Crystallographic Data Centre database (CCDC). Despite the poor resolution of the data obtained, the broadened peaks are still located at the distinct angles, confirming the purity of a 5-ASA powder and the formation of chloride salt in both 5-ASA

solution and 5-ASA precipitates. The diffractogram profiles suggest an anhydrous salt is formed in 5-ASA solution sample. A mixture of a monohydrate and anhydrous forms is present in 5-ASA precipitates, since peaks distinctive for both were found in the sample. For example, peaks at 16 °, 17.5 °, 20.8 °, and 28.8 ° can be found in both CCDC entry of 5-ASA Cl^- and 5-ASA precipitates sample, but are not present in CCDC entry of 5-ASA Cl^- . H_2O.

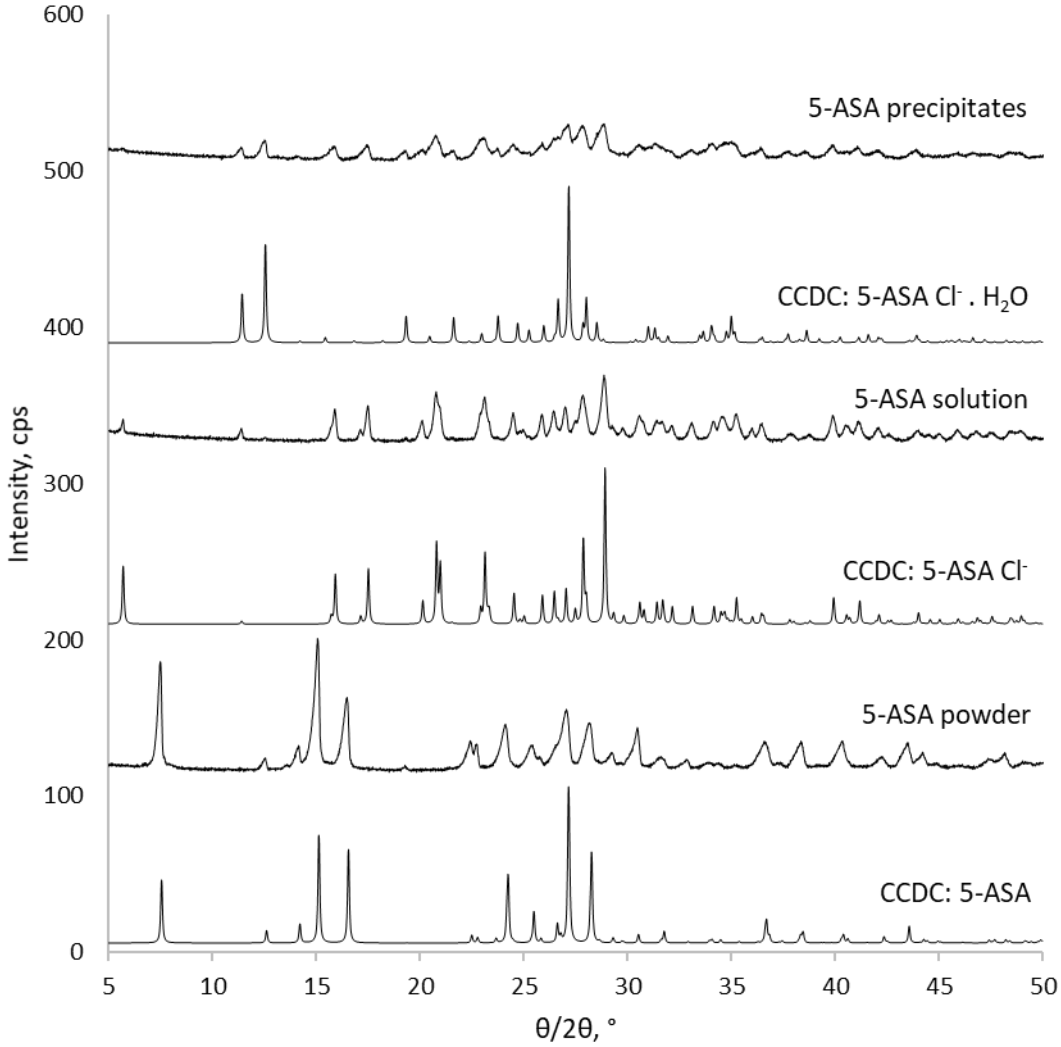

Figure 4.21. PXRD diffractograms of 5-ASA powder, freeze dried 5-ASA solution and freeze dried 5-ASA precipitates compared with entries for 5-ASA, 5-ASA chloride and 5-ASA chloride monohydrate from CDC database, showing 5-ASA precipitates are mixture of 5-ASA chloride and 5-ASA chloride monohydrate.

Potential effect of acidification on the blank zein particles was studied alongside the physico-chemical characterisation of the drug loaded particles, which were compared to their corresponding physical mixes. Physical mixes (referred to as 5-ASA-zein phys. mix of corresponding loading) were prepared by ball milling (10 min, 10 Hz) of freeze dried 5-ASA precipitates and acidified zein NPs of corresponding HCl concentration.

The TGA analysis did not show any significant difference in the thermogram profiles of the zein powder, blank zein NPs, and acidified blank zein NPs. 10 ± 1 % of each of the samples were decomposed at 275 °C (see Figure 4.22). In the drug loaded particles as well as the physical mixes, a decreasing trend of a decomposition temperature was observed with increasing 5-ASA (and HCl) concentration (see Figure 4.23). Decomposition temperatures were also decreased in all particle samples compared to their corresponding physical mix. This might be associated with the changes in the protein secondary structure when particles are loaded with the 5-ASA, as the similar decomposition temperature decrease was found in the blank EHDA zein particles. Both drug loaded particles and their physical mixes in the drug loading range of 5 – 20% showed similar thermogram profiles to the ones of blank zein NPs. Neither the drug loaded particles, nor their physical mixes showed a similar trend in their first step weight loss as the 5-ASA solution and 5-ASA precipitates and therefore, the TGA was not further considered as a loading efficiency assay method. The comparison of degradation rates (10 ± 1% weight loss) of drug loaded nanoparticles (5, 10, and 20% drug loading) and their corresponding physical mixes is shown in the Table 4.5.

Table 4.5. Comparison of temperatures, at which 10 ± 1% weight loss occurred in physical mixes and precipitated nanoparticles with 5, 10, and 20% drug loading, obtained by TGA.

Drug loading	Physical mix	Precipitated NPs
5%	270 °C	265 °C
10%	250 °C	225 °C
20%	223 °C	220 °C

However, 50% 5-ASA loading showed three-step decomposition profiles for both drug loaded NPs and its physical mix, which is summarised in the Table 4.6.

Table 4.6. Comparison of weight losses (TGA) in each degradation step of 5-ASA-zein NPs (50%) and its corresponding physical mix.

Degradation step	5-ASA-zein phys. mix (50%)	5-ASA-zein NPs (50%)
1	14 ± 1% weight loss at 212 °C (onset at 145 °C)	14 ± 1% weight loss at 190 °C (onset at 125 °C)
2	32 ± 1% weight loss at 275 °C	42 ± 1% weight loss at 260 °C
3	30 ± 2% weight loss at 370 °C	30 ± 2% weight loss at 370 °C

The three-step decomposition profile of the 50% drug loaded samples and their corresponding physical mix might suggest these particles are overloaded, since showing the typical two-step decomposition profile of the 5-ASA precipitates incorporated into the zein profile (creating the third step). However, the absence of the two-step profile in the physical mixes in the range of 5 – 20% contradicts this theory. Therefore, further analysis was performed to make any conclusions.

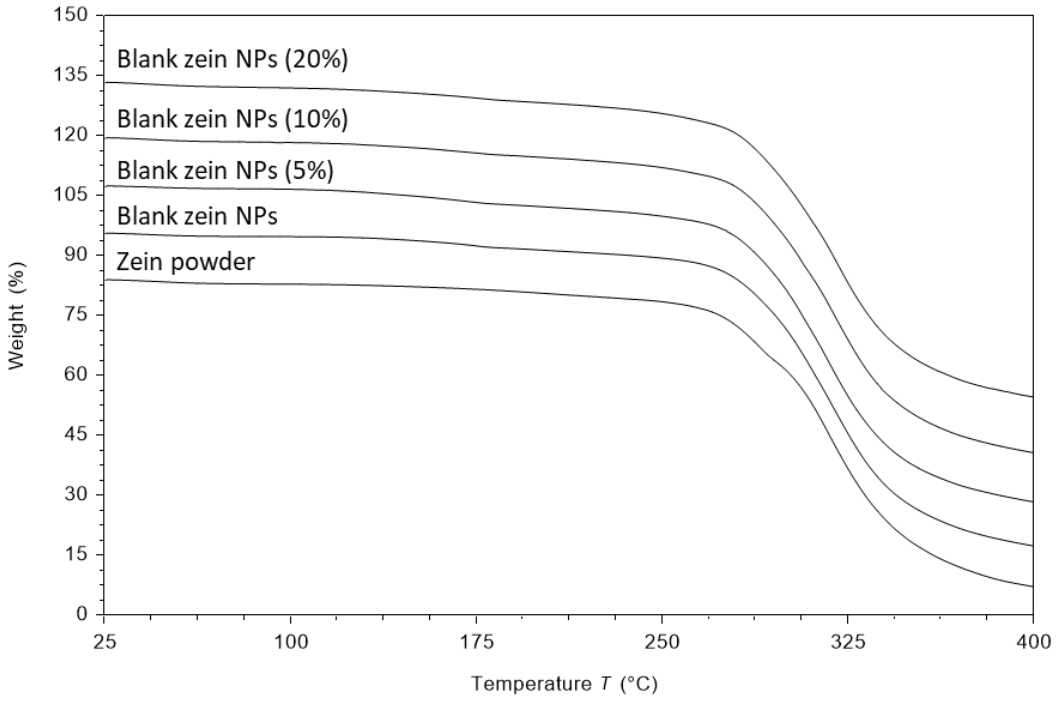

Figure 4.22. TGA thermograms of the non-acidified and acidified blank zein NPs compared to the pure zein powder, showing no significant change in their profiles.

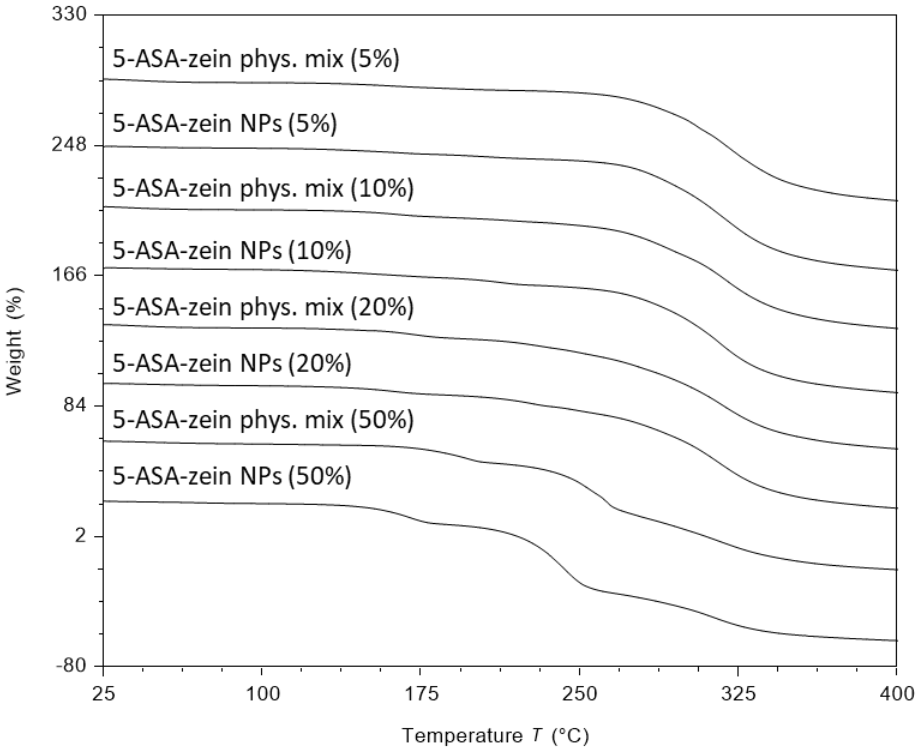

Figure 4.23. TGA thermograms of the 5-ASA-zein NPs compared to their corresponding physical mixes, showing increased decomposition rates with increased 5-ASA concentration.

In the Figure 4.24, the DSC analysis showed the increase of the glass transition temperature in the blank zein NPs, both non-acidified and acidified (mid-point at 167 °C for all), compared to the glass transition of the pure zein powder (161 °C). This suggests that the method of particle preparation, which is also a zein purification step (as commercial zein contains various zein secondary structures with different solubilities in the aqueous ethanol), and/or freeze drying might affect the structure of zein. Since all the particle samples showed their glass transition at the same temperature, the concentration of the HCl in the production step does not seem to affect the protein structure. The increase of the T_g suggests the protein folded into a more stable form, since the glass transition of the proteins is correlated to protein un-folding.[197]

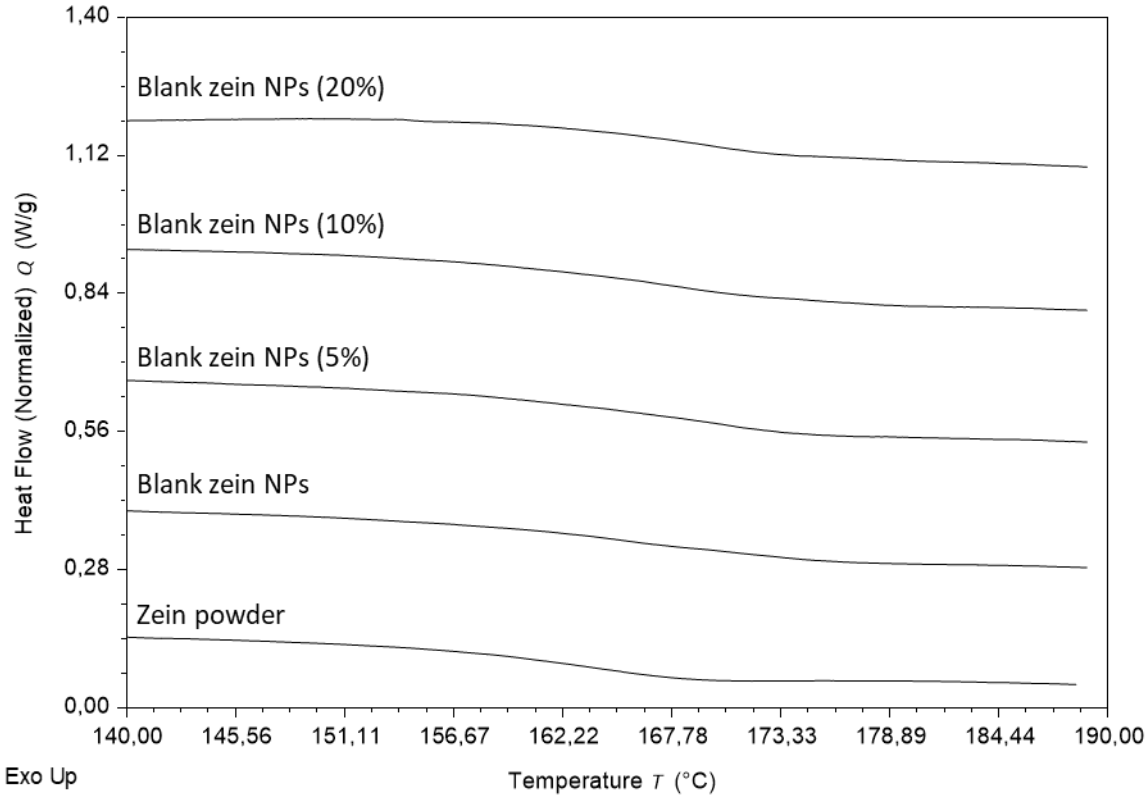

Figure 4.24. The DSC thermograms of the non-acidified and acidified blank zein NPs compared to the pure zein powder, showing the shift of the glass transition mid-point to the higher temperature (167 °C) in the freeze-dried NPs samples compared to the raw zein powder (161 °C).

Glass transition depression was observed in all drug loaded particle samples compared to the corresponding physical mixes (see Figure 4.25). The depression decreased with increasing drug concentration (from 162 °C to 153 °C for 5% loading, from 160 °C to 155 °C for 10% loading, and from 159 °C to 157 °C for 20% loading), suggesting the drug loading efficiency is the highest at the lowest (5%) drug loading.

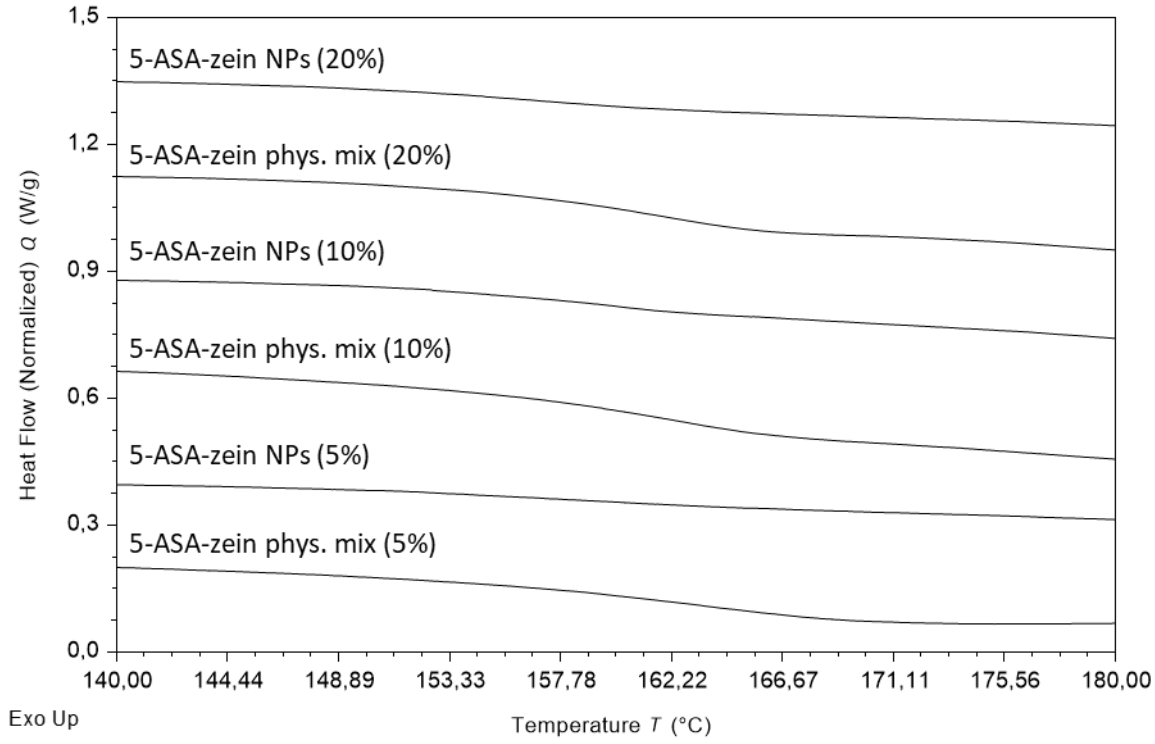

Figure 4.25. The DSC thermograms of 5-ASA-zein NPs showing glass transition depression compared to their corresponding physical mixes.

Further molecular analysis was performed by ATR-FTIR. Blank zein NPs, both non-acidified and acidified, did not show any significant band shift compared to the pure zein powder (see Figure 4.26), suggesting no significant change in the secondary structure even though the relative intensities of the amide III band decreased in both non-acidified and acidified particles. ATR-FTIR spectra of the drug loaded NPs compared to their physical mixes (see Figure 4.27) support the theory suggested by the DSC data – the highest drug loading efficiency can be seen in the particles with the lowest drug loading (5%). Although, the 5% loading is on the border of the instrument sensitivity, the bands at e.g., 797, 848, 1086, 1207, and 1299 cm^{-1} (assigned to the 5-ASA precipitates earlier in this chapter) were clearly observed in the spectrum of the 5-ASA-zein phys. mix (5%), while not found in the spectrum of 5-ASA-zein NPs (5%) which copied a profile of the blank zein NPs. The number and the intensity of the bands assigned to the 5-ASA precipitates increase with the increasing 5-ASA concentration in both physical mixes and drug loaded NPs. However, a decreased number and intensity of those bands were observed in both 5-ASA-zein NPs (10%) and 5-ASA-zein NPs (20%), when compared to their corresponding physical mixes.

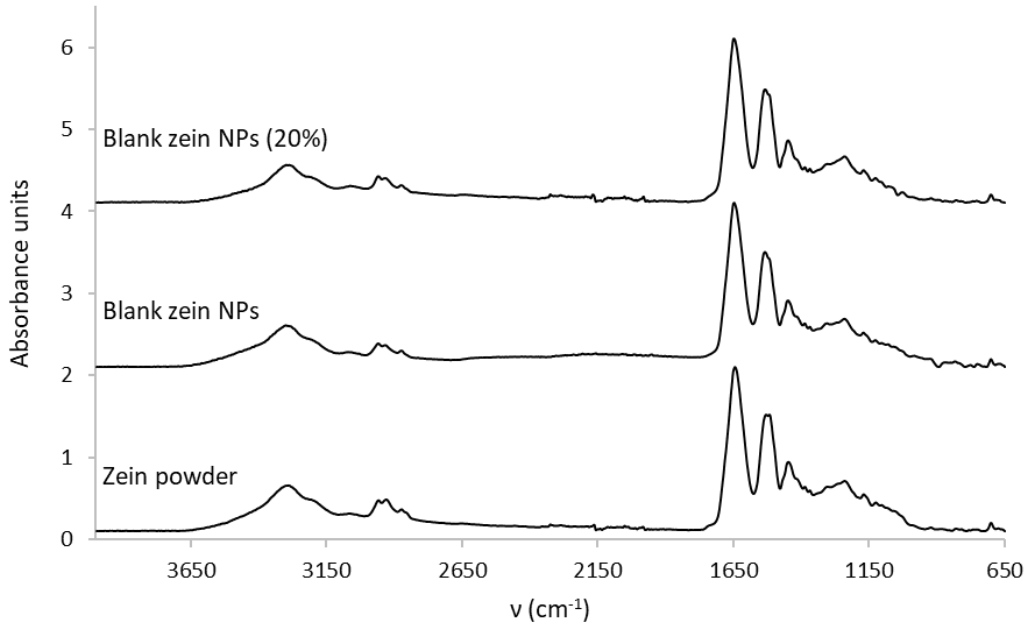

Protein Band	Pure zein		Blank zein NPs		Blank zein NPs (20%)	
	ν (cm^{-1})	RI (%)	ν (cm^{-1})	RI (%)	ν (cm^{-1})	RI (%)
Amide I, ~1650 cm^{-1}	1645	100	1647	100	1649	100
Amide II, ~1530 cm^{-1}	1529	72	1533	70	1533	69
Amide II, ~1515 cm^{-1}	1518	72	1520	66	1520	66
C-N Stretch, ~1445 cm^{-1}	1448	45	1448	40	1448	38
Amide III, ~1240 cm^{-1}	1240	34	1242	29	1240	28

Figure 4.26. ATR-FTIR spectra and a table of important protein bands observed in blank zein NPs, blank zein NPs (20%), and pure zein powder showing no significant effect of precipitation and/or acidification on the position of these bands.

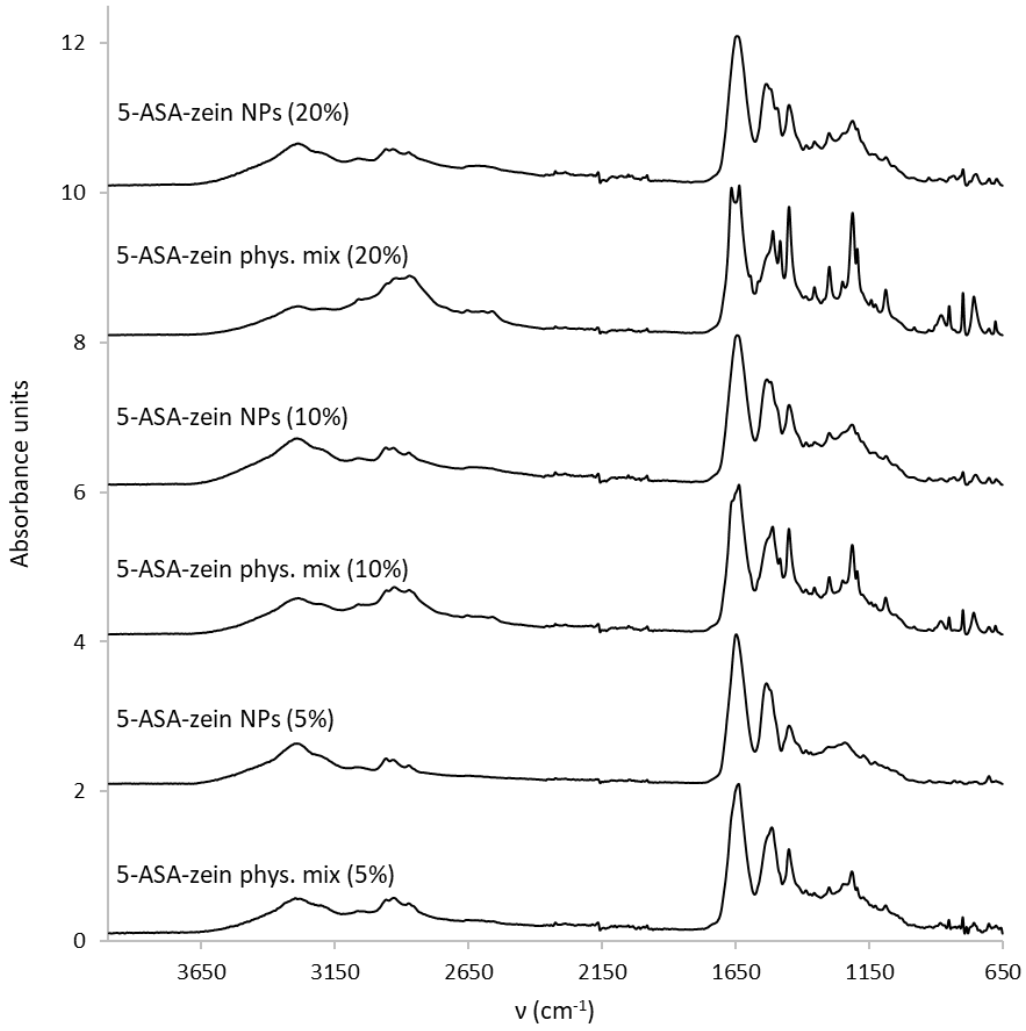

Figure 4.27. ATR-FTIR spectra of 5-ASA-zein NPs compared to their corresponding physical mixes, showing increased number and intensity of the bands assigned to the 5-ASA precipitates with increased 5-ASA concentration in both physical mixes and drug loaded NPs. 5-ASA precipitates' bands were not observed at 5-ASA-zein NPs (5%). Both 5-ASA-zein NPs (10%) and 5-ASA-zein NPs (5%) showed decreased number and intensity of these peaks compared to their corresponding mixes.

Finally, PXRD analysis was performed to study the crystallinity of the samples as well as their stability over the time. In the Figure 4.28, crystalline peaks at 31, 32, and 45° were observed in all acidified blank zein NPs compared to the fully amorphous non-acidified blank zein NPs. The low number of the peaks suggest the HCl added in the precipitation step formed a mineral chloride salt (halide). Therefore, the diffractograms were compared to the most common halides found in the nature (NaCl, KCl, $MgCl_2$, $CaCl_2$), since the zein powder used in these experiments is extracted from a natural corn source and purified to the extent of 98%. NaCl shares two peaks (32° and 45°) with the acidified blank zein particles. The second most intensive peak in the $MgCl_2$ is found at 31°, which is also the most intensive peak found in the acidified blank zein particles. However, no other MgCl2 peaks were found

in the acidified particles. The absence of the rest of the $MgCl_2$ peaks in the diffractograms of acidified blank zein particles could be caused by the low concentration of this impurity in the samples. This suggests a mixture of sodium and possibly magnesium and other ions are present in the zein powder.

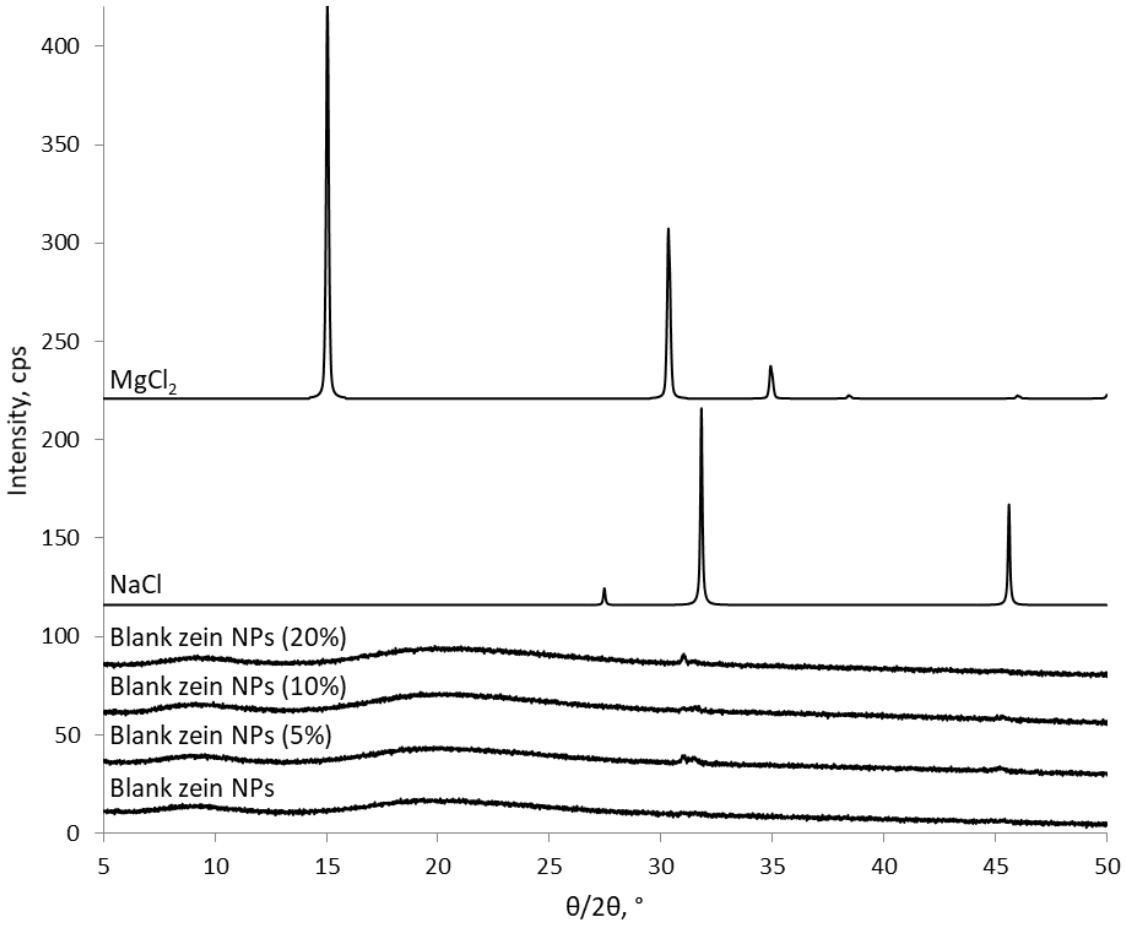

Figure 4.28. PXRD diffractograms of non-acidified and acidified blank zein NPs compared to simulated diffractogram of $MgCl_2$, suggesting pure zein powder contains magnesium impurity.

In the Figure 4.29, diffractograms of drug loaded NPs and their corresponding physical mixes are compared. The number and the intensity of the peaks assigned to the 5-ASA Cl^- and 5-ASA Cl^- . H_2O increased with increasing 5-ASA concentration in both drug loaded NPs and physical mixes, while each drug loaded NPs sample showed a decreased number and intensity of these peaks when compared to its corresponding physical mix. Peaks associated with the 5-ASA salts were not observed at 5-ASA-zein NPs (5%) and 5-ASA-zein NPs (10%). This suggests the PXRD analysis is another piece of evidence supporting the theory of the decreasing loading efficiency with the increasing drug loading concentrations.

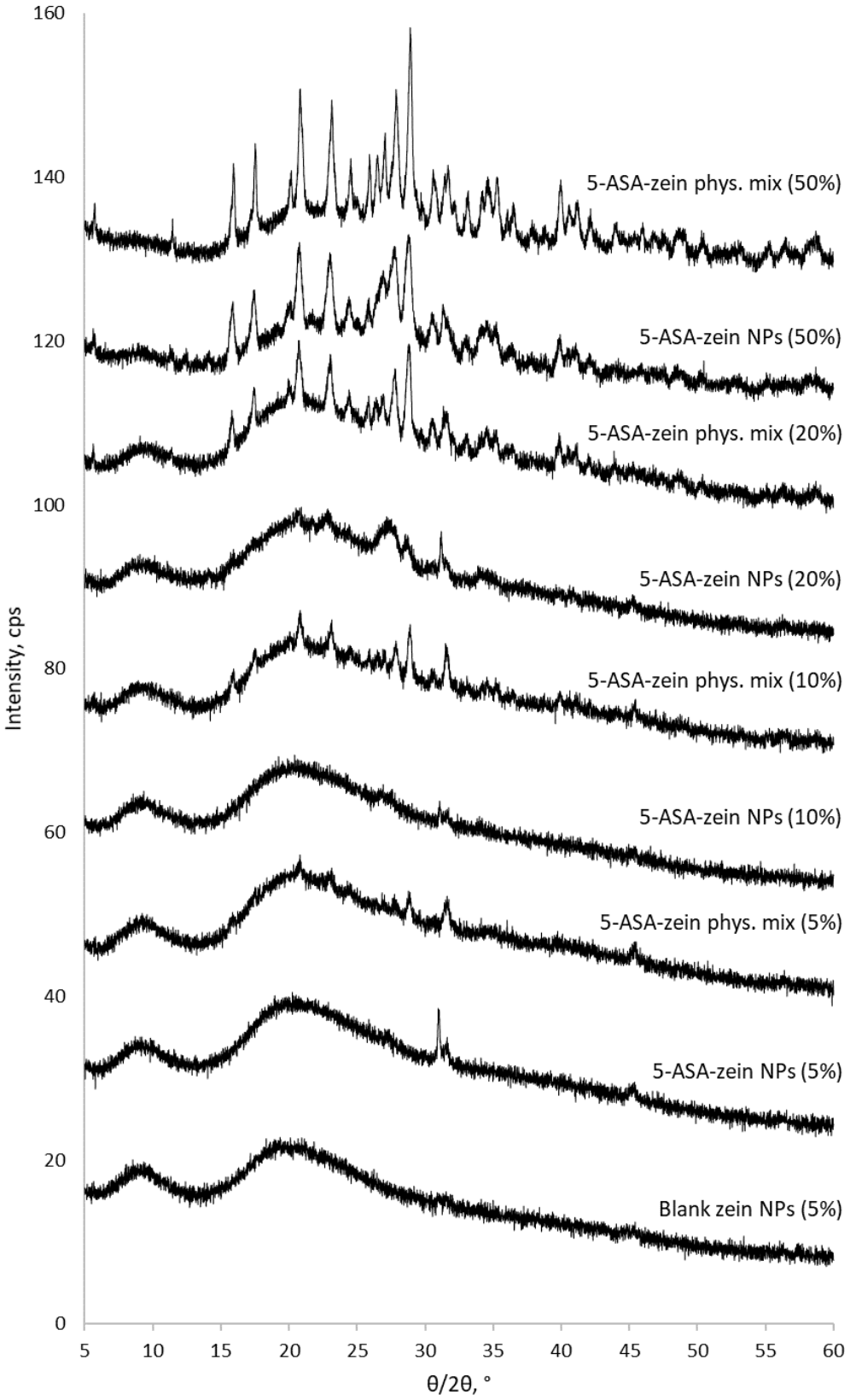

Figure 4.29. PXRD diffractograms of 5-ASA-zein NPs compared to their corresponding physical mixes, showing increased number and intensity of the peaks assigned to the 5-ASA chlorides with increased 5-ASA concentration in both physical mixes and drug loaded NPs. 5-ASA salts' peaks were not observed at 5-ASA-zein NPs (5%) and 5-ASA-zein NPs (10%). Both 5-ASA-zein NPs (20%) and 5-ASA-zein NPs (50%) showed decreased number and intensity of these peaks compared to their corresponding mixes.

The Figure 4.30 shows PXRD data for the stability study of the acidified blank zein NPs (A) and drug loaded NPs (B). The diffractograms of each formulation were obtained immediately after preparation (day 0) and after 15 days. Both blank and drug loaded formulation showed the same trend of increased intensity of the impurity halide peaks with increased concentration of HCl in the preparation step after 15 days. The intensity of the peaks belonging to the 5-ASA chloride salt did not change over the time in any of the drug loaded samples. This suggests the drug stays stable in the freeze dried formulations. However, the continuous crystallization of the impurity halide could cause unwanted leakage of the drug from the particles.

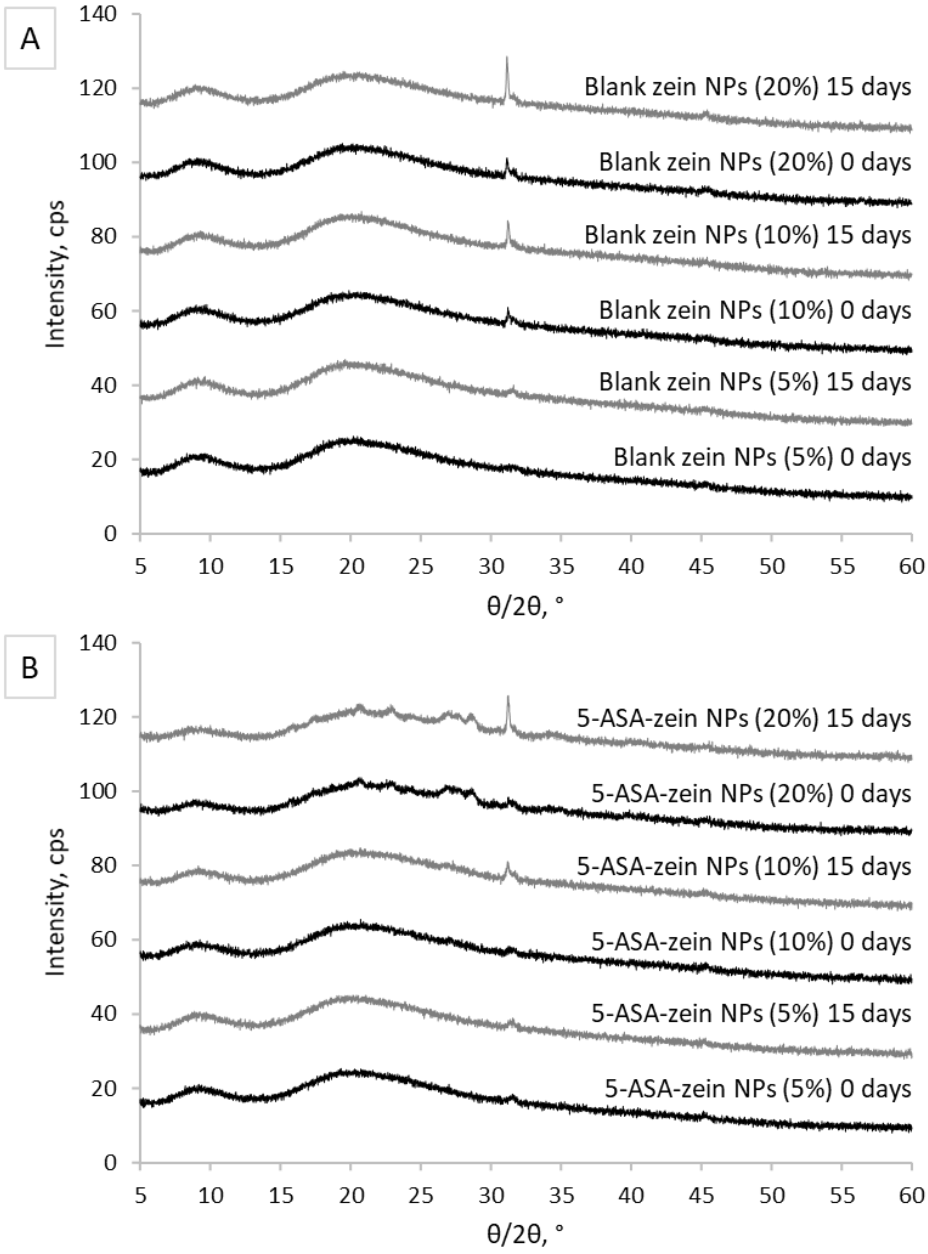

Figure 4.30. PXRD stability study showing diffractograms of (A) acidified blank zein NPs and (B) 5-ASA-zein NPs at 0 and 15 days, suggesting stability of the protein and the drug over the period, contrary to the $MgCl_2$ gradual crystallisation.

Finally, the drug loading efficiency (DLE) and the drug release were assessed. The LC-MS method was developed to assay the 5-ASA concentration in the samples. The LC-MS method was selected due to the inaccuracy of the UV-VIS spectrophotometry caused by the signal of water soluble impurities in zein interfering with the 5-ASA signal. These impurities follow irregular release pattern and therefore, the subtraction of the signal was not possible to use in the 5-ASA quantification. The DLE was assessed from 23.34% EtOH supernatant, using centrifuge filter units. Each filter unit was washed and reused twice for measuring of

replicates, which potentially created high irreproducibility of the measurements. DLE of 53%, 56%, and 31% was measured in the first replicate of 5-ASA-zein NPs (5%), 5-ASA-zein NPs (10%), and 5-ASA-zein NPs (20%), respectively. However, these values rapidly decreased with the replicates. Therefore, the method was planned to be reviewed and DLE experiments were supposed to be repeated. However, due to the COVID-19 pandemic, these experiments were not finished. The Figure 4.31 shows the drug release profiles of the 5-ASA from 5-ASA zein NPs (5%) and 5-ASA zein NPs (10%) in PBS buffer in pH = 7.4, mimicking the colonic pH. The only significant difference at cumulative drug release (CDR) was found at the 10 min time point, where the 5-ASA zein NPs (5%) released almost twice more of the drug than 5-ASA zein NPs (10%). However, the overall profiles were sustained for both nanosuspensions, showing CDR of $86 \pm 14\%$ and $74 \pm 21\%$ at 2 hours for 5-ASA zein NPs (5%) and 5-ASA zein NPs (10%) formulations, respectively. This drug release behaviour corresponds with findings in the literature, where A. Berardi et al.[198] observed the drug diffuses from the zein rapidly at the beginning until the protein swells sufficiently and closes its pores, creating a barrier for further water intake and consequently slowing the diffusion of the drug. Considering zein mucoadhesive properties and renewal time of colonic mucus (4 - 6h), this suggests the formulation is a suitable candidate for colon targeting drug delivery systems. This theory should be proved by performing the same drug release study in pH=1.2, to observe the drug release profile of the particles in the conditions of stomach. However, this was another experiment which was not finished due to the time and cost reasons associated with the COVID-19 pandemic.

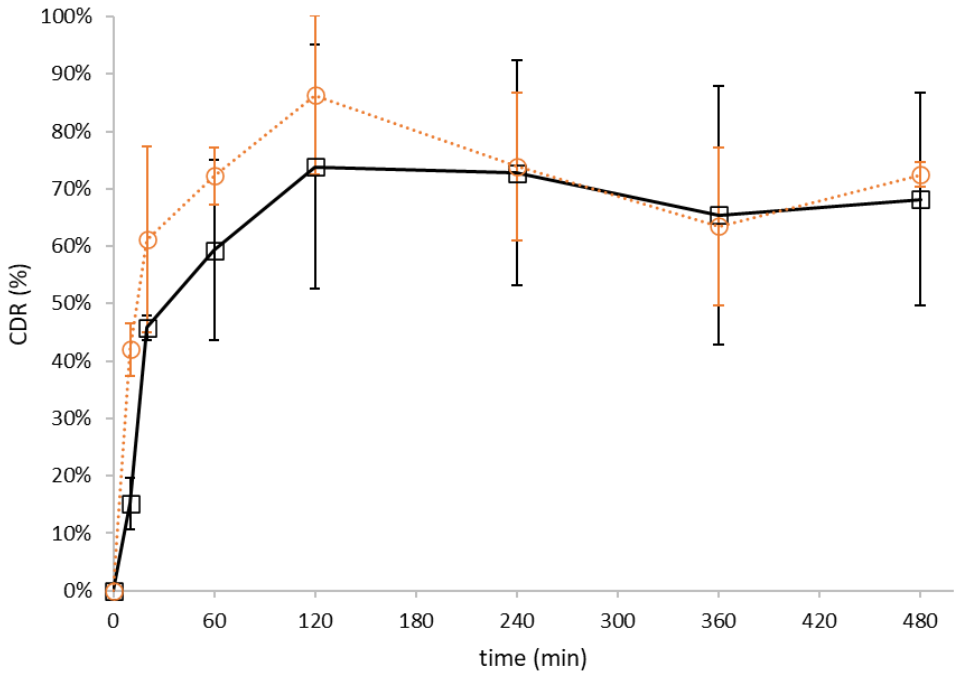

Figure 4.31. Cumulative drug release from 5-ASA-zein NPs (5%) (orange dashed line with circles) and 5-ASA-zein NPs (10%) (black solid line with squares) in PBS buffer at pH = 7.4., assayed with LC-MS.

4.4 Conclusion

Zein nanoparticles were prepared by two methods, electrospray and precipitation (anti-solvent). The electrospray method showed a very low yield compared to the precipitation technique. TEM and SEM images proved the size of zein NPs did not change significantly with the process conditions adjustments and both EHDA and precipitated NPs were obtained in the similar size range. Only the precipitated NPs were loaded with 5-ASA. Neither blank, nor drug loaded precipitated NPs changed their size after freeze drying. Precipitated particles were spherical, and their size did not change significantly when drug was loaded. On the other hand, both spherical and non-spherical particles were obtained by EHDA.

PXRD together with ATR-FTIR confirmed the 5-ASA was successfully loaded into the particles up to 10% 5-ASA/zein ratio (w/w) in form of chloride salt. Drug loaded NPs shown significantly higher degree of amorphous state compared to their corresponding physical mixes. Crystalline peaks in blank zein NPs at 31, 32, and 45° were associated to a mixture of halides (NaCl and possibly $MgCl_2$) that is generated during the precipitation step due to impurities in zein powder. The size of 5-ASA loaded zein NPs in suspension (DLS analysis) was stable for 8 days. The freeze dried form (PXRD analysis) was stable for 15 days. However, the halides gradually crystallised out of the formulation over the time.

LC-MS method was developed to assay 5-ASA loading efficiency of the zein NPs (filter centrifuge units) and drug release from the NPs suspension (dialysis tubes). In vitro drug release data showed a sustained release profile at pH = 7.4, which was used to mimic colonic pH. $86 \pm 14\%$ and $74 \pm 21\%$ of the drug was released within 2 hours from 5-ASA zein NPs (5%) and 5-ASA zein NPs (10%), respectively. Despite the fast release profile, the formulations were considered suitable for colon targeting drug delivery systems, suggesting the particles will adhere to the mucus of colon and release the drug within the mucus renewal time.

Two experiments (drug loading efficiency and drug release at pH = 1.2) were not finished due to the time and cost reasons associated with the COVID-19 pandemic.

5 INCORPORATION OF THE 5-AMINOSALICYLIC ACID LOADED ZEIN NANOPARTICLES INTO HPMCAS FIBERS & FACTORS AFFECTING THE ENTERIC PROPERTIES OF THE HPMCAS FIBERS

5.1 Introduction

The precipitated zein nanoparticles (NPs) loaded with 5-aminosalicylic acid (5-ASA) were intended to be incorporated into the HPMCAS fibers by the electrospinning method, as it would be a single step incorporation technique. It was proposed that using a co-axial nozzle: the 5-ASA-zein NPs nanosuspension as a core (inner) feed solution and HPMCAS solution loaded with paracetamol (PAR) and hydrocortisone (HYD) as a shell (outer) feed solution, would lead to the evenly distributed drug loaded NPs incorporated into the inner diameter of the enteric fibers. This would potentially lead to a release of the 5-ASA from the zein NPs only in the colonic pH. A diagram of the proposed formulation is shown in the Figure 5.1, where inner structure of the final fiber (after solvent evaporation) is schemed on the left and its cross section on the right. The optimal conditions for electrospinning of the HPMCAS polymer are discussed in the Chapter 3, including the most suitable solvent (binary mixture of acetone and DMSO, (3:2; v/v)) and relative humidity of 30 ± 2%.

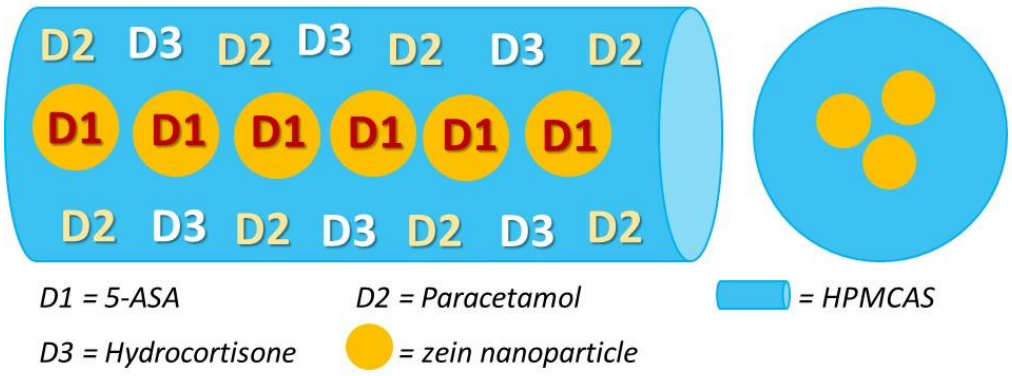

Figure 5.1. Diagram of incorporation of 5-ASA (D1) loaded zein nanoparticles into HPMCAS fibers containing paracetamol (D2) and hydrocortisone (D3) by co-axial electrospinning; cross section on the right.

In the first part of this chapter, the challenges faced during incorporating of the 5-ASA-zein NPs and following adjustments of the proposed method are described as well as the obtained drug release profile. The following part of this chapter discusses the lack of the enteric properties of the electrospun HPMCAS fibers (previously described in the Chapter 3). Following a hypothesis that the enteric properties of the polymer decreases with the

decreasing diameter of the fibers, filament extrusion was used to prepare single and multi-drug loaded HPMCAS filaments (using same drug loading ratio as in the electrospun fibers) of three different diameters. The drug release profiles obtained from the dissolutions of these filaments were further compared with the profiles of the electrospun fibers. All prepared formulations were imaged with SEM and characterised with TGA, (M)DSC, ATR-FTIR, and PXRD.

5.2 Materials and Methods

5.2.1 Materials

5-aminosalicylic acid (5-ASA) and Hydrocortisone (HYD) were purchased from Acros Organics, US. Paracetamol (PAR) was purchased from Sigma Aldrich, US. HPMCAS (grade H) and PVP k90 were kindly gifted by Ashland, US. PEO (300,000) was purchased from (Sigma-Aldrich, US). Zein was purchased from ACROS Organics, US. Acetone was purchased from VWR, France. DMSO was purchased from Fisher Scientific, UK. Ethanol (EtOH) was purchased from VWR, France. MilliQ (MQ) water was produced using a Purelab ultra (ELGA LabWater, UK). Hydrochloric acid, Perfluoro(methylcyclohexane), and PBS tablets were purchased from Sigma-Aldrich, US.

5.2.2 Fabrication of the electrospun HPMCAS fibers with incorporated 5-ASA loaded zein NPs

The nanosuspension of the 5-ASA loaded zein NPs were prepared by an anti-solvent method described in the Chapter 4. The 10% 5-ASA loading was selected for the purpose of incorporation into the HPMCAS fibers since these particles showed high level of molecular dispersion and minimal crystallinity of the drug. Clear solutions of 20% HPMCAS (w/v) and appropriate concentration of PAR in binary solvent system of acetone:DMSO (3:2; v/v) were prepared as well as a 7.5% PVP (w/v) solution in MQ water containing according concentration of HYD.

Nanofiber electrospinning unit (Tong Li Tech, China), syringe pumps (Cole-Parmer, US), 22G, co-axial (20G - 26G) and tri-axial (18G - 22G - 30G) emitters (both Avectas:Spraybase, Ireland) and a rotating drum collector covered with grease proof paper were used for electrospinning of the formulation. Humidity in the system was controlled with N_2 flow and kept at RH = 30 ± 2% for all experiments. The details of the final method are further described in the Results and Discussion section (5.3).

5.2.3 Electrospinning of the multi-drug loaded HPMCAS fibers

Clear solution of 20% HPMCAS (w/v) and according concentrations of 5-ASA, PAR, and HYD in binary solvent system of acetone:DMSO (3:2; v/v) was electrospun using the nanofiber electrospinning unit (Tong Li Tech, China), a syringe pump (Cole-Parmer, US), 22G emitter (both Avectas:Spraybase, Ireland) and a rotating drum collector covered with grease proof paper, while the relative humidity was fixed at 30 ± 2% using N_2 flow.

The viscosity, surface tension, and conductivity of the feed solution were measured following the methods described in the Chapter 3.

5.2.4 Hot-Melt Extrusion of the drug loaded HPMCAS filaments

To study the effect of the fiber diameter on the enteric properties of the HPMCAS, blank and drug loaded HPMCAS filaments of three different diameters were extruded at 170 °C using co-rotating twin screw mini-extruder (HAAKE™ MiniLab II Micro Compounder, Thermo Electron, Karlsruhe, Germany). The physical mixtures of different binary and quaternary combinations were mixed using mortar and pestle for 3 minutes before they were fed into the extruder. The diameter of the filaments was at first controlled by the extruder nozzle to obtain the thickest diameter. Then the filaments were manually pulled out of the extruder to obtain a middle and the thinnest diameters.

The thickest diameter of the filaments was measured by a digital clipper. The two thinner diameters were measured manually from the images obtained by an optical microscope (Linkam Scientific Instruments Ltd, Surry, UK). Each thickness of each filament was measured ten times, when only the parts with steady diameter were selected.

5.2.5 Imaging of the electrospun and extruded formulations

SEM analysis was performed to image the electrospun formulations and to visualise the surface and cross sections of the extruded filaments. The samples were directly attached onto SEM specimen stubs by double-sided tape and coated with gold using a Polaran SC7640 sputter gold coater (Quorum Technologies) prior to imaging. The coated samples were scanned by Gemini 300 series scanning electron microscope (Zeiss, Germany). The Image J software was used to measure the fiber diameter and the size of the beads, when 100 values were averaged for each.

Fluorescence emission spectra of the double filtered 5% zein (w/v) solution in 70% EtOH aq. (v/v) and the 7.5% PVP (w/v) solution in MQ water were recorded with a FS5

Spectrofluorometer (Edinburgh Instruments, UK) using a quartz cell cuvette. The excitation wavelength was set at 405 nm. The same excitation wavelength was then used to image the 5-ASA-zein NPs (10%) in the final formulation with a ZEISS LSM 980 (Zeiss, Germany) **confocal fluorescence microscope (CFM)**. The Image J/Fiji software was used for analysis of the images.

5.2.6 Physico-chemical characterisation of the electrospun and extruded formulations

TGA, **(M)DSC, ATR-FTIR,** and **PXRD** analysis was performed following the methods described in the Chapter 3.

5.2.7 *In vitro* drug release

Drug release profiles from multi-drug loaded samples were obtained from dissolution experiments described in the Chapter 3. The drugs were quantified by LC-MS: 50×2.1mm 2.6μ Kinetex XB C18 column (Phenomenex, USA) and an Acquity UHPLC system (Waters). The conditions of the LC-MS method are also described in the Chapter 3.

Drug release from single-drug loaded extrudates was performed in shaking water bath (100 rpm) at 37 ˚C, using closed glass vials. The extrudates were transferred from hydrochloric solution (pH = 1.2) into PBS buffer (pH = 7.4) after two hours by a pair of tweezers. The dissolution was performed under sink conditions, when the sink volume was 10 ml and the samples taken at each time point were 0.3 ml. The sink volume was kept constant with the corresponding buffer. The data was analysed by **UV-VIS spectrophotometry**, using a CLARIOstar® Plus microplate reader (BMG Labtech, Germany) and a quartz 96 well plate.

5.3 Results and Discussion

5.3.1 Incorporation of the 5-ASA loaded zein nanoparticles into HPMCAS fibers by electrospinning technique

As schemed in the Introduction in the Figure 5.1, the experiments of incorporation of 5-ASA-zein NPs into the HPMCAS fibers by co-axial electrospinning were performed. For this purpose, 5-ASA-zein NPs (10%) suspension (core feed solution) was used in combination with a 20% HPMCAS (w/v) solution in acetone:DMSO (3:2, v:v) containing 0.05% PAR and 0.04% HYD (shell feed solution). However, no matter what combination of the flow rates was used, the HPMCAS solution precipitated in the presence of the acidified nanoparticle solution (0.018M HCl) due to the polymer pH dependent solubility. Therefore, a tri-axial electrospinning using a pure solvent as a middle layer was proposed to obtain the design schemed in the Figure 5.1. The solvent used to solubilise the HPMCAS shell solution, acetone:DMSO (3:2, v:v), was trialled first. This was followed by MQ water and finally by the perfluoro(methylcyclohexane), which is immiscible with both feed solutions solvents. However, none of these solvents created sufficient barrier in between the nanosuspension and the HPMCAS solution and the precipitation of the HPMCAS was not prevented. Thus, using a solution of the polymer which is soluble in a wide range of pH as a middle layer was proposed. This would create a design which is sketched in the Figure 5.2. For this purpose, PVP k90 and PEO (300,000) polymers were selected. 10% PVP and 4% PEO solutions in MQ water were prepared and trialled as a middle solution at different feed rates in the tri-axial electrospinning. Nevertheless, using these polymer solutions as a barrier in between the nanosuspension and the HPMCAS solution and the precipitation of the HPMCAS was not yet again prevented.

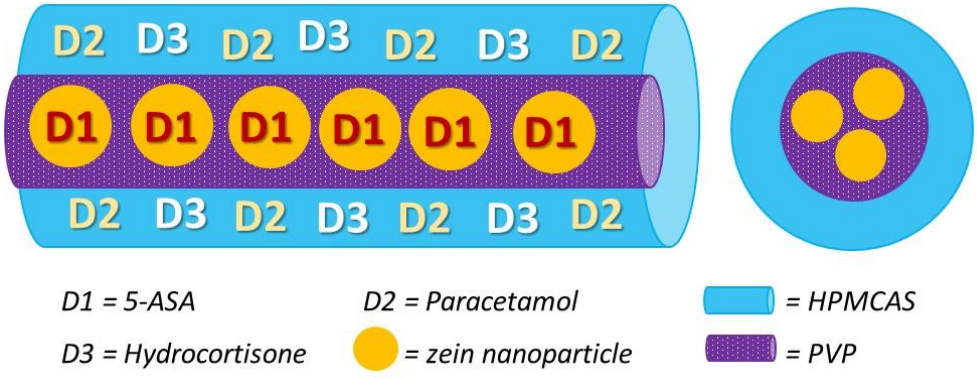

Figure 5.2. Diagram of incorporation of 5-ASA (D1) loaded zein nanoparticles into HPMCAS fibers containing paracetamol (D2) and hydrocortisone (D3) by tri-axial electrospinning, using a pH independent polymer such as PVP as a middle layer; cross section on the right.

Due to these challenges, a layered drug delivery system design shown in the Figure 5.3 was proposed (Figure A shows a cross section of the final formulation, Figure B shows a schematic look from the top). The system consisted of three layers, electrospun directly on each other at relative humidity 30 ± 2%. Layer 1 (bottom) and layer 3 (top) are HPMCAS fibers loaded with PAR electrospun through a scanning single nozzle on a rotating drum coated with a grease proof baking paper. The middle layer is created by HYD loaded PVP fibers with incorporated 5-ASA-zein NPs electrospun through a stationary co-axial nozzle (core feed solution: 5-ASA-zein NPs nanosuspension, shell feed solution: PVP loaded with HYD) on a stationary drum. Using a stationary nozzle and collector together with a shorter nozzle tip-collector distance were proposed to seal the middle layer from all sides to avoid immediate dissolution of the PVP polymer when hydrated, since a stationary electrospinning coats the collector in a circular shape.

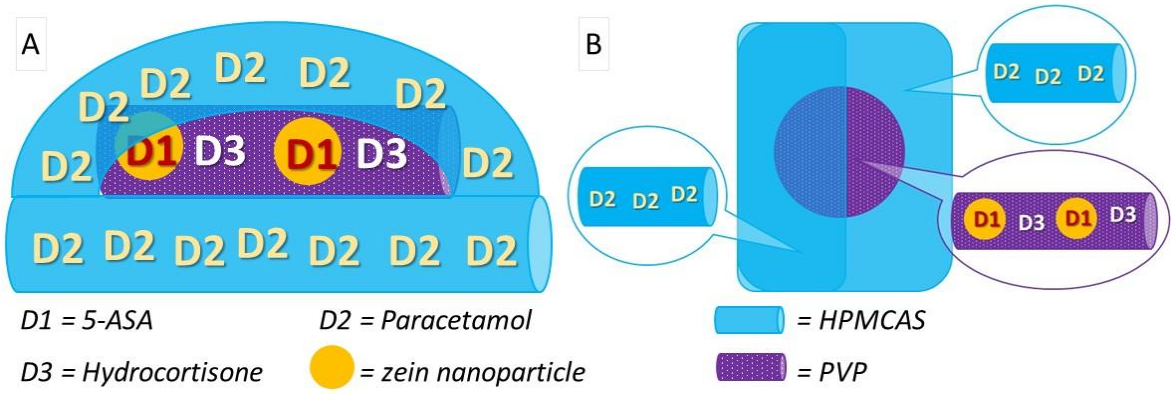

Figure 5.3. Diagram of a proposed layered drug delivery system design, showing (A) a cross-section of the final formulation and (B) a view from the top.

The electrospinning parameters of the layered formulation are summarised in the Table 5.1. The system was produced in triplicates, which were prepared on the same collector. First, layer 1 (HPMCAS-PARmin) was electrospun onto a rotating drum as a base for all three triplicates. Then rotating of the drum was stopped and three spots of layer 2 were electrospun onto the layer 1 with sufficient gaps in between each other, using a stationary co-axial nozzle (inner: 5-ASA-zein NPS (10%), outer: PVP-HYD, further referred to as "5-ASA-zein NPs – PVP-HYD"). Finally, the drum collector started to rotate again and a layer 3 (HPMCAS-PARmin) was electrospun over the three replicates of layer 2, sealing the formulation. The triplicates were separated using a pair of scissors (following guides which were marked on the uncovered part of the paper during the electrospinning process) and peeled of the grease proof paper. The table also lists concentrations of the excipients and the

drugs, and the used solvents. The concentrations of the drugs were adjusted considering the LC-MS LODs, so all three drugs could be quantified at the same time and none of the drugs would overload the detector. Each replicate of the layer 2 was electrospun for 25 minutes due to the minimal occurrence of the co-axial electrospinning process instabilities during this period. After this 25-minute period, the frequency of the electrospinning instabilities rapidly increased over the time. Since the nanosuspension of 5-ASA-zein NPS (10%) was fed through the nozzle at 0.15 ml/h flow rate to avoid said instabilities of the process, each replicate contained only ~ 95 μg of 5-ASA. From this, the concentrations of HYD and PAR were calculated based on their flow rates and time of the electrospinning. The times of the electrospinning of the layers 1 and 3 were set to 75 minutes each, to assure the bottom and top layers are thick enough and the whole formulation is easy to peel of the grease proof paper. This resulted in a ~0.05%, ~0.15%, and ~0.04% drug loading of PAR, 5-ASA, and HYD, respectively.

Table 5.1. Summary of electrospun feed solutions, process conditions, and calculated final drug loading of the layered drug delivery system prepared in triplicates on the same grease proof paper at RH = 30 ± 2% (layer 1 electrospun first, then three times layer 2 with sufficient gaps in between each other, followed by layer 3).

	Layer 1 & 3	**Layer 2**	
		Inner	Outer
Polymer conc. (w/v)	20% (HPMCAS)	1.58% (Zein)	7.5% (PVP)
Drug Conc. (mg/ml)	0.1 (PAR)	1.5 (5-ASA)	0.2 (HYD)
Solvent	acetone:DMSO (3:2; v/v)	23.34% EtOH + HCl (0.018M)	MQ water
Nozzle Gauge	22	26	20
Flow Rate (ml/h)	0.72	0.15	0.3
Distance (cm)	20	11	
Scan (cm)	2	0	
Drum Rotation (rpm)	60	0	
Negative Voltage (kV)	0	-4.6	
Positive Voltage (kV)	9.9 (Layer 1) 10.7 (Layer 3)	9.1 (replicate 1); 9.3 (replicate 2); 9.6 (replicate 3)	
Time (min)	75 (each)	3 x 25	
Final Drug Loading	~0.05%	~0.15%	~0.04%

The triplicates prepared following the parameters from the Table 5.1 were used for the drug release experiment, which is discussed further in this chapter. The same parameters were then used to prepare samples for SEM to observe the structure of the formulation at different

stages of the electrospinning. The representative SEM scans are showed in the Figure 5.4. First, the layer 1 was imaged on its own (Figure A). Beaded HPMCAS-PARmin fibers were observed in this layer. Then the layer 2 was electrospun on the layer 1 and imaged (Figures D – F). Figure D shows the overall structure of the layer 2 (5-ASA-zein NPs – PVP-HYD), consisting of microparticles, beaded fibers, and solidified drops/aggregates. The beaded nanofibers are shown in Figure E, using higher magnification due to the large size difference in between the particles and the fiber diameter. It was suggested that the beaded nanofibers are created by PVP and the microparticles are either core shell particles consisted of zein NPs core coated with PVP shell, or reprecipitated zein NPs into microparticles. The solidified drops/aggregates were suggested to be aggregates of zein NPs, potentially mixed with solidified PVP, created by the instabilities of the Taylor cone. Figure F suggests the layer 2 is not mixing with layer 1 and so the potential of the layers 1 and 3 to create enteric coating of the layer 2. Finally, the layer 3 was imaged, when electrospun on layers 1 and 2 (Figure B), showing the structure of the beaded HPMCAS-PARmin fibers did not change significantly by electrospinning on the layers 1 and 2. The whole formulation was also imaged upside down (bottom of layer 1), which confirmed the structure of the fibers stays intact after peeling from the substrate (Figure C).

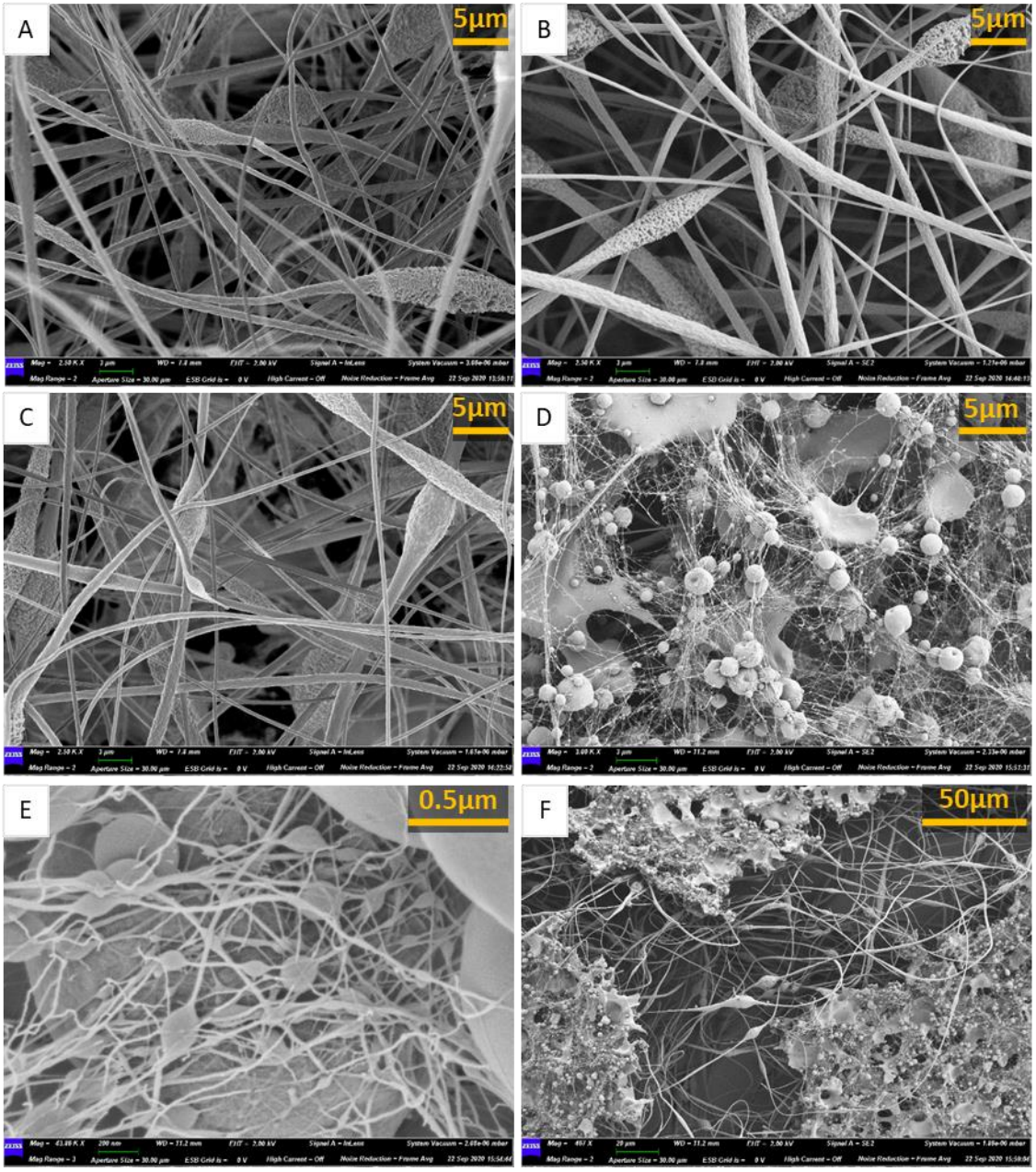

Figure 5.4. Representative SEM scans of the layered drug delivery system observing the formulation at the different stages of the electrospinning process. The HPMCAS-PARmin beaded fibers created (A) layer 1 and (B) layer 3. Scanning the finished formulation upside down confirmed the structure of (C) the layer 1 stayed unchanged after peeling it of the substrate. (D) A mix of particles, fibers, and solidified drops/aggregates were found in co-axially electrospun layer 2 (inner: 5-ASA zein NPS (10%), outer: PVP-HYD), where a higher magnification showed (E) beads on the fibers. Scans (B), (C), and (F) confirmed the layer 2 did not mix with the layers 1 and 3, where scan (F) was obtained before the formulation was sealed with layer 3 and by cracking of the layer 2 to expose the layer 1 beneath.

The distribution of the fiber diameter and the bead length/width ratio were closely studied in all three layers (see Figure 5.5). Figures A and B show comparisons of HPMCAS-PARmin fiber diameter and bead length/width ratio, respectively, in the layers 1 (solid) and 3 (dotted). Fiber diameter distribution histogram showed four maxima in both layers, where three of them were shared in the 100 – 200, 600 – 700, and >1000 nm ranges. However, the layer 1 showed a fourth maximum at 400 – 500 nm, while the layer 3 at 300 – 400 nm range. The layer 1 also did not show any fibers in the <100 and 900 – 1000 nm ranges, while 3% of the fibers in the layer 3 were found in each of this diameter range. The bead length/width ratio in the layer 1 (solid) showed two maxima at <1.5 and 2 – 3 ranges, while only one maximum was observed in the layer 3 at 1.5 – 2 range. Only 3% of the fibers in the layer 1 were found in each of the 3 – 4 and >4 bead/length ratio ranges, while 10% and 8% of the beads with these ratios were found in the layer 3. The differences in both fiber diameter and the bead length/width ratio distributions amongst the layers 1 and 2 are suggested to be caused by the different substrates since layer 1 was electrospun directly on the grease proof paper covering the stainless steel, while the layer 3 was electrospun on the layers 1 and 2 - creating a dense fiber (and particle) layer in between the collector and the jet, causing the need for higher voltage. Figure 5.5 C and D describe the fiber diameter and the bead length/width ratio distributions, respectively, of the PVP-HYD fibers in the layer 2. These fibers showed a tailing fiber diameter distribution peak with a maximum at 10 – 20 nm range (C) and a peak with maximum at 1.5 – 2 bead length/width ratio range. This suggests that the PVP-HYD fibers electrospun under the conditions used for the preparation of this formulation are not showing thick enough diameter to serve as an outer carrier of the 5-ASA-zein (10%) NPs whose diameter was ~10 times larger in the feed solution (125 ± 45 nm). The mean bead width and the mean bead length were estimated to be 87 ± 72 nm and 137 ± 97 nm, respectively. If the bead was considered a cylinder, then maximum of 8 spherical NPs could have been incorporated into one bead (maximum volume of the bead divided by the minimum volume of the NP). However, this calculation does not account for the packing gaps in between the particles.

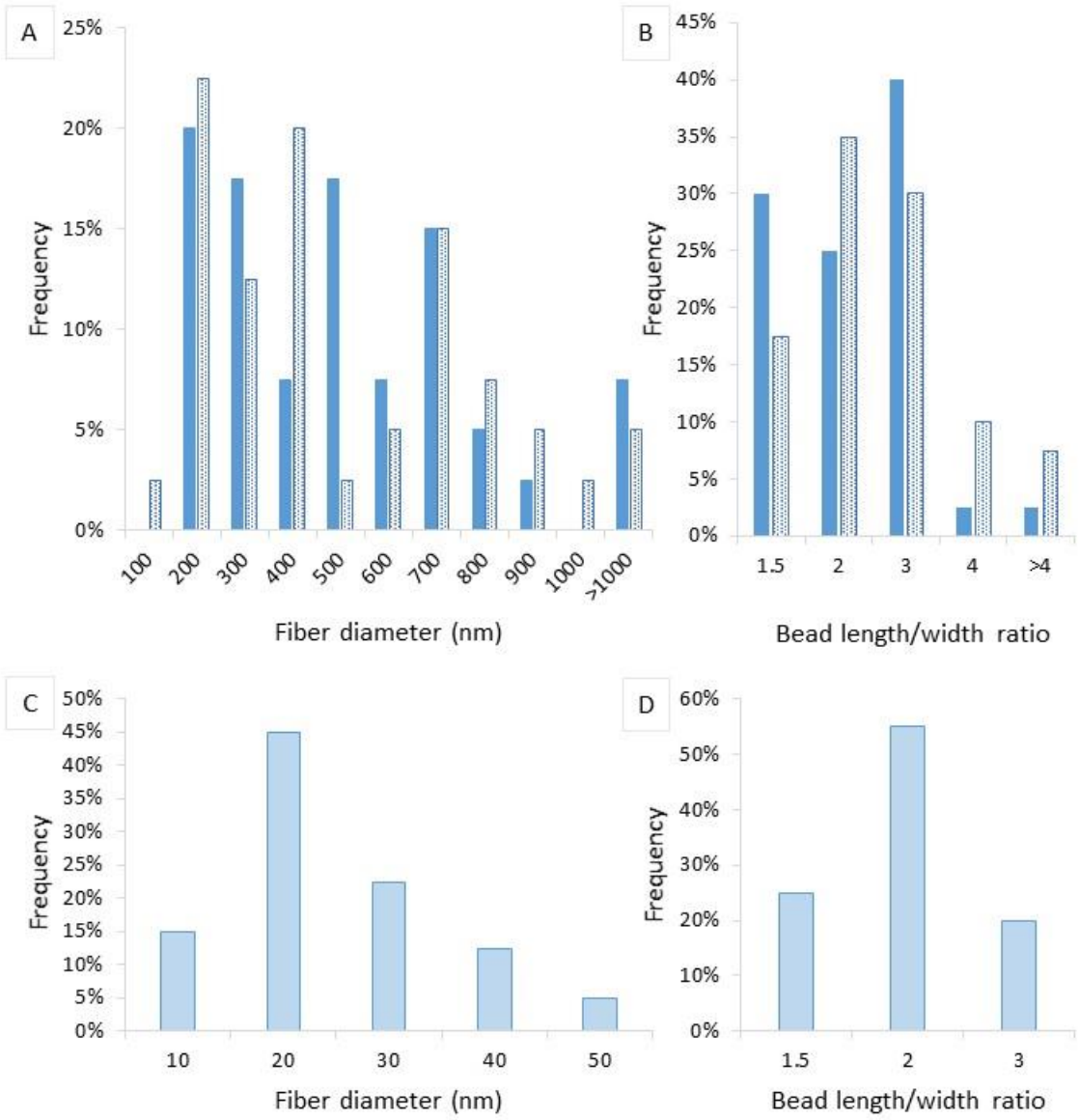

Figure 5.5. Histograms of (A, C) fiber diameter and (B, D) bead length/width ratio distributions of (A, B) HPMCAS-PARmin fibers (showing layer 1 as solid and layer 3 as dotted columns) and (C, D) PVP-HYD fibers; showing the change of substrate affected the distribution patterns in HPMCAS-PARmin fibers and insufficient fiber diameter of PVP-HYD to incorporate 5-ASA-zein NPs of ~10 times higher diameter.

Since particles of approximately 10 times larger diameter than the diameter of the 5-ASA-zein (10%) NPs were found in the layer 2, two theories of their material content were proposed as mentioned earlier - the microparticles are either core shell particles consisted of zein NPs core coated with PVP shell, or reprecipitated zein on its own. Confocal fluorescence microscopy (CFM) was used to obtain complementary data (see Figure 5.6), taking the advantage of strong fluorescence of zein and minimal fluorescence of PVP, when excited at 405 nm (Figure A). For this purpose, the layer 2 was electrospun directly on a glass cover slip for ~2 min. Figure B shows the image of the layer 2 without the excitation, Figure C is the fluorescent image excited at 405 nm, and Figure D is the overlay of figures B and C. Figure E is a 3D fluorescent map (excitation at 405 nm) showing spherical zein microparticles and large aggregates formed by a combination of spherical and deformed zein particles. The spherical particles were manually measured from both SEM and CFM images. Their diameter distributions are compared in the Figure 5.7. Both SEM and CFM methods showed the maximum abundance of the particles with 0.5 – 1 μm diameter (38% and 50%, respectively). SEM technique showed a tailing peak, when 3% of the particles were found in the 2.5 – 3 μm diameter range. On the other hand, the CFM method showed another maximum at 1.5 - 2 μm diameter range (13%) and no particles were found in the 2.5 – 3 μm diameter range. These inconsistencies could have been caused by the change of the substrate from grease proof paper to glass cover slip, necessary for the CFM imaging. The smallest diameters of the spherical particle found were 296 and 343 nm, measured by SEM and CFM, respectively. This confirms the theory of reprecipitation of the zein NPs into larger particles during the electrospinning process since the maximal diameter of the NPs in the feed solution was 170 nm. The reprecipitation as well as the aggregation might be caused by the excess of water coming from the PVP-HYD feed solution and mixing of the core and shell feed solutions within the Taylor cone, causing pH fluctuations. The reprecipitation process together with the aggregation were proposed to be the main reasons of the electrospinning instabilities. Although, the reprecipitation was confirmed by the CFM, the possibility that the reprecipitated zein particles were coated with a thin layer of PVP-HYD or that the aggregates were mixtures of the zein clusters and solidified PVP-HYD solution could have not been eliminated due to the low resolution of the technique.

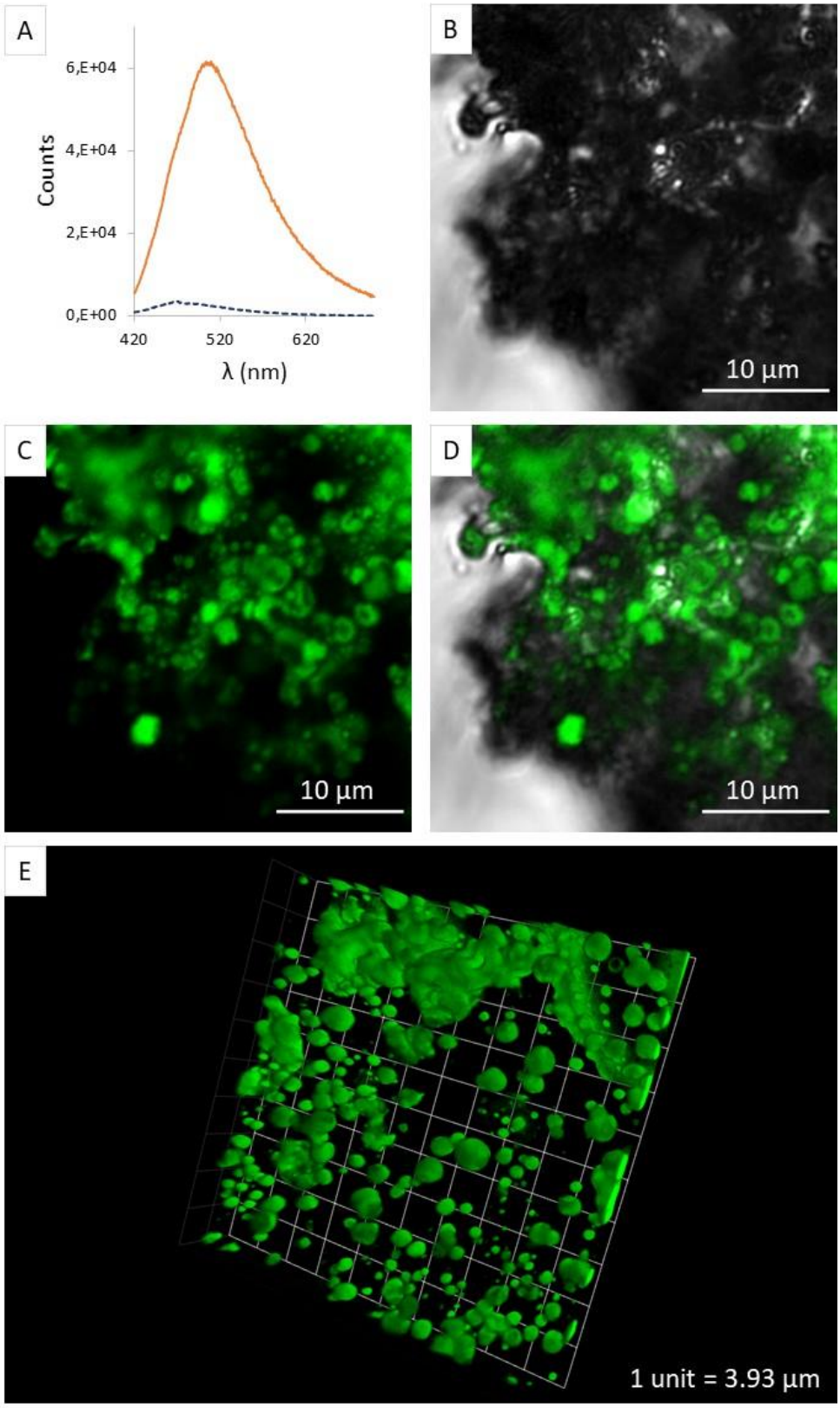

Figure 5.6. Representative Confocal Fluorescent Microscopy (CFM) images of the layer 2 and (A) a fluorescence emission spectrum of double filtered 5% zein solution in 70% EtOH aq. (v/v) (solid orange line) compared to the 7.5% PVP solution in MQ water (dashed dark blue line) at the 405 nm excitation. The CFM shows the layer 2 (B) without the excitation and (C) excited at 405 nm. The overlay of figures B and C is shown in Figure D. Figure E is a 3D fluorescent map (excitation at 405 nm) of the layer 2 sample, showing spherical zein particles and their large aggregates (please notice the scale of the units).

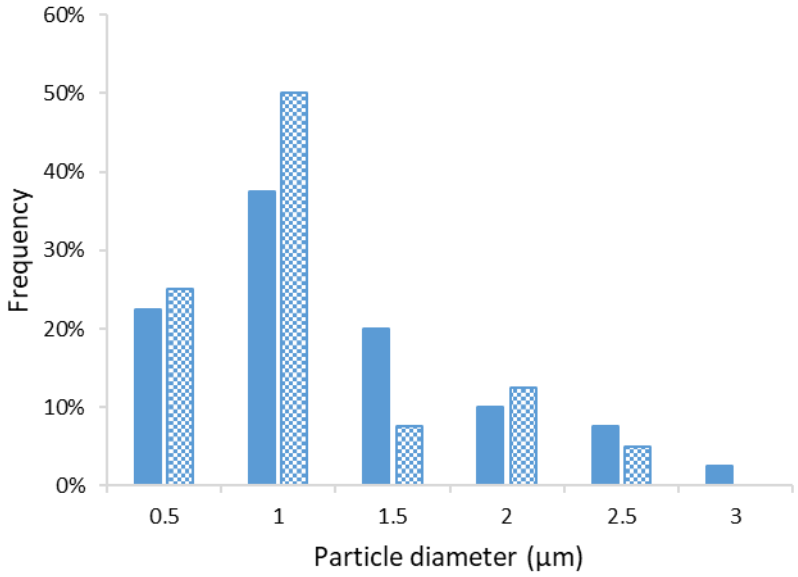

Figure 5.7. The histograms of particle diameter distribution in the layer 2 estimated from SEM (solid) and CFM (checked) images, showing the maximum abundance of the particles is within 0.5 – 1 µm diameter range and confirming the particles are reprecipitated zein NPs (potentially covered with a thin PVP layer).

The individual layers were characterised with TGA and the thermograms were compared to the corresponding physical mixes and individual materials. In the Figure 5.8, a thermogram of PVP powder was compared to the 5-ASA-zein NPs – PVP-HYD fibers (layer 2) and its physical mix. In all three thermograms a 10 ± 2% weight loss was observed in the 25 – 75 °C range, which is a common characteristic of a PVP polymer. No significant moisture uptake was detected in the layer 2 fibers (<1% weight loss in the 75 – 100 °C range). The decomposition temperature of the PVP was found at 410 °C, when additional 10 ± 1% weight loss was observed above 75 °C. This decomposition temperature was decreased to 390 °C and 380 °C for 5-ASA-zein NPs – PVP-HYD physical mix and fibers, respectively. The decrease of the decomposition temperature in the physical mix was associated with the faster decomposition rate of zein. The increased decomposition rate observed in the fibrous form could be explained by the increased surface to volume ratio caused by the electrospinning process. The thermogravimetric analysis of the HPMCAS-PARmin fibrous layer, its corresponding physical mix, and HPMCAS raw powder is also shown in the Figure 5.8. No significant weight loss at 100 °C was detected in the HPMCAS-PARmin fibers (<2%), suggesting minimal water uptake by the sample. Despite the fast decomposition rate of PAR, no change in the decomposition temperature was observed in the HPMCAS-PARmin physical mix compared to the HPMCAS raw powder (10 ± 1% weight

loss at 310 °C for both), suggesting that either the TGA was not sensitive enough to detect the ~0.05% PAR loading or the drug loading was not high enough to affect the polymer properties. However, the decomposition temperature of the HPMCAS-PARmin fibers decreased to 300 °C, suggesting again that the increased surface to volume ratio leads to a faster decomposition rate.

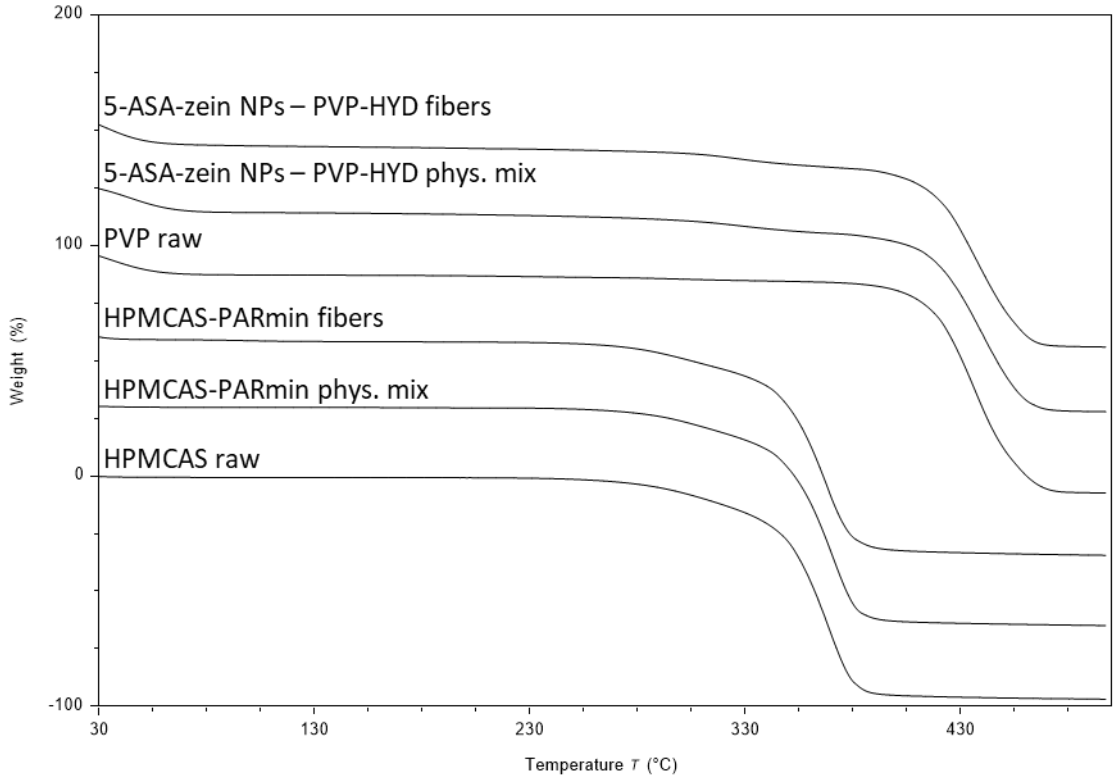

Figure 5.8. TGA thermograms of 5-ASA-zein NPs – PVP-HYD (layer 2) and HPMCAS-PARmin (layers 1 & 3) fibres showing no significant moisture uptake and faster decomposition rate compared to their corresponding physical mixes.

MDSC thermogram of the HPMCAS-PARmin fibers (layers 1 & 3) showed no significant shift of glass transition mid-point (123 °C) compared to both HPMCAS-PARmin physical mix and HPMCAS raw powder (see Figure 5.9 A), which corresponds with the TGA analysis. On the other hand, the MDSC thermogram of the 5-ASA-zein NPs – PVP-HYD fibers (layer 2) showed a depression of the glass transition (173 °C) compared to the DSC thermogram of a corresponding physical mix (175 °C). The glass transition mid-point of the PVP polymer was observed at 177 °C (see Figure 5.9 B). This suggests the glass transition of the 5-ASA-zein NPs – PVP-HYD physical mix was depressed due to the addition of the amorphous 5-ASA-zein NPs (10%) which showed glass transition at 155 °C, when analysed

separately. The glass transition was further depressed by the electrospinning process, suggesting the HYD was molecularly dispersed in the fibers.

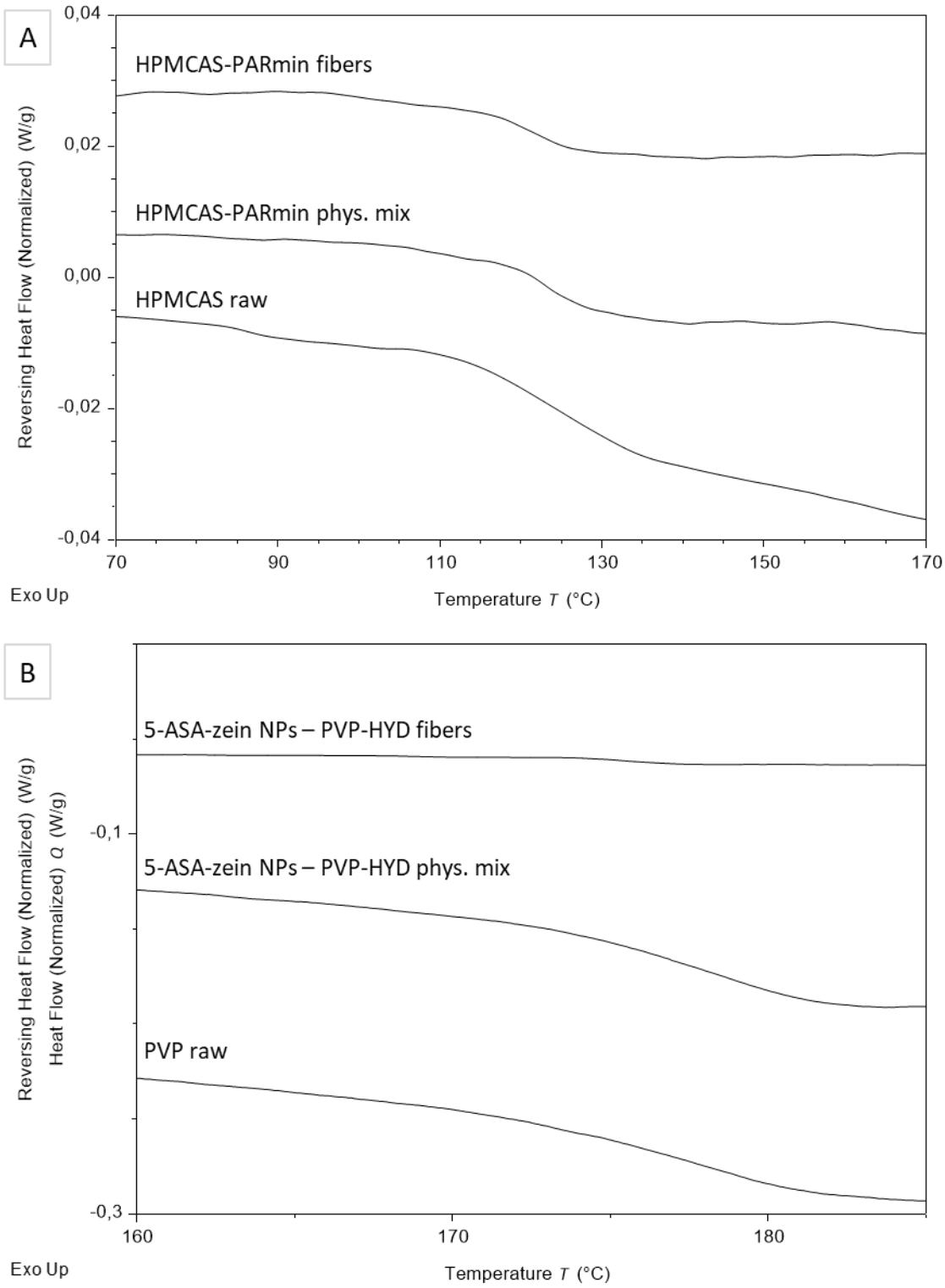

Figure 5.9. MDSC thermograms of the (A) HPMCAS-PARmin fibers and (B) 5-ASA-zein NPs – PVP-HYD fibers compared to the according physical mixes and polymer powders; (A) showing no significant shift in the glass transition of the HPMCAS-PARmin fibers (layers 1 & 3) and (B) suggesting molecular dispersion of the HYD in the electrospun layer 2.

The ATR-FTIR analysis of the HPMCAS-PARmin fibers (layers 1 & 3) showed no additional bands or their significant shifts compared to the corresponding physical mix as well as the raw HPMCAS powder (see Figure 5.10). Observing no bands belonging to PAR in the physical mix was expected as the ~0.05% paracetamol loading is not sufficient to be detected with the ATR-FTIR method and also the potential effect of the drug on the polymer would be too small at this concentration ratio. However, a broadening of the reference peak (~1050 cm^{-1}, RI = 100%) was observed in the HPMCAS-PARmin fibers, when compared with the corresponding physical mix and the unprocessed HPMCAS powder. This explains the increase in relative intensity of all the other bands in the HPMCAS-PARmin fibers, as the maximum intensity of the reference peak decreases (see the table in the Figure 5.10). The broadening of the reference peak may be associated with presence of a wider range of polymer conformations created by electrospinning.

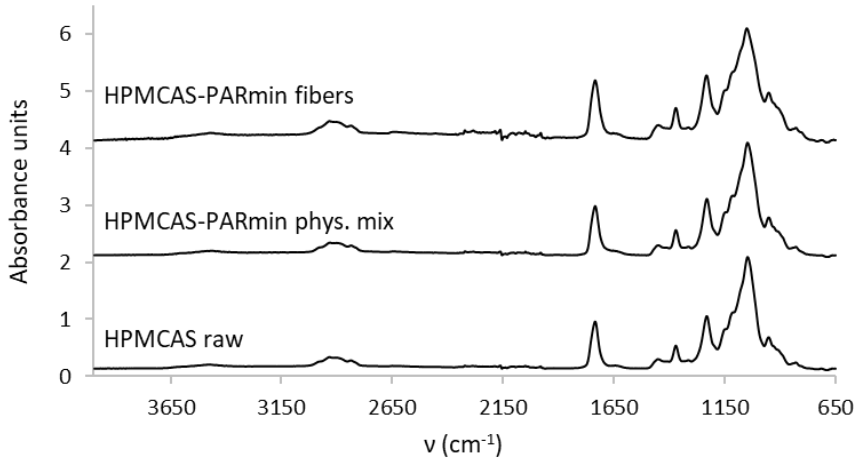

HPMCAS raw		HPMCAS-PARmin phys. mix		HPMCAS-PARmin fibers	
v (cm^{-1})	**RI (%)**	**v (cm^{-1})**	**RI (%)**	**v (cm^{-1})**	**RI (%)**
2936	12%	2934	13%	2934	19%
2839	9%	2837	10%	2837	15%
1736	43%	1736	45%	1736	55%
1645	4%	1649	5%	1649	8%
1452	10%	1450	10%	1450	15%
1371	22%	1371	24%	1371	30%
1315	9%	1315	9%	1315	13%
1232	48%	1231	51%	1232	59%
1047	100%	1047	100%	1051	100%
953	29%	953	35%	953	44%
829	7%	829	9%	829	13%

Figure 5.10. ATR-FTIR absorption spectra and a table of the bands' wavenumbers and relative intensities of the HPMCAS-PARmin fibers compared to its corresponding physical mix and raw HPMCAS powder, showing no significant shift of the bands but increase in relative intensity of all peaks after electrospinning.

The fibrous layer 2 was also characterised by the ATR-FTIR (see Figure 5.11). The spectra of the 5-ASA-zein NPs – PVP-HYD fibers and its physical mix are suggested to be two different combinations of the spectra belonging to the raw PVP powder and the 5-ASA-zein NPs (10%), as shown in the table in the Figure 5.11. The bands belonging to the 5-ASA-zein NPs (10%) are more prevalent in the physical mix than in the electrospun fibers, suggesting the reprecipitated particles in the layer 2 may be coated with a thin PVP shell. The maximum at 3296 cm^{-1} found in the physical mix could correspond to the 5-ASA-zein NPs (10%) band observed at 3290 cm^{-1}. No maximum at this region was found in the spectra of the electrospun layer 2 or the raw PVP powder. Compared to the raw PVP powder, another additional band was observed at 1537 and 1545 cm^{-1} in the spectra of the 5-ASA-zein NPs – PVP-HYD physical mix and the fibers, respectively. This band corresponds to the 5-ASA-zein NPs (10%) band found at 1531 cm^{-1}, which is the amide II peak. The relative intensity of this band is almost twice higher in the physical mix (25%) than in the fibers (13%) and the band is significantly shifted in the fibers compared to the physical mix. This shift could be caused by a minor change in the zein spectrum of the reprecipitated particles. However, no significant shift was observed in the amide I region (1645 – 1650 cm^{-1}), suggesting no significant change in the secondary structure of the protein. All the other bands, which were assigned as overlapping with or directly belonging to the 5-ASA-zein NPs (10%) in the physical mix and fibers spectra, were significantly shifted. This suggests the ball milling and the electrospinning might affect the materials' interaction. However, this phenomenon should be studied with less complex samples. The spectrum of hydrocortisone is not shown in this figure due to its undetectable (~0.04%) loading.

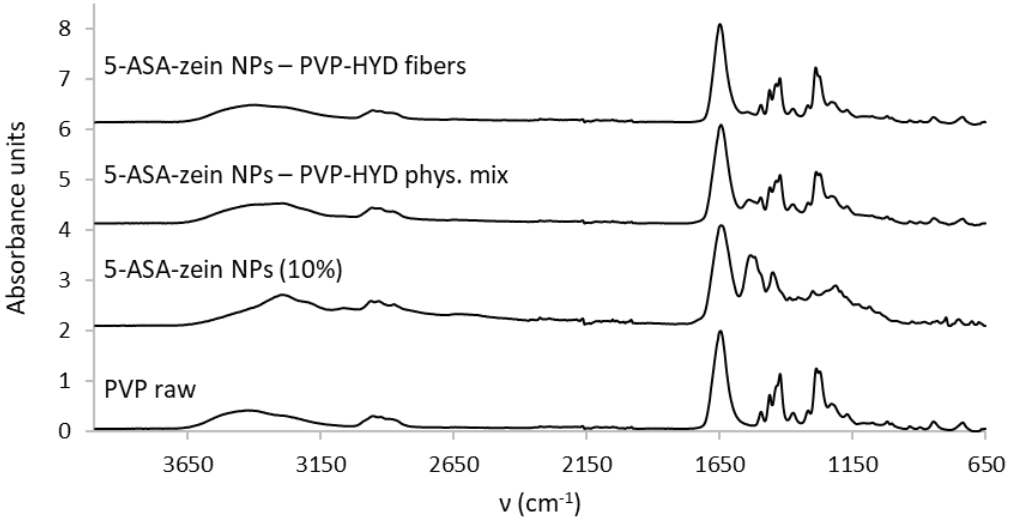

PVP raw		5-ASA-zein NPs – PVP-HYD phys. mix		5-ASA-zein NPs – PVP-HYD fibers		5-ASA-zein NPs (10%)	
v (cm^{-1})	RI (%)	v (cm^{-1})	RI (%)	v (cm^{-1})	RI (%)	v (cm^{-1})	RI (%)
3423	21%	3398	21%	3396	20%	x	x
x	x	3296	22%	x	x	3290	31%
2951	15%	2955	18%	2953	14%	2959	25%
2922	14%	2928	17%	2926	14%	2932	25%
2891	13%	2878	14%	2893	12%	2874	21%
1645	100%	1643	100%	1649	100%	1643	100%
x	x	1537	25%	1545	13%	1531	70%
x	x	x	x	x	x	1518	69%
1493	19%	1495	28%	1495	20%	x	x
1460	36%	1460	38%	1462	34%	x	x
x	x	x	x	x	x	1448	53%
1421	57%	1421	50%	1423	46%	x	x
1373	19%	1373	21%	1373	16%	x	x
1317	21%	1315	23%	1317	19%	x	x
1286	63%	1286	53%	1288	57%	1298	35%
1273	60%	1273	51%	1275	49%	x	x
1229	27%	1229	29%	1229	23%	1213	40%
1169	17%	1171	19%	1171	15%	x	x
845	10%	843	7%	845	8%	847	4%
735	9%	735	7%	735	8%	750	7%

Figure 5.11. ATR-FTIR absorption spectra and a table of the bands' wavenumbers and relative intensities of the 5-ASA-zein NPs – PVP-HYD fibers compared to its corresponding physical mix, raw PVP powder, and

5-ASA-zein NPs (10%), suggesting the zein in the 5-ASA-zein NPs (10%) changed its secondary structure after the reprecipitation within the electrospinning process.

The PXRD diffractograms of the fibrous layers and their corresponding physical mixes, both HPMCAS-PARmin and 5-ASA-zein NPs – PVP-HYD, showed no crystalline peak. This suggests the drug loading in both types of the electrospun layers were indetectable by PXRD. These diffractograms are compared to the diffractograms of unprocessed polymers and drugs in the Figure 5.12.

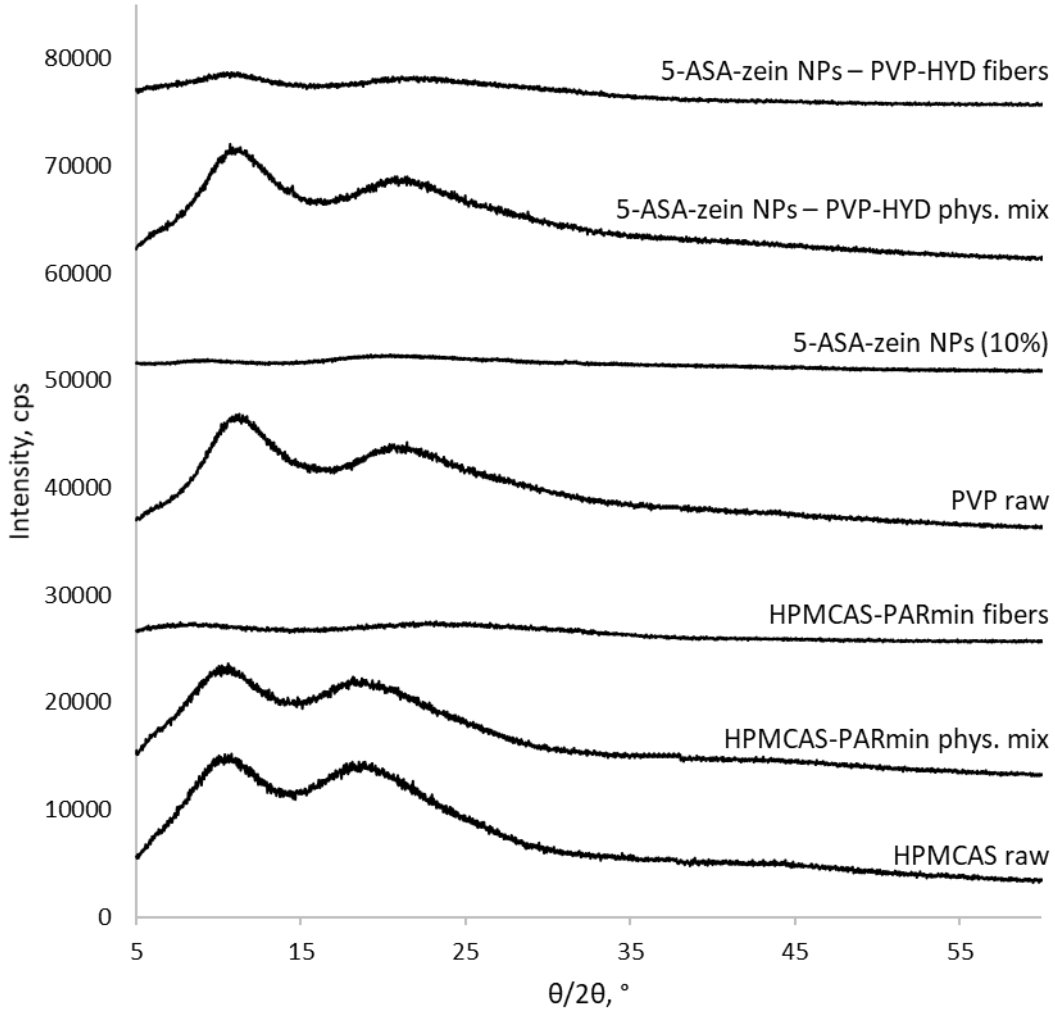

Figure 5.12. PXRD diffractograms of HPMCAS-PARmin and 5-ASA-zein NPs – PVP-HYD fibers, their physical mixes, the raw polymers, and the 5-ASA-zein NPs (10%); showing no crystalline peaks in any of the physical mixes or the electrospun samples.

The layered formulation was tested for drug release properties following the same method as in the dissolution of the MIX-HPMCAS fibers in Chapter 3, using LC-MS as a quantification technique. The cumulative drug release profiles (CDR) of all three drugs are shown in the Figure 5.13. 5-ASA showed a release profile following the same trends as in the release from the MIX-HPMCAS fibers or the 5-ASA-zein NPs (10%), when 56 ± 8% of the drug was released within 2 hours in pH = 1.2, followed by a plateau in pH = 7.4. The release of HYD in pH = 1.2 was significantly faster when compared with the release from the MIX-HPMCAS fibers, showing 36 ± 8% release at 2 hours in pH = 1.2, while total release of the drug at 8 hours was not significantly different from the total release observed in the MIX-HPMCAS fibers. The faster release of HYD in the acidic pH was associated with the high solubility of PVP in such conditions as well as with the increased surface to volume ratio due to the significantly lower diameter of the PVP-HYD fibers when compared with the MIX-HPMCAS fibers. No release of PAR was detected within the first two hours in pH = 1.2, followed by a slow release in pH = 7.4 reaching a total release of 12 ± 3% at 8 hours. This dissolution experiment showed the HPMCAS-PARmin fibers are not behaving as an enteric coating of the 5-ASA-zein NPs - PVP-HYD fibers, releasing more than 10% of the 5-ASA and HYD, each. However, the PAR release profile suggested the low drug loading could lead to a significantly slower drug release rate as well as preserving of the HPMCAS enteric properties after electrospinning.

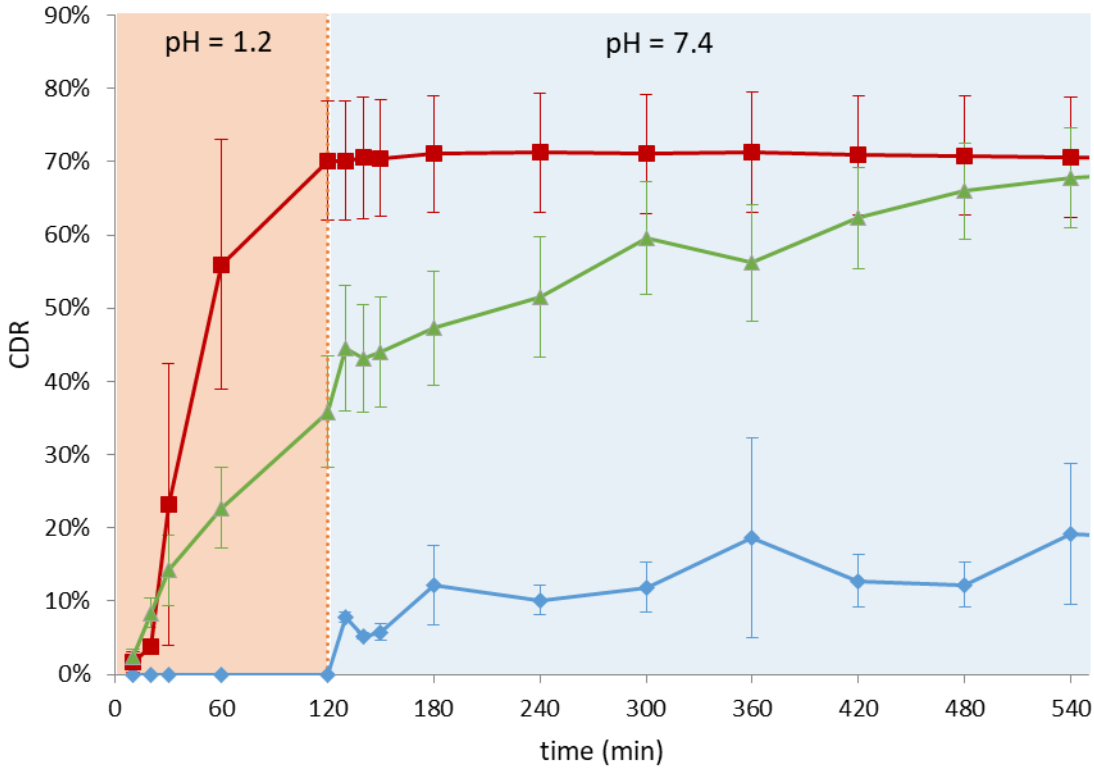

Figure 5.13. Cumulative drug release (CDR) from the layered formulation, simulating the pH transition from stomach acidic pH = 1.2 to colonic pH = 7.4 at 2 hour time point. Blue diamonds show release of PAR, red squares release of 5-ASA, and green triangles release of HYD.

5.3.2 Effects of drug loading on the enteric properties of the electrospun HPMCAS fibers

As the PAR release from the layered formulation suggested the low drug loading could lead to a significantly slower drug release rate as well as preserving of the HPMCAS enteric properties after electrospinning, the effect of the minimal drug loading levels was studied more closely. For this purpose, HPMCAS fibers containing 0.05% of PAR, 0.05% of HYD, and 0.15% of 5-ASA were prepared by a single nozzle electrospinning technique, following the conditions set up for the MIX-HPMCAS fibers (20% (w/v) solution of HPMCAS in acetone:DMSO (3:2; v:v) plus according concentrations of the drugs, 22G nozzle, 0.72 ml/h feed rate, 20 cm nozzle-collector distance, RH = 30 ± 2%, grease proof paper on a rotating drum: 60 rpm, 50 mm/s scan over 2 cm). The chamber temperature was 17.3 °C and the positive voltage was gradually increased from 11.92 kV to 17.22 kV over the course of 3.5 hours to keep the Taylor cone stable. The produced fibers are further referred to as MIX-HPMCASmin. Even though the need for gradual increase of the voltage suggests an

instability of the electrospinning process, only 13 beads were found in 9 different locations of the MIX-HPMCASmin fiber mat scanned by the SEM (see representative scans in the Figure 5.14 A, B), compared to >100 beads found in the same number of locations of the blank HPMCAS fibers. However, the diameter of the fiber was broadly distributed across 130 - 3078 nm range, where fibers with the diameter of 400 - 500 nm were the most abundant but creating only 20% of the whole sample (see Figure 5.14 C). None of the 13 beads found was spherical and 54% of the beads showed bead length/width ratio greater than 4 (see Figure 5.14 D).

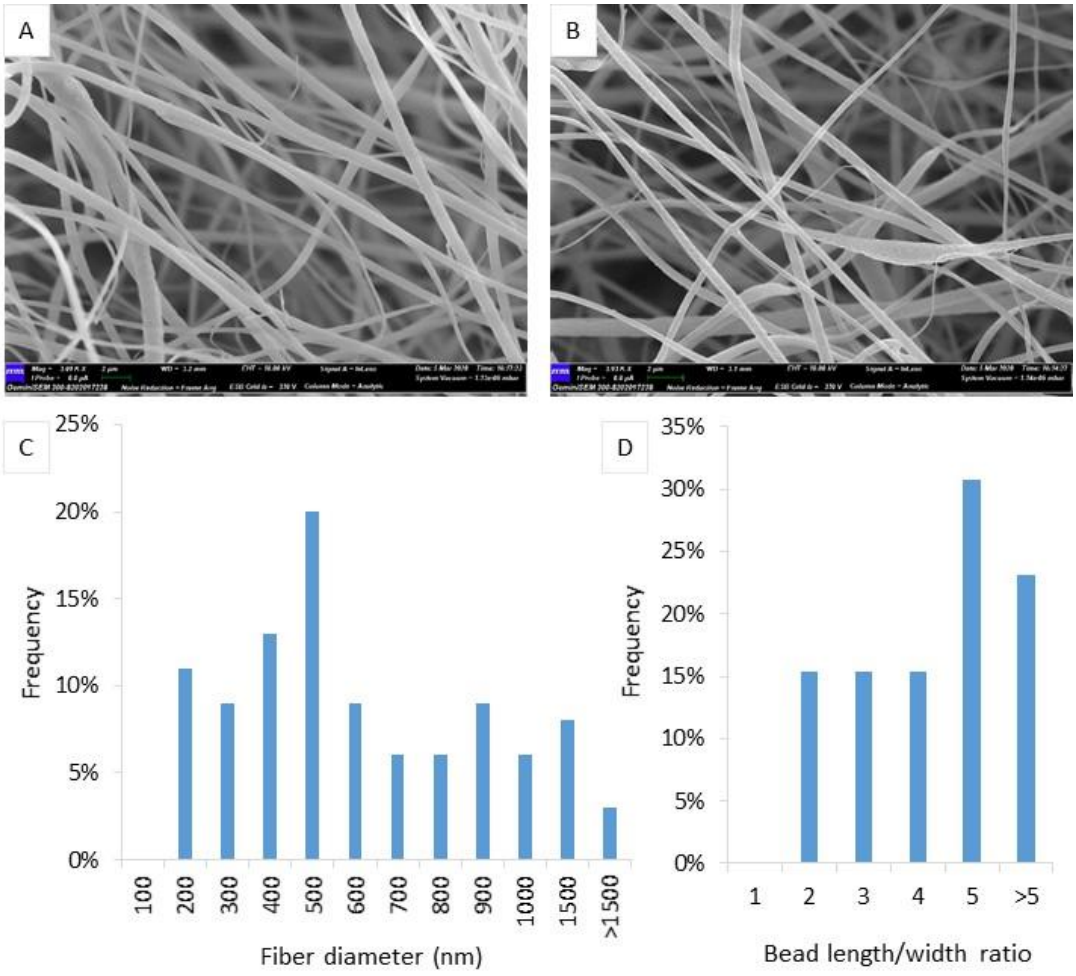

Figure 5.14. Representative (A,B) SEM scans of the MIX-HPMCASmin fibers showing (C) broad distribution of the fiber diameter and low total number of the beads, which were (D) predominantly elongated.

The low abundance of beads in the MIX-HPMCASmin fibers led to a study of the properties of the feed solution. No significant difference in viscosity, conductivity, and surface tension was observed in comparison with the blank HPMCAS solution. However, the processing temperature of the MIX-HPMCASmin fibers was 7.2 °C lower than for the blank HPMCAS

fibers causing significant changes in these parameters (increased viscosity and surface tension, decreased conductivity).

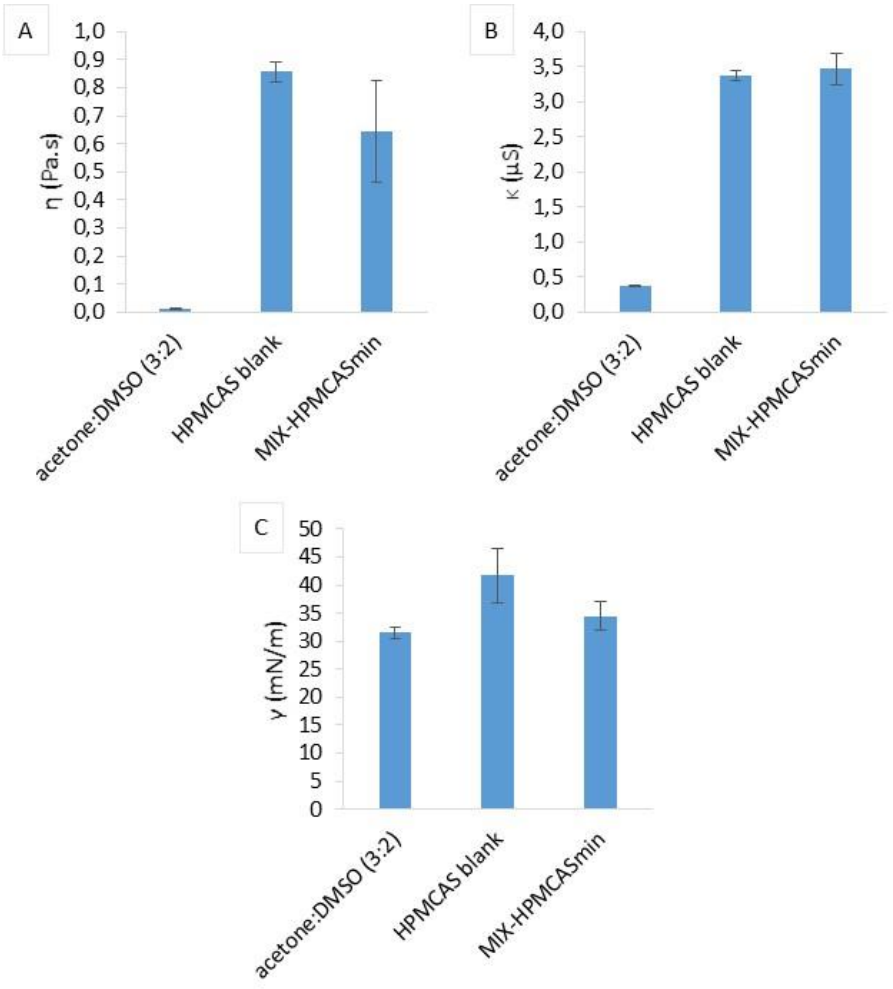

Figure 5.15. Solution properties of MIX-HPMCASmin compared to blank HPMCAS solution and the solvent binary mixture in terms of: (A) viscosity (η) measured at shear rate of 28.4 s^{-1}, (B) conductivity (κ) measured at 20 - 22 °C, and (C) surface tension (γ) measured at 21 ˚C.

The TGA analysis of the MIX-HPMCASmin fibers in the Figure 5.16 shows a faster decomposition rate (10 ± 1% weight loss at 300 °C), when compared to the corresponding physical mix and raw HPMCAS powder (both showing 10 ± 1% weight loss at 310 °C). This could be associated with the surface to volume ratio of the sample. The MDSC analysis of the MIX-HPMCASmin fibers in the Figure 5.17 shows the glass transition depression (mid-point at 119 °C) compared to the corresponding physical mix and raw HPMCAS powder (both showing mid-point at 123 °C). The absence of the melting peaks in the physical mix might be explained by the low drug loading levels which were not detectable by the MDSC method.

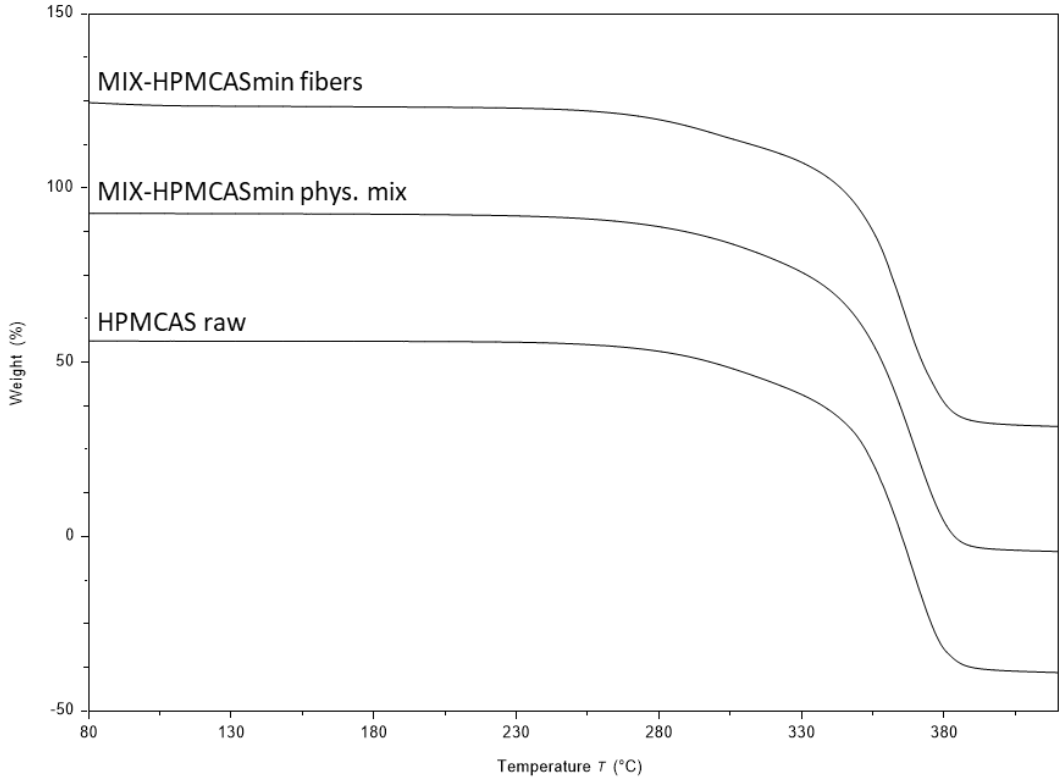

Figure 5.16. The TGA thermograms of the MIX-HPMCASmin fibers, its corresponding physical mix, and unprocessed HPMCAS powder, showing a faster decomposition rate in the fibrous sample compared to its physical mix.

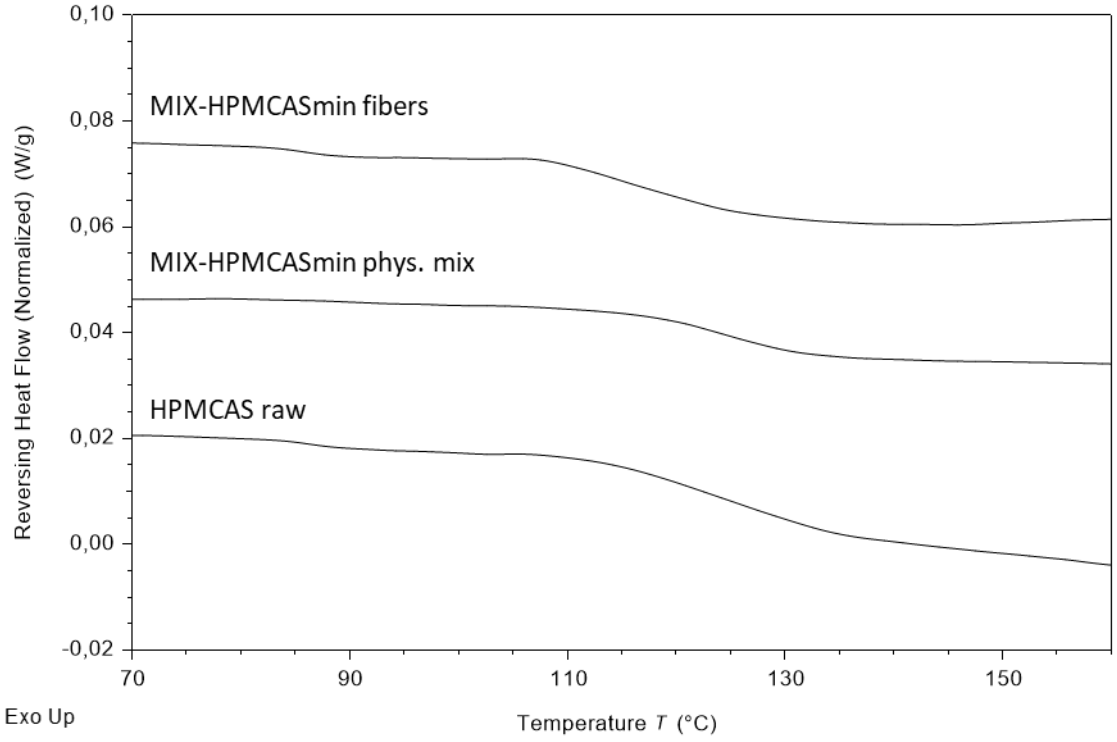

Figure 5.17. The MDSC thermograms of the MIX-HPMCASmin fibers, its corresponding physical mix, and unprocessed HPMCAS powder, showing a glass transition depression in the fibrous sample compared to its physical mix.

The ATR-FTIR spectrum of the MIX-HPMCASmin fibers was identical to the spectra of the MIX-HPMCASmin physical mix and unprocessed HPMCAS powder (see Figure 5.18), suggesting the drug loading levels were undetectable by the ATR-FTIR technique. The drugs were not detectable by the PXRD technique either, showing no crystalline peaks in either of the fibrous sample or its physical mix (see Figure 5.19).

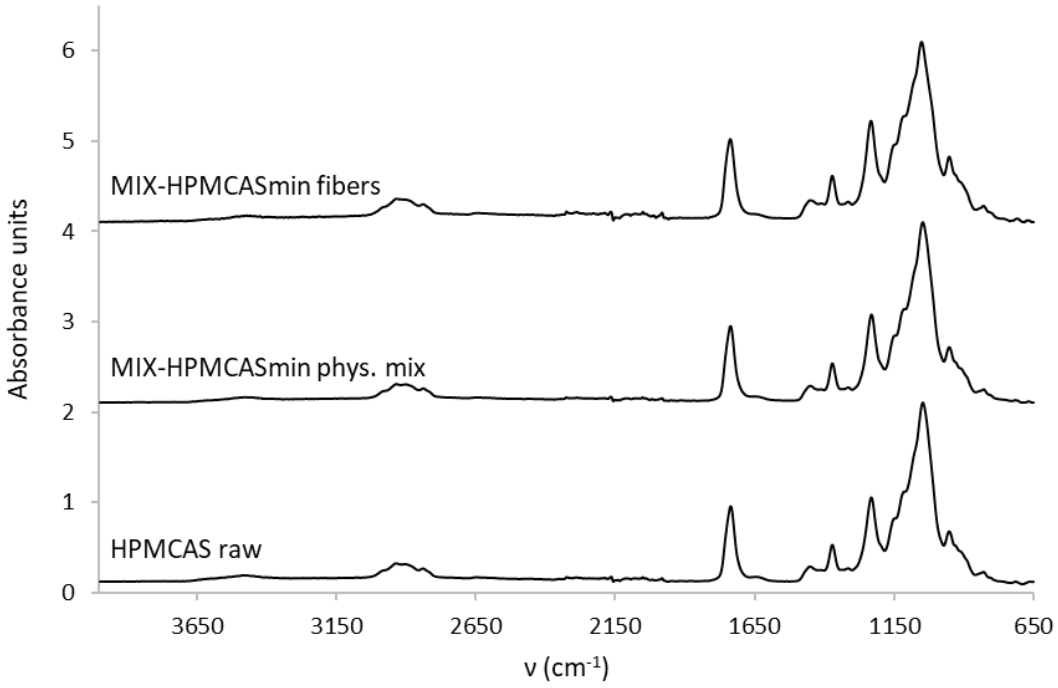

Figure 5.18. ATR-FTIR spectra of the the MIX-HPMCASmin fibers, its corresponding physical mix, and unprocessed HPMCAS powder, showing no band shifts or change in the relative intensities of the bands after electrospinning.

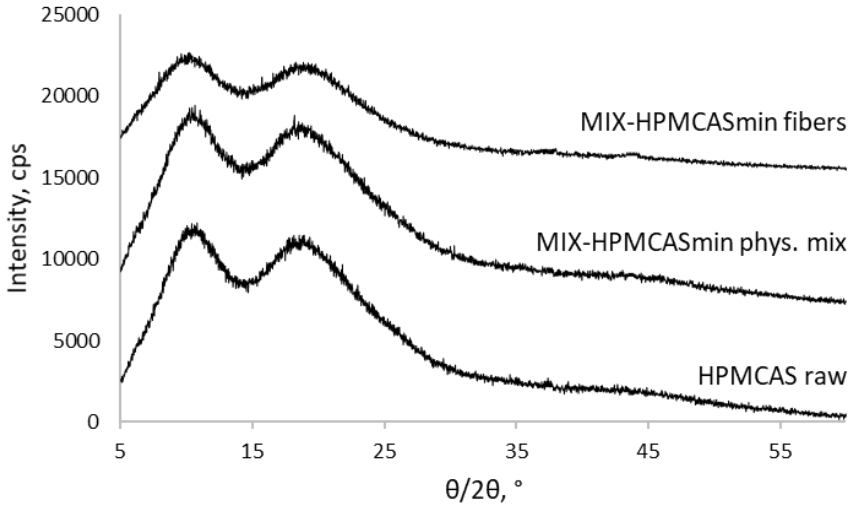

Figure 5.19. PXRD diffractograms of the the MIX-HPMCASmin fibers, its corresponding physical mix, and unprocessed HPMCAS powder, showing no crystalline peaks in the physical mix and the fibrous samples.

Following the same dissolution conditions as in the case of the MIX-HPMCAS fibers and the layered formulation, the drugs were quantified over 8 hours using LC-MS. The cumulative drug release profiles of the three drugs are showed in the Figure 5.20. More than 10% of each drug was released within first two hours in pH = 1.2, suggesting the enteric properties of HPMCAS were not preserved despite the total drug loading of 0.25%. When transferred into colonic pH, both PAR and HYD showed steady sustained release, while the 5-ASA reached a plateau. However, the reliability and accuracy of the LC-MS method should be studied more closely due to the low drug concentrations, especially after the pH transfer. Since the drug masses released in the acidic pH were not transferred into the vessels with colonic pH and therefore, the drug concentrations within the vessel came nearer to the LOD.

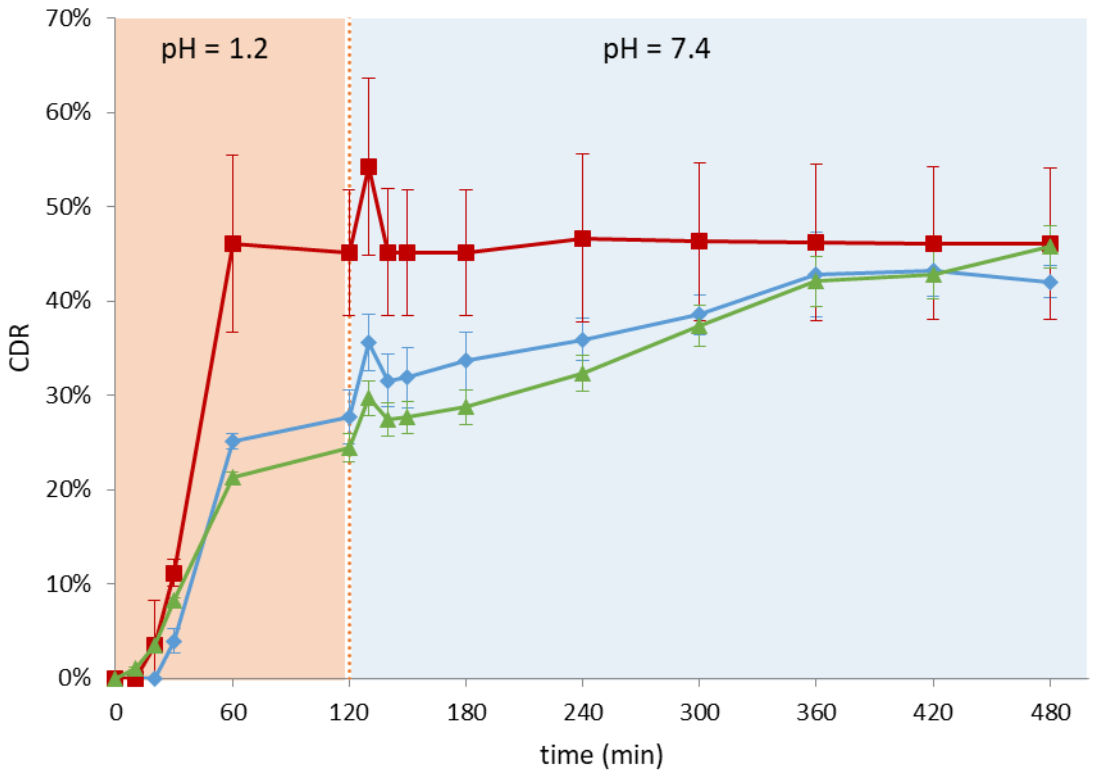

Figure 5.20. Cumulative drug release (CDR) from the electrospun MIX-HPMCASmin formulation, simulating the pH transition from stomach acidic pH = 1.2 to colonic pH = 7.4 at 2 hour time point. Blue diamonds show release of PAR, red squares release of 5-ASA, and green triangles release of HYD.

5.3.3 Effects of fiber diameter on the enteric properties of the HPMCAS

It was proposed that the enteric properties of the HPMCAS could be affected by the diameter of the fibers. As the HPMCAS swells at pH above 7 by absorption of water and allows free

movement of the drug, while much slower diffusion of the drug occurs in the acidic pH. However, the low diameter in the electrospun fibers seem to allow sufficient diffusion of the drug to cause a significant drug loss. For this study, filaments of three different diameters were prepared by the hot melt extrusion (HME). The drug-polymer ratios of the electrospun fibers in the Chapter 3 were kept and following filaments were prepared: blank HPMCAS extrudates, 5-ASA-HPMCAS extrudates (7% of 5-ASA), PAR-HPMCAS extrudates (8% of PAR), HYD-HPMCAS extrudates (2% of HYD), and MIX-HPMCAS extrudates (mixture of the three drugs, 17% of total drug loading). Even though the mid-point of the glass transition of the HPMCAS was found at 123 °C, the optimal extruding temperature of the polymer was found at 170 °C. At this temperature, it was possible to manually control the diameter of the filament to achieve three significantly different diameters (including the one controlled by the extruder nozzle). In the Figure 5.21, representative photos of the filaments are shown. The blank HPMCAS extrudates were clear yellow. The yellow colour intensified after adding paracetamol, while faded with addition of hydrocortisone. Once 5-ASA was added, the filaments became dark brown and opaque, while darker shade was observed at the MIX-HPMCAS extrudates due to lower concentration of the HPMCAS polymer. The brittleness of the filaments was also increased in both cases. This suggests the 5-ASA was oxidised and polymerised within the filaments, so the initial content of the 5-ASA needs to be assayed closely before the drug release studies.

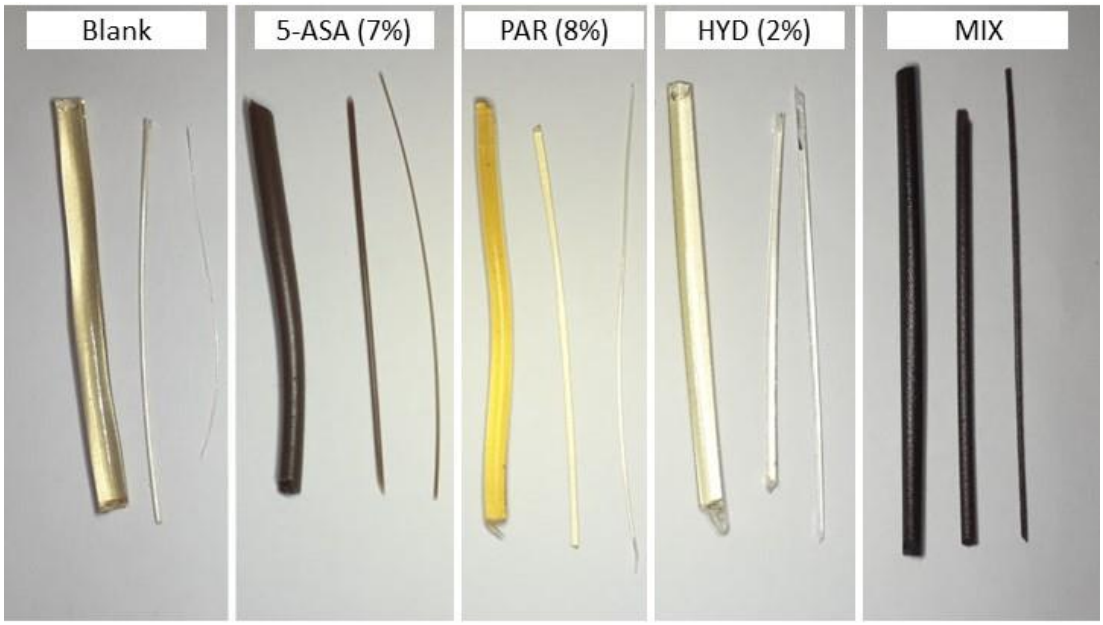

Figure 5.21. Representative photos of extruded blank HPMCAS, 5-ASA-HPMCAS, PAR-HPMCAS, HYD-HPMCAS, and MIX-HPMCAS filaments of three different manually controlled diameters, showing a colour change depending on the drug used in the composition.

The blank and single drug loaded filaments were stored in the desiccator at RH = 0% for 6 months before they were characterised due to the COVID-19 pandemic. The MIX-HPMCAS filaments were prepared fresh but also stored in the desiccator at RH = 0% in between experiments.

The morphology of the extruded filaments was imaged by SEM, when a surface and a cross section of each filament were scanned. The cross section was prepared by snapping of the filament manually to avoid any morphological changes caused by the increased pressure created by tools such as scalpel. In the Figure 5.22, representative SEM scans of the blank HPMCAS extrudates are shown. The surface (figure A) of the filament was smooth with occasional bumps. When the filaments with manually decreased (stretched out) diameter were snapped, they created a wood-like structure (figure B), while the filament with the highest diameter (controlled by the extruder nozzle) showed flaky structure (figures C and D).

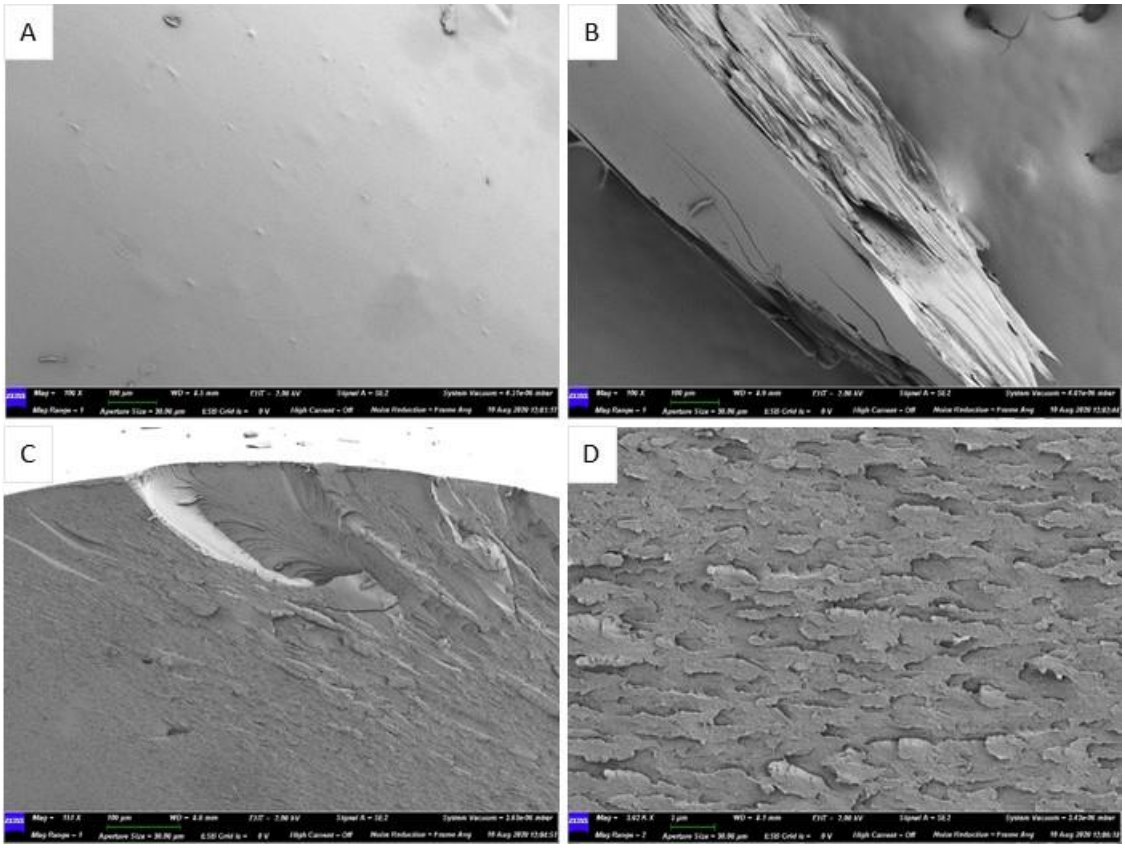

Figure 5.22. Representative SEM scans of the blank HPMCAS extrudates showing (A) smooth surface with occasional bumps, (B) wood like structure on the cross section of the filaments with manually controlled diameters, and (C – D) a flaky structure on the cross section of the thickest filaments with diameter controlled by the extruder's nozzle.

In the Figure 5.23, the surface and cross section of the drug loaded filaments with the thickest diameters (controlled by the extruder's nozzle) are shown. The 5-ASA-HPMCAS filaments showed a wood-like surface (A1) and plate drug crystals on the cross section (A2). The presence of the 5-ASA crystals was expected since the extrusion temperature (170 °C) was significantly lower than the drug's melting point. However, the 5-ASA decomposes before its melting and therefore, the extrusion temperature was kept at the optimal temperature for the HPMCAS polymer processing to avoid any drug decomposition. Smooth surface with occasional bumps as well as smooth cross section were observed in the scans of the PAR-HPMCAS extrudates (B1 and B2, respectively). Smooth surface was also observed in the HYD-HPMCAS extrudates (C1). However, the HYD-HPMCAS filaments showed a semolina-like structure (C2), suggesting the HYD might not have been fully molecularly dispersed due to its higher melting temperature (onset at 223 °C) compared to the processing temperature (170 °C). The MIX-HPMCAS filaments showed a rough surface (D1) similar to the 5-ASA-HPMCAS filaments, although slightly smoother. The plate crystals were also observed on the cross section of the MIX-HPMCAS filaments (D2) due to insufficient processing temperature to melt the 5-ASA.

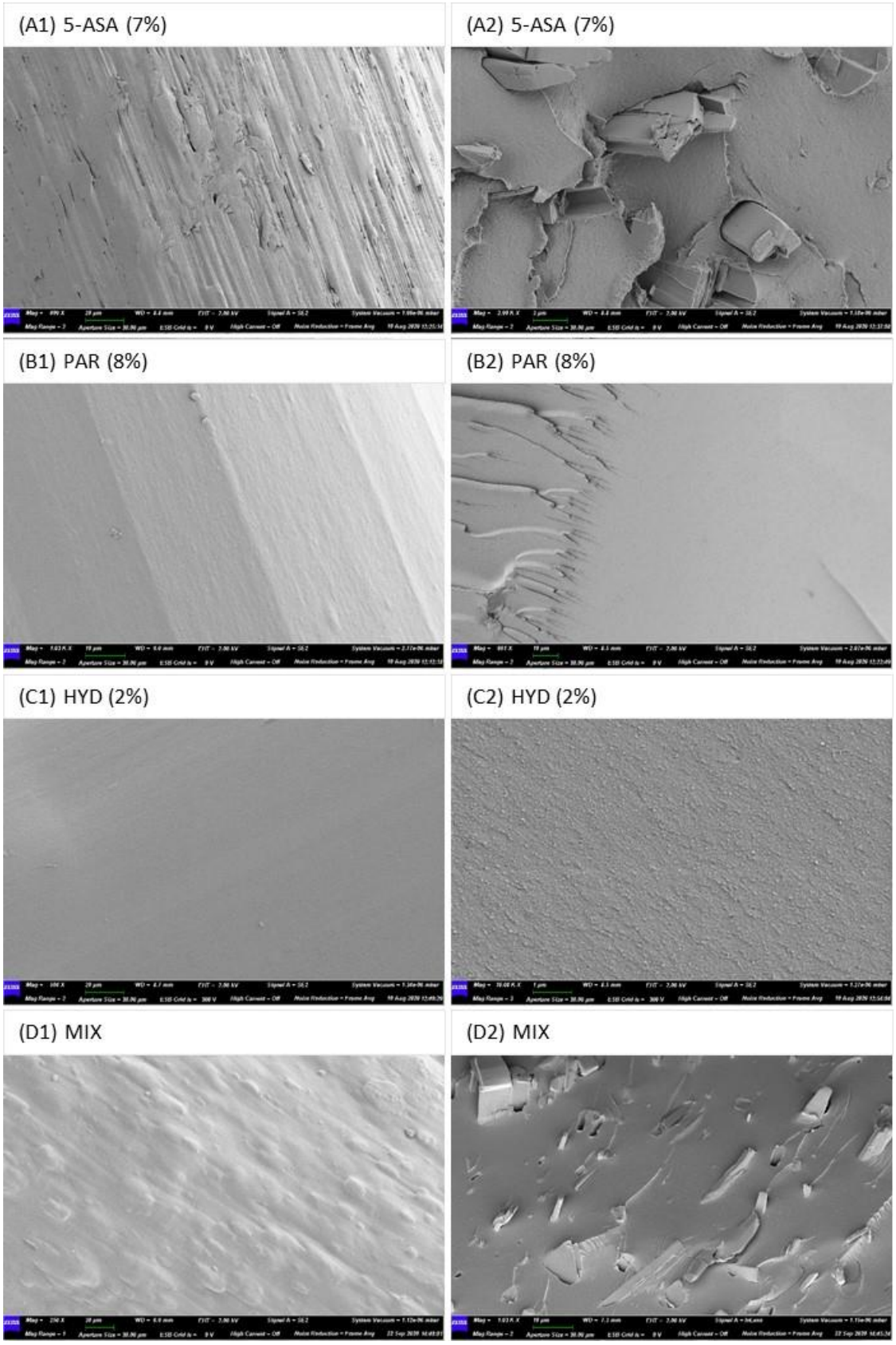

Figure 5.23. Representative SEM scans of the drug loaded extruded filaments: (A) 5-ASA-HPMCAS extrudates, (B) PAR-HPMCAS extrudates, (C) HYD-HPMCAS extrudates, and (D) MIX-HPMCAS extrudates showing the structure of (1) the filament surface and (2) the cross section of the filaments with diameter controlled by the extruder's nozzle.

All the extruded filaments were characterised with TGA, while <1.5% of weight loss was observed at 100 °C in each of them. The minimal moisture content was expected since the samples were stored at desiccator with RH = 0%. No significant difference of the decomposition rate was observed in the blank HPMCAS, 5-ASA-HPMCAS, HYD-HPMCAS, and MIX-HPMCAS extrudates compared to their physical mixes, showing 10 ± 1% weight loss at 310 °C, 270 °C, 315 °C, and 245 °C, respectively. Only PAR-HPMCAS extrudates showed faster decomposition rate compared (10 ± 1% weight loss at 280 °C) to its physical mix (10 ± 1% weight loss at 290 °C), which could be associated with an early onset of the PAR decomposition (155 °C).

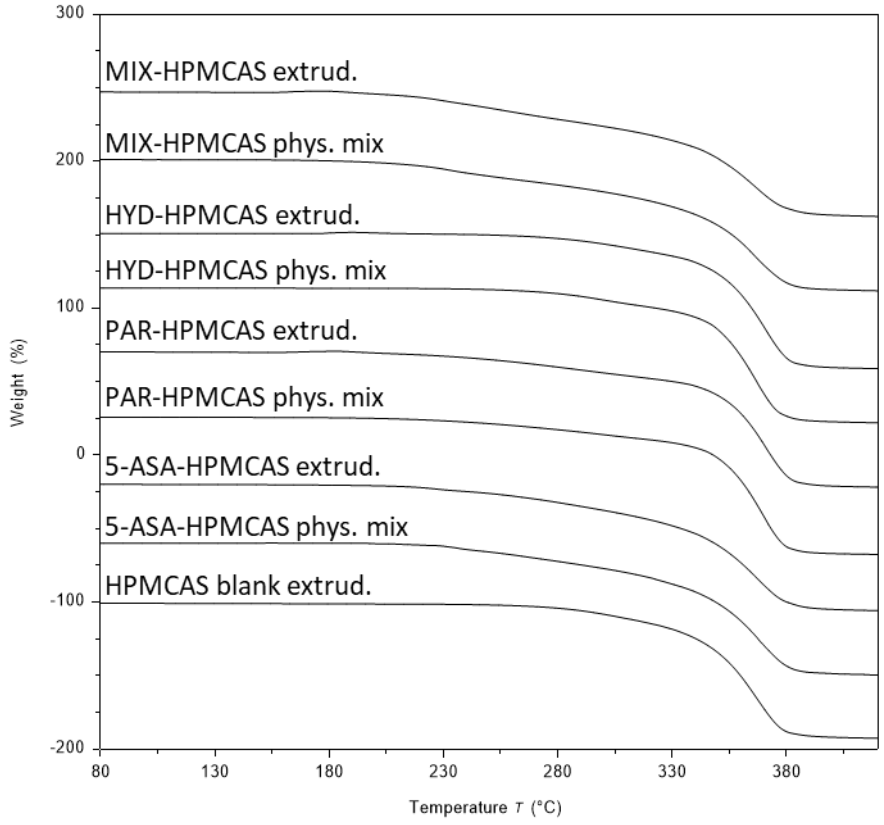

Figure 5.24. TGA thermograms of the drug loaded extruded filaments compared to the thermograms of the corresponding physical mixes and blank HPMCAS extrudates.

The MDSC analysis showed a significant depression of the glass transition in all drug loaded extruded samples compared to their corresponding physical mixes (see Figure 5.25), suggesting molecular dispersion of the drugs within the filaments. The glass transition mid-point of the blank HPMCAS extrudates was found at 120 °C, which is 3 °C lower than the unprocessed HPMCAS powder. The 5-ASA-HPMCAS extrudates showed a glass transition mid-point temperature at 121 °C compared to the corresponding physical mix which showed a glass transition at 124 °C. This suggests, that even though the 5-ASA

crystals were observed on the cross section of the filaments by SEM, some of the drug could have been molecularly dispersed in the filaments to some degree. PAR-HPMCAS extrudate showed 13 °C depression of the glass transition mid-point (95 °C) compared to its corresponding physical mix (108 °C). The glass transition mid-point of HYD-HPMCAS extrudates depressed to 119 °C from 125 °C and the one of MIX-HPMCAS extrudates depressed to 95 °C from 111 °C, when compared to their corresponding physical mixes.

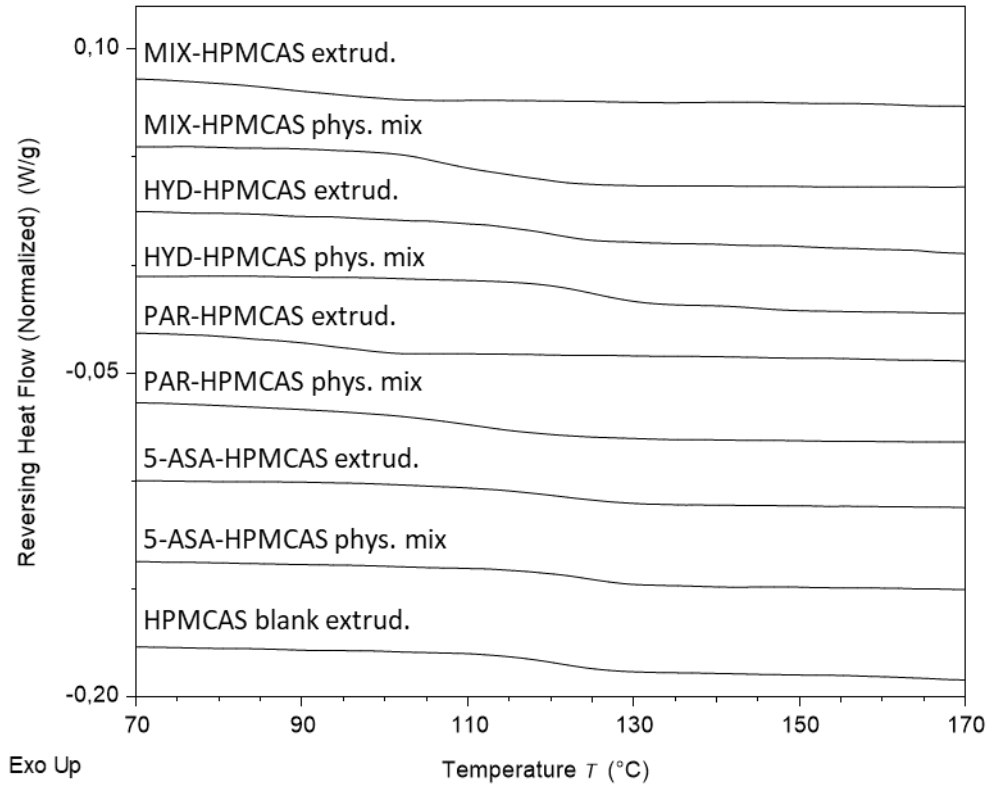

Figure 5.25. MDSC thermograms of the drug loaded extruded filaments compared to the thermograms of the corresponding physical mixes and blank HPMCAS extrudates.

The ATR-FTIR spectra of all extruded samples were compared to their corresponding physical mixes and unprocessed HPMCAS powder. The band with highest absorption intensity and therefore, 100% relative intensity, was found at ~1047 cm^{-1} in all spectra and was associated with HPMCAS. The spectrum of the blank HPMCAS extrudates showed a broadened reference peak (~1050 cm^{-1}, RI = 100%) compared to the spectrum of the raw HPMCAS, suggesting presence of a wider range of polymer conformations after extrusion (see Figure 5.26).

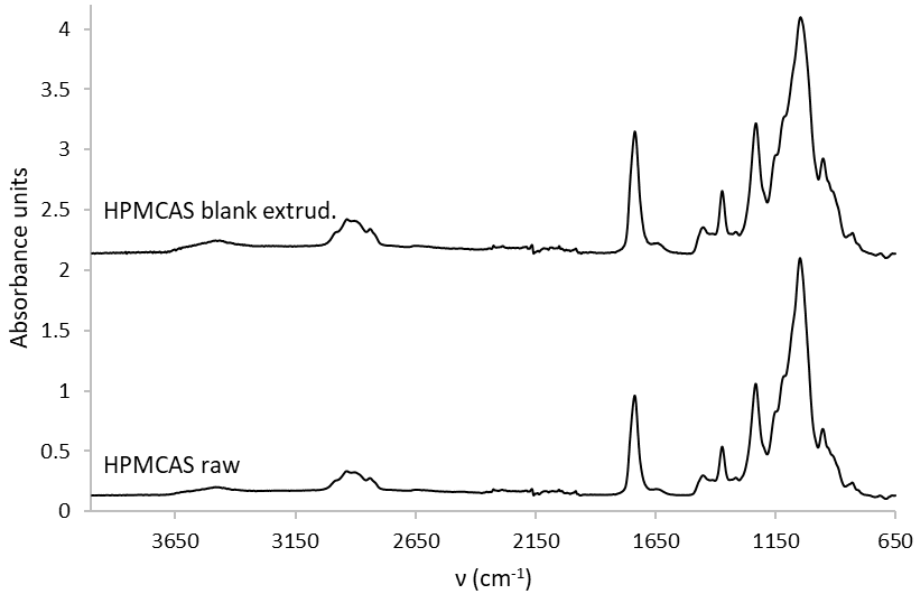

Figure 5.26. ATR-FTIR spectrum of extruded blank HPMCAS filaments compared to raw HPMCAS, showing a broadened peak at ~1050 cm^{-1} in the filament sample.

No significant band shifts or intensity changes were found in between the spectra of the 5-ASA-HPMCAS extrudates and its corresponding physical mix (see Figure 5.27). This agrees with the previous findings of the 5-ASA crystals in the extruded filaments.

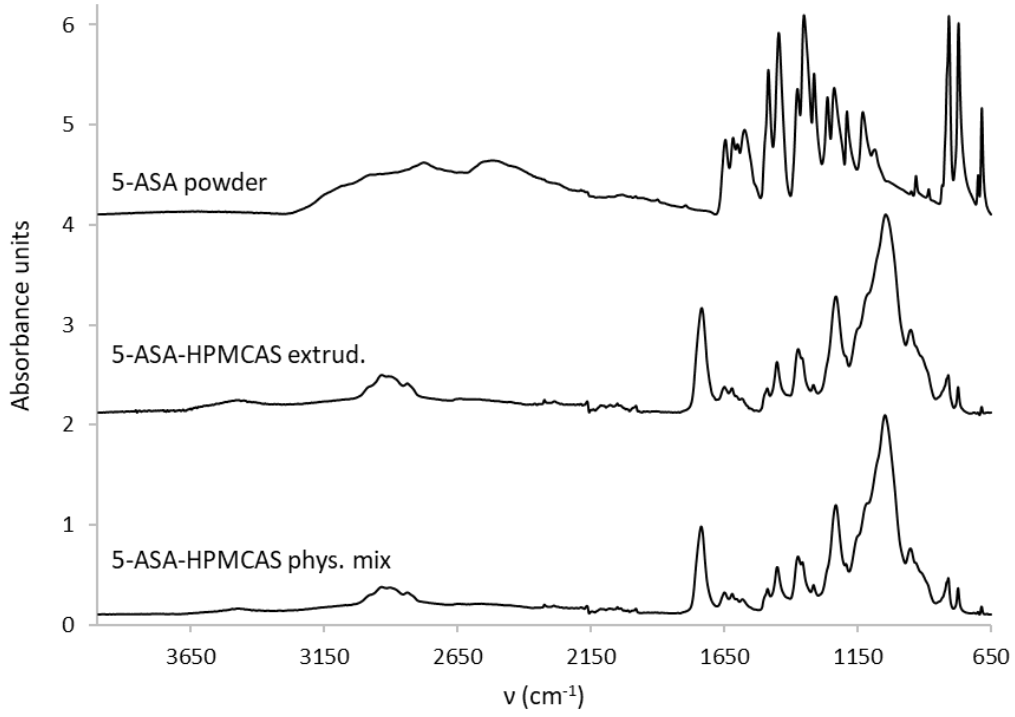

Figure 5.27. ATR-FTIR spectrum of extruded 5-ASA-HPMCAS filaments compared to its corresponding physical mix and 5-ASA powder, confirming presence of crystalline form of 5-ASA in the filaments.

A spectrum of the HYD-HPMCAS physical mix showed a sharp peak at 1643 cm^{-1}, which was the only band belonging to the hydrocortisone, as all the other peaks were associated with the HPMCAS (see Figure 5.28). This band became a broad shoulder in HYD-HPMCAS extrudates, confirming the HYD was at least partially molecularly dispersed.

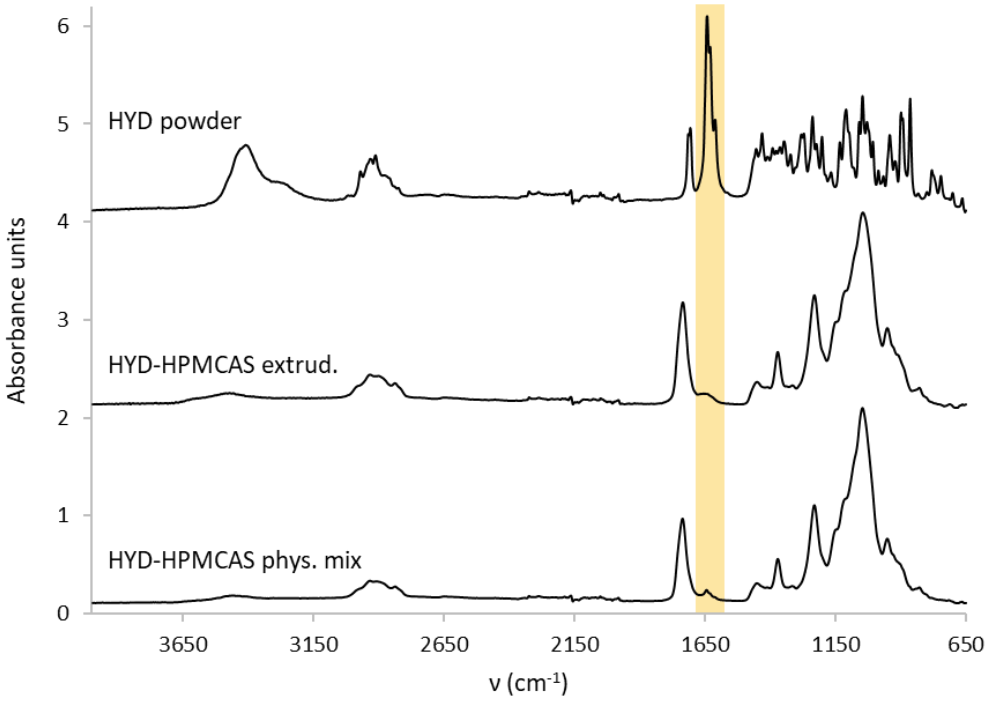

Figure 5.28. ATR-FTIR spectrum of extruded HYD-HPMCAS filaments compared to its corresponding physical mix and HYD powder, suggesting molecular dispersion of the drug in the filaments.

Figure 5.29 shows a comparison of the ATR-FTIR spectrum of extruded PAR-HPMCAS filaments compared to its corresponding physical mix and PAR powder at two different regions of interest and a corresponding table of the highlighted bands describing their exact wavenumber and relative intensity. Spectrum of PAR-HPMCAS physical mix showed a band at 3323 cm^{-1}, which disappeared in the spectrum of the extruded filaments (see Figure 5.29 A), suggesting the drug is in the amorphous form after extruding. Further significant changes in the spectrum of the PAR-HPMCAS filaments compared to its corresponding physical mix are shown in the Figure 5.29 B, where the bands of interest are highlighted in yellow and their exact wavenumbers and relative intensities are described in the accompanying table.

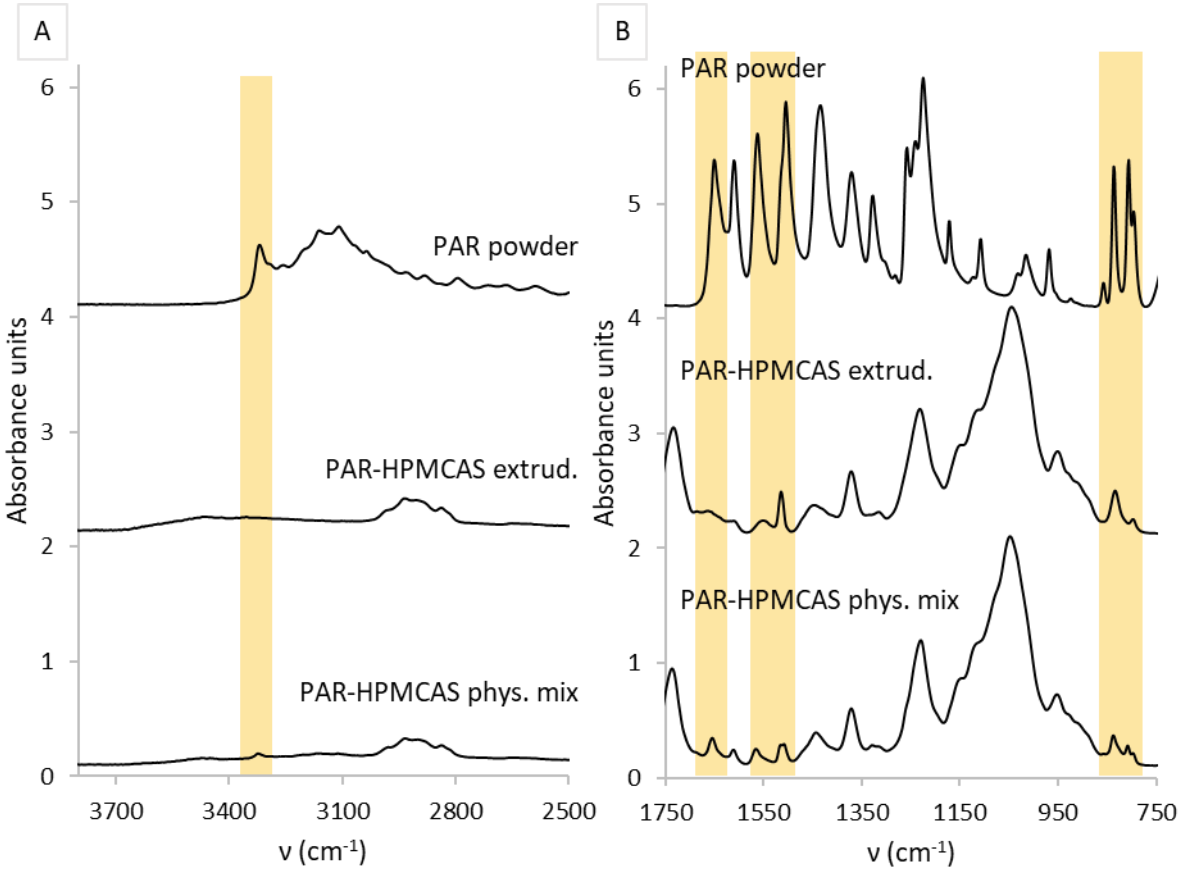

PAR-HPMCAS phys. mix		PAR-HPMCAS extrudates	
ν (cm^{-1})	RI	ν (cm^{-1})	RI
3323	5%	-	-
-	-	1686	11%
1655	13%	1644	12%
1566	8%	1551	7%
1508	10%	1514	20%
837	14%	833	20%

Figure 5.29. ATR-FTIR spectrum of extruded PAR-HPMCAS filaments compared to its corresponding physical mix and PAR powder showing (A) a disappearance of a band at 3323 cm^{-1}, suggesting the drug is in the amorphous form after extruding, and (B) further significant changes in the spectrum of the filaments. The bands of interest are highlighted in yellow and their exact wavenumbers and relative intensities are described in the accompanying table.

The ATR-FTIR spectrum of the MIX-HPMCAS extrudates was a combination of the 5-ASA-HPMCAS and PAR-HPMCAS extrudates spectra. The significant shifts, changes in relative intensities, and association of these bands compared to the MIX-HPMCAS physical mix are shown in the Figure 5.30 and Table 5.2.

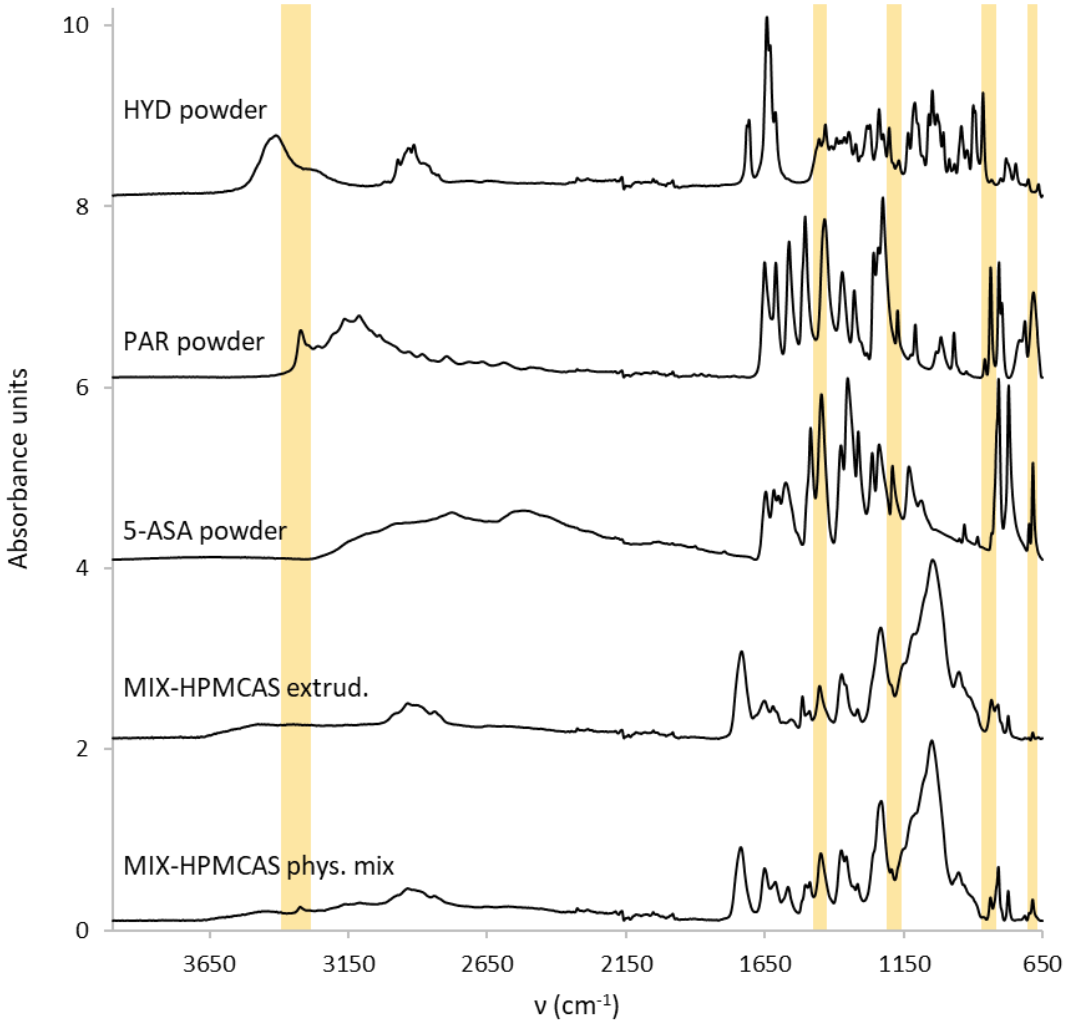

Figure 5.30. ATR-FTIR spectrum of extruded MIX-HPMCAS filaments compared to its corresponding physical mix and individual drug powders, significant changes in the spectrum are highlighted in yellow.

Table 5.2. Table of the significant changes/shifts, changes in relative intensities, and association of the ATR-FTIR bands of the MIX-HPMCAS extrudates compared to its corresponding physical mix.

MIX-HPMCAS phys. mix			**MIX-HPMCAS extrudates**		
***v* (cm^{-1})**	***RI***	**Association**	***v* (cm^{-1})**	***RI***	**Association**
3321	8%	PAR-HPMCAS phys. mix	-	-	PAR-HPMCAS extrud.
-	-	Overlap with more intense bands of PAR-HPMCAS phys. mix	1583	10%	5-ASA-HPMCAS extrud.
1566	19%	PAR-HPMCAS phys. mix	1555	11%	PAR-HPMCAS extrud.
1502	20%	PAR-HPMCAS phys. mix	1514	24%	PAR-HPMCAS extrud.
1448	37%	Overlap with more intense bands of PAR-HPMCAS phys. mix	1452	30%	5-ASA-HPMCAS extrud.
1194	29%	5-ASA-HPMCAS phys. mix	-	-	Overlap with more intense bands of PAR-HPMCAS extrud.
837	13%	PAR-HPMCAS phys. mix	833	22%	PAR-HPMCAS extrud.
687	12%	5-ASA-HPMCAS & PAR-HPMCAS phys. mixes	685	4%	5-ASA-HPMCAS & PAR-HPMCAS phys. mixes

The PXRD analysis in the Figure 5.31 show amorphous diffractograms of the PAR-HPMCAS and HYD-HPMCAS extrudates compared to their physical mixes which both showed crystalline peaks belonging to each of the drugs. This confirms the molecular dispersion of both drugs within the HPMCAS filaments. However, crystalline peaks associated with 5-ASA at 7.56 °, 15.14 °, and 16.54 ° were observed in both diffractograms of 5-ASA-HPMCAS and MIX-HPMCAS filaments, confirming the presence of the 5-ASA crystals within both extrudates.

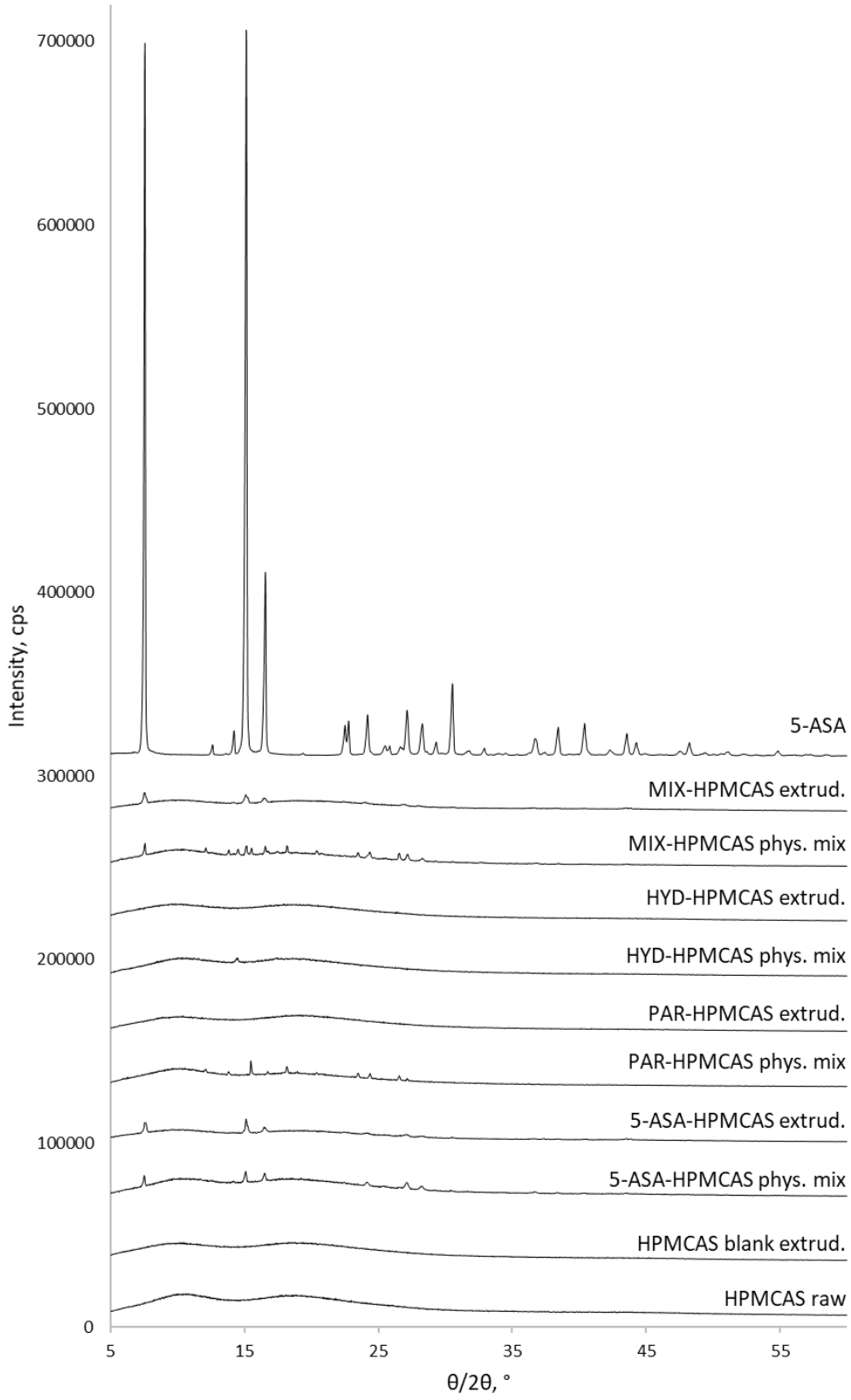

Figure 5.31. PXRD diffractograms of extruded blank HPMCAS, 5-ASA-HPMCAS, PAR-HPMCAS, HYD-HPMCAS, and MIX-HPMCAS filaments compared to the diffractograms of their corresponding physical mixes and raw HPMCAS and 5-ASA, suggesting the PAR and HYD were molecularly dispersed in the extrudates, while the 5-ASA stayed mostly in a crystal form after extrusion.

To study the effect of the filament diameter on the enteric properties of the HPMCAS, the three different diameters of each single drug loaded filament were first measured. The thickest diameter (a), which was controlled by the extruder nozzle, was measured by the digital calliper. The two thinner diameters (b, c) were manually estimated from the images obtained by the optical microscope. The mean diameters and their standard deviations (SD) are shown in the Table 5.3. Ten measurements were taken for each diameter.

Table 5.3. Diameters of the single drug loaded extruded filaments used for the drug release study.

	5-ASA-HPMCAS			**PAR-HPMCAS**			**HYD-HPMCAS**		
	a (µm)	**b (µm)**	**c (µm)**	**a (µm)**	**b (µm)**	**c (µm)**	**a (µm)**	**b (µm)**	**c (µm)**
Mean size	2100	617.1	332.6	1900	717.6	245.0	2100	738.1	269.9
SD	100	42.7	60.9	100	25.8	52.3	100	32.4	18.5

The dissolution study of the different diameters of the single drug loaded filaments was performed in closed glass vials placed in the shaking water bath (100 rpm) at 37 °C. The filaments were first placed into acidic buffer (pH = 1.2) for two hours and then transferred into PBS buffer pH = 7.4 for next 6 hours. The buffer volume was kept fixed by adding fresh buffer into the vials after each time point sample was taken. The drug concentrations were quantified by the UV-VIS spectrophotometry. In the Figure 5.32, the drug release profiles of the three single drug loaded filaments and each of their diameters are shown compared to the release profiles obtained for the electrospun single drug loaded samples. Figure A shows the release profiles of the 5-ASA-HPMCAS filaments compared to the 5-ASA-HPMCAS (both drug loading of 7%), figure B shows the release profiles of the PAR-HPMCAS filaments compared to the PAR-HPMCAS (both drug loading of 8%), and figure C shows the release profiles of the HYD-HPMCAS filaments compared to the HYD-HPMCAS (both drug loading of 7%). The thickest diameter (a) of the extruded filaments is represented by the green triangles, the middle diameter (b) is represented by the yellow squares, and the thinnest diameter (c) is represented by the dark blue diamonds. The pink empty circles belong to the release profiles of the electrospun formulations. The filament structure stayed unchanged after the two hours in the acidic pH and the filaments were therefore easily transferred. In the pH = 7.4, the filaments started to swell, which is characteristic for HPMCAS polymer.[143] Before calculating the cumulative drug release, the real drug concentration present in the filaments was measured by dissolving fresh filaments completely in the PBS buffer (pH = 7.4) in triplicates, resulting in clear solutions. The

measured drug loadings of the 5-ASA, PAR, and HYD were 5.9 ± 0.5%, 7.3 ± 0.8%, and 2.1 ± 0.1%, respectively. This suggests, the 5-ASA was partially decomposed by the extrusion process, which agrees with the dark brown colour of the filaments. The PAR might have been partially decomposed as well during the extrusion process, considering its early onset of decomposition (155 °C) occurring before the extrusion temperature (170 °C) and the high standard deviation of the real drug loading measurements. The mean values of the real drug loading measurements were further used as the 100% of the drug content in the filaments.

The enteric properties of the HPMCAS polymer were not preserved in any of the PAR-HPMCAS extrudates samples, showing 11 ± 2%, 13 ± 1%, and 41 ± 5% cumulative drug release after 2 hours in pH = 1.2 buffer. On the other hand, no drug was released from both 5-ASA-HPMCAS and HYD-HPMCAS extrudates of all three diameters in the acidic pH. Following trends observed in other enteric polymers, in particular Eudragits (as already discussed in Chapter 3)[185], the diffusion of PAR from HPMCAS extrudates in acidic media could be explained by its low molecular weight and weak acidity.

Even though the PAR-HPMCAS extrudates did not behave as an enteric formulation, all the obtained data suggest the diameter of the filament plays a key role in the drug release rate. The bigger the diameter of the filament was, the slower the drug release was. The dependence of the drug release in acidic media on the filament diameter was also observed in other enteric polymers such as Eudragit L100[199] and Eudragit FS100[200]. In the latter case, Balogh et al.[200] compared release of poorly soluble spironolactone from Eudragit electrospun fibers and extruded filaments. The electrospun fibers of ~0.4 – 0.8 μm diameter did not fulfil the enteric requirements despite spironolactone's higher molecular weight (417 g/mol). However, less than 5% of the drug was released from ground extrudates (particles of <400 μm diameter).

The drug release study of the MIX-HPMCAS extrudates was not performed due to time and cost reasons associated with the COVID-19 pandemic.

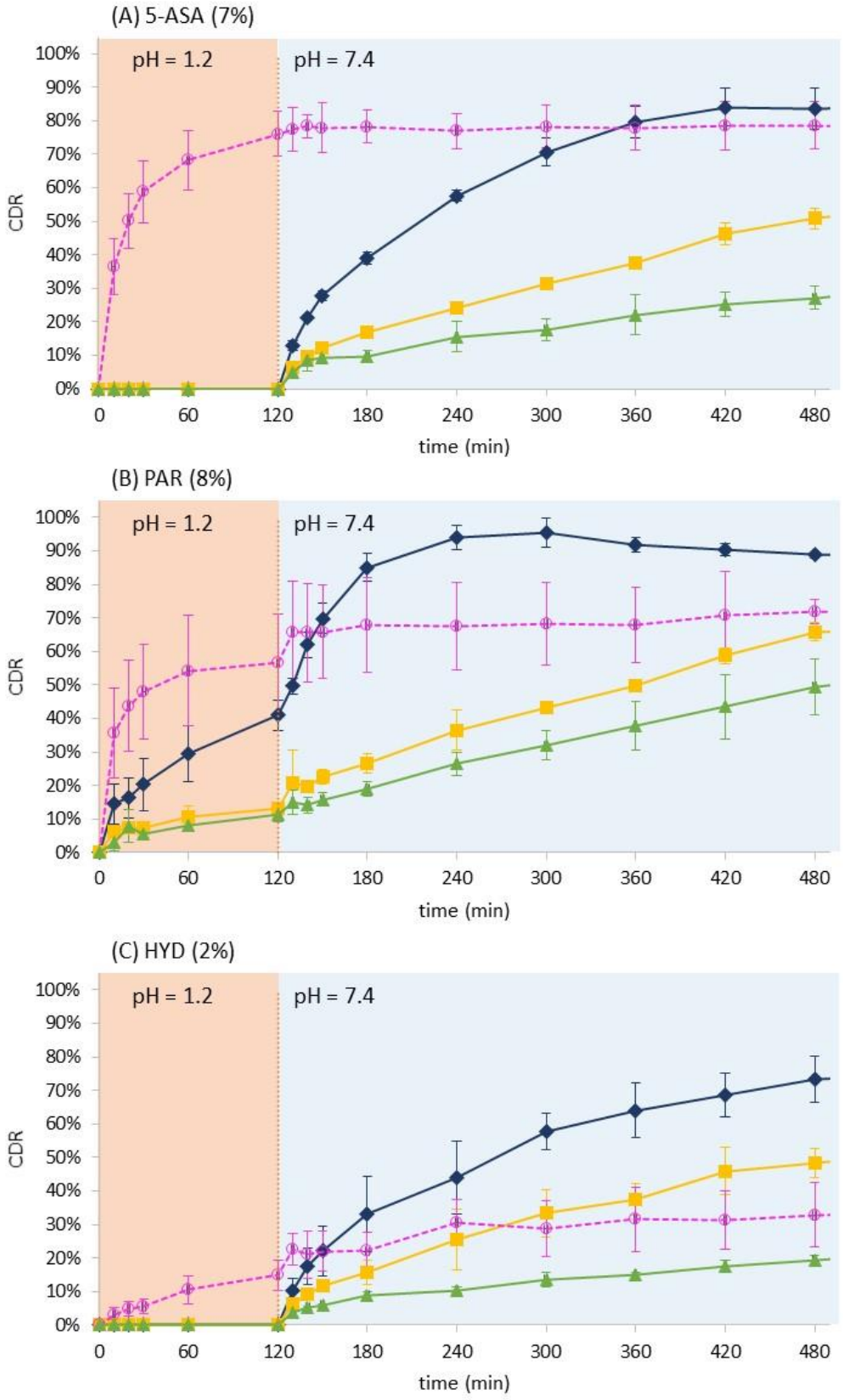

Figure 5.32. The cumulative drug release profiles of the (A) 5-ASA-HPMCAS, (B) PAR-HPMCAS, and (C) HYD-HPMCAS extruded filaments compared to the corresponding electrospun formulations (pink empty circles). The thickest diameter (a) of the extruded filaments is represented by the green triangles, the middle diameter (b) by the yellow squares, and the thinnest diameter (c) by the dark blue diamonds.

5.4 Conclusion

First, the incorporation of the 5-ASA loaded zein NPs into the HPMCAS fibers by electrospinning and its challenges were discussed in this chapter. Even though tri-axial electrospinning using either (immiscible) solvent or pH independent polymer solutions as a middle layer in between the nanosuspension and the HPMCAS solution was trialled, the one step incorporation technique was not achieved due to the precipitation of the HPMCAS polymer in the presence of the acidified nanosuspension.

This led to redesigning the formulation into a layered composition consisted of three layers. The middle layer was created by the co-axial electrospinning: 5-ASA-zein NPs (10%) as a core and 7.5% PVP solution in MQ water with 0.04% HYD as a shell. This was sealed from all sides by the (single nozzle) electrospun HPMCAS-PARmin (0.05% of PAR) fibers. The SEM and CFM imaging showed the 5-ASA-zein NPs (10%) reprecipitated into 0.5 – 1 μm particles within the process. Due to the instability of the co-axial electrospinning process (probably caused by the reprecipitation of zein particles), the middle layer could have been electrospun for 25 minutes only, which led to the minimal drug loading levels of all three drugs, so they could be assayed by the LC-MS without overloading the MS detector. Even though the electrospun HPMCAS-PARmin layers were not a sufficient enteric coating of the 5-ASA-zein particles within the PVP-HYD fibers and both 5-ASA and HYD were rapidly diffused from the formulation in pH = 1.2, the PAR was not released before the formulation was transferred into the colonic pH.

This finding led to a brief study of the effect the low drug loading levels could have on the enteric properties of the HPMCAS electrospun fibers. For this purpose, MIX-HPMCASmin fibers containing 0.05% PAR, 0.05% HYD, and 0.15% 5-ASA (0.25% drug loading in total) were electrospun using a single nozzle. These fibers showed a minimal beading when compared with the blank HPMCAS fibers (described in Chapter 3), even though same electrospinning conditions beside temperature were used. The viscosity, surface tension, and conductivity of these two feed solutions were not significantly different either. Therefore, the temperature effect on the HPMCAS fiber structure should be investigated in the future. Despite the minimal drug loading levels, the enteric properties of the HPMCAS fibers were not preserved in this case, diffusing all three drugs above the 10% limit in the pH = 1.2. This suggests that either the 0.25% total drug loading is too high or the combination of the drugs

itself affects the enteric properties. This also should be investigated more closely in the future.

At last, the effect of the fiber diameter on the enteric properties was studied. For this purpose, the hot-melt extrusion was used to prepare drug loaded HPMCAS filaments of three different diameters. The extrusion temperature was fixed at 170 °C, which was found to be the optimal temperature for processing of the HPMCAS of the grade H and also a safe temperature to avoid major drug losses due to their decomposition. The SEM scans showed the blank HPMCAS filaments had smooth surface with occasional bumps and a flaky structure on a cross section. The PAR-HPMCAS (8% drug loading) filaments showed smooth surface and cross section. The HYD-HPMCAS (2% drug loading) showed smooth surface and a semolina-like structure on the cross section. Both 5-ASA-HPMCAS (7% drug loading) and MIX-HPMCAS (17% drug loading in total) filaments showed bark-like surface and plate 5-ASA crystal on their cross sections. The drug release study was performed only for the single drug loaded filaments due to the time and cost reasons associated with the COVID-19 pandemic. However, a strong pattern of the increasing drug release rate with the decreasing filament/fiber diameter was observed. Out of the three extruded single drug loaded formulations, only the PAR-HPMCAS extrudates were not fulfilling the enteric requirements (at any diameter). On the other hand, both 5-ASA-HPMCAS and HYD-HPMCAS extrudates showed 0% drug release in pH = 1.2 for all three studied diameters. These results suggest that enteric properties can be achieved above a critical diameter. Although the diameter of electrospun fibers can be controlled by e.g., polymer solution flow rate and the applied voltage, the maximum fiber diameters reported in literature are ~10 μm,[201] which presents limitation of the electrospinning technique.

6 CONCLUSION AND FUTURE WORK

This project provided an insight into processing of HPMCAS polymer by electrospinning technique. The HPMCAS was confirmed to be electrospinnable without adding any additives (Chapter 3), despite the contradictory reports in the literature.[170] Beaded HPMCAS fibers were obtained from 20% (w/v) HPMCAS solution in acetone:DMSO (3:2, v:v). The morphology of the fibers was significantly affected by relative humidity, showing thinner and broken fibers with more spherical beads in decreased humidity (RH = 23 ± 2%). Other factors such as feed solution viscosity, conductivity, and surface tension contributing to the electrospinnability and resulting fiber diameter size and surface morphology were discussed, although no significant effects of these parameters on the morphology of blank fibers were observed. Significantly reduced beading was observed in the MIX-HPMCASmin fibers, containing all three model drugs (5-aminosalicylic acid, hydrocortisone, paracetamol) in minimal drug-polymer ratios. Although no significant difference in the properties of the feed solution was observed in this case, the electrospinning process itself was performed at significantly reduced temperature. Since all the studied physico-chemical properties of the feed solutions are temperature dependant, it was suggested the temperature might be one of the key factors affecting the fiber morphology, which should be further studied in the future.

As one of the main objectives of the project was to prepare multi-drug loaded HPMCAS electrospun formulations, three model drugs were mixed with the HPMCAS electrospinning feed solution to produce multidrug loaded fibers (MIX-HPMCAS fibers). These fibers (Chapter 3) were also significantly affected by the relative humidity, showing significant fusing at RH>30 ± 2%. Therefore, drug loaded formulations were electrospun at RH = 30 ± 2% and the fibers were collected on a rotating drum to assure even thickness of the fibrous mat. Control single drug loaded samples were prepared at the same electrospinning conditions, in order to compare drug release profiles from the fibrous formulations (Chapter 3). None of the formulations fulfilled the enteric requirements, as more than 10% of each drug was released within 2 hours in pH = 1.2 from the HPMCAS fibers even though the polymer did not dissolve. However, hydrocortisone (HYD) showed significantly slower release in pH = 1.2 compared with the more hydrophilic 5-aminosalicylic acid (5-ASA) and paracetamol (PAR). It was suggested the release rate of the drug was affected by the physico-chemical properties of the drugs, especially their molecular weight, hydrophobicity, acidity/basicity, and solubility in water. However, the ratio of the drug and polymer within the formulation might play a role in the drug diffusion

in pH = 1.2 too. To test whether drug loading capacity of the fibers was not exceeded in the MIX-HPMCAS and single drug loaded fibers, MIX-HPMCASmin fibers containing all three drugs in minimal drug-polymer ratios (5-ASA: 0.15%, PAR: 0.05%, HYD: 0.05%) were prepared (Chapter 5). Despite the minimal concentrations of the drugs, the HPMCAS fibers did not behave as an enteric carrier, releasing more than 10% of each drug within 2 hours in pH = 1.2. Interestingly, the diffusion rate of the hydrocortisone followed the same profile as in the case of paracetamol, which was loaded into the fibers at the same drug-polymer ratio. The comparison of cumulative drug release (CDR) after 2 hours in pH =1.2 from the MIX-HPMCAS fibers, single drug loaded fibers, and the MIX-HPMCASmin fibers is shown in the Table 6.1. (M)DSC, ATR-FTIR, and PXRD analyses confirmed the drugs were molecularly dispersed in all drug loaded fibrous samples.

Table 6.1. Comparison of cumulative drug release (CDR) after 2 hours in pH =1.2 from the MIX-HPMCAS fibers, single drug loaded fibers, and the MIX-HPMCASmin fibers (drug to polymer ratio referred to as DL).

Drug	MIX-HPMCAS		Single drug loaded fibers		MIX-HPMCASmin	
	DL	**CDR**	**DL**	**CDR**	**DL**	**CDR**
5-ASA	7%	65 ± 8%	7%	76 ± 7%	0.15%	45 ± 7%
PAR	8%	66 ± 6%	8%	57 ± 15%	0.05%	28 ± 3%
HYD	2%	19 ± 4%	2%	15 ± 4%	0.05%	25 ± 2%

Since none of the electrospun drug loaded HPMCAS formulation showed enteric properties, it was proposed that the enteric properties might depend on the surface to volume ratio of the formulation fibers and subsequently the diameter of the fibers. For this purpose, single drug loaded extrudates containing the same drug-polymer ratios (DL) as the single drug loaded fibers were prepared at three different diameters (~1800 - 2100, ~580 - 760, ~200 - 390 μm). For comparison, the diameter of the electrospun fibers was in the ~0.2 - 0.4 μm range. Molecular dispersion of the paracetamol and hydrocortisone was observed in the HPMCAS extrudates. However, the 5-aminosalysilic acid was loaded into the extruded filaments in a crystalline form. Despite its crystalline form, the 5-ASA was not released in the pH = 1.2 from the extrudates of any diameter. Enteric properties were also observed at the hydrocortisone loaded extrudates of all three diameters. However, diffusion of the paracetamol from the extrudates of all three diameters was observed, when even the lowest surface to volume ratio studied in this project was not enough to keep the enteric properties of the HPMCAS. The diffusion rate of the paracetamol increased with the

decreasing diameter of the extrudates/fibers, although no significant difference was observed in between the thickest and medium diameters of the extrudates. The comparison of the cumulative drug release (CDR) after 2 hours in pH =1.2 from the single drug loaded extrudates and electrospun fibers of different diameters is summarised in the Table 6.2. In pH = 7.4, the drug release rate increased with the decreasing diameter for all single drug loaded extrudates, independently of the drug. These findings suggest the surface to volume ratio is a key factor influencing the enteric properties of the formulations. It was suggested that enteric properties of the fibers could be achieved above a critical diameter. Diameter of electrospun fibers can be controlled by polymer concentration, polymer solution flow rate and/or the applied voltage. Although, as mentioned earlier, fibers of ~10 μm diameter are the biggest fibers reported in the literature so far.[201] However, the physico-chemical properties of the drug also affect the diffusion significantly, particularly its molecular weight and acidity/basicity (low molecular weight and basicity of the drugs lead to their faster diffusion into acidic media).

Table 6.2. Comparison of cumulative drug release after 2 hours in pH =1.2 from the single drug loaded extrudates and electrospun fibers of different diameters (drug to polymer ratio referred to as DL).

Drug	DL	Extrudates			Fibers
		~ 1800 - 2100 μm	**~ 580 - 760 μm**	**~ 200 - 390 μm**	**~ 0.2 - 0.4 μm**
5-ASA	7%	0%	0%	0%	76 ± 7%
PAR	8%	11 ± 2%	13 ± 1%	41 ± 5%	57 ± 15%
HYD	2%	0%	0%	0%	15 ± 4%

To deliver the 5-ASA into the colon without any drug loss in the acidic environment while still using the HPMCAS electrospun fibers, encapsulation of the drug into the nanoparticles and their subsequent incorporation into the fibers was proposed. For this purpose, spherical 5-ASA loaded zein nanoparticles (NPs) were prepared by nanoprecipitation as this method showed higher yield than the electrospray (Chapter 4). To dissolve 5-ASA in sufficient concentrations, the solution was acidified with hydrochloric acid. PXRD together with ATR-FTIR confirmed the 5-ASA was successfully loaded into the particles up to 10% 5-ASA/zein ratio (w/w) in form of chloride salt. Drug loaded NPs shown significantly higher degree of amorphous state compared to their corresponding physical mixes. Drug release in PBS buffer of pH = 7.4 (mimicking the colonic environment) showed a sustained profile, when 86 ± 14% and 74 ± 21% of the drug was released within 2 hours from

5-ASA zein NPs (5% 5-ASA/zein ratio) and 5-ASA zein NPs (10% 5-ASA/zein ratio), respectively. As the particles are expected to adhere to the colonic mucus due to the zein mucoadhesion properties, the formulations were considered suitable for colon targeting drug delivery systems despite their fast release profiles. Due to the time and cost reasons associated with the COVID-19 pandemic, drug loading efficiency and drug release in pH = 1.2 experiments were not finished. Other suggested future experiments are studies of the key factors affecting the particle size distribution (e.g., mixing process) and stability of the nanosuspensions as change of the nanosuspension pH caused significant agglomeration of the particles. For this purpose, a sodium caseinate was proposed as the most promising stabiliser.[186]

The incorporation of the 5-ASA loaded zein NPs into the HPMCAS fibers by electrospinning was not achieved due to the precipitation of the HPMCAS polymer in the presence of the acidified nanosuspensions (Chapter 5). This led to redesigning the formulation into a layered composition consisted of three layers. The middle layer was created by the co-axial electrospinning: 5-ASA-zein NPs (10%) as a core and 7.5% PVP solution in MQ water with 0.04% HYD as a shell. This was sealed from all sides by the (single nozzle) electrospun HPMCAS-PARmin (0.05% of PAR) fibers. The SEM and CFM imaging showed the 5-ASA loaded zein NPs reprecipitated from the diameter of 125 ± 45 nm into 0.5 – 1 μm within the process. The electrospun HPMCAS-PARmin layers were not a sufficient enteric coating of the 5-ASA-zein particles within the PVP-HYD fibers and both 5-ASA and HYD were rapidly diffused from the formulation in pH = 1.2.

REFERENCES

1. Jairath, V. & Feagan, B. G. Global burden of inflammatory bowel disease. *The Lancet Gastroenterology and Hepatology* vol. 5 2–3 (2020).

2. Chourasia, M. K. & Jain, S. K. Pharmaceutical approaches to colon targeted drug delivery systems. *J. Pharm. Pharm. Sci.* **6**, 33–66 (2003).

3. Lai, S. K., Wang, Y. Y. & Hanes, J. Mucus-penetrating nanoparticles for drug and gene delivery to mucosal tissues. *Adv. Drug Deliv. Rev.* **61**, 158–171 (2009).

4. J. Hill & Irving, M. H. Anatomy and physiology of the colon, rectum, and anus. in *ABC of Colorectal Diseases* (ed. D. J. Jones) 1–4 (BMJ Books, 1999).

5. Scanlon, V. C. & Sanders, T. The Digestive System. in *Essentials of Anatomy and Physiology* 396–421 (F. A. Davis Company, 2011).

6. Lai, S. K., Wang, Y. Y. & Hanes, J. Mucus-penetrating nanoparticles for drug and gene delivery to mucosal tissues. *Adv. Drug Deliv. Rev.* **61**, 158–171 (2009).

7. Ensign, L. M., Cone, R. & Hanes, J. Oral drug delivery with polymeric nanoparticles: The gastrointestinal mucus barriers. *Adv. Drug Deliv. Rev.* **64**, 557–570 (2012).

8. Ensign, L. M., Schneider, C., Suk, J. S., Cone, R. & Hanes, J. Mucus penetrating nanoparticles: Biophysical tool and method of drug and gene delivery. *Adv. Mater.* **24**, 3887–3894 (2012).

9. Lai, S. K., Wang, Y. Y., Wirtz, D. & Hanes, J. Micro- and macrorheology of mucus. *Adv. Drug Deliv. Rev.* **61**, 86–100 (2009).

10. Geibel, J. P. Secretion and Absorption By Colonic Crypts. *Annu. Rev. Physiol.* **67**, 471–490 (2005).

11. Scott, N. A. & Thompson, D. G. Inflammatory bowel disease. in *ABC of Colorectal Diseases* (ed. Jones, D. J.) 55–60 (BMJ Books, 1999).

12. Inflammatory bowel disease (Latest modification: 15-Jan-2015): Martindale: The Complete Drug Reference. https://www.medicinescomplete.com/mc/martindale/current/670-a7-1-r.htm?q=inflammatory bowel disease&t=advanced&ss=tr&tot=28&p=1#_hit.

13. Inflammatory bowel disease - NHS Choices. http://www.nhs.uk/Conditions/inflammatory-bowel-disease/Pages/Introduction.aspx.

14. Hua, S., Marks, E., Schneider, J. J. & Keely, S. Advances in oral nano-delivery systems for colon targeted drug delivery in inflammatory bowel disease: Selective targeting to diseased versus healthy tissue. *Nanomedicine Nanotechnology, Biol. Med.* **11**, 1117–1132 (2015).

15. Docherty, M. J., Jones, R. C. W. & Wallace, M. S. Managing pain in inflammatory bowel disease. *Gastroenterol. Hepatol.* **7**, 592–601 (2011).

16. Feagins, L. A. & Cryer, B. L. Do Non-steroidal Anti-inflammatory Drugs Cause Exacerbations of Inflammatory Bowel Disease? doi:10.1007/s10620-009-1042-7.

17. Kefalakes, H., Stylianides, T. J., Amanakis, G. & Kolios, G. Exacerbation of inflammatory bowel diseases associated with the use of nonsteroidal anti-inflammatory drugs: myth or reality? doi:10.1007/s00228-009-0719-3.

18. Rampton, D. S. & Sladen, G. E. Relapse of ulcerative proctocolitis during treatment with no-steroidal anti-inflammatory drugs. *Postgrad. Med. J.* **57**, 297–299 (1981).

19. Walt, R. P., Hawkey, C. J. & Langman, M. J. Colitis associated with non-steroidal anti-inflammatory drugs. *British medical journal (Clinical research ed.)* vol. 288 238 (1984).

20. Rutherford, D., Stockdill, G., Hamer-Hodges, D. W. & Ferguson, A. Proctocolitis induced by salicylate. *British Medical Journal* vol. 288 794 (1984).

21. Kaufmann, H. J. & Taubin, H. L. Nonsteroidal anti-inflammatory drugs activate quiescent inflammatory bowel disease. *Ann. Intern. Med.* **107**, 513–516 (1987).

22. Bombardier, C. *et al.* Comparison of Upper Gastrointestinal Toxicity of Rofecoxib and Naproxen in Patients with Rheumatoid Arthritis. *N. Engl. J. Med.* **343**, 1520–1528 (2000).

23. Laine, L. *et al.* Serious lower gastrointestinal clinical events with nonselective NSAID or Coxib use. *Gastroenterology* **124**, 288–292 (2003).

24. Bresalier, R. S. *et al.* Cardiovascular Events Associated with Rofecoxib in a Colorectal Adenoma Chemoprevention Trial. *N. Engl. J. Med.* **352**, 1092–1102 (2005).

25. Solomon, S. D. *et al.* Cardiovascular Risk Associated with Celecoxib in a Clinical Trial for Colorectal Adenoma Prevention. *N. Engl. J. Med.* **352**, 1071–1080 (2005).

26. World Health Organization. *World health statistics 2019: monitoring health for the SDGs, sustainable development goals*. (2019).

27. World Health Organization. *Global action plan for the prevention and control of noncommunicable diseases 2013-2020*. (2013).

28. World Economic Forum and Harvard School of Public Health. *The Global Economic Burden of Non-communicable Diseases*. (2011).

29. Vermeire, E., Hearnshaw, H., Van Royen, P. & Denekens, J. Patient adherence to treatment: Three decades of research. A comprehensive review. *J. Clin. Pharm. Ther.* **26**, 331–342 (2001).

30. García-Pérez, L. E., Álvarez, M., Dilla, T., Gil-Guillén, V. & Orozco-Beltrán, D. Adherence to therapies in patients with type 2 diabetes. *Diabetes Ther.* **4**, 175–194 (2013).

31. Kavanagh, O. N., Albadarin, A. B., Croker, D. M., Healy, A. M. & Walker, G. M. Maximising success in multidrug formulation development: A review. *J. Control. Release* **283**, 1–19 (2018).

32. Stewart, D. *et al.* The behaviors and experiences of the community pharmacy team on the provision of multi-compartment compliance aids. *Res. Soc. Adm. Pharm.* **14**, 347–355 (2018).

33. Raimi-Abraham, B. T., Garcia del Valle, A., Varon Galcera, C., Barker, S. A. & Orlu, M. Investigating the physical stability of repackaged medicines stored into commercially available multicompartment compliance aids (MCAs). *J. Pharm. Heal. Serv. Res.* **8**, 81–89 (2017).

34. Church, C. & Smith, J. How stable are medicines moved from original packs into compliance aids? *Pharm. J.* **276**, 75–76 (2006).

35. Edirisinghe, S., Raimi-Abraham, B. T., Gilmartin, J. F. M. & Orlu-Gul, M. Multi-compartment compliance aids (MCAs): Application to the geriatric community. *Eur. Geriatr. Med.* **6**, 65–68 (2015).

36. Elliott, R. A. Appropriate use of dose administration aids. *Aust. Prescr.* **37**, 46–50 (2014).

37. Wald, N. J. & Law, M. R. A strategy to reduce cardiovascular disease by more than 80%. *Br. Med. J.* **326**, 1419–1423 (2003).

38. Huffman, M. D., Xavier, D. & Perel, P. Uses of polypills for cardiovascular disease and evidence to date. *Lancet* **389**, 1055–1065 (2017).

39. Patel, S. J. *et al.* Combination Drug Products for HIV—A Word of Caution for the Transplant Clinician. *Am. J. Transplant.* **16**, 2479–2482 (2016).

40. Pourkavoos, N. Unique Risks, Benefits, and Challenges of Developing Drug-Drug Combination Products in a Pharmaceutical Industrial Setting. *Comb. Prod. Ther.* **2**, (2012).

41. Das, N., Dhanawat, M., Dash, B., Nagarwal, R. C. & Shrivastava, S. K. Codrug: An efficient approach for drug optimization. *Eur. J. Pharm. Sci.* **41**, 571–588 (2010).

42. Svartz, N. Salazopyrin, a new sulfanilamide preparation. *Acta Med. Scand.* **110**, 577–598 (1942).

43. Croft, D. N., Cuddigan, J. H. P. & Sweetland, C. Gastric Bleeding and Benorylate, a New Aspirin. *Br. Med. J.* **3**, 545–547 (1972).

44. Monteleone, G. *et al.* Mongersen, an Oral SMAD7 Antisense Oligonucleotide, and Crohn's Disease. *N. Engl. J. Med.* **372**, 1104–1113 (2015).

45. Adawiyah, N., Moniruzzaman, M., Hawatulaila, S. & Goto, M. Ionic liquids as a potential tool for drug delivery systems. *Medchemcomm* **7**, 1881–1897 (2016).

46. Zeng, Q. Z., Ouyang, J., Zhang, S. & Zhang, L. Structural characterization and dissolution profile of mycophenolic acid cocrystals. *Eur. J. Pharm. Sci.* **102**, 140–146 (2017).

47. Zhou, Z. *et al.* Resveratrol cocrystals with enhanced solubility and tabletability. *Int. J. Pharm.* **509**, 391–399 (2016).

48. Thipparaboina, R., Kumar, D., Chavan, R. B. & Shastri, N. R. Multidrug co-crystals: Towards the development of effective therapeutic hybrids. *Drug Discov. Today* **21**, 481–490 (2016).

49. Bary, A. R., Tucker, I. G. & Davies, N. M. Considerations in the use of hydroxypropyl-β-cyclodextrin in the formulation of aqueous ophthalmic solutions of hydrocortisone. *Eur. J. Pharm. Biopharm.* **50**, 237–244 (2000).

50. Cortes, J. E. *et al.* Phase II, multicenter, randomized trial of CPX-351 (cytarabine:Daunorubicin) liposome injection versus intensive salvage therapy in adults with first relapse AML. *Cancer* **121**, 234–242 (2015).

51. Green, M. R. *et al.* Abraxane®, a novel Cremophor®-free, albumin-bound particle form of paclitaxel for the treatment of advanced non-small-cell lung cancer. *Ann. Oncol.* **17**, 1263–1268 (2006).

52. Tamames-Tabar, C., García-Márquez, A., Blanco-Prieto, M. J., Serre, C. & Horcajada, P. MOFs in pharmaceutical technology. in *Bio- and Bioinspired Nanomaterials* 83–112 (Wiley-VCH Verlag GmbH & Co. KGaA, 2014).

53. Eubank, J. F. *et al.* Porous, rigid metal(III)-carboxylate metal-organic frameworks for the delivery of nitric oxide. *APL Mater.* **2**, (2014).

54. McKinlay, A. C. *et al.* Nitric oxide adsorption and delivery in flexible MIL-88(Fe) metal-organic frameworks. *Chem. Mater.* **25**, 1592–1599 (2013).

55. Park, H. & Park, K. Polymers in Pharmaceutical Products. in *Polymers of Biological and Biomedical Significance* 2–15 (American Chemical Society, 1993). doi:10.1021/bk-1994-0540.ch001.

56. Farah, S., Anderson, D. G. & Langer, R. Physical and mechanical properties of PLA, and their functions in widespread applications — A comprehensive review. *Adv. Drug Deliv. Rev.* **107**, 367–392 (2016).

57. Makadia, H. K. & Siegel, S. J. Poly Lactic-co-Glycolic Acid (PLGA) as biodegradable controlled drug delivery carrier. *Polymers (Basel).* **3**, 1377–1397 (2011).

58. Sivasankaran, S. & Jonnalagadda, S. Advances in controlled release hormonal technologies for contraception: A review of existing devices, underlying mechanisms, and future directions. *J. Control. Release* **330**, 797–811 (2021).

59. Kelleher, J. F. *et al.* A comparative study between hot-melt extrusion and spray-drying for the manufacture of anti-hypertension compatible monolithic fixed-dose combination products. *Int. J. Pharm.* **545**, 183–196 (2018).

60. Ziaee, A. *et al.* Spray drying ternary amorphous solid dispersions of ibuprofen – An investigation into critical formulation and processing parameters. *Eur. J. Pharm. Biopharm.* **120**, 43–51 (2017).

61. Zardetto, S. & Rosa, M. D. Effect of extrusion process on properties of cooked, fresh egg pasta. *J. Food Eng.* **92**, 70–77 (2009).

62. Kuhs, M., Moore, J., Kollamaram, G., Walker, G. & Croker, D. Predicting optimal wet granulation parameters for extrusion-spheronisation of pharmaceutical pellets using a mixer torque rheometer. *Int. J. Pharm.* **517**, 19–24 (2017).

63. Huber, J. Pharmacokinetics of Implanon®: An integrated analysis. *Contraception* **58**, 85S-90S (1998).

64. Van Laarhoven, J. A. H., Kruft, M. A. B. & Vromans, H. In vitro release properties of etonogestrel and ethinyl estradiol from a contraceptive vaginal ring. *Int. J. Pharm.* **232**, 163–173 (2002).

65. Yoo, J. *et al.* Three-dimensional printing system and equipment assembly (US20140065194). (2014).

66. Leuner, C. & Dressman, J. Improving drug solubility for oral delivery using solid dispersions. *Eur. J. Pharm. Biopharm.* **50**, 47–60 (2000).

67. Riekes, M. K. *et al.* Development of enteric-coated fixed dose combinations of amorphous solid dispersions of ezetimibe and lovastatin: Investigation of formulation and process parameters. *Int. J. Pharm.* **520**, 49–58 (2017).

68. Jacobs, E. E., Gronowicz, G., Hurley, M. M. & Kuhn, L. T. Biomimetic calcium phosphate/polyelectrolyte multilayer coatings for sequential delivery of multiple biological factors. *J. Biomed. Mater. Res. - Part A* **105**, 1500–1509 (2017).

69. Palmer, A. C. & Sorger, P. K. Combination Cancer Therapy Can Confer Benefit via Patient-to-Patient Variability without Drug Additivity or Synergy. *Cell* **171**, 1678-1691.e13 (2017).

70. Philip, A. K. & Philip, B. Colon targeted drug delivery systems: a review on primary and novel approaches. *Oman Med J* **25**, 79–87 (2010).

71. Amidon, S., Brown, J. E. & Dave, V. S. Colon-Targeted Oral Drug Delivery Systems: Design Trends and Approaches. *AAPS PharmSciTech* **16**, 731–741 (2015).

72. Schiller, C. *et al.* Intestinal fluid volumes and transit of dosage forms as assessed by magnetic resonance imaging. *Aliment. Pharmacol. Ther.* **22**, 971–979 (2005).

73. Macfarlane, G. T., Gibson, G. R. & Cummings, J. H. Comparison of fermentation reactions in different regions of the human colon. *J. Appl. Bacteriol.* **72**, 57–64 (1992).

74. Bown, R. L., Gibson, J. A., Sladen, G. E., Hicks, B. & Dawson, A. M. Effects of lactulose and other laxatives on ileal and colonic pH as measured by a radiotelemetry device. *Gut* **15**, 999–1004 (1974).

75. Christl, S. U. & Scheppach, W. Metabolic consequences of total colectomy. *Scand. J. Gastroenterol. Suppl.* **32**, 20–24 (1997).

76. Hebden, J. M., Blackshaw, P. E., Perkins, A. C., Wilson, C. G. & Spiller, R. C. Limited exposure of the healthy distal colon to orally-dosed formulation is further exaggerated in active left-sided ulcerative colitis. *Aliment. Pharmacol. Ther.* **14**, 155–161 (2000).

77. Stubbs, J. B. *et al.* A noninvasive scintigraphic assessment of the colonic transit of nondigestible solids in man. *J. Nucl. Med.* **32**, 1375–1381 (1991).

78. Chourasia, M. K. & Jain, S. K. Polysaccharides for colon targeted drug delivery. *Drug Deliv.* **11**, 129–148 (2004).

79. Yang, L., Chu, J. S. & Fix, J. A. Colon-specific drug delivery: New approaches and in vitro/in vivo evaluation. *Int. J. Pharm.* **235**, 1–15 (2002).

80. Friend, D. R. New oral delivery systems for treatment of inflammatory bowel disease. *Adv. Drug Deliv. Rev.* **57**, 247–265 (2005).

81. Challa, T., Vynala, V. & Allam, K. V. Review Article COLON SPECIFIC DRUG DELIVERY SYSTEMS : A REVIEW ON PRIMARY AND NOVEL APPROACHES. *Int. J. Pharm. Sci. Rev. Res.* **7**, 171–181 (2011).

82. Dehghan, M. H. G. *et al.* Assessment of Isomalt for Colon-Specific Delivery and Its Comparison with Lactulose. *AAPS PharmSciTech* **14**, 53–59 (2013).

83. Pozzi, F., Furlani, P., Gazzaniga, A., Davis, S. S. & Wilding, I. R. The TIME CLOCK* system: a new oral dosage form for fast and complete release of drug after a predetermined lag time. *J. Control. Release* **31**, 99–108 (1994).

84. Steed, K. P. *et al.* The use of pharmacoscintigraphy to focus the development strategy for a novel 5-ASA colon targeting system ® (' 'TIME CLOCK ' ' system). *J. Control. Release* **49**, 115–122 (1997).

85. Reddy, S. N. *et al.* Colonic motility and transit in health and ulcerative colitis. *Gastroenterology* **101**, 1289–97 (1991).

86. Vassallo, M. *et al.* Transit through the proximal colon influences stool weight in the irritable bowel syndrome. *Gastroenterology* **102**, 102–8 (1992).

87. Ohe, M. R. von der, Camilleri, M., Kvols, L. K. & Thomforde, G. M. Motor Dysfunction of the Small Bowel and Colon in Patients with the Carcinoid Syndrome and Diarrhea. *N. Engl. J. Med.* **329**, 1073–1078 (1993).

88. Cruz, E. *et al.* Oros Push-Stick for Controlled Delivery of Active Agents. (2010).

89. Swanson, D. R., Barclay, B. L., Wong, P. S. & Theeuwes, F. Nifedipine gastrointestinal therapeutic system. *Am. J. Med.* **83**, 3–9 (1987).

90. Xiao, B. & Merlin, D. Oral colon-specific therapeutic approaches toward treatment of inflammatory bowel disease. *Expert Opin. Drug Deliv.* **9**, 1393–1407 (2012).

91. Collnot, E. M., Ali, H. & Lehr, C. M. Nano- and microparticulate drug carriers for targeting of the inflamed intestinal mucosa. *J. Control. Release* **161**, 235–246 (2012).

92. Hua, S. Orally administered liposomal formulations for colon targeted drug delivery. *Front. Pharmacol.* **5**, 138 (2014).

93. Beloqui, A. *et al.* Budesonide-loaded nanostructured lipid carriers reduce inflammation in murine DSS-induced colitis. *Int. J. Pharm.* **454**, 775–783 (2013).

94. Lamprecht, A., Schä, U. & Lehr, C.-M. Size-Dependent Bioadhesion of Micro-and Nanoparticulate Carriers to the Inflamed Colonic Mucosa. *Pharm. Res.* **18**, 788–793 (2001).

95. Wachsmann, P., Moulari, B., Béduneau, A., Pellequer, Y. & Lamprecht, A. Surfactant-dependence of nanoparticle treatment in murine experimental colitis. *J. Control. Release* **172**, 62–68 (2013).

96. Lamprecht, A., Yamamoto, H., Takeuchi, H. & Kawashima, Y. Nanoparticles Enhance Therapeutic Efficiency by Selectively Increased Local Drug Dose in Experimental Colitis in Rats. *J. Pharmacol. Exp. Ther.* **315**, 196–202 (2005).

97. Niebel, W., Walkenbach, K., Béduneau, A., Pellequer, Y. & Lamprecht, A. Nanoparticle-based clodronate delivery mitigates murine experimental colitis. *J. Control. Release* **160**, 659–665 (2012).

98. Lautenschläger, C., Schmidt, C., Lehr, C.-M., Fischer, D. & Stallmach, A. PEG-functionalized microparticles selectively target inflamed mucosa in inflammatory bowel disease. *Eur. J. Pharm. Biopharm.* **85**, 578–586 (2013).

99. Coco, R. *et al.* Drug delivery to inflamed colon by nanoparticles: Comparison of different strategies. *Int. J. Pharm.* **440**, 3–12 (2013).

100. Gradauer, K. *et al.* Liposomes coated with thiolated chitosan enhance oral peptide delivery to rats. *J. Control. Release* **172**, 872–878 (2013).

101. Jubeh, T. T., Barenholz, Y. & Rubinstein, A. Differential Adhesion of Normal and Inflamed Rat Colonic Mucosa by Charged Liposomes. *Pharm. Res.* **21**, 447–453 (2004).

102. Meissner, Y., Pellequer, Y. & Lamprecht, A. Nanoparticles in inflammatory bowel disease: Particle targeting versus pH-sensitive delivery. *Int. J. Pharm.* **316**, 138–143 (2006).

103. Lamprecht, A. *et al.* Biodegradable Nanoparticles for Targeted Drug Delivery in Treatment of Inflammatory Bowel Disease. *J. Control. Release* **192**, 202–208 (2014).

104. Cu, Y. & Saltzman, W. M. Controlled Surface Modification with Poly(ethylene)glycol Enhances Diffusion of PLGA Nanoparticles in Human Cervical Mucus. *Mol. Pharm.* **6**, 173–181 (2009).

105. Tang, B. C. *et al.* Biodegradable polymer nanoparticles that rapidly penetrate the human mucus barrier. *Proc. Natl. Acad. Sci. U. S. A.* **106**, 19268–19273 (2009).

106. Yang, M. *et al.* Nanoparticle penetration of human cervicovaginal mucus: The effect of polyvinyl alcohol. *J. Control. Release* **192**, 202–208 (2014).

107. Vong, L. B., Tomita, T., Yoshitomi, T., Matsui, H. & Nagasaki, Y. An Orally Administered Redox Nanoparticle That Accumulates in the Colonic Mucosa and Reduces Colitis in Mice. *Gastroenterology* **143**, 1027-1036.e3 (2012).

108. Moulari, B., Pertuit, D., Pellequer, Y. & Lamprecht, A. The targeting of surface modified silica nanoparticles to inflamed tissue in experimental colitis. *Biomaterials* **29**, 4554–4560 (2008).

109. Bhavsar, M. D. & Amiji, M. M. Gastrointestinal distribution and in vivo gene transfection studies with nanoparticles-in-microsphere oral system (NiMOS). *J. Control. Release* **119**, 339–348 (2007).

110. Bhavsar, M. D., Tiwari, S. B. & Amiji, M. M. Formulation optimization for the nanoparticles-in-microsphere hybrid oral delivery system using factorial design. *J. Control. Release* **110**, 422–430 (2006).

111. Laroui, H. *et al.* Targeting Intestinal Inflammation With CD98 siRNA/PEI–loaded Nanoparticles. *Am. Soc. Gene Cell Ther.* (2013) doi:10.1038/mt.2013.214.

112. Wilson, D. S. *et al.* Orally delivered thioketal nanoparticles loaded with TNF-α–siRNA target inflammation and inhibit gene expression in the intestines. *Nat. Mater.* **9**, 923–928 (2010).

113. Hua, S. Targeting sites of inflammation: intercellular adhesion molecule-1 as a target for novel inflammatory therapies. *Front. Pharmacol.* **4**, 127 (2013).

114. Mane, V. & Muro, S. Biodistribution and endocytosis of ICAM-1-targeting antibodies versus nanocarriers in the gastrointestinal tract in mice. *Int. J. Nanomedicine* **7**, 4223–37 (2012).

115. Nguyen, D. N., Clasen, C. & Van den Mooter, G. Pharmaceutical Applications of Electrospraying. *J. Pharm. Sci.* **105**, 2601–2620 (2016).

116. Jaworek, A. Micro- and nanoparticle production by electrospraying. *Powder Technol.* **176**, 18–35 (2007).

117. Hamdallah, S. I. *et al.* Microfluidics for pharmaceutical nanoparticle fabrication: The truth and the myth. *Int. J. Pharm.* **584**, 119408 (2020).

118. Jaworek, A. & Sobczyk, A. T. Electrospraying route to nanotechnology: An overview. *J. Electrostat.* **66**, 197–219 (2008).

119. Xie, J., Jiang, J., Davoodi, P., Srinivasan, M. P. & Wang, C. H. Electrohydrodynamic atomization: A two-decade effort to produce and process micro-/nanoparticulate materials. *Chem. Eng. Sci.* **125**, 32–57 (2015).

120. Smith, D. P. H. The Electrohydrodynamic Atomization of Liquids. *IEEE Trans. Ind. Appl.* **IA-22**, 527–535 (1986).

121. Barrero, A. & Loscertales, I. G. Micro- and Nanoparticles via Capillary Flows. *Annu. Rev. Fluid Mech.* **39**, 89–106 (2007).

122. Scheideler, W. J. & Chen, C. H. The minimum flow rate scaling of Taylor cone-jets issued from a nozzle. **104**, (2014).

123. Sridhar, R. & Ramakrishna, S. Electrosprayed nanoparticles for drug delivery and pharmaceutical applications. *Biomatter* **3**, e24281 (2013).

124. Pande, M. & Bhaskarwar, A. *Nanoparticles: Preparation and Characterization*. (Momentum Press ® LLC, 2016).

125. Kashchiev, D. *Nucleation*. (Elsevier Science, 2000).

126. Sear, R. P. Heterogeneous and homogeneous nucleation compared: Rapid nucleation on microscopic impurities. *J. Phys. Chem. B* **110**, 4985–4989 (2006).

127. Thanh, N. T. K., Maclean, N. & Mahiddine, S. Mechanisms of nucleation and growth of nanoparticles in solution. *Chem. Rev.* **114**, 7610–7630 (2014).

128. Sinha, B., Müller, R. H. & Möschwitzer, J. P. Bottom-up approaches for preparing drug nanocrystals: Formulations and factors affecting particle size. *Int. J. Pharm.* **453**, 126–141 (2013).

129. Vekilov, P. G. Nucleation. *Cryst. Growth Des.* **10**, 5007–5019 (2010).

130. Cao, G. & Wang, Y. *Nanostructures and Nanomaterials Synthesis, Properties, and Applications*. (World scientific, 2011).

131. Williams, C., Panaccione, R., Ghosh, S. & Rioux, K. Optimizing clinical use of mesalazine (5-aminosalicylic acid) in inflammatory bowel disease. *Therap. Adv. Gastroenterol.* **4**, 237–48 (2011).

132. Mesalazine: Martindale: The Complete Drug Reference. https://www.medicinescomplete.com/mc/martindale/current/16887-a.htm?q=5-ASA&t=search&ss=text&tot=256&p=1#mS16887-a.

133. Papich, M. G. Mesalamine. in *Saunders Handbook of Veterinary Drugs (Small and Large Animals)* 497–498 (Elsevier, 2016). doi:10.1016/B978-0-323-24485-5.00370-3.

134. Dash, A. K. & Brittain, H. G. Mesalamine. in *Analytical Profiles of Drug Substances and Excipients* (ed. Brittain, H. G.) vol. 25 209–242 (Academic Press, 1998).

135. National Center for Biotechnology Information. Mesalamine | C7H7NO3 - PubChem. *PubChem Compound Summary for CID 4075, Mesalamine* (2021).

136. Hydrocortisone | Martindale: The Complete Drug Reference.

137. IBD Relief. Hydrocortisone for Crohn's disease and ulcerative colitis.

138. Suitchmezian, V., Jeß, I. & Näther, C. Structural, thermodynamic, and kinetic aspects of the trimorphism of hydrocortisone. *J. Pharm. Sci.* **97**, 4516–4527 (2008).

139. Paracetamol | Martindale: The Complete Drug Reference.

140. Wang, I. C. *et al.* Polymorph transformation in paracetamol monitored by in-line NIR spectroscopy during a cooling crystallization process. *AAPS PharmSciTech* **12**, 764–770 (2011).

141. National Center for Biotechnology Information. Hydrocortisone | C21H30O5 - PubChem. *PubChem Compound Summary for CID 5754, Hydrocortisone* (2021).

142. National Center for Biotechnology Information. Acetaminophen | C8H9NO2 - PubChem. *PubChem Compound Summary for CID 1983, Acetaminophen* (2021).

143. Ashland/PC-12624.6. *AquaSolve: Hydroxypropylmethylcellulose acetate succinate - Physical and chemical properties*. (2016).

144. Lai, L. F. & Guo, H. X. Preparation of new 5-fluorouracil-loaded zein nanoparticles for liver targeting. *Int. J. Pharm.* **404**, 317–323 (2011).

145. Shukla, R. & Cheryan, M. Zein: the industrial protein from corn. *Ind. Crops Prod.* **13**, 171–192 (2001).

146. Elzoghby, A. O., Samy, W. M. & Elgindy, N. A. Protein-based nanocarriers as promising drug and gene delivery systems. *J. Control. Release* **161**, 38–49 (2012).

147. Zhong, Q. & Jin, M. Zein nanoparticles produced by liquid–liquid dispersion. *Food Hydrocoll.* **23**, 2380–2387 (2009).

148. Ashland. *PVP K-90 polymer*. *Product Data 4849* (2013).

149. Karavas, E., Georgarakis, E., Sigalas, M. P., Avgoustakis, K. & Bikiaris, D. Investigation of the release mechanism of a sparingly water-soluble drug from solid dispersions in hydrophilic carriers based on physical state of drug, particle size distribution and drug-polymer interactions. *Eur. J. Pharm. Biopharm.* **66**, 334–347 (2007).

150. Bhardwaj, N. & Kundu, S. C. Electrospinning: A fascinating fiber fabrication technique. *Biotechnol. Adv.* **28**, 325–347 (2010).

151. Jaeger, R., Bergshoeft, M. M., Martin, C. & Vancso, S. G. J. Electrospinning of Ultra-thin Polymer Fibers. *Macromol. Symp.* **127**, 141–150 (1998).

152. Teo, W. E. & Ramakrishna, S. A review on electrospinning design and nanofibre assemblies. *Nanotechnology* **17**, (2006).

153. Bazilevsky, A. V., Yarin, A. L. & Megaridis, C. M. Co-electrospinning of core-shell fibers using a single-nozzle technique. *Langmuir* **23**, 2311–2314 (2007).

154. Sun, Z., Zussman, E., Yarin, A. L., Wendorff, J. H. & Greiner, A. Compound Core-Shell Polymer Nanofibers by Co-Electrospinning. *Adv. Mater.* **15**, 1929–1932 (2003).

155. Jiang, Y. N., Mo, H. Y. & Yu, D. G. Electrospun drug-loaded core-sheath PVP/zein nanofibers for biphasic drug release. *Int. J. Pharm.* **438**, 232–239 (2012).

156. Xie, J., Lim, L. K., Phua, Y., Hua, J. & Wang, C. H. Electrohydrodynamic atomization for biodegradable polymeric particle production. *J. Colloid Interface Sci.* **302**, 103–112 (2006).

157. Rezvanpour, A., Attia, A. B. E. & Wang, C. H. Enhancement of particle collection efficiency in electrohydrodynamic atomization process for pharmaceutical particle fabrication. *Ind. Eng. Chem. Res.* **49**, 12620–12631 (2010).

158. Rezvanpour, A., Krantz, W. B. & Wang, C. H. Scaling analysis of the electrohydrodynamic atomization (EHDA) process for pharmaceutical particle fabrication. *Chem. Eng. Sci.* **80**, 81–90 (2012).

159. Rezvanpour, A. & Wang, C. H. The effects of auxiliary electric field within the electrohydrodynamic atomization encapsulation chamber on particle size, morphology and collection efficiency. *Chem. Eng. J.* **239**, 8–18 (2014).

160. Haberkorn, H., Franke, D., Frechen, T., Goesele, W. & Rieger, J. Early stages of particle formation in precipitation reactions - Quinacridone and boehmite as generic examples. *J. Colloid Interface Sci.* **259**, 112–126 (2003).

161. Tao, J., Chow, S. F. & Zheng, Y. Application of flash nanoprecipitation to fabricate poorly water-soluble drug nanoparticles. *Acta Pharm. Sin. B* **9**, 4–18 (2019).

162. Thorat, A. A. & Dalvi, S. V. Liquid antisolvent precipitation and stabilization of nanoparticles of poorly water soluble drugs in aqueous suspensions: Recent developments and future perspective. *Chem. Eng. J.* **181**–**182**, 1–34 (2012).

163. Cheng, J. *et al.* Formulation of functionalized PLGA-PEG nanoparticles for in vivo targeted drug delivery. *Biomaterials* **28**, 869–876 (2007).

164. Kakran, M., Sahoo, N. G., Li, L. & Judeh, Z. Fabrication of quercetin nanoparticles by anti-solvent precipitation method for enhanced dissolution. *Powder Technol.* **223**, 59–64 (2012).

165. Wang, Z., Chen, J. F., Le, Y., Shen, Z. G. & Yun, J. Preparation of ultrafine beclomethasone dipropionate drug powder by antisolvent precipitation. *Ind. Eng. Chem. Res.* **46**, 4839–4845 (2007).

166. Budhian, A., Siegel, S. J. & Winey, K. I. Haloperidol-loaded PLGA nanoparticles: Systematic study of particle size and drug content. *Int. J. Pharm.* **336**, 367–375 (2007).

167. Limayem Blouza, I., Charcosset, C., Sfar, S. & Fessi, H. Preparation and characterization of spironolactone-loaded nanocapsules for paediatric use. *Int. J. Pharm.* **325**, 124–131 (2006).

168. Van Eerdenbrugh, B. *et al.* A screening study of surface stabilization during the production of drug nanocrystals. *J. Pharm. Sci.* **98**, 2091–2103 (2009).

169. Verma, S., Kumar, S., Gokhale, R. & Burgess, D. J. Physical stability of nanosuspensions: Investigation of the role of stabilizers on Ostwald ripening. *Int. J. Pharm.* **406**, 145–152 (2011).

170. Balogh, A., Azs Farkas, B. & Krist Of Nagy, Z. Pharmaceutical Nanotechnology Novel Alternating Current Electrospinning of Hydroxypropylmethylcellulose Acetate Succinate (HPMCAS) Nanofibers for Dissolution Enhancement: The Importance of Solution Conductivity. (2017) doi:10.1016/j.xphs.2017.02.021.

171. Examples of the calculation of shear rates :: Anton Paar Wiki.

172. Fashandi, H. & Karimi, M. Pore formation in polystyrene fiber by superimposing temperature and relative humidity of electrospinning atmosphere. (2012) doi:10.1016/j.polymer.2012.10.003.

173. İçoğlu, H. İ. & Oğulata, R. T. Effect of Ambient Parameters on Morphology of Electrospun Poly (Trimethylene Terephthalate) (Ptt) Fibers. *Tekst. ve Konfeksiyon* 215–223 (2017).

174. Htike, H. H., Long, C. & Sukigara, S. The effect of relative humidity on electrospinning of poly- (vinyl alcohol) with soluble eggshell membrane. *J. Text. Eng.* **58**, 9–12 (2012).

175. Hardick, O., Stevens, B. & Bracewell, D. G. Nanofibre fabrication in a temperature and humidity controlled environment for improved fibre consistency. *J. Mater. Sci.* **46**, 3890–3898 (2011).

176. Golin, A. P. Humidity Effect on the Structure of Electrospun Core-Shell PCL-PEG Fibers for Tissue Regeneration Applications. (The University of Western Ontario, 2014).

177. Liang, T., Parhizkar, M., Edirisinghe, M. & Mahalingam, S. Effect of humidity on the generation and control of the morphology of honeycomb-like polymeric structures by electrospinning. *Eur. Polym. J.* **61**, 72–82 (2014).

178. Raghavan, B. K. & Coffin, D. W. Control of inter-fiber fusing for nanofiber webs via electrospinning. *J. Eng. Fiber. Fabr.* **6**, 1–5 (2011).

179. Nezarati, R. M., Eifert, M. B. & Cosgriff-Hernandez, E. Effects of humidity and solution viscosity on electrospun fiber morphology. *Tissue Eng. - Part C Methods* **19**, 810–819 (2013).

180. Fong, H., Chun, I. & Reneker, D. H. Beaded nanofibers formed during electrospinning. *Polymer (Guildf).* **40**, 4585–4592 (1999).

181. Choi, J. S. *et al.* Effect of organosoluble salts on the nanofibrous structure of electrospun poly(3-hydroxybutyrate-co-3-hydroxyvalerate). *Int. J. Biol. Macromol.* **34**, 249–256 (2004).

182. Liu, M., Wang, X., Wang, Y. & Jiang, Z. Controlled stimulation-burst targeted release by pH-sensitive HPMCAS/theophylline composite nanofibers fabricated through electrospinning. *J. Appl. Polym. Sci.* **137**, 48383 (2020).

183. Shen, X. *et al.* Electrospun diclofenac sodium loaded Eudragit® L 100-55 nanofibers for colon-targeted drug delivery. *Int. J. Pharm.* **408**, 200–207 (2011).

184. Illangakoon, U. E., Yu, D. G., Ahmad, B. S., Chatterton, N. P. & Williams, G. R. 5-Fluorouracil loaded Eudragit fibers prepared by electrospinning. *Int. J. Pharm.* **495**, 895–902 (2015).

185. Burgess, K., Li, H., Abo-Zeid, Y., Fatimah & Williams, G. R. The effect of molecular properties on active ingredient release from electrospun eudragit fibers. *Pharmaceutics* **10**, (2018).

186. Patel, A., Hu, Y., Tiwari, J. K. & Velikov, K. P. Synthesis and characterisation of zein-curcumin colloidal particles. *Soft Matter* **6**, 6192–6199 (2010).

187. Gomez-Estaca, J., Balaguer, M. P., Gavara, R. & Hernandez-Munoz, P. Formation of zein nanoparticles by electrohydrodynamic atomization: Effect of the main processing variables and suitability for encapsulating the food coloring and active ingredient curcumin. *Food Hydrocoll.* **28**, 82–91 (2012).

188. Bhushani, J. A., Kurrey, N. K. & Anandharamakrishnan, C. Nanoencapsulation of green tea catechins by electrospraying technique and its effect on controlled release and in-vitro permeability. *J. Food Eng.* **199**, 82–92 (2017).

189. Si, Y. *et al.* Characterization of electrical current and liquid droplets deposition area in a capillary electrospray. *Results Eng.* **9**, 100206 (2021).

190. de la Mora, J. F. & Loscertales, I. G. The current emitted by highly conducting Taylor cones. *J. Fluid Mech.* **260**, 155–184 (1994).

191. Cai, S. & Singh, B. R. Identification of β-turn and random coil amide III infrared bands for secondary structure estimation of proteins. *Biophys. Chem.* **80**, 7–20 (1999).

192. Sessa, D. J. & Woods, K. K. Purity assessment of commercial zein products after purification. *JAOCS, J. Am. Oil Chem. Soc.* **88**, 1037–1043 (2011).

193. Haynes, W. M. *CRC handbook of chemistry and physics : a ready-reference book of chemical and physical data.* (CRC Press, 2014).

194. Malvern Panalytical. Dynamic Light Scattering (DLS)|Common Terms Defined|Malvern Panalytical. https://www.malvernpanalytical.com/en/learn/knowledge-center/Whitepapers/WP111214DLSTermsDefined (2017).

195. Jensen, J., Cornett, C., Olsen, C. E., Tjørnelund, J. & Hansen, S. H. Identification of major degradation products of 5-aminosalicylic acid formed in aqueous solutions and in pharmaceuticals. *Int. J. Pharm.* **88**, 177–187 (1992).

196. Bouman, J. *et al.* Controlled Release from Zein Matrices: Interplay of Drug Hydrophobicity and pH. *Pharm. Res.* **33**, 673–685 (2016).

197. Swenson, J., Jansson, H., Hedström, J. & Bergman, R. Properties of hydration water and its role in protein dynamics. *J. Phys. Condens. Matter* **19**, (2007).

198. Berardi, A., Rahim, S. A., Bisharat, L. & Cespi, M. Swelling of zein matrix tablets benchmarked against HPMC and ethylcellulose: Challenging the matrix performance by the addition of co-excipients. *Pharmaceutics* **11**, 1–15 (2019).

199. Da Costa, F. F. P., Araújo, E. S., Nascimento, M. L. F. & De Oliveira, H. P. Electrospun Fibers of Enteric Polymer for Controlled Drug Delivery. *Int. J. Polym. Sci.* **2015**, (2015).

200. Balogh, A. *et al.* Controlled-release solid dispersions of Eudragit® FS 100 and poorly soluble spironolactone prepared by electrospinning and melt extrusion. *Eur. Polym. J.* **95**, 406–417 (2017).

201. Cramariuc, B. *et al.* Fiber diameter in electrospinning process. *J. Electrostat.* **71**, 189–198 (2013).